EVALUATION AND TARGETING OF GEOTHERMAL ENERGY RESOURCES IN THE SOUTHEASTERN UNITED STATES

Progress Report

John K. Costain and Lynn Glover, III
Principal Investigators

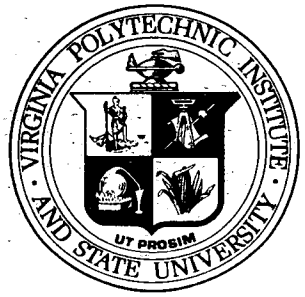

Virginia Polytechnic Institute and State University
Blacksburg, Virginia 24061

October 1, 1979 — March 31, 1980

PREPARED FOR THE U.S. DEPARTMENT OF ENERGY
UNDER CONTRACT NO. DE - AC05 - 78ET27001

DISCLAIMER

Master

VPI&SU-78ET27001-8

EVALUATION AND TARGETING OF GEOTHERMAL ENERGY RESOURCES IN THE SOUTHEASTERN UNITED STATES

Progress Report

John K. Costain and Lynn Glover III

Principal Investigators

Department of Geological Sciences

Virginia Polytechnic Institute and State University

Blacksburg, VA 24061

October 1, 1979 - June 30, 1980

PREPARED FOR THE U. S. DEPARTMENT OF ENERGY UNDER

CONTRACT NO. DE-AC05-78ET27001

(Formerly ET-78-C-05-5648)

TABLE OF CONTENTS

Abstract and Overview

A continuing objective of this program is to characterize the crystalline basement underlying the Atlantic Coastal Plain in terms relevant to evaluating its radiogenic heat production. Three articles in this report deal with this objective. Farrar summarizes three years of work on the geologic mapping and tectonic interpretation of the easternmost North Carolina Piedmont along the Coastal Plain boundary. This study provides the geologic data base for the interpretation of regional aeromagnetic and gravity data in the exposed Piedmont, and the extrapolation of this interpretation to Piedmont rocks covered by Coastal Plain sediments. Farrar also reports the petrography of the CP14A core from Southport, N. C. G. Russell and W. Russell, in a continuing program of dating Coastal Plain basement rocks, report the Rb/Sr whole rock and mineral ages of granite from the CP25A core from Portsmouth, Va. This partially confirms the eastward younging of belts of granite in the Piedmont and under the Coastal Plain. The granite at Portsmouth has the highest heat flow measured to date.

Gleason completes depth to basement maps of the Atlantic Coastal Plain from New Jersey to Georgia with his maps covering New Jersey to Virginia, and South Carolina. Gleason also gives a drilling status report for the program.

Four reports characterize portions of Atlantic Coastal Plain sediments. McConnell summarizes the stratigraphic and structural framework of the Virginia Coastal Plain, and begins an effort to assess the structural control on distribution and geometry of Coastal Plain aquifers and zones of potentially low thermal conductivity. Svetlichny and Lambiase present a correlation of the Coastal Plain portion of the Crisfield, Md. deep test hole (DGT-1) with other deep holes in the Eastern Shore of Maryland and Virginia. They conclude that corelations are good, with minor modifications as a result of the additional data provided by DGT-1. Svetlichny gives a stratigraphic correlation of seven southeastern Virginia heat-flow-determination holes with a deep test well at Norfolk, Va. He finds that because the drill cuttings were unreliable, the gamma logs give the best correlations between holes. Lambiase reviews the stratigraphy of the Atlantic Coastal Plain south of North Carolina. He suggests that carbonate in the Tertiary section in this area will result in somewhat higher thermal conductivity than in the northern Coastal Plain. In part because of the carbonate distribution, thermal conductivity may stay relatively constant to basement in the southern Coastal Plain, making possible more accurate temperature estimates from shallow holes as compared to estimates made in the northern Coastal Plain.

McClung continues the survey of temperature profiles of existing USGS observation wells and other available Atlantic Coastal Plain wells, with temperature logs of Georgia wells. Perry presents an updated compilation of heat flow and heat generation in Coastal Plain and Piedmont holes. Coruh describes the new computer system aquired for the processing of VIBROSEIS data.

Laczniak presents an analysis of the relation between energy output and well spacing in a typical Atlantic Coastal Plain geothermal doublet system (ie. a two well system, with separate pumping and injection wells). The analysis confirms that 55°C geothermal water presents a useful energy resource in the Atlantic Coastal Plain.

RESEARCH OBJECTIVES

The objective of this research is to develop and apply targeting procedures for the evaluation of low-temperature radiogenically-derived geothermal resources in the eastern United States utilizing geological, geochemical, and geophysical data.

The optimum sites for geothermal development in the tectonically-stable Eastern United States will probably be associated with areas of relatively high heat flow derived from crustal igneous rocks containing relatively high concentrations of radiogenic heat-producing elements. The storage of commercially-exploitable geothermal heat at accessible depths (1-3 km) will also require favorable reservoir conditions in rocks overlying a radiogenic heat source. In order to systematically locate these sites, a methodology employing geological, geochemical, and geophysical prospecting techniques is being developed and applied. The distribution of radiogenic sources within the igneous rocks of various ages and magma types will be determined by a correlation between radioelement composition and the bulk chemistry of the rock. Surface sampling and measurement of the radiogenic heat-producing elements are known to be unreliable as they are preferentially removed by ground-water circulation and weathering. The correlation between the bulk chemistry of the rock (which can be measured reliably from surface samples) and radiogenic heat generation is being calibrated by detailed studies at a number of locations in the eastern United States

Initial studies are developing a methodology for the location of radiogenic heat sources buried beneath the insulating sedimentary rocks of the Atlantic Coastal Plain. Choice of a drill site in the Atlantic Coastal Plain with a high geothermal resource potential depends on favorable:

(1) concentration of radiogenic elements in granitic rocks beneath a sedimentary insulator;
(2) thermal conductivity of the sedimentary insulator;
(3) thickness of the sedimentary insulator; and
(4) reservoir conditions in the permeable sedimentary rocks overlying the radiogenic heat source.

Because it is not economically feasible to select drilling sites on the Atlantic Coastal Plain without geophysical and geological models, it is advisable to base the development of these models on a substantial and accurate data base which can be partially derived from the exposed rocks of the Piedmont and enhanced by basement studies beneath the Atlantic Coastal Plain.

PERSONNEL OF PROGRAM

October 1, 1979 - June 30, 1980

GEOLOGY AND PETROLOGY, Lynn Glover III, Principal Investigator

J. A. Speer, Research Associate
S. S. Farrar, Research Associate
S. W. Becker, Research Associate
R. L. McConnell, Research Associate
R. J. Gleason, Research Associate
G. Russell, Research Associate
W. Russell, Analytical Chemist
J. Reilly, Graduate Research Assistant
C. Newton, Graduate Research Assistant
S. Dickerson, Laboratory Technician
N. Evans, Graduate Research Assistant
C. Harris, Graduate Research Assistant
C. R. Miner, Laboratory Technician
M. W. Dellers, Secretary

GEOPHYSICS, John K. Costain, Principal Investigator

L. D. Perry, Research Associate
J. J. Lambiase, Research Associate
S. Dashevsky, Research Specialist
M. Svetlichny, Research Specialist
W. McClung, Research Specialist
S. Higgins, Research Specialist
C. Coruh, Visiting Associate Professor
M. McKinney, Laboratory Aide
B. Thoreson, Computer Programmer (part-time)
M. Hoffman, Laboratory Technician
D. Hostvedt, Laboratory Technician
K. King, Computer Programmer
R. Laczniak, Graduate Research Assistant
M. Bahorich, Graduate Research Assistant
Bielanski, E., Graduate Research Assistant
P. Dysart, Graduate Research Assistant
P. W. Glosh, Secretary

ADMINISTRATIVE ASSISTANT
Patricia Hubble

BOOKKEEPER
Mildred Memitt

DRAFTSMAN-PHOTOGRAPHER
Eric Raitch

DRILLING STAFF

W. G. Coulson, Supervisor and Core Driller
J. Childress, Core Driller
G. Childress, Core Driller Helper
R. Dalton, Core Driller Helper
R. Bowman, Core Driller Helper
R. Gravley, Core Driller Helper
A. Davison, Core Driller Helper
R. Stilwell, Core Driller Helper
P. Stone, Core Driller Helper
J. Acuff, Core Driller Helper
B. Coulson, Core Driller Helper
S. Long, Secretary

VIBROSEIS SEISMIC DATA ACQUISITION STAFF

W. Shumate, Laboratory Instrument Maker
W. Ranck, Laboratory Instrument Maker
W. Davis, Laboratory Mechanic
H. Neuburg, Research Associate
J. Sheridan, Laboratory Technician
J. McCoy, Laboratory Technician
K. Smith, Laboratory Technician
C. Chalmers, Laboratory Technician
E. Clayton, Laboratory Technician
J. Davies, Laboratory Technician
M. Dilg, Laboratory Technician
L. Field, Laboratory Technician
C. Whiting, Laboratory Technician
J. Munsey, Laboratory Technician
S. Long, Secretary

PAPERS PUBLISHED

Speer, J.A, 1978, Molybdenum mineralization in the Liberty Hill and Winnsboro plutons, South Carolina, Ec. Geol., v. 73, p. 558-561.

Glover, L. III, 1979, General geology of the East Coast with emphasis on potential geothermal energy regions: a detailed summary, Proceedings: A Symposium of geothermal energy and its direct uses in the eastern United States - Geothermal Resources Council Special Report No. 5, p. 9-11.

Costain, J.K, 1979, Geothermal exploration methods and results: Atlantic Coastal Plain. Proceedings: A Symposium of geothermal energy and its direct uses in the eastern United States - Geothermal Resources Council Special Report No. 5, p. 13-22.

Speer, J. A., S. W. Becker, and S. S. Farrar, 1980, Field relations and petrology of the postmetamorphic, coarse-grained granitoids and associated rocks of the southern Appalachian Piedmont, In Wones, D. R., ed., The Caledonides in the USA: Department of Geological Sciences, Virginia Polytechnic Institute and State University Memoir number 2, p. 137-148.

Perry, L. D., J. K. Costain and P. A. Geiser, 1979, Heat flow in western Virginia and a model for the origin of thermal springs in the folded Appalachians, Jour. of Geophysical Research, v. 84, n. B12, p. 6875-6883.

Bourland, W. C. and S. S. Farrar, 1979, Tectogenesis of the rocks surrounding the Winnsboro Intrusive Complex, South Carolina Geology, v. 24, p. 1-18.

Gleason, R. J., J. J. Lambiase, and S. S. Dashevsky, 1979, Mid-Atlantic and southeastern low-to-moderate temperature program: Geologic setting and targeting procedure, In Goethermal Energy and the Eastern U.S., Johns Hopkins University, Applied Physics Laboratory, Ch. VII, 9 p.

Costain, J. K., L. Glover, III, and A. K. Sinha, 1979, Low-temperature geothermal resource potential of the eastern United States, EOS, Transactions, American Geophysical Union.

PAPERS SUBMITTED FOR PUBLICATION

Muffler, L. J. P., J. K. Costain, D. Foley, E. A. Sammel and W. Younguist, 1979, Nature and distribution of geothermal energy, Proceedings: Klamath Falls Symposium on Geothermal Energy, in press.

Lambiase, J. J., S. S. Dashevsky, J. K. Costain, R. J. Gleason and W. S. McClung, 1979, Geothermal resource potential of the Northern Atlantic Coastal Plain, submitted to Geology.

Speer, J. A., 1979, Prograde metamorphism of the pelitic rocks in the contact aureole and xenoliths of the Liberty Hill pluton, South Carolina, submitted to Amer. Jour. of Science.

Gleason, R. J., 1980, Structure contour map of basement below North Carolina Coastal Plain and Continental Shelf, submitted to Southeastern Geology.

ABSTRACTS PUBLISHED TO DATE

Geiser, P.A. and J.K. Costain, 1977, Evaluation of the geothermal potential of the hot springs of northwestern Virginia, Abstracts of ANS Topical Meeting on Energy and Mineral Resource Recovery. Golden, Colorado, April 12-14, p. 33.

Geiser, P.A. and J.K. Costain, 1977, Structural controls of thermal springs in the Warm Springs anticline, Virginia, Abstracts, Geol. Soc. America SE Section, Winston-Salem, North Carolina.

Costain, J.K., L. Glover III, A.K. Sinha, 1977, Low-temperature geothermal resources in the eastern United States, Program with Abstracts, Annual Meeting of Geological Society of America, Seattle, Washington.

Costain, J.K. and A.K. Sinha, 1978, Relationship between heat flow and heat generation in the southeastern United States, Program with Abstracts, Geological Society of America, SE Section Meeting, April.

Costain, J.K., A new model for the linear relationship between heat flow and heat generation, Transactions, American Geophysical Union, 59:p. 392.

Becker, S.W., 1978, Petrology of the Cuffytown Creek pluton, Geol. Soc. Amer. Abstracts with Programs, v. 10.

Farrar, S.S., 1979, Tectonics of the fault bounded Raleigh block, eastern Piedmont, North Carolina, Geol. Soc. Amer., Abstracts with Programs, v. 11.

Farrar, S.S., 1979, Lithology and metamophism of Raleigh block, eastern Piedmont, North Carolina, Geol. Soc. Amer. Abstracts with Programs, v. 11, p. 177-178.

Lambiase, J. J., M. Svetlichny, S. S. Dashevsky, B. U. Conrad, and J. K. Costain, 1979, Detailed temperature logging as a useful tool for lithologic interpretation, AAPG Abstracts, p. 120.

Speer, J. A., S. W. Becker, and S. S. Farrar, 1979, Field relations and petrology of the post metamorphic, coarse-grained granites and associated rocks in the Southern Appalachian Piedmont, Abstracts, the Caledonides in the USA I.G.C.P. project, Caledonide Orogen, p. A9.

Speer, J. A., 1979, Magnetic anomalies coinciding with metamorphic isograds in the Liberty Hill aureole, South Carolina, Geol. Soc. Amer. Abstracts with Programs, 11, 522.

Gleason, R. J., J. J. Lambiase, and S. S. Dashevsky, 1979, Mid-Atlantic and southeastern low-to-moderate temperature program: Geo-

logic setting and targeting procedures - Introduction and heat source investigations, Minutes from Geothermal Energy Technical Interchange Meeting, Ch. VII, p. 1 - 9.

Lambiase, J. J. and R. J. Gleason, 1980, Atlantic Coastal Plain low-temperature geothermal program, State Coupled Geothermal Program Meeting, January.

Farrar, S. S., 1980, Use of aeromagnetic, gravity, and LANDSAT data in the reconnaissance geologic mapping of the Raleigh block, eastern Piedmont, North Carolina, Geol. Soc. Amer. Abstract with Programs, v. 12, p. 176.

TALKS GIVEN TO DATE

Geiser, P. A., 1977, Evaluation of the geothermal potential of hot springs in Northwestern Virginia, American Nuclear Society, Denver, Colorado, April.

Geiser, P. A. and J. K. Costain, 1977, Structural controls of thermal springs in the Warm Springs Anticline, Southeastern Geological Society of America, Winston-Salem, North Carolina, April. (Speaker: P. A. Geiser)

Costain, J. K., 1977, Low-temperature resources of the eastern United States, Second NATO-CCMS Meeting on Dry Hot Rock Geothermal Energy, Los Alamos Scientific Labortory, Los Alamos, New Mexico, June.

Costain, J. K., 1977, Low-temperature geothermal resources of the eastern United States, Geological Society of Washington, Washington, D.C., October.

Costain, J. K., 1977, Low-temperature geothermal resources in the eastern United States, 1977 Annual Meeting of the Geological Society of America, November.

Costain, J. K., 1977, Low-temperature geothermal resources in the eastern United States, Potomac Geophysical Society, November.

Costain, J. K., 1978, Geothermal resource potential of the eastern United States, Geothermal Resource Conci Special Short Course No. 7, "Geothermal Energy: A National Opportunity" (The Federal Impact), Washington, D.C., May.

Costain, J. K., 1978, Geothermal resource potential of the eastern United States, Nordic Symposium on Geothermal Energy, Gothenburg, Sweden, May.

Costain, J. K., 1979, Geothermal resources of the Atlantic Coastal Plain, The Energy Technology Conference and Exposition, Washington, D.C., February.

Dashevsky, S. S., 1979, Geothermal resource potential of the Atlantic Coastal Plain, Smithfield, Virginia Rotary Club, May.

Lambiase, J. J., 1979, Geothermal resource potential of the Atlantic Coastal Plain, North-South Carolina section of the American Institute of Mining Engineers, Raleigh, North Carolia, March.

Lambiase, J. J., S. S. Dashevsky, R. J. Gleason and J. K. Costain, 1979, Geothermal resource potential of the Atlantic Coastal Plain, 2nd Symposium n the Southeastern Coastal Plain, Americas, Georgia, March. (Speaker: J. J. Lambiase)

Lambiase, J. J., M. Svetlichny, S. S. Dashevsky, B. U. Sans, and J. K. Costain, 1979, Detailed temperature logging as a useful tool for lithologic interpretation, American Association of Petroleum Geologists Annual Meeting, Houston, Texas, March. (Speaker: J. J. Lambiase)

Speer, J. A., S. W. Becker and S. S. Farrar, 1979, Field relations and petrology of the post metamorphic, coarse-grained granites and associated rocks in the Southern Appalachian Piedmont, Blacksburg, VA, I.G.C.P. Caledonides in the USA, August. (Speaker: J. A. Speer).

Speer, J. A., 1979, Magnetic anomalies coinciding with metamorphic isograds in the Liberty Hill aureole, South Carolina, Geol. Soc. of America, March.

Farrar, S. S., 1979, Tectonics of the fault-bounded Raleigh block, eastern Piedmont, North Carolina, Geol. Soc. Amer., March.

Farrar, S. S., 1979, Lithology and metamorphism of Raleigh block, eastern Piedmont, North Carolina, Geol. Soc. Amer., March.

Farrar, S. S., 1980, Use of aeromagnetic, gravity, and LANDSAT data in the reconnaissance geologic mapping of the Raleigh block, eastern Piedmont, North Carolina, Geol. Soc. Amer., March.

Gleason, R. J., J. J. Lambiase, and S. S. Dashevsky, 1979, Mid-Atlantic and southeastern low-to-moderate temperature program; Geologic setting and targeting procedures - Introduction and heat source investigations, Geothermal Energy Technical Interchange Meeting, Oct. 29 - 31, Coolfont, Berkeley Springs, WV (Speaker: R. J. Gleason).

Gleason, R. J., 1980, Heat source investigations in the Piedmont and basement beneath the Atlantic Coastal Plain, DGE/DGRM Resource Assessment/Commercialization Planning Meeting, January 21-24, Salt Lake City, UT.

Lambiase, J. J., 1980, Atlantic Coastal Plain low temperature program, DGE/DGRM Resource Assessment/Commercialization PlanningMeeting, January 21-24, Salt Lake City, UT.

PROGRESS

A. OROGENIC STUDIES LABORATORY

GEOLOGY OF THE RALEIGH BLOCK AND THE ADJACENT PIEDMONT OF NORTH CAROLINA

Stewart S. Farrar

Orogenic Studies Laboratory

INTRODUCTION

The tectonic interpretation of the southern Appalachians is evolving rapidly, spurred on by the advent of geophysical data (reflection seismology, aeromagnetic and gravity surveys) (Clark and others, 1978; Cook and others 1979; Hatcher and Zietz, 1978; Long, 1979) which have been interpreted to indicate that some, if not all (Harris and Bayer, 1979) of the Appalachian Piedmont is allochthonous. The easternmost Piedmont has received less attention than the west. Studies in the South Carolina Kiokee belt (Secor and Snoke, 1978; Snoke and others, 1980) and in the eastern Virginia Piedmont (Bobyarchick and Glover, 1979; Durrant and others, 1980) have indicated a late Paleozoic, Alleghanian, metamorphic and/or deformational event which probably included the formation of at least some of the major mylonite zones which comprise the Eastern Piedmont fault system of Hatcher and others (1977). The tectonic relation of this Alleghanian activity to the approximately synchronous thrusting in the western Appalachians is not at all clear. What is clear is the need for more detail in the surface geology of the eastern North Carolina Piedmont, between the Virginia and South Carolina study areas.

Although the eastern Piedmont of North Carolina has been described in terms of metamorphic belts - the high grade Raleigh belt, and the low grade Carolina slate belt and Eastern slate belt (King, 1955; Fisher and others, 1970; Parker, 1968, 1979) - this subdivision is useful only as an approximation of metamorphic conditions in the area. The belts cannot be used as a basis for stratigraphic subdivision because major lithologic units cross from low-grade into high-grade belts.

This paper attempts to develop a foundation on which more detailed studies of this area can build. This is done by defining "tectonic blocks" bounded by major mylonite zones. Across the mylonite zones there are discontinuities of lithology, structure, and metamorphic grade. Within the blocks, a gross stratigraphy can be developed, major structures can be mapped out, and metamorphism can be discussed as an extension of the traditional belt concept.

The Raleigh block is thus a tectonic unit, comprising the Raleigh metamorphic belt and part of the Eastern slate metamorphic belt (Fig.

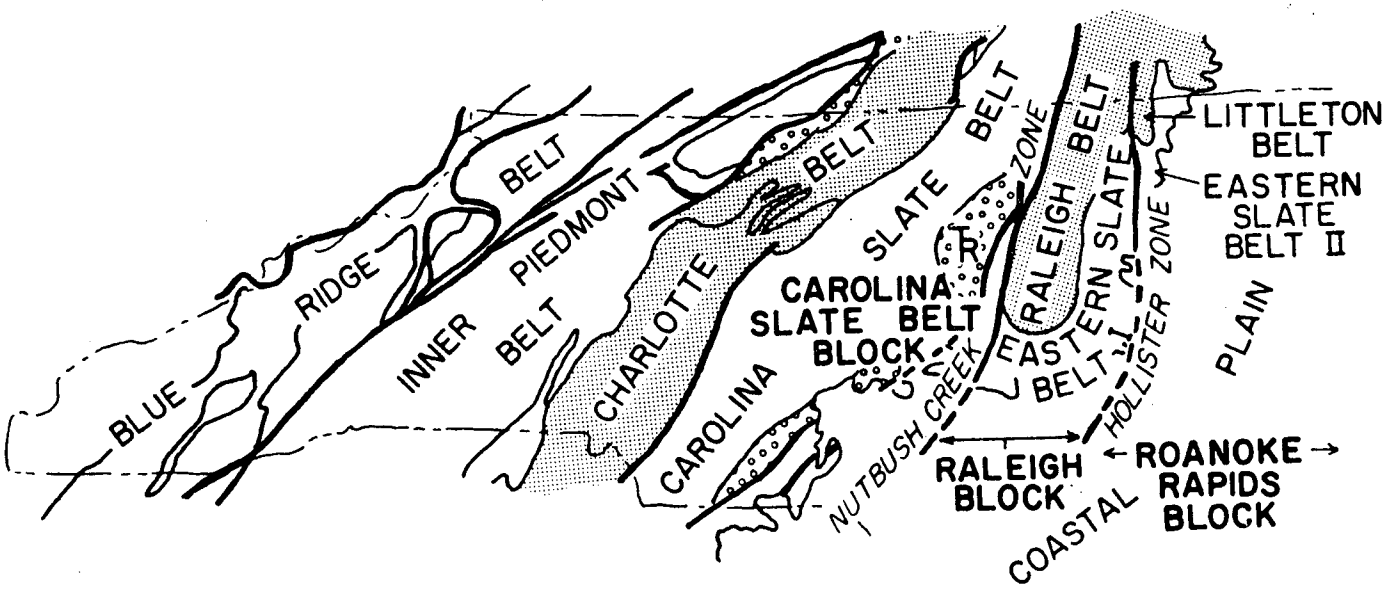

Figure 1. Generalized geology of North Carolina modified from Fisher and others (1970) to show tectonic blocks of this study.

1). The Raleigh block is bounded on the west by the Nutbush Creek mylonite zone, which separates it from the Carolina slate belt block, and on the east by the Hollister mylonite zone, which separates it from the Roanoke Rapids block. The approximate boundaries of the area studied are the Durham Triassic Basin on the west, Coastal Plain sediment cover on the south and east, and the Virginia state line on the north. This area includes the easternmost Carolina slate belt block, the Raleigh block, and the Roanoke Rapids block.

Within the study area, only syn-tectonic to post-tectonic granitiod plutons have been dated, giving ages in the range 320 to 285 Ma (Kish and Fullagar, 1978; Fullagar and Butler, 1979, A. K. Sinha, unpub. data). The metasedimentary, metavolcanic, and pre-metamorphic intrusive rocks are assumed to be late Precambrian to early Paleozoic in age, as are those of the Carolina slate belt to the west (Glover and Sinha, 1973; St. Jean, 1973; Black, 1978; Wright and Seiders, 1980).

Published studies of this area include: structural reconnaissance of the entire area (Parker, 1968); Wake County in the southwest (Parker, 1979); the northwest (Parker, 1963); the northeast (Mundorff, 1946); and the south and west (Wilson and Carpenter, 1975).

STRATIGRAPHY

Lithostratigraphic units in this area have been described only in the Raleigh area (Parker, 1979) and in the northwest (Parker, 1963). An attempt is made here to develop broad lithostratigraphic units for the entire study area. These formations (Fig. 2) have been defined with the assistance of aeromagnetic, gravity, and LANDSAT data in addition to structural interpretation. Outcrop control is very sparse in much of the area, particularly so in the south and east. The stratigraphy is described separately for each tectonic block (Fig. 3). Correlation between blocks is possible only in the sense that they contain similar rock types of probably the same general age.

Carolina Slate Belt Block

Only that part of the Carolina slate belt block east of the Durham Triassic basin is described in this study. This block lies to the west of the Nutbush Creek mylonite zone. This mylonite forms a sharp boundary where it dips steeply in the north and south, but in the Raleigh area it is a diffuse zone dipping moderately westward (see Structure). The stratigraphic sequence given here is subject to modification because, without top-bottom criteria, pre-tectonic relations between formations are not known. In present attitude the Cary Formation underlies the Fuquay-Varina Complex. The Beaverdam Complex intrudes the Cary Formation, and the Vance County Trondjemite intrudes rocks exposed to the west of the study area.

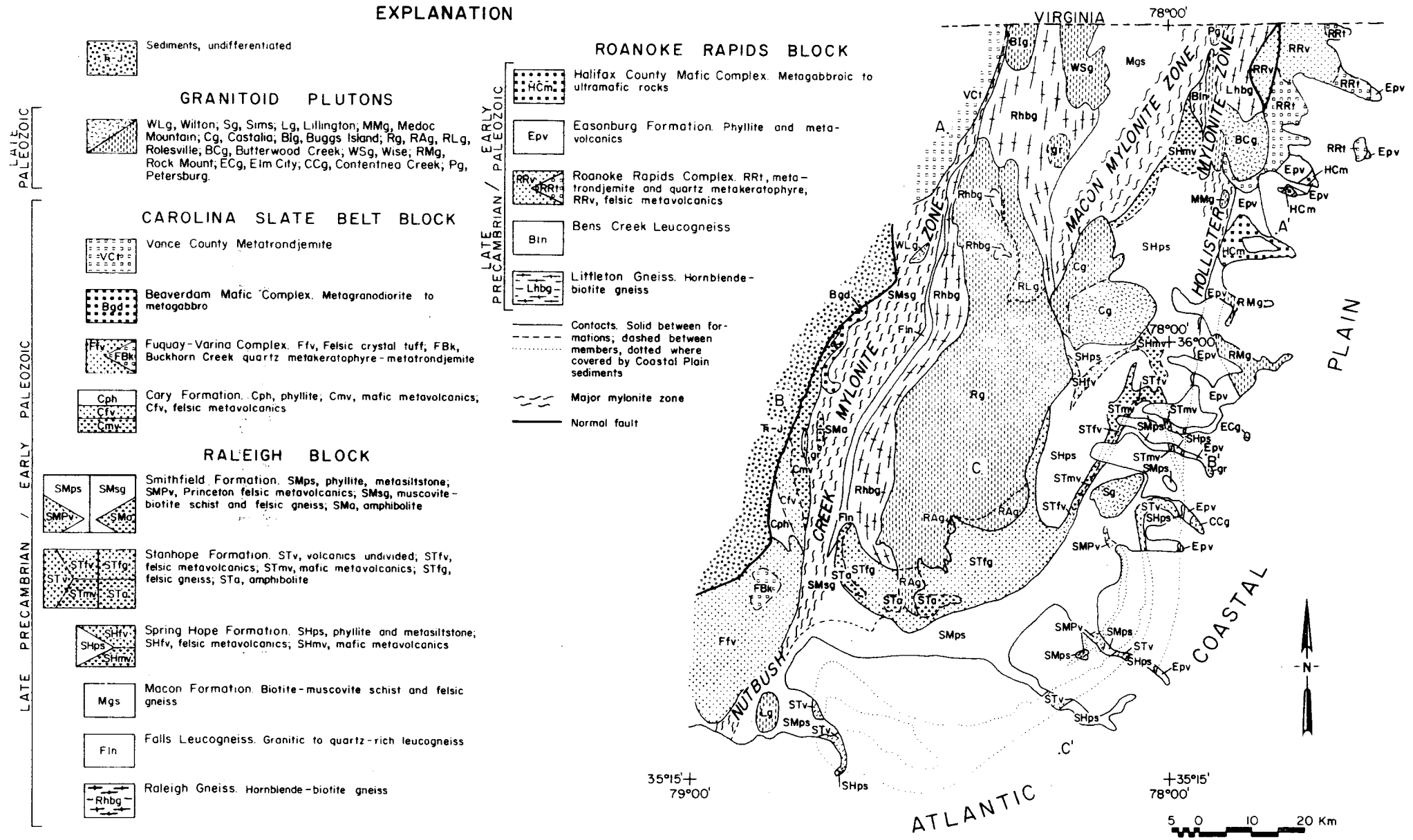

Figure 2. Geologic map of the northeastern Piedmont of North Carolina, showing formations as defined herein.

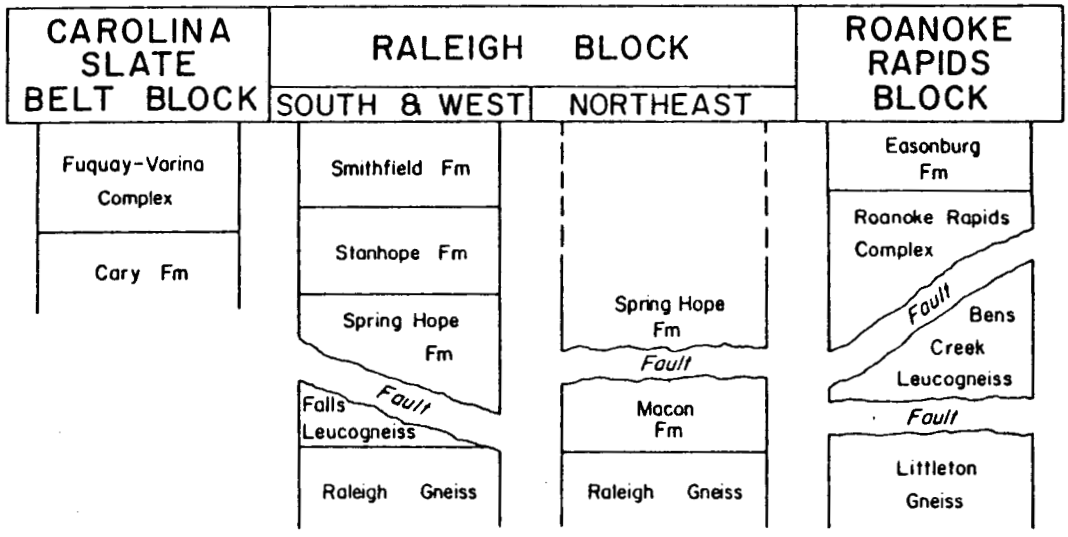

Figure 3. Stratigraphic sections of the Raleigh block and adjacent areas of the northeastern Piedmont of North Carolina.

Cary Formation

From bottom to top, as presently exposed, the Cary Formation comprises three members. Quartz-chlorite-epidote greenstone (Cmv) is overlain by felsic metatuff (Cfv) and quartz-albite crystal metatuff with the assemblage opaque + epidote + chlorite + muscovite + quartz + albite. This, in turn, is overlain by opaque-epidote-chlorite-quartz-muscovite phyllite (Cph). Most of this formation is below or at biotite grade, greenschist facies metamorphism (Parker, 1979). Parker (1979) included these rocks, and the western part of the Fuquay-Varina Complex in his Cary sequence. Because of the spatial relation of hypabyssal quartz keratophyre intrusions centered in a large mass of felsic volcanic rocks in the Fuquay-Varina area, these rocks are described separately as the Fuquay-Varina Complex. Fortson (1958) also described some of the lithologic units included in the Cary Formation.

Fuquay-Varina Complex

The greenschist grade Fuquay-Varina Complex comprises the Buckhorn Creek hypabyssal trondjemite-quartz keratophyre pluton (FBk, Fig. 2), the smaller Sunset Lake quartz keratophyre pluton or dike (not shown on map); and extensive felsic plagioclase-crystal tuff (Ffv). The Buckhorn Creek pluton comprises fine-grained, light gray-to-tan trondjemite-quartz keratophyre with albite and subordinate quartz phenocrysts in a granophyric groundmass of quartz + albite + minor to moderate amounts of K-feldspar. Accessory minerals include muscovite, biotite, titanite, garnet, epidote, allanite, and opaques. An apparently subordinate facies of the pluton has the same mineralogy but has a non-granophyric groundmass. The Buckhorn Creek pluton is well exposed along Buckhorn Creek, 6 km west of Fuquay-Varina. The smaller Sunset Lake intrusion crops out 7 km north of Fuquay-Varina at the spillway of Sunset Lake. This hypabyssal intrusion comprises granophyric quartz keratophyre with quartz and albite phenocrysts, and porphyritic quartz keratophyre with quartz and albite phenocrysts in a non-granophyric, fine-grained groundmass of quartz + albite + minor K-feldspar. Both facies have accessory biotite, muscovite, epidote, titanite, and opaques. The Buckhorn Creek and Sunset Lake intrusions have been previously described as granites (Parker, 1979).

These hypabyssal intrusions occur in the center of an approximately 7 km thick pile of felsic crystal tuff, with albite and some quartz phenocrysts in a groundmass of albite + quartz; minor K-feldspar, with accessory muscovite, biotite, calcite, epidote, garnet, titanite, and opaques. Interlayered with the crystal tuff at 0.5 to 2 m thick beds of muscovite schist and biotite schist. The occurrence of the hypabyssal intrusions, with porphyritic and granophyric textures, cutting a thick pile of crystal tuff of similar composition suggests that the plutons may have cut their own extrusive piles in forming the Fuquay-Varina Complex.

Rocks of the Fuquay-Varina Complex are cut by three foliations, among which relations are difficult to establish. The S_3 foliation, a muscovite-biotite foliation, is particularly strong in the schistose

layers, and weak in the felsic layers. In general, S_3 increases in strength eastward into the Nutbush Creek mylonite zone. Metamorphic grade in the Fuquay-Varina complex increases from apparently below biotite grade in the west to biotite-almandine grade in the east.

Beaverdam Mafic Complex

The Beaverdam Mafic Complex (Bgd, Fig. 2) is an intermediate to mafic intrusive complex metamorphosed to greenschist facies, as described by Parker (1979). It crops out in the general area of the intersection of NC Route 50 and NC Route 98, 15 km east of Durham. According to Parker (1979), the northeastern part of the complex is mostly gabbro, originally comprising pyroxene and calcic plagioclase as its major minerals, now altered to hornblende (some actinolite), oligoclase and clinozoisite. It also includes zones of pyroxenite altered to hornblendite. The southwestern portion of the complex is more felsic, ranging from quartz diorite to granodiorite with plentiful enclaves - including autoliths of the gabbroic facies. The quartz diorite and granodiorite now have the metamorphic assemblage chlorite + epidote + opaque + muscovite + minor microcline + quartz + albite (± hornblende). This is a premetamorphic complex of probable slate belt age, but it has not been isotopically dated.

Vance County Trondjemite

The Vance County Trondjemitic pluton (VCt, Fig. 2) (Vance County granitic pluton of Foose and others, 1980, and Casadevall and Rye, 1980; albite granodiorite of Parker, 1963) is a greenschist to lowermost amphibolite grade, sodic plagioclase-rich intrusion. Seriate plagioclase is generally albite, but includes oligoclase along the eastern border, which may be at lower amphibolite grade adjacent to the Nutbush Creek mylonite zone. The remainder of the assemblage is chlorite + biotite + minor K-feldspar + quartz. The easternmost border of the pluton is mylonitized in the Nutbush Creek mylonite zone. Tungsten mineralization is important along the western contact of the pluton (outside the map area) (Foose and others, 1980; Casadevall and Rye, 1980). Only the eastern contact of the Vance County pluton was examined in this study.

Raleigh Block

The Raleigh block, comprising the central, major portion of the mapped area, ranges in metamorphic grade from middle greenschist facies in the south and east to middle amphibolite facies in the north. A stratigraphic sequence can be defined with some confidence in the low-grade portion of the block, and with increasingly less confidence in higher grade areas. Different map units have been defined within formations for the higher grade rocks, even where they can be traced with some confidence from low-grade areas. This distinction is made in order to emphasize the interpretative step in correlating texturally distinct metasedmentary and metavolcanic rocks of the Eastern slate belt with higher grade rocks which lack protolith textures.

Raleigh Gneiss

This formation was described by Parker (1979) as Injected Gneisses and Schists. The Raleigh Gneiss, as defined here, comprises biotite gneiss, biotite-hornblende gneiss, amphibolite, and minor muscovite-biotite schist and muscovite-quartz-feldspar pegmatite. The major portion of the formation consists of interlayered leucocratic biotite gneiss (C.I. = 2-5) and more mafic biotite-hornblende-bearing gneiss (C.I. = 10-15). The mineral assemblage is quartz, plagioclase ($An_{23}Ab_{76}Or_1$), perthitic microcline, biotite (Fe/(Fe+Mg) = 0.57), hornblende (Fe/(Fe+Mg) = 0.64) and accessory opaques, zircon, titanite, apatite, allanite, and garnet. Retrograde minerals include chlorite, muscovite, epidote, and hematite.

Numerous thin amphibolite layers occur within the Raleigh Gneiss. Their mineral assemblage is plagioclase, hornblende, biotite, and accessory quartz, epidote, titanite, opaques, and hematite. Small pegmatite bodies, comprising quartz-K feldspar-plagioclase-muscovite within the Raleigh Gneiss are concentrated in the eastern half of the formation, near the Rolesville granite.

Thin biotite-muscovite schist and biotite schist layers occur within the Raleigh Gneiss. In the northern Raleigh belt, west of the Wise pluton, the assemblages sillimanite + staurolite + garnet + muscovite, and sillimanite + biotite + garnet + muscovite occur in these schist layers. No aluminosilicates have been found in the southern half of the Raleigh Gneiss.

Falls Leucogneiss

Parker (1979) includes this gneiss as the easternmost rock type in his "Felsic Gneisses and Schists." The Falls granitic leucogneiss, as defined here, is a fine-grained, light tan to white, magnetite-plagioclase-quartz-microcline gneiss (C.I. = 1-3) with accessory garnet, biotite, titanite, allanite, apatite, chlorite, muscovite, epidote, and zircon. The Falls leucogneiss is 1.0-1.5 km thick and is continuous along strike for at least 40 km (Fig. 2). Very weak layering - concentrations of quartz with biotite, garnet, and epidote - shows tight to isoclinal minor folds. The axes of these folds and the parallel concentration of the mafic minerals form a very strong lineation which is characteristic of this unit; in some areas it is a pencil gneiss. Several saprolite outcrops of hornblende-plagioclase amphibolite within the leucogneiss suggest that the formation may be as much as 10 to 15 percent amphibolite.

Plagioclase in the leucogneiss is albite ($An_6Ab_{93}Or_1$) and the microcline is microperthitic with a bulk composition of about $An_0Ab_8Or_{92}$. Biotite is of an intermediate composition with Fe/(Fe + Mg) = 0.56.

Macon Formation

The Macon Formation, defined here, comprises muscovite-biotite-quartz-plagioclase gneiss, quartz-muscovite schist, aluminous schist, phyllonite, and biotite-quartz-K feldspar-albite leucogneiss. The Macon Formation is characterized by textures of dynamic to mylonitic deformation. Mineral assemblages indicate various metamorphic grades, from relict sillimanite grade assemblages in lesser deformed rocks to chlorite grade in phyllonite.

The dominant rock type of the Macon Formation is muscovite-quartz-biotite-K feldspar-plagioclase gneiss with accessory epidote, chlorite, opaques, apatite, and titanite. The gneiss has abundant plagioclase augen and scattered microcline augen. Plagioclase augen compositions vary from $An_{21}Ab_{78}Or_1$ to $An_{28}Ab_{71}Or_1$. The texture of this gneiss is suggestive of dynamic metamorphism approaching mylonitic conditions. The typical outcrop is interlayered plagioclase-microcline augen gneiss and protomylonite. Both apparently have lower amphibolite grade assemblages with stable biotite and oligoclase - even in the protomylonite. In the central and eastern part of the formation, mylonitic textures at lower grade are superimposed on the amphibolite grade assemblages. Extent of deformation varies from protomylonite to phyllonite. The mylonite has classic fluxion structure around plagioclase porphyroclasts. The biotite in the groundmass at higher metamorphic grade has been replaced by chlorite and muscovite in the mylonites. The K-feldspar and plagioclase prophyroclasts are progressively replaced by muscovite, albite, and quartz. The final stage of this process is phyllonite with the assemblage muscovite + chlorite + quartz + opaques $\pm$ tourmaline. The phyllonite has the mineral assemblage of phyllite, but texturally shows isoclinally folded and refolded microfolds in a fine mylonitic layering, and scattered feldspar porphroclasts.

Relatively minor pelitic to aluminous schists record the retrogressive metamorphism accompanying mylonitization. In two outcrops near the western border of the Macon Formation, the schist has the greenschist grade assemblage chloritoid + muscovite + quartz + hematite + chlorite, with relict sillimanite in the chloritoid and muscovite. One of these outcrops also has relict garnet with chlorite and hematite rims. The chloritoid and some muscovite have grown across the prexisting foliation in which the sillimanite lies. Muscovite schist along the eastern border of the formation has the assemblage muscovite + quartz + chlorite + opaque and contains relict staurolite and garnet. Kyanite has also been reported along this eastern boundary (Stoddard and McDaniel, 1979). Eastward from the Macon Formation metamorphic grade drops to greenschist facies in the Spring Hope Formation of the eastern Carolina slate belt.

The Geologic Map of North Carolina (N. C. Dept. of Conservation and Development, 1958) shows part of the area of the Macon Formation as felsic metavolcanic rocks. This study indicates that these rocks are mylonites and ultramylonites of plagioclase-rich gneisses, lacking the protolith textures necessary to determine whether or not they are vol-

canic in origin. Structural position suggests that the Macon Formation may be, at least in part, equivalent to the Stanhope Formation.

Spring Hope Formation

The Spring Hope Formation, defined here, comprises interlayered phyllite, metamudstone-metasiltstone, and felsic and mafic metavolcanic rocks.

Phyllite (SHps) is the most plentiful component, comprising about 60 percent of the formation. The mineral assemblage is quartz + muscovite ± chlorite ± albite ± opaques. Compositional layering shows as banding on the strong muscovite foliation. This foliation is commonly crenulated by at least two later foliations. In some areas of lesser developed foliation, graded bedding is preserved in tightly folded metasiltstone-metamudstone layers.

Metavolcanic rocks comprise the remaining 40 percent of the formation. Felsic metavolcanic rocks (SHfv), including plagioclase crystal metatuff, quartz-plagioclase crystal-lithic metatuff, and quartz keratophyre metaporphyry, comprise about 25 to 30 percent. The quartz keratophyre metaporphyry is exposed in a roadcut where a county road crosses the Seaboard Coast Railroad 2.5 km west of Spring Hope. Felsic metatuff is well exposed immediately south of the Castalia pluton. Greenstone-metabasalt (SHmv) comprises 10 to 15 percent of the Spring Hope Formation. Greenstone layers, some with quartz amygdules, crop out at the spillway of Boddies Mill Pond about 2 km southeast of the Castalia pluton. Four kilometers east of Spring Hope a temporary gravel pit for route I-95 construction exposed interlayered felsic and mafic metavolcanic rocks. One layer is scoriaceous, with a fine-grained groundmass of albite + epidote + quartz + opaque, and amygdules of quartz and epidote. Only major areas of felsic and mafic metavolcanic rocks are mapped separately; other outcrops of metavolcanic rocks occur within areas mapped as dominantly phyllite.

Stanhope Formation

The Stanhope Formation is best defined in the greenschist grade Eastern slate belt, where it consists of massive greenstone-metabasalt (STmv, Fig. 2) overlain by felsic crystal and lapilli tuff (STfv), with thin interbedded phyllitic layers in the felsic tuff. As metamorphic grade increases into the Raleigh belt, the greenstone is recrystallized to amphibolite (STa) and the felsic metavolcanic rocks to quartz-plagioclase gneiss (STfg). The Stanhope Formation is generaly 1.5-2.0 km thick and is continuous along strike for more than 200 km around the Smithfield synform (see Fig. 2, and STRUCTURE). The ratio of felsic to mafic metavolcanic rocks is variable, but the formation appears to average about 40 percent mafic, 40 percent felsic, with 20 percent phyllite-metamudstone interlayered with the felsic rocks.

The best exposed section through the Stanhope Formation is along minor tributaries of the Tar River, along both sides of NC Route 581, about 2 km north of the community of Stanhope. Massive greenstone-metabasalt at the base of the formation comprises epidote + quartz ± chlorite ± actinolite ± albite ± calcite ± opaques. Most igneous textures and mineralogy have been lost to recrystallization, but quartz amygdules are preserved in some outcrops. Felsic metavolcanic rock overlying the greenstone comprises albite crystal and crystal-lithic metatuff with at least one lapilli stone layer 2-3 m thick. These felsic tuffs have 1-2 m thick interlayers of chlorite-muscovite phyllite.

Under upper greenschist and lower amphibolite grade conditions, rocks of the Stanhope formation lose most of their distinctive volcanic textures. The felsic tuff and plagioclase-quartz crystal tuff are recrystallized to a fine-grained, plagioclase-rich gneiss (STfg). In some lesser deformed areas, the relict plagioclase phenocrysts are plentiful. The mineral assemblage comprises plagioclase (albite or oligoclase) + quartz + minor K-feldspar + muscovite + epidote + opaque ± garnet ± calcite ± titanite ± biotite. Within the felsic gneiss are muscovite schist layers which are the recrystallized equivalent of phyllite layers occurring in the felsic metavolcanic rocks at lower grade. There are good exposures of the felsic gneiss member along Swift Creek 10 to 15 km northwest of Smithfield. The mafic metavolcanic rocks which occur as greenstones in the Stanhope Formation have been recrystallized to opaque oxide-quartz-plagioclase-hornblende amphibolite (STa). Intermediate grade samples of quartz-chlorite-albite-epidote-amphibole amphibolite occur in the southeastern part of the amphibolite member. The amphibolite member is well exposed along Middle Creek, 6 to 8 km east of Willow Springs.

Smithfield Formation

Metasiltstone-metamudstone and phyllite (SMps), and subordinant felsic metavolcanic rocks (SMPv) comprise the Smithfield Formation, as defined here, which is exposed in the trough of the Smithfield synform (see Fig. 2, and STRUCTURE). This is interpreted to be the uppermost exposed portion of the Eastern slate belt. Outcrop width of the formation is as much as 25 km, and formation thickness is estimated at 8 to 10 km. As the Raleigh belt is approached, recrystallization within the Smithfield rocks increases, forming an interlayered sequence of schist and gneiss (SMsg).

Metasiltstone, metamudstone, and phyllite comprise the metasedimentary portion of this formation in the Eastern slate belt. The metamudstone-metasiltstone is generally green-gray, with the assemblage quartz + muscovite + chlorite + albite + epidote + opaques ± titanite. Graded bedding is common on the scale of a few millimeters, with quartz + albite-rich layers grading into muscovite + chlorite-rich layers. Rare quartz-rich layers have magnetite + zircon heavy mineral concentrations. Bedding is cut by at least two, and in some cases three, foliations. S_1 is a strong planar orientation of muscovite and chlorite which cuts bedding. S_2 and S_3 are crenulation foliations.

Phyllite is very rich in muscovite, with the assemblage muscovite + quartz + chlorite ± albite ± tourmaline ± hematite ± opaques. S_1 and S_2 foliations are particularly strong in the phyllite. Bedding is commonly isoclinally folded, and is visible as color or mineralogical banding on foliation surfaces, producing a strong lineation. These metasedimentary rocks of the Smithfield Formation are exposed in several stream valleys northwest of Smithfield, and in the spillway of Holts Pond, 3 km southwest of Smithfield.

Felsic metavolcanic rocks of the Smithfield Formation occur in one unit, which is exposed in the spillway of another Holts Pond 2 km west of Princeton, NC, and at the two Nello Teer quarries northeast of Princeton. This felsic metavolcanic sequence, here named the Princeton member, is dominated by plagioclase and plagioclase-quartz crystal metatuffs. Within the sequence are several felsic flows with flow layering defined by alternating albite-, muscovite-, and epidote-rich layers. These flows are amygdaloidal, with quartz-filled vesicles up to 2 to 3 cm in diameter in some layers. The amygdules are flattened in the plane of combined $S_1 + S_2$.

The Smithfield Formation has a characteristic aeromagnetic anomaly pattern (see Geophysics). The metasediments cause a flat low anomaly which is interrupted by a high amplitude, short wavelength high corresponding to the Princeton felsic metavolcanic member along the southeastern limb of the synform. A mirror image of this short wavelength aeromagnetic high occurs along the northwestern limb of the synform. Although outcrops have not been found, it is assumed that the felsic metavolcanic member also occurs along this anomaly.

The felsic metavolcanic rocks are minor in volume in this formation, but crop out quite well because of their high resistance to erosion. Near Princeton these rocks form a topographic ridge which protrudes through Coastal Plain cover and is visible on LANDSAT images.

Gneisses and schists of the high grade portion of the Smithfield Formation (SMsg) comprise: (1) muscovite-biotite-quartz-albite gneiss (felsic metavolcanic rock); (2) quartz-muscovite schist and muscovite quartzite; (3) muscovite-biotite schist; (4) muscovite graphite schist; (5) amphibolite. This map unit comprises parts of two map units of Parker (1979) - Mica Gneisses and Schists with Interlayered Hornblende Gneiss, and part of Felsic Gneisses and Schists.

Muscovite-biotite-quartz-albite gneiss with accessory tourmaline, microcline, opaques, apatite, chlorite, titanite, and calcite comprises most of the western third of the map unit. This gneiss is very fine-grained, with a strong foliation of the micas which cuts across isoclinal folds of the compositional layering. Some relict plagioclase phenocrysts remain in the deformed and recrystallized groundmass as evidence of the volcanic origin of this rock type.

An amphibolite body lies within the quartz-albite-muscovite-biotite gneiss. The least deformed portions of this amphibolite consist of hornblende and plagioclase with fine-grained opaque inclusions concen-

trated in the hornblende. The opaque inclusions, which were probably exsolved from igneous clinopyroxene, show a relict ophitic texture indicating that this was a gabbroic intrusion, and not a basalt flow equivalent to those in the Stanhope Formation to the southeast.

East of the felsic gneiss (metavolcanic) unit is a zone of interlayered and complexly folded felsic gneiss, muscovite quartzite, muscovite-biotite schist, and muscovite-graphite schist. Some felsic layers in this unit have relict plagioclase phenocrysts - these layers appear to be felsic crystal metatuffs. The muscovite quartzite and schists are amphibolite grade equivalents of the metamudstone and metasiltstone of the Smithfield Formation. Variable metamorphic grade in this area results in a great variety of pelitic mineral assemblages, ranging from retrograde greenschist assemblages in some of the Nutbush Creek mylonite rocks to kyanite-staurolite grade adjacent to the Falls leucogneiss on the east. These assemblages are discussed under Metamorphism.

Roanoke Rapids Block

The Roanoke Rapids block, comprising the eastern edge of the exposed Piedmont, ranges in metamorphic grade from middle greenschist facies to middle amphibolite facies. Because of the lack of outcrop, due to Coastal Plain overlap, the stratigraphic sequence cannot be defined with any confidence. The formations to the north, the Bens Creek Leucogneiss, Littleton Gneiss and the Roanoke Rapids Complex, are the best exposed; the other formations are based on very sparse outcrops.

Littleton Gneiss

The Littleton gneiss (Lhbg), as defined here, is essentially identical to the Raleigh gneiss. It comprises biotite gneiss, hornblende-biotite gneiss, and minor amphibolite and muscovite-biotite schist. As in the Raleigh gneiss, the more leucocratic (C.I. = 3-5) biotite gneiss predominates over the more mafic hornblende-biotite gneiss (C.I. = 10-15). The typical mineral assemblage of the hornblende-biotite gneiss is hornblende + biotite + oligoclase + quartz + microcline, with accessory opaques, zircon, titanite, allanite, and apatite; and secondary epidote, muscovite, and chlorite. This gneiss is best exposed along Deep Creek, 2.5 km southwest of Summit in the Thelma quadrangle.

Bens Creek Leucogneiss

The Bens Creek leucogneiss (Bln), as defined here, is a fine-grained, light tan to white, albite-quartz-microcline gneiss (C.I. = 1-3). Biotite, magnetite, garnet, titanite, apatite, chlorite, epidote, calcite and zircon are accessories. The gneiss is quartz-rich, and some workers have described it as a quartzite. The highest quartz content observed in this study is about 40 percent. The fine grain size and isoclinal folding with near horizontal fold axes in this area suggest that this unit has been mylonitized - not surprising, since it

is sandwiched between the Macon and Hollister mylonite zones. This unit occurs on the border of the Littleton gneiss (separated for the most part by the Butterwood Creek granite) in a position equivalent to that of the Falls leucogneiss which is adjacent to the Raleigh gneiss. Mineral assemblages occurring in the adjacent Macon and Littleton formations suggest that the Bens Creek leucogneiss has been subjected to amphibolite grade metamorphism. The leucogneiss is well exposed within 1 km northwest of Littleton along the east side of Little Stone House Creek.

Roanoke Rapids Complex

The Roanoke Rapids complex, as defined here, comprises greenschist grade hypabyssal intrusive (RRt) and extrusive (RRv) felsic to intermediate rocks. The hypabyssal intrusion, which may also have been the center of volcanism, is immediately south of Roanoke Rapids. It is irregular in shape and approximately 20 km in diameter. It is surrounded by felsic metavolcanic rocks, with interlayered metasediments of probable volcanic origin.

The hypabyssal intrusion ranges from trondjemitic to quartz dioritic in composition. The mineral assemblage comprises albite + amphibole + biotite + quartz + Kfeldspar + epidote + chlorite + muscovite + titanite + opaque. The intrusion is cut by quartz keratophyre dikes which have quartz and albite phenocrysts in a granophyric quartz-K feldspar-albite groundmass. The intrusive rocks are characterized by the high content of sodic feldspar, relative lack of K-feldspar, and by greenschist mineral assemblages.

Extrusive rocks of the Roanoke Rapids Complex comprise plentiful plagioclase crystal and crystal-lithic metatuff, and relatively rare felsic flows. A probable flow of quartz keratophyre is exposed 2 km northwest of Thelma, N. C. This body consists of albite phenocrysts connected by thin films of quartz-albite-Kfeldspar granophyre to form layers. The layers are separated by lenticles of quartz. This rock is interpreted to have been a flow or lava dome of crystal mush which crystallized rapidly to produce the granophyric texture and lock in vapor. Quartz fills the large flattened vesicles. A weak foliation parallel to this flattening suggests that there was tectonic as well as the expected gravitational flattening of the vesicles.

Metamorphosed pyroclastic rocks, and metasediments derived from them, are common in the area surrounding the Roanoke Rapids intrusion. Crystal and crystal-lithic metatuff interlayered with phyllite and metagraywacke occur along the raceway below the Roanoke Rapids dam and along both the north and south shores of Roanoke Rapids Lake. The crystal metatuff has albite and quartz phenocrysts in a groundmass of albite + quartz + microcline + muscovite $\pm$ calcite $\pm$ epidote $\pm$ biotite $\pm$ chlorite $\pm$ titanite $\pm$ garnet $\pm$ opaques. The crystal-lithic metatuff and crystal-lithic lapilli metatuff have albite and quartz phenocrysts and lapilli as large as 10 cm in diameter in a groundmass of albite + quartz + epidote + chlorite $\pm$ calcite $\pm$ opaques. The lapilli have sharp contacts with the groundmass and are commonly rounded; smaller

fragments are commonly angular. Flattening in the plane of S_1 or S_2 foliation is common. Lapilli include: very fine-grained, felty, albite-quartz groundmass with albite phenocrysts; fine-grained, equigranular quartz-albite groundmass with quartz and albite phenocrysts; and fragments of intrusive rocks of the complex. No nonvolcanic lithic fragments have been found.

Metasedimentary rocks of the complex include muscovite-quartz-chlorite phyllite and a volanogenic metagraywacke with the assemblage quartz + albite + calcite + epidote + chlorite + opaques. The metagraywacke is particularly well exposed along NC Route 48 on the south side of the Roanoke River at Roanoke Rapids. The phyllite is exposed along Deep Creek, 1 km south of Roanoke Rapids Lake.

The complex has also been intruded by dikes which vary from quartz keratophyre to diabase in composition. Some of the mafic dikes, metamorphosed to greenstone, are exposed in the raceway of the Roanoke Rapids dam.

Easonburg Formation

The Easonburg Formation (Epv), as defined here, includes interlayered felsic volcanic and phyllitic rocks exposed south of the Roanoke Rapids complex and to the east of the Hollister mylonite zone. These rocks are exposed only sporadically in the deeper stream valleys which cut the overlying Coastal Plain sediments. The best exposures are felsic plagioclase crystal metatuff along the Tar River 2 km south of Easonburg; and chlorite-muscovite phyllite along Swift Creek 2 km south of Hilliardston in the Red Oak quadrangle. This formation may be equivalent to the Spring Hope Formation to the west, but it cannot be correlated with confidence across the Hollister mylonite zone.

Halifax County Mafic Complex

The Halifax County mafic and ultramafic rocks have been described briefly by Stoddard and Teseneer (1978). They comprise metamorphosed gabbroic and ultramafic rocks, now comprising chlorite, amphibole, serpentine, with some relict clinopyroxene, olivine and saussuritized plagioclase. Rocks of this formation are very poorly exposed.

Granitoids

The northeastern Piedmont of North Carolina has been intruded by numerous syn- and post-tectonic granitoid plutons. Granitoids occurring in amphibolite grade country rock have a generally syntectonic appearance, with a moderate to weak biotite foliation (S_3, and in some cases S_2) parallel to country rock foliation. Feldspars and quartz in these granitoids show minor to moderate recrystallization. Granitoids occurring in greenschist grade country rock more commonly are post-tectonic in appearance. Foliation is weak to absent. The foliation which does occur is commonly an igneous flow foliation, and is generally parallel to the contacts of the pluton.

Rolesville Granite Batholith

The Rolesville granite was named by Stuckey (1965) for a small community near a large quarry in the granite. It was described as a batholith by Parker (1968). The Rolesville batholith comprises three texturally-defined granite facies, and a border facies which contains a large component of country rock gneiss. Modal composition averages for 19 samples of Rolesville granite point-counted on slabs and thin sections are: plagioclase 37%; K-feldspar 33%; quartz 25%; and C.I. 5% (Becker and Farrar, 1977).

The Rolesville main facies (Rg) consists of medium- to coarse-grained biotite granite, with weak compositional layering cut by a later weak to moderate biotite foliation. K-feldspar is microperthitic microcline with an average composition of $An_0Ab_8Or_{92}$. Plagioclase generally has weak oscillatory zoning in the range $An_{18}Ab_{81}Or_1$ to $An_{24}Ab_{75}Or_1$. Thin albite rims are common. Biotite has Fe/(Fe+Mg) = 0.58. Accessory minerals include allanite, opaques, zircon, apatite, and titanite. There is commonly some alteration of biotite to chlorite, and plagioclase is slightly to moderately saussuritized. Secondary minerals include chlorite, epidote, muscovite, calcite, and hematite.

The Archers Lodge porphyritic facies (RAg) which constitutes much of the southern margin of the batholith contains microcline macroperthite phenocrysts 1-4 cm in length. Quartz, biotite, plagioclase, and microcline microperthite averaging 4-5 mm in length comprise the groundmass. Accessory and secondary minerals are the same as in the Rolesville main phase.

The Louisburg facies (RLg) occurs along the northern border of the Rolesville batholith. It is a foliated, fine- to medium-grained biotite granite, with quartz and feldspar averaging 1 to 2 mm in length. Microcline in the Louisburg facies is microperthitic with an average composition of $An_0Ab_6Or_{92}$. Plagioclase is normally zoned with $An_{22}Ab_{77}Or_1$ to $An_{19}Ab_{80}Or_1$, and albite rims. Accessories present are zircon, apatite, allanite, and opaques; hematite, chlorite, epidote, and muscovite occur as secondary minerals. Saussuritization of plagioclase is minor.

All facies of the Rolesville batholith have been cut by aplite and pegmatite dikes a few centimeters to tens of centimeters thick. The main facies of the Rolesville is cut by large dikes of biotite leucogranite which are apparently from a late stage of the granite melt. The leucogranite has microcline microperthite ($An_0Ab_7Or_{93}$), and plagioclase ($An_{14}Ab_{85}Or_1$). The minor biotite is almost completely altered to chlorite. Saussuritization of the plagioclase is relatively strong.

Castalia Granite

The Castalia pluton (Cg), mapped by Julian (1972), is a medium- to coarse-grained biotite granite. The central and eastern part of the pluton is essentially unfoliated. The northwestern part has a weak foliation parallel to regional country rock foliation, and closely

resembles the Rolesville main facies. The average grain size is approximately 5 mm. The K-feldspar is microcline microperthite. Plagioclase is weakly to moderately zoned $An_{29}Ab_{70}Or_1$ to $An_{18}Ab_{81}Or_1$. The plagioclase is moderately saussuritized. Secondary minerals are chlorite, epidote, calcite, muscovite, and garnet. Accessory minerals are titanite, zircon, allanite, apatite, and opaques. The unfoliated portion of the pluton is notable for its uniformity of texture and composition. The Rb/Sr age of the Castalia is 313 $\pm$ 13 Ma (Fullagar and Butler, 1979).

Butterwood Creek Granite

The granite pluton described below is herein named the Butterwood Creek Granite (BCg), for Butterwood Creek which flows through the area of granite exposures south of Littleton, North Carolina (Figure 2). This area appears as granite, metavolcanic rocks and mica gneisses on the Geologic Map of North Carolina (N. C. Dept. of Conservation and Development, 1958).

The Butterwood Creek pluton has three facies. Most of the pluton consists of coarse-grained, amphibole-biotite granite with K-feldspar megacrysts. A more mafic, early facies occurs as autoliths and as a border facies of the pluton, but not in bodies large enough to be mapped separately. A third facies is a fine- to medium-grained muscovite-biotite leucogranite which occurs along the southwestern border of the pluton.

The eastern two-thirds of the Butterwood Creek is essentially undeformed and unfoliated. The coarse-grained, amphibole-biotite granite (C.I. = 5-8) has microcline perthite megacrysts (up to 2-3 cm, some with wiborgitic texture), quartz, plagioclase (0.5-1.5 cm, weak to moderate oscillatory zoning from $An_{23}Ab_{76}Or_1$ to $An_{19}Ab_{79}Or_2$). Biotite is of intermediate composition (Fe/(Fe+Mg) = 0.46), and the amphibole has Fe/(Fe+Mg) = 0.48. Quartz is slightly strained, and there has been minor recrystallization of the borders of plagioclase. Euhedral accessory titanite is plentiful. Other accessory minerals include opaques, zircon, apatite, and allanite. Secondary minerals include chlorite, muscovite, and epidote. Minor quartz veins cutting the granite contain trace amounts of molybdenite.

The more mafic medium-grained facies of the pluton occurs as autoliths and as a minor border facies. This is a biotite-amphibole granodiorite, with C.I. = 15 to 20. Mineral compositions are similar to those of the coarse-grained facies. Some antiwiborgite texture is present in the feldspars. This is believed to be an early facies of the pluton.

A fine- to medium-grained, muscovite-biotite leucogranite facies (C.I. = 1-2) occurs on the southwestern margin of the Butterwood Creek pluton. K-feldspar is microperthitic microcline with plentiful adjacent myrmekite. Plagioclase is oligoclase. Biotite is partially altered to chlorite, and muscovite is plentiful as an interstitial mineral - probably secondary is part, but possibly primary. Epidote

is a minor secondary mineral. Accessories include opaques and zircon. This poorly-exposed body is apparently a late facies of the Butterwood Creek.

The western third of the Butterwood Creek pluton is cut by the Hollister mylonite zone. As the mylonite zone is approached, a tectonic foliation is developed in the granite. In the coarse-grained facies, quartz is strongly deformed, with subgrain development; feldspars are fractured, with recrystallized edges; biotites are bent and kinked; titanites are fractured and rounded. No amphibole occurs in the deformed coarse-grained facies. Similar textural changes occur in the other facies, but the muscovite-biotite leucogranite appears to be less deformed, although it is foliated.

In the mylonite zone proper, grain size is greatly reduced, with zones of ultramylonite. Textural gradation suggests that this is all one pluton, but this is interpretive at best because of the lack of exposures. The Bens Creek leucogneiss, a leucogranitic mylonitic gneiss along the westernmost border of the pluton, was being mapped as country rock, but may also be a mylonitized portion of the Butterwood Creek pluton.

Medoc Mountain Granite

A small pluton of medium- to coarse-grained biotite granite (MMg) occurs about 2 km south of the Butterwood Creek pluton and may be part of the same intrusive complex. This pluton was not examined in the present study but has been described from surface and drill core samples by Robertson and others (1947) and Harvey (1974). The Boy Scout-Jones and Moss-Richardson molybdenite prospects are associated with this pluton. The pluton has been dated as 301 $\pm$ 6 Ma (Fullagar and Butler, 1979). The granite is described as unfoliated, but faulted and fractured in some areas. Cu-Mo mineralization is associated with quartz veins cutting the granite and surrounding phyllite. There is minor to moderate alteration of the granite with secondary minerals including chlorite, muscovite, epidote, and carbonate.

Sims Granite

The Sims granite (Sg) (also known as the Conner Stock) is a coarse-grained, unfoliated biotite granite dated by Wedemeyer and Spruill (1980) at 287 $\pm$ 9 Ma. It is an approximately elliptical pluton with a long axis of about 10 km, and has a thin layer of Coastal Plain sediments over most of the eastern half of the pluton. Mineralogically, the Sims comprises perthitic microcline, quartz, moderately zoned plagioclase (from about An_{20} to An_{16}) which is moderately to strongly saussuritized. Biotite has Fe/(Fe+Mg) = 0.56 and is moderately altered to chlorite.

A pelitic xenolith from the Sims has the assemblage biotite-andalusite-fibrolite-quartz-muscovite. At the contact of the granite, the quartz-muscovite phyllite has been recrystallized to a coarse-grained quartz-muscovite hornfels.

Rocky Mount Granitoid

The Rocky Mount pluton (RMg), which lies along the Piedmont-Coastal Plain boundary, has been briefly described by Watson and Laney (1906), Mundorff (1946), Councill (1954), and Parker (1968). The pluton is exposed along the Tar River and its tributaries in and west of the city of Rocky Mount, and along Swift Creek northwest of Rocky Mount. It is mostly covered by Coastal Plain sediments. The pluton, as outlined from water well and aeromagnetic data, corresponds to a -30 milligal gravity anomaly (Dept. of Defense Gravity Data, 1976).

The Rocky Mount pluton comprises three major facies: biotite monzogranite, exposed along the Tar River and its tributaries in and near Rocky Mount; hornblende-biotite granodiorite, exposed only in the RM1 drillcore, located in the center of the gravity anomaly, 1 km south of Battleboro, N. C.; and biotite-hornblende tonalite which crops out along Swift Creek, forming the northwestern boundary of the pluton.

The biotite monzogranite is light gray, equigranular, medium- to fine-grained, weakly to moderately foliated, with a color index (C.I.) of 2-3. Biotite (up to 1.0-1.5 mm) is the only ferromagnesian silicate. Maximum grain size of the microperthitic and perthitic microcline, plagioclase, and quartz is 2-4 mm. The feldspars are sub- to anhedral, quartz is strained, with some subgrain development. The quartz is flattened slightly parallel to the foliation defined by the biotite. The plagioclase (An_{15}) has weak normal zoning, and weakly to moderately saussuritized cores. Accessory minerals include apatite, zircon, allanite, magnetite, and small euhedral titanite, secondary minerals include moderate development of epidote and chlorite after biotite, and minor epidote, calcite, and muscovite from saussuritization of plagioclase. Enclaves of fine-grained biotite-hornblende tonalite are common in some outcrops, and may be related to the coarser-grained tonalite which occurs to the north.

The RM1 drillcore comprises medium- to coarse-grained hornblende-biotite granodiorite, which has not been found in the exposed portion of the pluton. Minor facies in the core include a dike of fine-grained biotite monzogranite, and several 1-2 cm thick quartz-feldspar pegmatite and aplite veins. The hornblende-biotite granodiorite has euhedral to subhedral plagioclase, somewhat strained, up to 0.5-1.0 cm long, and with oscillatory zoning An_{32-23}, which comprises up to 45 modal percent of the rock. Anhedral quartz and sub- to anhedral microcline perthite comprise 20 to 25 modal percent each. Biotite, pleochroic tan to brown, and amphibole, pleochroic tan to green-brown to blue-green, and commonly twinned, comprise the ferromagnesian silicates. The average of three modes has 7 percent biotite and 2 percent amphibole. Both the biotite and amphibole commonly occur as euhedral inclusions in plagioclase and microcline. Accessory minerals include large, 2-3 mm long, euhedral titanite, apatite, allanite, zircon, pyrite, and magnetite(?). Secondary minerals include minor chlorite and epidote after biotite, and minor epidote and calcite after plagioclase. Within the core, there are zones of alteration adjacent to calcite + epidote + quartz-filled fractures. This alteration involves

the formation of abundant chlorite + epidote from amphibole and biotite, and the saussuritization of plagioclase.

Hornblende-biotite tonalite is medium-gray, medium-grained, weakly foliated, with 55 modal percent plagioclase (An_{40-30}, up to 5-8 mm), 20 percent quartz (2-4 mm), 10-15 percent each of biotite and amphibole (2-4 mm), and very minor microcline microperthite. Accessory minerals include apatite, zircon, and large, 1-3 mm, euhedral titanites. Secondary minerals, which are very minor, include traces of epidote, calcite, and muscovite from the saussuritization of plagioclase.

Other Granites

The Elm City granite (ECg) lies to the southwest of the Rocky Mount pluton, separated from it by Coastal Plain cover, and lying outside the aeromagnetic anomaly of the Rocky Mount pluton. The Elm City pluton is a medium- to coarse-grained biotite granite which is exposed in an abandoned quarry alongside the Atlantic Coast Line railroad about 3.5 km north of Elm City, North Carolina. Water wells (Mundorff, 1946) suggest a limited extent of the granite under Coastal Plain cover. The mineralogy is microcline perthite, quartz, plagioclase (approximately An_{20}, with slight zoning and minor saussuritization), biotite (commonly altered to chlorite), with accessory allanite, zircon, and opaques, and secondary epidote, muscovite, and chlorite. This pluton is also described in Councill (1954).

The Contentnea Creek granite, (CCg) described by Councill (1954) and Watson and Laney (1906), is a coarse-grained biotite granite exposed in fractured condition along Contentnea Creek south of Wilson, North Carolina. It was not examined in this study.

The Wilton granite (WLg) is a small pluton about 3 km east of Wilton in Granville County, within the Nutbush Creek mylonite zone. It is a pink, medium-grained, foliated biotite granite. Its Rb/Sr age is 285 $\pm$ 10 Ma (Fullagar and Butler, 1979). Its mineral assemblage is microcline perthite, plagioclase, quartz, biotite; with accessory opaques, allanite, titanite, zircon; and secondary chlorite, muscovite, and calcite. There is some saussuritization of plagioclase, and biotite is commonly altered to chlorite. C.I. is 2 to 5. The granite has been weakly deformed, having moderately to strongly strained quartz. Plentiful fractures have quartz-molybdenite-sulfide mineralization.

The Buggs Island (BIg) and Wise (WSg) granites are medium-grained, foliated, biotite granites, similar to the Rolesville. The Buggs Island pluton, most of which lies in Virginia, has been dated by Rb/Sr at 313 $\pm$ 8 Ma (Kish and Fullagar, 1978). It lies in the Raleigh belt, but is bounded on the west by the Nutbush Creek mylonite zone. The Wise pluton lies within the northern Raleigh belt, and has not been dated.

The Lillington granite (Lg) is a medium-grained, foliated, biotite granite cropping out south of Lillington near the southwesternmost

exposures of the Raleigh block east of the Nutbush Creek mylonite zone. This granite has been dated at Rb/Sr 290 Ma (Kish and Fullagar, 1978).

METAMORPHISM

Rocks of the eastern Piedmont of North Carolina have been metamorphosed under medium pressure (Barrovian) metamorphic conditions. Metamorphic grade in this area has been previously described in terms of belts - the low grade Carolina slate belt and Eastern slate belt, and the high grade Raleigh belt (King, 1955; Parker, 1968). The character of these belts and the locations of their boundaries have remained rather ill-defined.

In this study, the eastern North Carolina Piedmont has been divided into tectonic blocks, bounded by major mylonite zones (Fig. 1). Because there are metamorphic, as well as tectonic, discontinuities across these mylonite zones, the metamorphic belt concept has been applied to individual blocks. Within the study area, the Carolina slate belt block and the greenschist grade Carolina slate belt are coincident (Fig. 1). Their eastern boundary is the western edge of the Nutbush Creek mylonite zone. The Raleigh block (Fig. 1) comprises the Raleigh belt, which in this study is restricted to the area of amphibolite grade rocks, and the Eastern slate belt I, which comprises the greenschist grade rocks of the block. The Raleigh block is bounded on the west by the Nutbush Creek mylonite zone and on the east by the Hollister mylonite zone. East of the Hollister zone is the Roanoke Rapids block (Fig. 1), comprising the amphibolite grade rocks of the Littleton belt, and the greenschist grade rocks of the Eastern slate belt II.

The Carolina slate belt has a narrow chlorite zone along the edge of the Durham Triassic basin (Fig. 4). This chlorite zone is assumed to continue under the Triassic basin and into the main portion of the Carolina slate belt west of the study area. There is a wide biotite + almandine zone between the chlorite zone and the Nutbush Creek mylonite. A reported occurrence of kyanite + staurolite west of the Beaverdam Mafic Complex (ST, Fig. 4) (E. F. Stoddard, pers. comm., 1979) presents the possibility that some of the assemblages mapped in this zone may be retrograde from amphibolite facies assemblages.

The greenschist grade Eastern slate belt I comprises a wide chlorite zone in the east and south, extending under Coastal Plain cover, and much narrower biotite, almandine, and chloritoid zones adjacent to the Raleigh belt and in the Nutbush Creek mylonite zone (Fig. 4). At the scale of this map, the appearance of biotite nearly coincides with the appearance of almandine and chloritoid in rocks of appropriate pelitic composition.

The Eastern slate belt I-Raleigh belt boundary is defined here as the boundary between the greenschist and amphibolite facies in the sense of Greenwood (1976), using a group of reactions, rather than single reaction, to define the approximate facies boundary in a var-

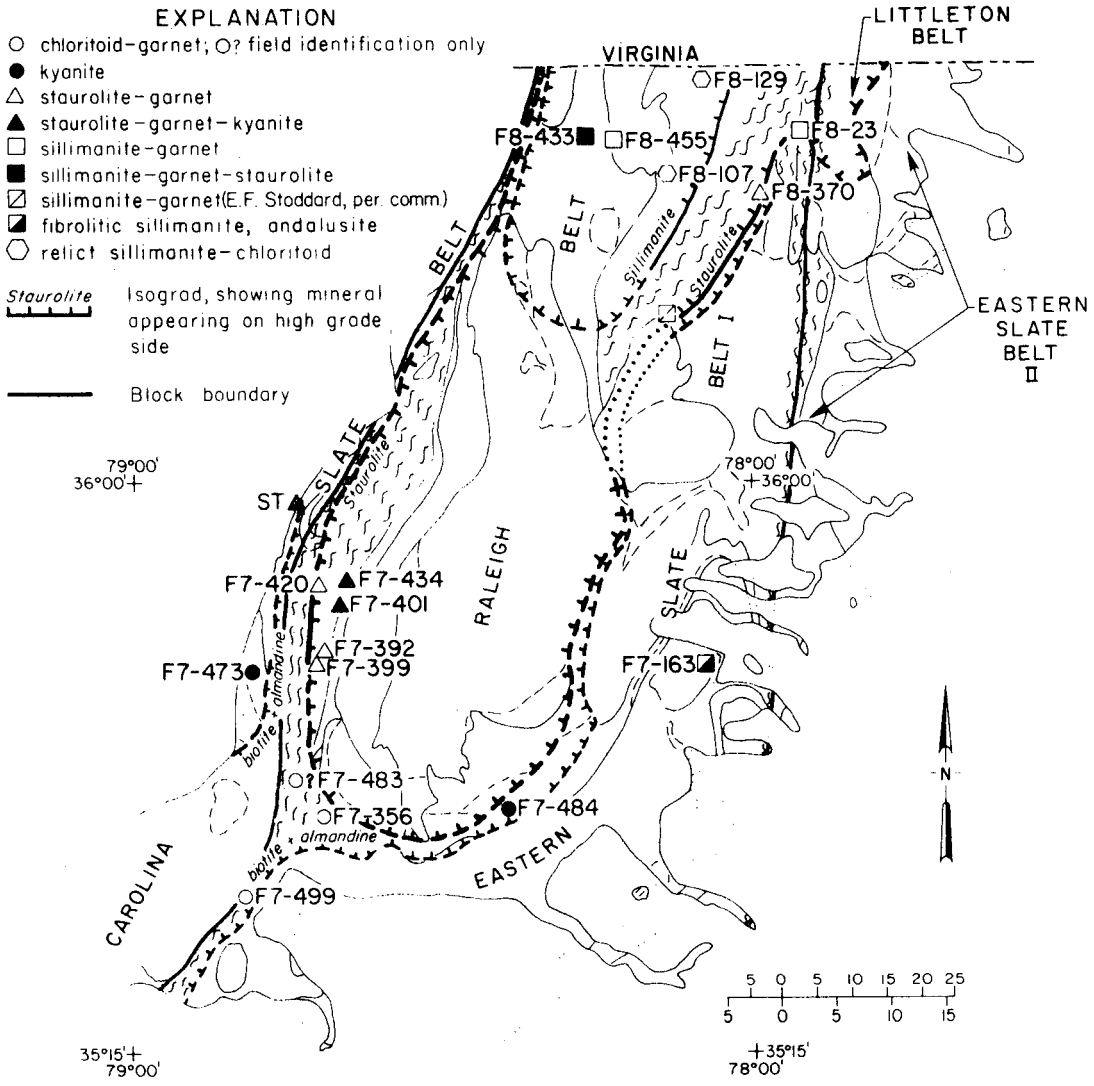

Figure 4. Map of metamorphic grade distribution in the northeastern Piedmont of North Carolina.

iety of rock compositions. In the pelitic rocks of the Smithfield and Macon formations, the staurolite-in isograd is used to define this contact. In the Smithfield Formation southwest and west of Raleigh, this isograd (Fig. 4) approximately coincides with that of Parker (1979), although Parker extended it farther southwest, whereas, this study suggests that it curves southeastward. The staurolite-in isograd also occurs along the eastern border of the Macon Formation in the northeastern Raleigh belt. The isograd in this area is approximated from the one staurolite-bearing sample found in this study (SF8-370, Fig. 4) and several occurrences reported by Stoddard and McDaniel (1979). The Raleigh belt contact is approximated as the change from albite to more calcic plagioclase in mafic metavolcanic rocks, and the contact is extrapolated across major units of felsic metavolcanic rocks. The contact is very poorly controlled along the eastern side of the Rolesville batholith. The northwestern Raleigh belt is bounded on the west by the Nutbush Creek mylonite zone which cuts off the northern end of the Smithfield Formation. From approximately Henderson northward, biotite-hornblende gneiss of the Raleigh belt is in fault contact, along the Nutbush Creek mylonite zone, with the greenschist grade Vance County pluton of the Carolina slate belt.

Within the Raleigh belt, metamorphic grade increases toward the center and to the north (Fig. 4). The highest grade pelitic rocks in the southern Raleigh belt are quartz-muscovite-biotite-garnet-staurolite-kyanite schists in the easternmost Smithfield formation (F7-434, F7-401, Fig. 4), adjacent to the Falls Leucogneiss. In the northern Raleigh belt, sillimanite is regionally developed. The highest grade assemblage observed is muscovite-quartz-sillimanite-garnet-staurolite in a schist layer within biotite-hornblende gneiss (SF8-433, Fig. 4).

The amphibolite grade Littleton belt (named here, Fig. 4) of the Roanoke Rapids block is fault-bounded on the east, where it abuts Eastern slate belt rocks of the biotite zone. The Hollister mylonite zone cuts the Littleton belt on the west, where it is in contact with Eastern slate belt I and the Raleigh belt. The post-metamorphic Butterwood Creek granite separates the Littleton belt from Eastern slate belt rocks on the south. The Littleton belt is thus terminated on three sides, but continues northward into Virginia.

Eastern slate belt II is variably at chlorite and biotite grade. General lack of exposures limits the mapping of metamorphic grade in this area.

Mineralogy

A table of mineral assemblages, grouped according to tectonic block, formation, and map unit is provided as Appendix I. The mineral assemblages are generalized for the map unit except for the pelitic rocks. For the pelitic samples shown in Figure 4, the individual thin section mineral assemblage is given under the appropriate formation. The pelitic mineral assemblages, and the metamorphic temperature and pressure conditions derived from them, are discussed below.

Mineralogy of Metapelites

Kyanite

Kyanite occurs in at least two localities in the chlorite or biotite zone (F7-473 and F7-484, Fig. 4). These are quartz-kyanite-pyrophyllite occurrences, and the low temperature occurrence of kyanite is apparently compositionally controlled. Elsewhere in the study area, kyanite occurrence is in pelitic compositions (F7-434, F7-401) where it appears slightly to the high-grade side of the appearance of staurolite.

Kyanite is the only aluminosilicate reported in the southern Raleigh belt, and kyanite with staurolite has been reported as loose grains in saprolite along the eastern border of the Macon formation (Stoddard and McDaniel, 1979), but it has not been reported elsewhere in the northern Raleigh belt of North Caolina.

Sillimanite

Sillimanite occurs on a regional scale in the northern Raleigh belt. At location SF8-433 (Fig. 4) sillimanite occurs in the assemblage muscovite-quartz-sillimanite-garnet-staurolite in a thin schist layer within hornblende-biotite gneiss. Elsewhere in the northern Raleigh belt sillimanite occurs along the western edge of the Macon Formation as a relict mineral with garnet in a muscovite-chloritoid schist (SF8-107 and SF8-129, Fig. 4), in a muscovite quartzite northwest of the Castalia pluton (Stoddard and McDaniel, 1979), and in a muscovite schist in southern Virginia (F8-352). The occurrences adjacent to the Castalia pluton, the Wise pluton (SF8-455), and a probable xenolith in the northwestern border of the Butterwood Creek pluton (SF8-23) are in probable contact metamorphic assemblages. Fibrolitic sillimanite occurs in a xenolith from the Sims granite which intruded rocks in the chlorite zone of the Eastern slate belt.

Andalusite

The only known occurrence of andalusite in the study area is in a xenolith (with fibrolitic sillimanite) from the Neverson quarry in the Sims pluton.

Garnet

Compositions and zoning of garnet in the pelitic rocks agree well with metamorphic grade. In the chloritoid zone, garnet has high MnO and typical prograde zoning with decreasing MnO and increasing FeO and MgO from core to rim (F7-356, Table 1). At the staurolite-in isograd, the garnet has zoning similar to that of the chloritoid zone, but with a greater decrease in MnO and increase in FeO at the garnet rims (F8-370, F7-399-3, Table 1). In the highest grade portion of the southern Raleigh belt (with the assemblage quartz + muscovite + biotite + garnet + staurolite + kyanite) zoning in the garnet decreases, becomes more irregular, and the garnets have lower MnO than at lower grade (F7-401, Table 1). Garnet in the sillimanite-staurolite grade rocks of the northern Raleigh belt is essentially unzoned, having the highest FeO and MgO and the lowest MnO and CaO of garnet in the study area (F8-433, Table 1).

Biotite

Biotite from peltic rocks of the chloritoid zone (F7-499) is Fe-rich, with Fe/(Fe+Mg) = 0.73 (Table 2). In peltic rocks of the staurolite and staurolite-sillimanite zone, biotite is intermediate in composition with Fe/Fe+Mg = 0.46-0.50 (Table 2).

Plagioclase

Microprobe analyses of plagioclase in pelitic rocks show change of composition with increasing metamorphic grade into the Raleigh belt. Plagioclase coexisting with garnet and chloritoid in sample F7-499 is $An_5Ab_{94}Or_1$. Plagioclase coexisting with biotite + muscovite + garnet + staurolite $\pm$ kyanite in the Raleigh belt ranges from $An_{18}Ab_{81}Or_1$ (F7-401) to $An_{36}Ab_{63}Or_1$ (F7-434). At the scale of this study, the change in plagioclase compositions from albite to oligoclase coincides with the staurolite-in isograd.

Muscovite

Muscovites from the pelitic rocks of chloritoid grade and higher are close to ideal muscovite, with approximately 1 weight percent total iron as FeO and 1 weight percent Na_2O (Table 3). Muscovite from the sillimanite zone (F8-433), although texturally it locally appears to be retrograde, is the closest to ideal muscovite, suggesting crystallization at relatively high temperature (Miyashiro, 1973).

Staurolite

Staurolite in the Raleigh belt is constant in composition except for variation in ZnO which ranges from less than 0.5 to greater than 2.0 weight percent ZnO (staurolite analyses, Table 4).

TABLE 1. GARNET FROM PELITIC ROCKS OF THE RALEIGH BLOCK

	1		2		3		4		5		6		7		8	
SIO2	36.31		36.57		36.66		37.44		37.40		37.41		37.66		38.99	
TIO2	0.12		0.13		0.12		0.15		0.09		0.10		0.14		0.00	
A203	19.40		19.10		21.51		20.73		19.94		20.11		19.89		21.15	
FEO	26.20		28.82		33.97		26.38		31.01		34.00		34.06		35.06	
MGO	0.61		0.75		1.01		1.20		1.77		2.14		3.64		3.49	
MNO	8.88		6.67		4.28		12.30		7.44		3.96		1.90		1.88	
CAO	5.50		5.25		3.28		2.40		2.38		1.87		1.92		1.78	
NA20	0.01		0.0		0.02		0.01		0.0		0.01		0.0		0.0	
K20	0.01		0.02		0.02		0.01		0.01		0.02		0.03		0.01	
SUM	97.04		97.31		100.89		100.62		100.04		99.62		99.24		102.44	
SI	3.039	*	3.056	*	2.961	*	3.023	*	3.040	*	3.043	*	3.047	*	3.048	*
AL	0.0	3.039	0.0	3.056	0.039	3.000	0.0	3.023	0.0	3.040	0.0	3.043	0.0	3.047	0.0	3.048
AL	1.914	*	1.881	*	2.007	*	1.972	*	1.910	*	1.927	*	1.697	*	1.946	*
TI	0.008	1.921	0.008	1.889	0.007	2.014	0.009	1.982	0.006	1.916	0.006	1.934	0.009	1.905	0.005	1.953
FE	1.834	*	2.014	*	2.293	*	1.781	*	2.108	*	2.313	*	2.305	*	2.292	*
MG	0.076	*	0.093	*	0.122	*	0.144	*	0.214	*	0.259	*	0.439	*	0.407	*
MN	0.630	*	0.472	*	0.293	*	0.841	*	0.512	*	0.273	*	0.130	*	0.124	*
CA	0.493	*	0.470	*	0.284	*	0.206	*	0.207	*	0.163	*	0.166	*	0.149	*
NA	0.002	*	0.0	*	0.003	*	0.002	*	0.0	*	0.002	*	0.0	*	0.0	*
K	0.001	3.036	0.002	3.051	0.002	2.996	0.001	2.977	0.001	3.043	0.002	3.012	0.003	3.044	0.001	2.973
O	12.000	*	12.000	*	12.000	*	12.000	*	12.000	*	12.000	*	12.000	*	12.000	*
AL		60.47		66.04		76.67		59.88		69.30		76.89		75.80		77.11
PY		2.51		3.06		4.06		4.86		7.05		8.63		14.44		13.68
SP		20.76		15.46		9.78		26.28		16.84		9.07		4.28		4.19
GR		16.26		15.41		9.48		6.98		6.81		5.42		5.47		5.02
AL		72.21		78.08		84.70		64.38		74.36		81.29		80.19		81.19
PY		3.00		3.62		4.49		5.22		7.57		9.12		15.27		14.40
SP		24.79		18.30		10.81		30.40		18.07		9.59		4.53		4.41
AL		62.03		68.13		79.92		62.94		74.55		84.14		88.60		89.34
SP		21.29		15.97		10.20		29.72		16.12		9.93		5.01		4.85
GR		16.68		15.90		9.89		7.34		7.33		5.93		6.40		5.81
F/M		32.371		26.614		21.279		18.159		12.219		9.966		5.547		5.943
F/FM		0.970		0.964		0.955		0.948		0.924		0.909		0.847		0.856

1 F7-356 GAR CORE CID ZONE
2 F7-356 GAR RIM CID ZONE
3 F7-499 GAR* CID ZONE
4 F8-370 GAR CORE STAUR ZONE
5 F8-370 GAR MID** STAUR ZONE
6 F8-370 GAR RIM STAUR ZONE
7 F7-399-3 GAR CORE STAUR ZONE
8 F7-399-3 GAR MID*** STAUR ZONE

* Analysis used in biotite-garnet geothermometer

** Analysis used in garnet-staurolite geothermometer

*** Analysis used in both geothermometers

TABLE 1. GARNET FROM PELITIC ROCKS OF THE RALEIGH BLOCK

	9	10	11	12	13	14	15	16
SIO2	38.18	38.35	37.42	37.80	37.06	37.28	38.79	38.39
TIO2	0.23	0.06	0.08	0.10	0.06	0.10	0.06	0.05
A2O3	21.22	21.64	19.99	20.65	19.77	21.14	20.44	20.96
FEO	35.91	27.96	33.99	34.56	34.26	33.99	37.20	36.33
MGO	3.34	3.34	2.97	3.05	3.05	3.81	3.42	3.40
MNO	1.15	4.72	2.10	0.72	1.27	1.06	0.84	0.90
CAO	1.24	6.41	2.75	3.10	1.92	2.96	0.93	0.94
NA2O	0.04	0.02	0.02	0.0	0.0	0.0	0.01	0.01
K2O	0.03	0.03	0.02	0.02	0.04	0.02	0.01	0.02
SUM	101.34	102.73	99.34	100.20	97.43	100.36	101.70	101.00
SI	3.022 *	2.975 *	3.036 *	3.024 *	3.056 *	2.977 *	3.068 *	3.048 *
AL	0.0 3.022	0.025 3.000	0.0 3.036	0.0 3.024	0.0 3.056	0.023 3.000	0.0 3.068	0.0 3.048
AL	1.979 *	1.972 *	1.911 *	1.965 *	1.921 *	1.966 *	1.905 *	1.961 *
TI	0.014 1.993	0.004 1.975	0.005 1.916	0.006 1.971	0.004 1.925	0.006 1.972	0.004 1.908	0.003 1.964
FE	2.377 *	1.814 *	2.306 *	2.312 *	2.363 *	2.270 *	2.460 *	2.412 *
MG	0.394 *	0.386 *	0.359 *	0.364 *	0.375 *	0.453 *	0.403 *	0.402 *
MN	0.077 *	0.310 *	0.144 *	0.049 *	0.089 *	0.072 *	0.056 *	0.061 *
CA	0.105 *	0.533 *	0.239 *	0.266 *	0.170 *	0.253 *	0.079 *	0.080 *
NA	0.006 *	0.003 *	0.003 *	0.0 *	0.0 *	0.0 *	0.002 *	0.002 *
K	0.003 2.963	0.003 3.049	0.002 3.054	0.002 2.992	0.004 3.000	0.002 3.050	0.001 3.001	0.002 2.956
O	12.000 *	12.000 *	12.000 *	12.000 *	12.000 *	12.000 *	12.000 *	12.000 *
AL	80.49	59.61	75.65	77.32	78.86	74.46	82.05	81.63
PY	13.34	12.69	11.78	12.16	12.51	14.88	13.44	13.62
SP	2.61	10.19	4.73	1.63	2.96	2.35	1.88	2.05
GR	3.56	17.51	7.84	6.89	5.66	8.31	2.63	2.71
AL	83.46	72.26	82.08	84.86	83.60	81.21	84.27	83.90
PY	13.83	15.38	12.78	13.35	13.26	16.22	13.81	13.99
SP	2.71	12.35	5.14	1.79	3.14	2.57	1.93	2.11
AL	92.88	68.27	85.75	88.03	90.14	87.48	94.80	94.50
SP	3.01	11.67	5.37	1.86	3.38	2.76	2.17	2.37
GR	4.11	20.05	8.89	10.12	6.47	9.76	3.04	3.13
F/M	6.228	5.500	6.823	6.492	6.539	5.164	6.242	6.146
F/FM	0.862	0.846	0.872	0.867	0.867	0.838	0.862	0.860

9 F7-399-3 GAR RIM STAUR ZONE
10 F7-420-2 GAR MID** STAUR ZONE
11 F7-401 GAR CORE STAUR-KYAN ZONE
12 F7-401 GAR MID***STAUR-KYAN ZONE
13 F7-401 GAR RIM STAUR-KYAN ZONE
14 F7-434 GAR MID***STAUR-KYAN ZONE
15 F8-433 GAR CORE**STAUR-SIL ZONE
16 F8-433 GAR RIM STAUR-SIL ZONE

* Analysis used in biotite-garnet geothermometer
** Analysis used in garnet-staurolite geothermometer
*** Analysis used in both geothermometers

TABLE 2. BIOTITE FROM PELITIC ROCKS OF THE RALEIGH BLOCK

	1		2		3		4		5	
SIO2	34.08		34.77		35.61		38.07		36.87	
TIO2	1.83		1.78		1.56		1.56		1.57	
A2O3	19.45		19.23		19.43		20.04		19.24	
FEO	25.59		17.75		17.04		17.50		17.28	
MGO	5.40		10.27		10.75		10.90		11.15	
MNO	0.09		0.0		0.0		0.0		0.0	
CAO	0.04		0.04		0.02		0.06		0.04	
NA2O	0.05		0.12		0.31		0.12		0.16	
K2O	9.63		9.45		8.47		7.14		9.41	
H2O	3.84		3.88		3.92		4.07		4.01	
SUM	100.00		97.29		97.11		99.44		99.73	
SI	5.315	*	5.366	*	5.443	*	5.601	*	5.503	*
AL	2.685	8.000	2.634	8.000	2.557	8.000	2.399	8.000	2.497	8.000
AL	0.889	*	0.863	*	0.943	*	1.076	*	0.887	*
TI	0.215	*	0.207	*	0.179	*	0.173	*	0.176	*
FE	3.338	*	2.291	*	2.178	*	2.153	*	2.157	*
MN	0.012	*	0.0	*	0.0	*	0.0	*	0.0	*
MG	1.255	5.709	2.362	5.722	2.449	5.750	2.390	5.792	2.481	5.701
CA	0.007	*	0.007	*	0.003	*	0.009	*	0.006	*
NA	0.015	*	0.036	*	0.092	*	0.034	*	0.046	*
K	1.916	1.937	1.860	1.903	1.651	1.747	1.336	1.380	1.791	1.844
H	4.000	4.000	4.000	4.000	4.000	4.000	4.000	4.000	4.000	4.000
O	24.000	*	24.000	*	24.000	*	24.000	*	24.000	*
	F/M	2.668		0.970		0.889		0.901		0.870
	F/FM	0.727		0.492		0.471		0.474		0.465

1 F7-499 BIO CTD ZONE
2 F7-399-3 BIO STAUR ZONE
3 F7-401 BIO STAUR-KY ZONE
4 F7-434 BIO STAUR-KY ZONE
5 F7-420-2 BIO STAUR ZONE

TABLE 3. MUSCOVITE IN PELITIC ROCKS OF THE RALEIGH BLOCK

	1	2	3	4	5	6
SIO2	46.15	45.39	45.73	45.46	45.53	47.51
TIO2	0.08	0.50	0.09	0.66	0.47	0.22
A203	34.07	33.17	35.59	34.41	34.98	37.61
FEO	1.78	1.06	0.85	0.93	1.10	0.74
MGO	0.46	0.69	0.32	0.63	0.67	0.46
MNO	0.0	0.0	0.0	0.0	0.0	0.0
CAO	0.0	0.0	0.01	0.01	0.01	0.0
NA2O	0.73	1.18	1.49	1.34	1.11	1.09
K2O	9.77	9.09	8.20	8.90	8.57	7.35
H2O	4.41	4.33	4.42	4.40	4.41	4.60
SUM	97.45	95.41	96.70	96.74	96.85	99.58

SI	6.276	*	6.279	*	6.195	*	6.194	*	6.180	*	6.188	*
AL	1.724	8.000	1.721	8.000	1.805	8.000	1.806	8.000	1.820	8.000	1.812	8.000
AL	3.735	*	3.685	*	3.876	*	3.719	*	3.774	*	3.961	*
TI	0.008	*	0.052	*	0.009	*	0.066	*	0.048	*	0.022	*
FE	0.202	*	0.123	*	0.096	*	0.106	*	0.125	*	0.081	*
MN	0.0	*	0.0	*	0.0	*	0.0	*	0.0	*	0.0	*
MG	0.093	4.039	0.142	4.002	0.065	4.046	0.128	4.021	0.136	4.082	0.089	4.152
CA	0.0	*	0.0	*	0.001	*	0.001	*	0.001	*	0.0	*
NA	0.192	*	0.316	*	0.391	*	0.354	*	0.292	*	0.275	*
K	1.695	1.887	1.604	1.920	1.417	1.810	1.547	1.902	1.484	1.777	1.221	1.496
H	4.000	4.000	4.000	4.000	4.000	4.000	4.000	4.000	4.000	4.000	4.000	4.000
O	24.000	*	24.000	*	24.000	*	24.000	*	24.000	*	24.000	*
	F/M	2.171		0.862		1.490		0.828		0.921		0.903
	F/FM	0.685		0.463		0.598		0.453		0.479		0.474

1 F7-499 MU CTD ZONE
2 F7-399-3 MU STAUR ZONE
3 F8-370 MU STAUR ZONE
4 F7-401 MU STAUR-KY ZONE
5 F7-434 MU STAUR-KY ZONE
6 F8-433 MU STAUR-KY ZONE

TABLE 4. STAUROLITE FROM PELITIC ROCKS OF THE RALEIGH BLOCK

	1	2	3	4	5	6
SIO2	28.48	28.28	28.70	28.00	27.66	28.78
TIO2	0.66	0.44	0.66	0.71	0.71	0.33
A203	52.66	53.53	53.10	51.71	53.48	53.31
FEO	12.94	12.35	10.96	13.37	13.38	11.67
MGO	1.41	1.34	1.12	1.72	1.69	1.06
MNO	0.01	0.06	0.04	0.0	0.05	0.0
ZNO	0.24	1.00	2.35	0.37	0.52	2.39
CAO	0.0	0.01	0.0	0.01	0.01	0.02
NA2O	0.0	0.05	0.08	0.01	0.01	0.06
K2O	0.0	0.0	0.0	0.01	0.01	0.0
H2O	2.14	2.15	2.15	2.12	2.15	2.16
SUM	98.54	99.21	99.18	98.03	99.67	99.80

SI	7.980	*	7.882	*	8.002	*	7.924	*	7.706	*	7.998	*
AL	0.0	29.179	0.0	29.240	0.0	29.149	0.0	29.298	0.0	29.362	0.0	29.216
TI	0.139	*	0.092	*	0.138	*	0.151	*	0.149	*	0.069	*
FE	3.032	*	2.879	*	2.560	*	3.164	*	3.117	*	2.712	*
MN	0.002	*	0.014	*	0.009	*	0.0	*	0.012	*	0.0	*
MG	0.589	*	0.557	*	0.465	*	0.726	*	0.702	*	0.439	*
ZN	0.050	*	0.206	*	0.484	*	0.077	*	0.107	*	0.490	*
CA	0.0	*	0.003	*	0.0	*	0.003	*	0.003	*	0.006	*
NA	0.0	*	0.027	*	0.043	*	0.005	*	0.005	*	0.043	*
K	0.0	29.179	0.0	29.240	0.0	29.149	0.004	29.298	0.004	29.362	0.0	29.216
H	4.000	4.000	4.000	4.000	4.000	4.000	4.000	4.000	4.000	4.000	4.000	4.000
O	48.000	*	48.000	*	48.000	*	48.000	*	48.000	*	48.000	*
	F/M	5.153		5.197		5.521		4.361		4.459		6.177
	F/FM	0.837		0.839		0.847		0.813		0.817		0.861

1 F7-399-3 STAUR STAUR ZONE
2 F8-370 STAUR STAUR ZONE
3 F7-420-2 STAUR STAUR ZONE
4 F7-401 STAUR STAUR-KY ZONE
5 F7-434 STAUR STAUR-KY ZONE
6 F8-433 STAUR STAUR-SIL ZONE

Chloritoid

Chloritoid is constant in composition (chloritoid analyses, Table 5). Chloritoid in samples F7-499, and perhaps F7-356, in the southwestern part of the Smithfield Formation appear to be of prograde origin, while that in samples F8-107-1 and F8-129-2 from the Macon Formation pseudomorph sillimanite.

Metamorphic Temperatures Estimated from Biotite-Garnet and Garnet-Staurolite Geothermometers

Maximum metamorphic temperatures in the Raleigh belt and the adjacent highest grade portion of the Eastern slate belt, given in Table 6, are estimated from the biotite-garnet geothermometers of Thompson (1976), Perchuk (1977), and Ferry and Spear (1978). Analyses from Tables 1 and 2 were used in these determinations. For garnets with typical prograde zoning and narrow, apparently retrograde rims, the composition just inside the rim was used. This is under the assumption that the last prograde growth was at the highest temperature attained, and that the biotite with which it is paired has not changed significantly in composition during the retrograde event. The large amounts of MnO and CaO in the garnets of samples F7-499 and F4-420-2 make their temperatures suspect (Ferry and Spear, 1978).

In general, the temperatures given by these geothermometers appear to be reasonable in comparison to experimental univariant curves (for example Fig. 2 in Greenwood, 1976), with chloritoid stable in F7-499 at about 500°C, and staurolite without chloritoid stable at about 550°C and higher in the other rocks. Sample F7-401 appears to give too low a temperature (494-528°C) for its assemblage and sample location (Fig. 4).

Temperatures were also determined using the garnet-staurolite geothermometer of Perchuk (1977) (Table 7). The temperature of 550° for sample F7-434 agrees well with the garnet-biotite geothermometer of 570°. The garnet-staurolite pair for F7-401 gives a more reasonable temperature of 550° than the garnet-biotite pair, and it agrees with the temperature of the nearby F7-434 sample. This suggests that the biotite of F7-401 may have reequilibrated at a lower temperature than the garnet-staurolite.

Samples F8-370 and F8-433, which lack biotite for the garnet-biotite geothermometer give garnet-staurolite temperatures which are reasonable for their locations. Sample F8-370, from the northeasternmost Raleigh belt, adjacent to the greenschist grade Eastern slate belt rocks, gave 465°C, which is below the stability range of staurolite according to Ganguly (1972), but the sample is very close to the staurolite-in isograd. The only sillimanite-bearing sample (F8-433) gives a temperature of 635°, which appears to be quite reasonable, based on its mineral assemblage of coexisting staurolite + muscovite + sillimanite + quartz with no K-feldspar (see reactions in Fig. 2, Greenwood, 1976).

TABLE 5. CHLORITOID FROM PELITIC ROCKS OF THE RALEIGH BLOCK

	1		2		3		4	
SIO2	23.97		24.77		24.97		24.80	
TIO2	0.0		0.01		0.01		0.01	
A203	39.69		40.38		39.84		40.69	
FEO	24.99		25.37		24.05		24.71	
MGO	1.59		1.80		1.87		1.90	
MNO	0.65		0.32		0.49		0.31	
CAO	0.01		0.03		0.02		0.05	
NA2O	0.0		0.01		0.0		0.0	
K2O	0.0		0.02		0.0		0.02	
H2O	7.09		7.25		7.18		7.26	
SUM	97.99		99.96		98.43		99.75	
SI	2.026	2.026	2.047	2.047	2.085	2.085	2.047	2.047
AL	3.954	*	3.933	*	3.919	*	3.958	*
TI	0.0	3.954	0.001	3.934	0.001	3.920	0.001	3.958
FE	1.767	*	1.754	*	1.679	*	1.706	*
MN	0.047	*	0.022	*	0.035	*	0.022	*
MG	0.200	*	0.222	*	0.233	*	0.234	*
CA	0.001	*	0.003	*	0.002	*	0.004	*
NA	0.0	*	0.002	*	0.0	*	0.0	*
K	0.0	2.015	0.002	2.004	0.0	1.948	0.002	1.968
H	4.000	4.000	4.000	4.000	4.000	4.000	4.000	4.000
O	14.000	*	14.000	*	14.000	*	14.000	*
F/M		9.051		8.009		7.365		7.390
F/FM		0.901		0.889		0.880		0.881

1 F7-356 CTD
2 F7-499 CTD
3 F8-107-1 CTD
4 F8-129-2 CTD

Table 6. Raleigh block metamorphic temperatures from biotite-garnet geothermometers.

Sample	Thompson	Perchuk	Ferry & Spear
F7-499	510	513	497
F7-399-3	557	560	557
F7-401	508	528	494
F7-434	568	572	571
F7-420-2	575	554	581

Table 7. Raleigh block metamorphic temperatures from garnet-staurolite geothermometer (Perchuk, 1977).

Sample	Temperature
F8-370	465
F7-399-3	605
F7-401	550
F7-434	550
F7-420-2	>640
F8-433	635

Samples F7-399-3 and F7-420-2 appear to give garnet-staurolite temperatures that are too high. F7-399-3 at 605° versus 560° for biotite-garnet is in the range of possible temperatures, but F7-420-2 at >640° is off the chart of values which Perchuk (1977) gives, while the location of the sample would suggest a temperature of about 550°.

Retrograde, or Second Metamorphic, Event

In, and adjacent to, the major mylonite zones of this area, there is evidence of a late, generally lower grade, metamorphic event. In the Smithfield Formation west of Raleigh, there is a late greenschist assemblage superposed on the staurolite grade assemblage. For example, in sample F6-139 staurolite occurs only as inclusions in garnet porpyroblasts. The groundmass assemblage is quartz + plagioclase + biotite + opaques with a late foliation of chlorite, muscovite, and epidote. The rims of garnet in this area are commonly altered to chlorite. Elsewhere in the Nutbush Creek mylonite zone, retrogression is more complete, and the assemblage chlorite + albite + epidote + muscovite dominates the pelitic and semi-pelitic rocks. These rocks weather readily, and are difficult to sample.

The Macon Formation shows extensive evidence of a late metamorphic event. Samples F8-107 and F8-129 (Fig. 4) have extensive development of chloritoid which grew across a prexisting foliation. The chloritoid is pseudomorphic after sillimanite, relicts of which are preserved, in allignment with the early foliation, enclosed in the chloritoid. F8-129 has relict garnet, most of which has been altered to chlorite + hematite. Elsewhere in the Macon Formation, retrograde recrystallization associated with mylonitization has been complete, with resultant phyllonites comprising quartz + chlorite + muscovite + opaques + albite + tourmaline.

Contact Metamorphism

The Sims granite is the only pluton in the study area for which there is evidence of contact metamorphism. The Sims granite intruded chlorite grade phyllite and metasiltstone of the Eastern slate belt. The phyllite in immediate contact with the granite has recrystallized to a coarse-grained, muscovite-quartz hornfels. Within the pluton, a xenolith from the Neverson Quarry has the assemblage biotite + muscovite + quartz + andalusite + fibrolitic sillimanite. The muscovite of the groundmass appears to be pseudomorphic after a poikiloblastic mineral - perhaps cordierite? This is the only andalusite locality found in the study area.

Summary of P-T Conditions in the Raleigh Block

Pressure and temperature conditions in the Raleigh block are summarized in Figure 5, based on evidence from pelitic assemblages. The elongated box labelled ESB-RB is interpreted as the approximate P-T conditions of rocks encountered along a south to north traverse of the Raleigh block from the greenschist grade Eastern slate belt, across the staurolite-in isograd into the southern Raleigh belt with its

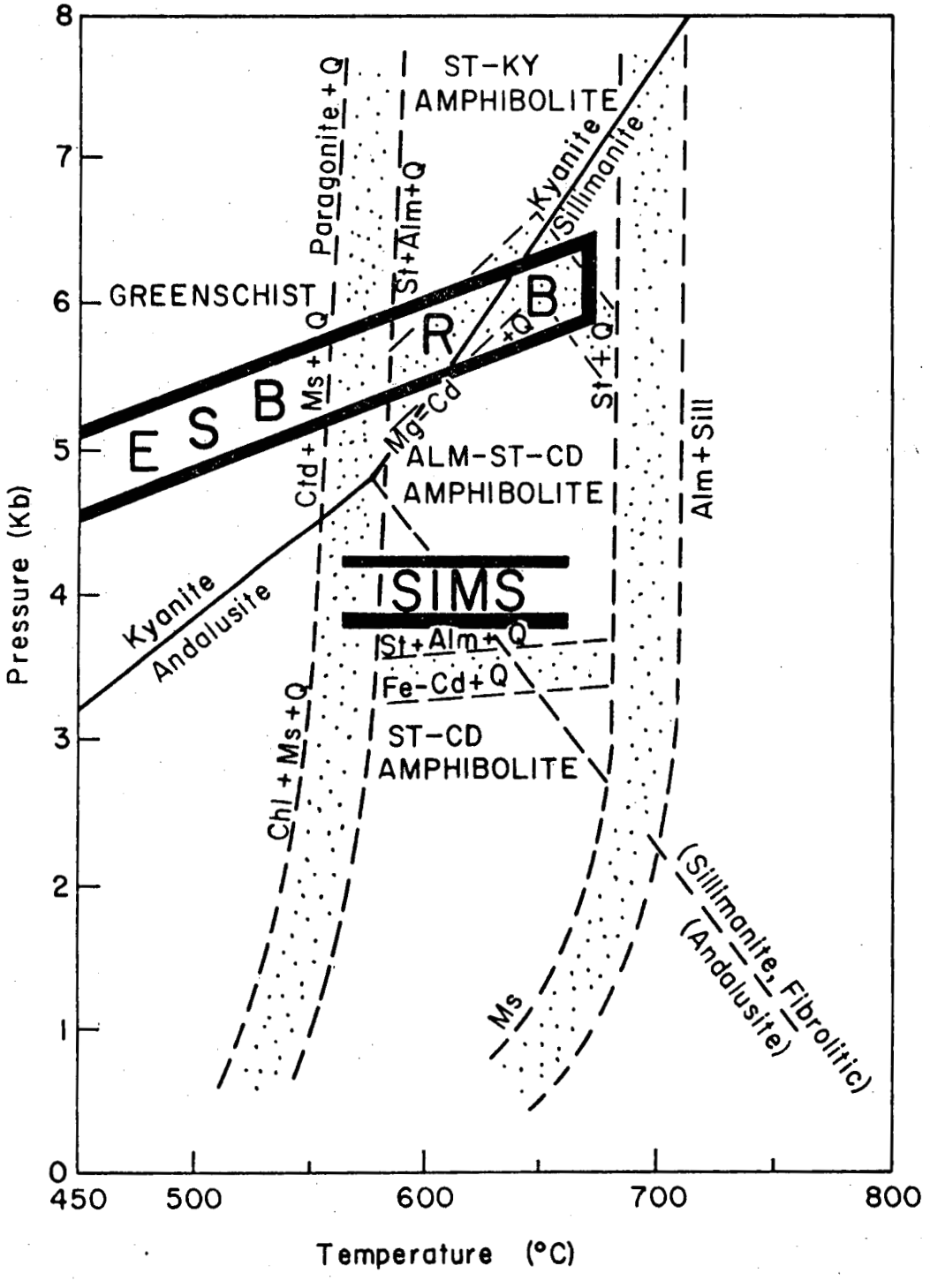

Figure 5. P-T conditions in the Raleigh block, estimated from mineral assemblages and geothermometers as discussed in the text. ESB = Eastern slate belt; RB = Raleigh belt; SIMS = contact aureole and xenoliths of the Sims pluton. Stability fields are from Greenwood (1976).

staurolite-kyanite assemblages, and continuing to the northern Raleigh belt with staurolite-sillimanite assemblages. Geothermometers, as discussed above, give temperatures ranging from 500° for chloritoid-bearing Eastern slate belt rocks to 550° to 570° for staurolite + kyanite and 635° for staurolite + sillimanite-bearing assemblages.

There is no numerical pressure control on this facies series, but the presence of the kyanite to sillimanite transition and the lack of regionally developed andalusite and cordierite indicate relatively high pressures, a Barrovian series, above the aluminosilicate triple point. The sloping field shown from about 5 kb to about 6 kb going from greenschist to amphibolite facies fits well for the temperature of transition from the kyanite to sillimanite stability field. The steepness of the slope is not known, but the general attitude is interpreted from the distribution of isograds and structure. The highest temperature, and assumed highest pressure, occur in the core of the regional scale, southward plunging, F_3 Wake-Warren antiform (see STRUCTURE). This antiform, which postdates the metamorphic maximum, is interpreted to have uplifted the northern Raleigh block with respect to the southern Raleigh block and the adjacent Carolina slate belt block; thus, the highest grade assemblages, in both temperature and pressure, of this area are exposed in the northern Raleigh block.

The pressure assigned to the contact metamorphism associated with intrusion of the Sims granite is less well defined because of a lack of data, but it clearly lies below the triple point, crossing the andalusite and sillimanite stability fields. There may have been regional uplift before intrusion of the Sims pluton, or the intrusion may have heated the rocks from a lower pressure-temperature position on the regional curve - there is no close control on regional metamorphic conditions in the vicinity of the Sims pluton.

STRUCTURE

The eastern Piedmont of North Carolina comprises tectonic blocks separated by major mylonite zones. Discontinuities of lithology, structure, and metamorphic grade occur across these mylonite zones, while within blocks there is continuity of lithologic units and structures. The area of this study comprises portions of three major blocks: the easternmost part of the Carolina slate belt block; the Raleigh block; and the Roanoke Rapids block. Rocks within each of these blocks appear to have been subjected to a minimum of three ductile deformational events, the sequence of which is best defined in the southern half of the Raleigh block.

Style of Deformation

S_0 in the greenschist grade belts of the study area is layering of sedimentary or igneous origin. In the amphibolite grade belts, S_0 is a compositional layering of indeterminate origin, most premetamophic textures having been destroyed at this grade.

The first deformation (D_1) produced a penetrative S_1 foliation, generally consisting of the planar orientation of minerals, and commonly including some compositional segregation into metamorphic layering parallel to this foliation. D_1 also resulted in F_1 isoclinal folding of the preexisting compositional layering (S_0). S_1 and S_0 are commonly parallel on the limbs of these folds, and in high grade rocks they can only be differentiated in the hinge zones of the F_1 folds. F_1 folds occur at microscopic to outcrop scale, but no map scale F_1 folds have been defined.

The second deformation (D_2) produced a moderate to strong S_2 foliation comprising the planar orientation of minerals axial planar to F_2 folds, and less commonly, a crenulation cleavage in mica-rich S_1. F_2 folds are tight to isoclinal, and can commonly be differentiated from F_1 folds only by interference of the two generations. F_2 folds range from microscopic to regional in scale. The best defined regional scale F_2 fold is the Smithfield synform discussed below.

D_3 produced open to tight folds. S_3 is a weak to strong crenulation cleavage in schistose rocks, and a weak foliation of micas in less micaceous lithologies. F_3 folds range from microscopic to regional scale structures, they are differentiated from F_2 folds through interference of the two generations and overprinting of the foliations. S_3 generally has a N to NNE strike in the mapped area. This is parallel to the axial surfaces of the regional F_3 structures.

D_4 produced a weak S_4 crenulation cleavage and small open to tight F_4 folds which fold S_3. D_4 appears to have been of only local importance and is not discussed further.

Structural Interpretation

The study area has been subdivided into domains which show the character of structures within the Raleigh block, and the abrupt changes which occur across the mylonite zones. Major structures, structural domains, and equal area stereographic projections of structural data are shown in Figure 6.

Carolina Slate Belt Block

Subarea I is the easternmost part of the Carolina slate belt block. It is characterized by moderate to shallow, westward-dipping foliations, and generally westward plunging minor structures. S_3 is particularly strong in this area, occurring as a well-developed crenulation cleavage and spaced cleavage in micaceous, and even quite felsic, rocks. Well developed S_3 is very similar in appearance to S_2, and they are probably commonly confused for one another in this area.

Nutbush Creek Mylonite Zone

Subarea II comprises the Nutbush Creek mylonite zone (Casadevall, 1977), which is part of the Eastern Piedmont fault system of Hatcher and others (1977). In the area of this study, the Nutbush Creek

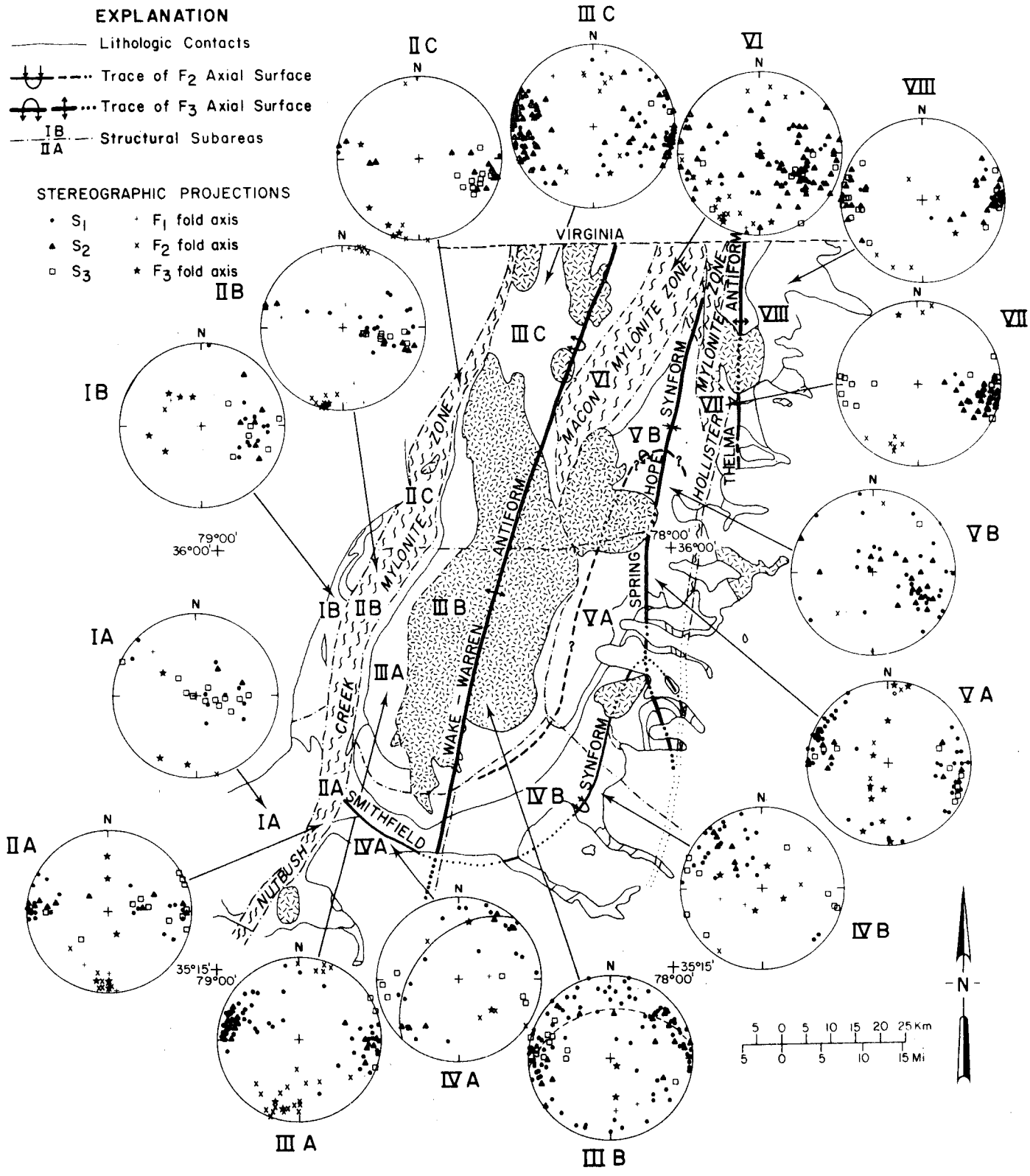

Figure 6. Major structures in the northeastern Piedmont of North Carolina, showing structural domains and equal area projections of data from these domains.

mylonite zone dips steeply westward near Lillington, N. C. in the south (subarea IIA), shallows and becomes relatively diffuse in the Raleigh, N. C., area (subarea IIB), then steepens to near vertical north of Henderson, N. C. (subarea IIC), where it is only a few hundred meters thick.

In subarea II, D_1 structures consist of isoclinal minor F_1 folds refolded by D_2. Plentiful F_2 folds are characterized by their tight to isoclinal form and strong axial plane and/or crenulation cleavage. S_3 occurs as a weak crenulation cleavage in lesser deformed rocks and a very strong mylonitic foliation and crenulation cleavage in mylonitized rocks. F_3 folds are generally, small open to tight structures.

The attitudes of mineral lineations and minor-fold hinge lines are typical of mylonite zones. These linear features are tightly grouped in a near horizontal attitude parallel to the length of the mylonite zone. The Nutbush Creek zone is typical of major mylonite zones in that the mylonitic textures are best developed in felsic rocks. Schists in the zone deform readily, but do not show the deformation well. Much of the movement in this area appears to have been in the tightly crenulated schists of the Smithfield Formation.

Wake-Warren F_3 Antiform

Subarea III comprises the F_3 Wake-Warren antiform (Parker, 1968), in the Raleigh belt. The western limb of this antiform (subarea IIIA) is characterized by steep to vertical foliation. Mineral lineations, as in subarea II, are near horizontal and trend parallel to strike of the rock unit, grouped around the attitude 10,S12W. S_1 and S_2 are strong axial planar foliations in this subarea. S_3 is a weak crenulation cleavage which increases in strength into the Nutbush Creek mylonite zone. There appear to be several tight to isoclinal map scale folds (probably F_2) in this area, but they were not be defined in this study. Parker (1979) describes folds in this area.

Subarea IIIB comprises the nose of the southern Raleigh belt portion of the Wake-Warren antiform. The complexity of F_1 and F_2 folding somewhat obscures the structures in stereographic projection (Fig. 6), but S_3 attitudes define the approximate F_3 axial surface N10E,70E. S_1 is widely dispersed, but poles to S_2 form a girdle defining the F_3 fold axis 50,S05E. F_2 folds in this subarea have axial surfaces dipping moderately southward - as is indicated by S_2 attitudes.

Subarea IIIC comprises the northern interior of the Raleigh belt. Structures in this area are poorly defined, but the general curvature of the foliation is similar to that of the western limb of the Wake-Warren antiform farther south. Here, however, the eastern limb is cut off in the Macon mylonite zone (Fig. 6).

Smithfield F_2 Synform

The Smithfield synform (Fig. 6) is a regional scale F_2 structure which has, in turn, been folded in the F_3 Wake-Warren antiform

(subarea IV) and F_3 Spring Hope synform (subarea V). The form of the Smithfield synform is characterized on the western limb of the Wake-Warren antiform (subarea IVA). On this limb of the F_3 structure, the F_2 Smithfield axial surface is approximately planar. In this area, S_1 forms a girdle defining the F_2 fold axis 45,S48E. The upright attitude of the synform in this area is indicated by the near vertical S_2 attitudes. The Smithfield synform is cut off on the west by the Nutbush Creek mylonite zone.

Subarea IVB encompasses that portion of the Smithfield synform on the eastern limb of the Wake-Warren antiform. In this area, poles to S_1 form a poor girdle defining the F_2 axis 0,N48E. This portion of the Smithfield synform is overturned to the north, with the axial surface N48E,55S, as generalized from S_2.

The Smithfield synform continues northeastward into subarea VA where it has been tightly folded in the Spring Hope synform, and is cut off on the east by the Hollister mylonite zone. Parallel and to the northwest of the Smithfield synform is a less well defined F_2 antiform. This is best shown by the outcrop pattern of the Stanhope Formation (Fig. 2) which is folded tightly in this antiform.

Spring Hope Synform

Subarea VA encompasses the F_3 Spring Hope synform south of the Castalia pluton (Fig. 6). The Spring Hope synform in this area is a tight, upright structure. Most foliations are tightly grouped on the limbs. The F_2 Smithfield synform has been refolded in the Spring Hope synform. The resultant F_3 folds plunge from both north and south into the trough of the Smithfield synform. The eastern limb of the Spring Hope synform is attenuated in the Hollister mylonite zone which cuts off the Smithfield synform, and forms the eastern boundary of the Raleigh block.

The Spring Hope synform north of the Castalia pluton (subarea VB) flattens out and becomes poorly defined. At its northern extremity, the synform is pinched out between the Macon and Hollister mylonite zones.

Macon Mylonite Zone

Subarea VI (Fig. 6) comprises the Macon mylonite zone. Rocks of this zone include protomylonite, mylonite, and phyllonite derived from gneisses of at least staurolite grade in the eastern Raleigh belt. The mylonitic foliation dips gently to moderately westward and has been folded, with the resultant complex foliation pattern in stereographic projection.

The dip of the mylonitic foliation under the Raleigh belt rocks suggests that this is a thrust fault with the amphibolite grade Raleigh belt rocks thrust eastward over the greenschist grade Eastern slate belt rocks.

Hollister Mylonite Zone

The Hollister mylonite zone, a branch of the eastern Piedmont fault system of Hatcher and others (1977), is a steeply-westward dipping zone of mylonite and phyllonite (subarea VII). Lineations (Fig. 6), as in the Nutbush Creek zone, are near horizontal and trend parallel to the strike of the zone. Aeromagnetic data (USGS, 1973c, 1976) indicates that the Hollister zone, which forms the eastern boundary of the Raleigh block, merges with the Augusta fault (Hatcher and others, 1977) under Coastal Plain cover to the south.

Although the Hollister mylonite zone, for most of its length, passes through Eastern slate belt rocks with no change in metamorphic grade, it is texturally distinct. The metavolcanic rocks outside the zone have a moderate muscovite-chlorite foliation but show only minor deformation of phenocrysts. Within the Hollister zone, isoclinal, and refolded isoclinal, folds dominate the texture. Phenocrysts are flattened and recrystallized, and a tight crenulation cleavage is commonly superposed on the phyllonite foliation.

The Hollister mylonite zone also passes through the Butterwood Creek granite. The southeastern part of the pluton, away from the mylonite zone, is essentially undeformed, with only slightly undulatory extinction of the quartz, and no measurable foliation. The part of the pluton close to the mylonite zone on the east, and all of the pluton to the west of the mylonite zone, has a strong tectonic foliation which increases in intensity to protomylonite and mylonite in the Hollister zone.

Roanoke Rapids Block

The Roanoke Rapids block comprises that part of the exposed North Carolina Piedmont east of the Hollister mylonite zone (subarea VIII). The pattern of rock types, metamorphic grade, and the few structural measurements in this area, suggest a southward plunging antiformal structure for this area, with the hornblende-biotite gneiss north of the Butterwood Creek granite at its core. Within the block, a high-angle fault separates the biotite-hornblende gneiss from felsic metavolanic rocks to the east. Lack of exposures prohibits more detailed structural interpretation of this area.

Structural Summary

The structural history of the easternmost North Carolina Piedmont is dominated by three major ductile deformational events. D_1 is represented by a strong foliation and minor folds. D_2 regional scale folding produced the Smithfield synform, a tight to isoclinal structure which is overturned to the north, and a poorly defined parallel antiformal structure to the northwest (Fig. 6, and cross section in Fig. 7c). D_3 refolded the rocks into a series of north-northeast trending, tight- to open-F_3 structures: the Wake-Warren antiform, Spring Hope synform, and Thelma antiform. These are, in part, separated from one another by major mylonite zones, the Nutbush Creek,

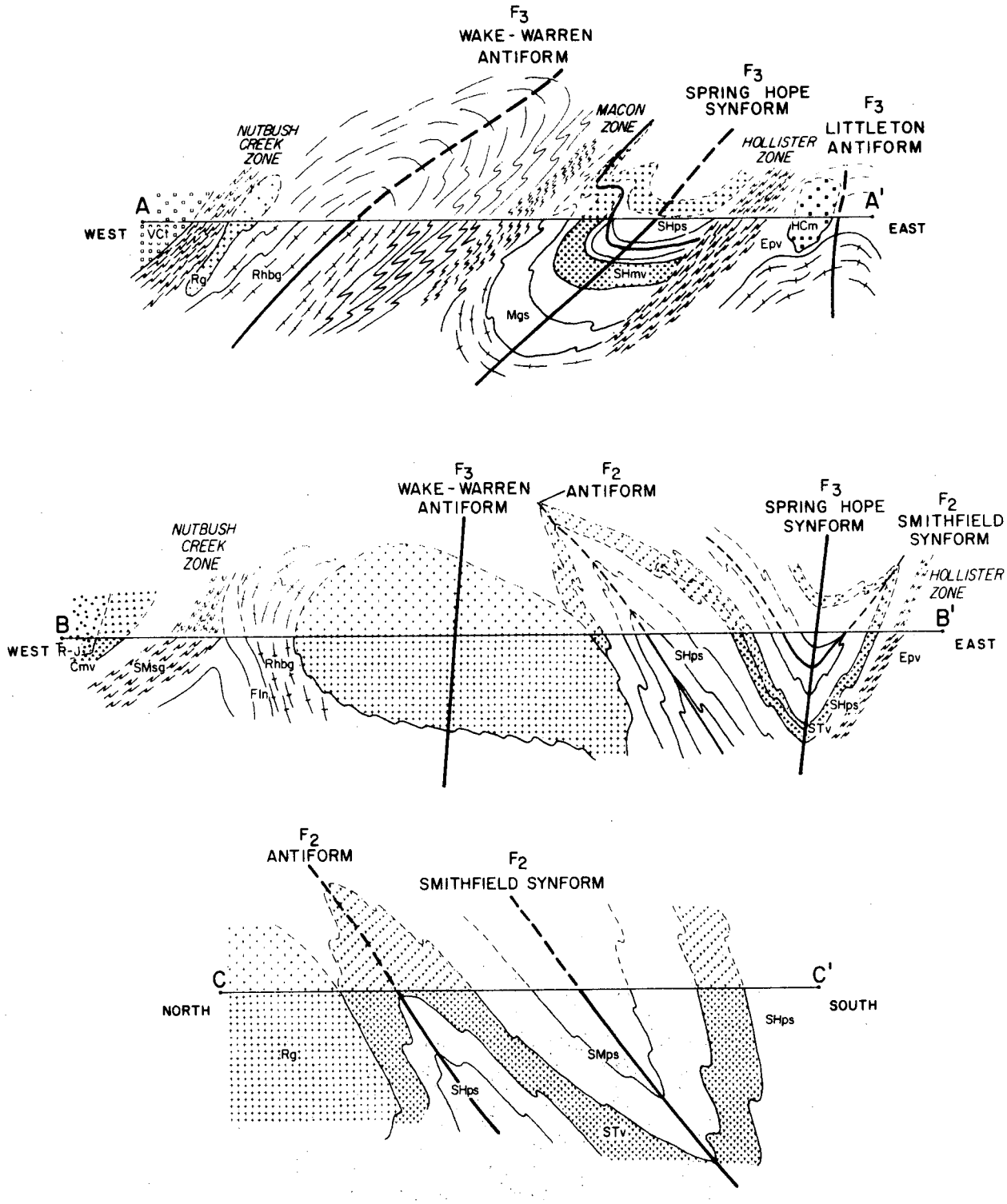

Figure 7. Schematic cross sections (locations, Fig. 7). (a) The northern Raleigh block; (b)the southern Raleigh block; (c) the Smithfield F_2 synform.

Macon, and Hollister zones, which developed on the attenuated limbs of the F_3 structures. Rather schematic E-W cross sections (Fig. 7a and 7b) show the approximate form and attitude of these southward-plunging folds. The Wake-Warren antiform is overturned to the East in the North (Fig. 7a), and approximately upright in the South (Fig. 7b). All three major mylonite zones dip moderately to steeply westward.

Geophysics

Aeromagnetic Anomalies

Aeromagnetic anomaly maps (USGS, 1973a,b,c, 1974, 1976, 1977a,b) were used extensively to define limits of stratigraphic units exposed only at widely scattered outcrops. This process was particularly useful in the southern half of the Raleigh block, where highly magnetic metavolcanic units contrast strikingly with low magnetic metasedimentary units. On the other hand, aeroamgnetic data could not differentiate between the Rolesville granite and surrounding hornblende-biotite gneiss. In general, the amphibolite grade gneisses and foliated granites have a flat magnetic signature, while the greenschist grade rocks have greater contrast in their magnetic character.

The Nutbush Creek and Hollister mylonite zones have distinct magnetic signatures where they dip steeply. Magnetic anomalies on either side of the mylonites end at these zones, or approach the zones asymptotically. The asymptotic approach is particularly evident in the Raleigh area along the Nutbush Creek zone, where moderately dipping rock units give relatively dispersed anomalies. The Macon mylonite zone has a less distinct magnetic signature, consisting of a series of parallel linear anomalies which have been openly folded. The only anomalies to cross the mylonite zones undeflected are those caused by post-metamorphic diabase dikes.

Gravity

In general, the Raleigh belt comprises relatively low density rocks, and the Carolina slate belt and Eastern slate belt comprise higher density rocks, based on Department of Defense Gravity Data (1976). Large granitoid bodies - for example, the Rolesville and Rocky Mount plutons - produce major gravity lows. Smaller plutons - for example, the Butterwood Creek and Sims plutons - are not well defined because of the wide spacing of gravity stations.

These contrasting gravity signatures add further definition to the attitudes of major mylonite zones. Where the dip of a mylonite zone is moderate to shallow, as in the Nutbush Creek mylonite zone near Raleigh, the gravity gradient from Carolina slate belt high to Raleigh belt low is gradual. In contrast, where the Nutbush Creek mylonite narrows and steepens north of Henderson, the mylonite exposures and aeromagnetic lineament coincide with the eastern edge of a steep gravity gradient from the Carolina slate belt into the Raleigh belt. This supports the interpretation of a steeply-westward dipping mylonitic zone, with Carolina slate belt rocks overlying Raleigh belt rocks.

In the areas of the Macon and Hollister mylonite zones, the gravity gradients are less abrupt. This agrees well with the shallow dip of the Macon zone, and the lack of contrast in rock types across the Hollister zone.

DISCUSSION AND CONCLUSIONS

The stratigraphic sequences within the Raleigh block and adjacent blocks of the northeastern North Carolina Piedmont comprise metasedimentary, metavolcanic, and metamorphosed shallow intrusive rocks which are probably equivalent in age to the late Precambrian and early Paleozoic Carolina slate belt rocks farther west which have been dated (Glover and Sinha, 1973; St. Jean, 1973; Fullagar, 1971; Black, 1978; Wright and Seiders, 1980). Hornblende-biotite gneiss of the Raleigh block and Roanoke Rapids block may possibly be older - they do not appear to be equivalent to any units in the Eastern slate belt, and they are apparently at the bases of the sections (Fig. 3).

The rocks of the Raleigh block and adjacent areas have been deformed in a minimum of three major ductile deformational events. Of these, D_1, although it produced a strong foliation and microscopic to mesoscopic folds, produced no mappable megascopic folds. D_2 and D_3 events produced microscopic to megascopic folds which dominate the map pattern. Tight F_2, regional-scale folds, including the Smithfield synform, were refolded by non-coaxial, open-to-close, F_3, regional-scale folds, the Wake-Warren, Spring Hope, and Thelma structures. These D_3 structures plunge moderately southward.

Three major mylonite zones, occurring on the limbs of the D_3 structures (Figs. 6 and 7), appear to have formed as a result of attenuation of F_3 fold limbs. Two of these mylonite zones - the Nutbush Creek and Hollister zones - divide the area into three blocks - the Carolina slate belt block, the Raleigh block, and the Roanoke Rapids block.

The major metamorphic event in this area appears to have been post- or syn-D_2 and pre-D_3. This is best illustrated in the southern Raleigh block, where the greenschist grade rocks of the Smithfield and Stanhope formations can be traced up grade along strike of S_0, and the S_2 axial surfaces, into the amphibolite grade rocks of the Crabtree and Clayton formations. Metamorphic isograds cut across the prexisting F_2 folds. In contrast, the isograds conform to the shape of the F_3 folds. Areas of highest metamorphic grade occur in northern, more uplifted, cores of the southward-plunging, F_3 antiforms. The lowest-grade rocks occur in F_3 synforms and in the southern part of the area.

Discontinuities of isograds occur along the mylonite zones, indicating that at least part of the movement on these zones occurred after the metamorphic peak. Retrograde metamorphism, associated with mylonitization, also testifies to the late movement along these zones, postdating the major metamorphic event. These three mylonite zones dip moderately to steeply westward, and the gravity data suggest that at least the Nutbush Creek zone dips westward to great depth. Sense

of movement on the mylonite zones is known only to the extent implied in the cross sections (Figs. 7a and 7b) which require that the high grade rocks of the Wake-Warren and Thelma antiforms were uplifted along these zones with respect to the lower grade Carolina and Eastern slate belt rocks. Horizontal movement on these zones has not been determined.

Recent K/Ar and Rb/Sr studies by Kish and others (1979) suggest that metamorphism in the Carolina slate belt to the west in the Albemarle area peaked at about 480 Ma, while rocks in the Raleigh belt - specifically the 313 $\pm$ 8 Ma old Buggs Island granite - were ductilly deformed much later. It has been suggested (Snoke and others, 1980; Durrant and others, 1980) that there is a belt of Alleghanian (Hercynian) metamorphism and/or deformation along the easternmost Piedmont from Georgia to Virginia. Metamorphism and the D_3 deformational event in the Raleigh block may also be of Alleghanian age.

REFERENCES

Becker, S. W. and Farrar, S. S., 1977, The Rolesville batholith: in, Costain and others, Evaluation and Targeting of Geothermal Resources in the Southeastern United States, Progress Report November 1, 1976 - March 31, 1977.

Black, W. W., 1978, Chemical characteristics and Rb/Sr ages of metavolcanics from the Carolina slate belt of North Carolina: Geological Society of America Abstracts with Programs, v. 10, p. 162-163.

Bobyarchick, A. R. and Glover, L., III, 1979, Deformation and metamorphism in the Hylas zone and adjacent parts of the eastern Piedmont in Virginia: Geological Society of America Bulletin, v. 90, p. 739-752.

Casadevall, T., 1977, The Nutbush Creek dislocation, Vance County, North Carolina, and Mecklenberg County, Virginia - a probable fault of regional significance: Geological Society of America Abstracts with Programs, v. 9, p. 127-128.

Casadevall, T., and Rye, R. O., 1980, The Tungsten Queen deposit, Hamme district, Vance County, North Carolina: A stable isotope study of a metaorphosed quartz-huebnerite vein: Economic Geology, v. 75, p. 523-537.

Clark, H. B., Costain, J. K., and Glover, L., III, 1978, Structural and seismic reflectin studies of the Brevard ductile deformation zone near Rosman, North Carolina: American Journal of Science, v. 278, p. 419-441.

Cook, F. A., Albaugh, D. S., Brown, L. D., Kaufman, S., Oliver, J. E., and Hatcher, R. D., Jr., 1979, Thin-skinned tectonics in the crystalline southern Appalachians; COCORP seismic-reflection profiling of the Blue Ridge and Piedmont: Geology, v. 7, p. 563-567.

Councill, R. J., 1954, Commercial granites of North Carolina: North Carolina Division of Mineral Resources Bulletin 67, 59 p.

Durrant, J. M., Sutter, J. F., and Glover, L., III, 1980, Evidence for an Alleghanian (Hercynian?) metamorphic event in the Piedmont province near Richmond, Virginia: Geological Society of America Abstracts with Programs, v. 12, p. 176.

Ferry, J. M. and Spear, F. S., 1978, Experimental calibration of the partitioning of Fe and Mg between biotite and garnet: Contributions to Mineralogy and Petrology, v. 66, p. 113-117.

Fisher, G. W., Pettijohn, F. J., Reed, J. C., Jr., and Weaver, K. N., eds.,1970, Tectonic map of the central and southern Appalachians; in, Studies of Appalachian Geology: Central and southern: New York, Interscience, 460 p.

Foose, M. P., Slack, J. F., and Casadevall, T., 1980, Textrual and structural evidence for a predeformation hydrothermal origin of the Tungsten Queen deposit, Hamme district, North Carolina: Economic Geology, v. 75, p. 515-522.

Fortson, C. W., 1958, Geology of the Crabtree Creek area, northwest of Raleigh, North Carolina (M.S. thesis): Raleigh, North Carolina State College, 101 p.

Fullagar, P. D. and Butler, J. R., 1979, 325 to 265 m.y.-old post-metamorphic granitic plutons in the Piedmont of the southeastern Appalachians: American Journal of Science, v. 279, p. 161-185.

Ganguly, J., 1972, Staurolite stability and related parageneses: Theory, experiments, and applications: Journal of Petrology, v. 13, p. 335-365.

Glover, L., III and Sinha, A. K., 1973, The Virgilina deformation, a late Precambrian(?) orogenic event in the central Piedmont of Virginia and North Carolina: American Journal of Science, v. 273-A, p. 234-251.

Greenwood, H. J., 1976, Metamorphism at moderate temperatures and pressures: in, Bailey, D. K. and Macdonald, R., eds., The Evolution of the Crystalline rocks: London, The Academic Press, p. 187-259.

Harris, L. D. and Bayer, K. C., 1979, Sequential development of the Appalachian orogen above a master decollement - A hypothesis: Geology: v. 7, p. 568-572.

Harvey, B. W., 1974, The microscopic petrography and ore microscopy of the Boy Scout-Jones molybdenum prospect, Halifax County, North Carolina (M.S. thesis): Raleigh, North Carolina State University, 85 p.

Hatcher, R. D., Jr. and Zietz, I., 1978, Thin crystalline thrust sheets in the southern Appalachian Inner Piedmont and Blue Ridge: Interpretation based on regional aeromagnetic data: Geological Society of America Abstracts with Programs, v. 10, p. 417.

Hatcher, R. D., Jr., Howell, D. E., and Talwani, P., 1977, Eastern Piedmont fault system: speculation on its extent: Geology, v. 5, p. 636-640.

Julian, E. L., 1972, The Castalia adamellite in Franklin and Nash Counties, North Carolina, and the petrogenesis of some associated aplites and pegmatites (M.S. thesis): Raleigh, North Carolina State University, 61 p.

King, P. B., 1955, A geologic section across the southern Appalachians: An outline of the geology in the segment in Tennessee, North Carolina, and South Carolina: in, Russell, R. J., ed., Guides to Southeastern Geology: Boulder, Co., Geological Society of America, p. 332-373.

Kish, S. A., and Fullagar, P. D., 1978, Summary of geochronological data for Late Paleozoic plutons from high grade metamorphic belts of the eastern Piedmont of North Carolina, South Carolina, and Virginia: in, Snoke, A. W., ed., Geological investigations of the eastern Piedmont, southern Appalachians: Carolina Geological Society, 1978 Guidebook, South Carolina Geological Survey, South Carolina State Development Board, p. 61-64.

Kish, S. A., Butler, J. R., and Fullagar, P. D., 1979, The timing of metamorphism and deformation in the central and eastern Piedmont of North Carolina: Geological Society of America Abstracts with Programs, v. 11, p. 184-185.

Long, L. T., 1979, The Carolina slate belt - Evidence of a continental rift zone: Geology, v. 7, p. 180-184.

Miyashiro, A., 1973, Metamorphism and metamorphic belts: London, Allen & Unwin, p. 202.

Mundorff, M. J., 1946, Ground water in the Halifax area, North Carolina: North Carolina Division of Mineral Resources Bulletin 51, 76 p.

North Carolina Department of Conservation and Development, Division of Mineral Resources, 1958, Geologic Map of North Carolina, scale 1:500,000.

Parker, J. M., III, 1963, Geologic setting of the Hamme tungsten district North Carolina and Virginia: U. S. Geological Survey Bulletin 1122-G, p. G1-G69.

Parker, J. M., III, 1968, Structure of easternmost North Carolina Piedmont: Southeastern Geology, v. 9, p. 117-131.

Parker, J. M., III, 1979, Geology and mineral resources of Wake County: North Carolina Division of Mineral Resources Bulletin 86, 122 p.

Perchuk, L. L., 1977, Thermodynamic control of metamorphic processes: in, Saxena and Bhattacharji, eds., Energetics of Geological Processes, Springer-Verlag, p. 286-352.

Robertson, A. F., McIntosh, F. K., and Ballard, T. J., 1947, Boy Scout-Jones and Moss-Richardson molybdenum deposits, Halifax County, N. C.: U. S. Bureau of Mines Report of Investigations 4156.

St. Jean, J., Jr., 1973, A new Cambrian trilobite from the Piedmont of North Carolina: American Journal of Science, v. 273-A, p. 196-216.

Secor, D. T., Jr., and Snoke, A. W., 1978, Stratigraphy, structure, and plutonism in the central South Carolina Piedmont: in, Snoke, A. W., ed., Geological investigations of the eastern Piedmont, southern Appalachians: Carolina Geological Society 1978 Guidebook, South Carolina Geological Survey, South Carolina State Development Board, p. 65-123.

Snoke, A. W., Kish, S. A., and Secor, D. T., Jr., 1980, Deformed Hercynian granitic rocks from the Piedmont of South Carolina: American Journal of Science (in press).

Stoddard, E. F. and McDaniel, R. D., 1979, Geology of the Raleigh belt in eastern Franklin and Warren Counties, North Carolina: A preliminary report: Geological Society of America Abstracts with Programs, v. 11, p. 214.

Stoddard, E. F. and Teseneer, R. L., 1978, Associated mafic and ultramafic igneous rocks, southwestern Halifax County, North Carolina: Geological Society of America Abstracts with Programs, v. 10, p. 199.

Stuckey, J. L., 1965, North Carolina: Its geology and mineral resources: Raleigh, North Carolina Department of Conservation and Development, 550 p.

Thompson, A. B., 1976, Mineral reactions in pelitic rocks: II. Calculation of some P-T-X (Fe-Mg) phase relations: American Journal of Science, v. 276, p. 425-454.

United States Geological Survey, 1973a, Aeromagnetic map of the Henderson quadrangle and parts of the Louisburg and Boydton quadrangles, North Carolina: U. S. Geological Survey Geophysical Investigations Map GP-884.

United States Geological Survey, 1973b, Aeromagnetic map of the Norlina quadrangle and parts of the Castalia and South Hill quadrangles, North Carolina: U. S. Geological Survey Geophysical Investigations Map GP-885.

United States Geological Survey, 1973a, Aeromagnetic map of the Essex-Roanoke Rapids area, North Carolina: U. S. Geological Survey, Geophysical Investigations Map GP-886.

United States Geological Survey, 1974, Aeromagnetic map of parts of the Greensboro and Raleigh 1° by 2° quadrangles, North Carolina: U. S. Geological Survey Open-file Map 74-29.

United States Geological Survey, 1976, Aeromagnetic maps of parts of Georgia, South Carolina, and North Carolina, Coastal Plains Regional Commission: U. S. Geological Survey Open-file Map 76-181.

United States Geological Survey, 1977a, Aeromagnetic map of north-central North Carolina: U. S. Geological Survey Open-file Map 77-192.

United States Geological Survey, 1977b, Aeromagnetic map of the south-central North Carolina: U. S. Geological Survey Open-file Map 77-205.

Watson, T. L. and Laney, F. B., 1906, The building and ornamental stones of North Carolina: North Carolina Geological Survey Bulletin 2, 283 p.

Wedemeyer, R. G. and Spruill, R. K., 1980, Geochemistry and geochronology of the Sims granite, eastern Carolina slate belt, North Carolina: Geological Society of America Abstracts with Programs, v. 12, p. 211.

Wilson, W. F. and Carpenter, P. A., 1975, Region J geology: A guide for North Carolina mineral resource development and land use planning: North Carolina Mineral Resources Section, Regional Geology Series 1, 76 p.

Wright, J. E. and Seiders, V. M., 1980, Age of zircon from volcanic rocks of the central North Carolina Piedmont and tectonic implications for the Carolina volcanic slate belt: Geological Society of America Bulletin, v. 91, p. 287-294.

Appendix 1. Mineral assemblages in rock units of the northeastern North Carolina Piedmont. Minerals are listed in order of decreasing abundance. Individual thin section assemblages are noted by sample numbers in parenthesis.

Carolina Slate Belt Block

Cary Formation

Greenstone

epidote + chlorite + quartz ± titanite

Quartz-albite crystal metatuff

albite + quartz + muscovite + chlorite + epidote + opaque

Phyllite

muscovite + quartz + chlorite + epidote + opaque

Kyanite metaquartzite

(F7-473) quartz + kyanite + pyrophyllite + hematite

Fuquay-Varina Formation

Buckhorn Creek Metatrondjemite-quartz metakeratophyre

albite + quartz + microcline + muscovite + biotite + titanite + epidote + allanite + opaque ± garnet

Albite-quartz crystal metatuff

albite + quartz + K-feldspar + muscovite + biotite ± chlorite ± garnet ± epidote ± titanite ± opaque ± calcite ± tourmaline ± hematite

Biotite schist

biotite + quartz + muscovite + albite + opaque

Beaverdam Mafic Complex

Metagabbro

hornblende + actinolite + oligoclase + clinozoisite (Parker,1979)

Quartz metadiorite-metagranodiorite

albite + quartz + microcline + muscovite + opaque + epidote + chlorite ± hornblende ± biotite ± garnet ± titanite ± apatite

Vance County Metatrondjemite

albite (and oligoclase) + quartz + K-feldspar + biotite + chlorite

Raleigh Block

Raleigh Gneiss

Hornblende-biotite gneiss

quartz + plagioclase ($An_{23}Ab_{76}Or_1$) + perthitic microcline + biotite (Fe/(Fe+Mg)=0.57) + hornblende (Fe/(Fe+Mg)=0.64) + opaque + zircon + titanite + apatite + allanite ± garnet + retrograde minerals (chlorite + muscovite + epidote ± hematite)

Muscovite schist

(F8-433) quartz + muscovite + garnet + sillimanite + staurolite + chlorite + hematite + tourmaline

(F8-455) quartz + muscovite + garnet + biotite + chlorite + sillimanite + hematite

Falls Leacogneiss

microcline + quartz + albite ($An_6Ab_{93}Or_1$) + magnetite ± garnet ± biotite ± titanite ± allanite ± apatite ± chlorite ± muscovite ± epidote ± zircon

Macon Formation

Quartz-plagioclase gneiss

plagioclase ($An_{21}Ab_{78}Or_1$-$An_{28}Ab_{71}Or_1$) + K-feldspar + quartz + biotite + muscovite + chlorite + epidote + opaques + apatite + titanite

Aluminous schist

(F8-107) muscovite + quartz + chloritoid + relict sillimanite + chlorite + opaque

(F8-129) muscovite + quartz + chloritoid + garnet + chlorite + relict sillimanite + tourmaline + opaque

Quartz-muscovite schist

(F8-370) quartz + muscovite + chlorite + garnet + staurolite + opaque + hematite

Phyllonite

muscovite + quartz + chlorite + opaque + tourmaline + hematite

Spring Hope Formation

Phyllite, metamudstone-metasiltstone

quartz + muscovite + chlorite ± albite ± opaque ± epidote ± hematite

Plagioclase and quartz-plagioclase crystal metatuff

quartz + albite + muscovite + opaque + epidote ± biotite

Greenstone-metabasalt

epidote + albite + quartz + opaque ± chlorite ± actinolite ± muscovite

Stanhope Formation

Greenstone-metabasalt

epidote + quartz ± chlorite ± actinolite ± albite ± calcite ± opaques ± biotite

Albite crystal and crystal-lithic metatuff

albite + quartz + muscovite + epidote + chlorite + opaque

Amphibolite

hornblende + plagioclase ± quartz ± opaque ± epidote ± chlorite ± titanite

Felsic gneiss

plagioclase + quartz + K-feldspar + muscovite + epidote + opaque ± titanite ± garnet ± calcite ± biotite

Smithfield Formation

Metasiltstone-metamudstone-phyllite

quartz + albite + muscovite + chlorite + epidote + opaques ± titanite ± zircon ± tourmaline ± hematite ± biotite

Princeton felsic metatuff and flows

albite + quartz + epidote + muscovite ± calcite ± opaque ± titanite ± zircon ± garnet

Muscovite-biotite-quartz-albite gneiss

albite + quartz + biotite + muscovite + microcline + opaque ± tourmaline ± apatite ± chlorite ± titanite ± calcite ± epidote

Quartz-muscovite schist and metaquartzite

quartz + muscovite + plagioclase + magnetite ± calcite

Muscovite-biotite schist

(F7-499) quartz + muscovite + chlorite + biotite + albite + garnet + opaque + chloritoid + tourmaline

(F7-399-3) quartz + plagioclase + muscovite + biotite + garnet + staurolite + chlorite + opaque

(F7-420-2) quartz + biotite + garnet + plagioclase + muscovite + staurolite + chlorite

(F7-401) quartz + biotite + muscovite + garnet + staurolite + kyanite + plagioclase + opaque + chlorite

(F7-434) quartz + biotite + muscovite + plagioclase + garnet + staurolite + kyanite

Muscovite-graphite schist

(F7-392) muscovite + staurolite + garnet + graphite + quartz

Amphibolite

hornblende + plagioclase + opaque + chlorite + epidote + quartz ± titanite

Roanoke Rapids Block

Littleton Gneiss

Hornblende-biotite gneiss

quartz + plagioclase (oligoclase) + microcline + biotite + hornblende + opaque ± zircon ± titanite ± allanite ± apatite + secondary (epidote + muscovite + chlorite)

Bens Creek Leucogneiss

microcline + quartz + albite + biotite + magnetite ± garnet ± titanite ± apatite ± chlorite ± epidote ± calcite ± zircon ± muscovite

Roanoke Rapids Complex

Metatrondjemite

albite + hornblende + actinolite + biotite + quartz + K-feldspar + epidote + chlorite + muscovite + titanite + opaque

Quartz metakeratophyre

albite + quartz + K-feldspar + biotite + epidote + muscovite + garnet

Quartz-plagioclase crystal-lithic metatuff

albite + quartz + microcline + muscovite ± calcite ± epidote ± biotite ± chlorite ± titanite ± garnet ± opaque

Phyllite

muscovite + quartz + chlorite ± epidote ± albite

Metagraywacke

quartz + albite + calcite + epidote + chlorite + opaque + muscovite ± opaque ± tourmaline

Easonburg Formation

Plagioclase crystal metatuff

albite + quartz + biotite + muscovite + epidote + chlorite + opaque

Phyllite

muscovite + quartz + chlorite + hematite

Halifax County Mafic Complex

Metagabbro

chlorite + amphibole + relict (clinopyroxene + olivine + plagioclase) + epidote + ? (Stoddard & Teseneer, 1978)

Ultramafic rocks

pyroxenite, wehrlite, lherzolite (Stoddard & Teseneer, 1978)

Petrography of the Basement Portion of the CP14A Drillcore, Southport, North Carolina

by
Stewart S. Farrar
Orogenic Studies Laboratory

Location

The CP14A drillhole, Lat. 33°56.9', Long. 78°00.0', near Southport, North Carolina, intercepted crystalline basement rocks at a depth of 479 m (1570 ft), and was continuously cored to a depth of 568 m (1864 ft), resulting in 89 m (294 ft) of 3.5 cm diameter core.

Petrography

The drillcore consists dominantly of tonalitic biotite-amphibole-quartz-plagioclase gneiss (samples 1707, 1779, and 1860, Table 1 and Fig. 1).

Within this gneiss many 1-10 cm thick layers of amphibolite gneiss (sample 1850, Table 1) occur parallel to the prominent tectonic foliation, which is defined by the planar orientation of minerals. There are also a few 1-2 cm thick aplite dikes and one leucotonalite dike (sample 1785.2, Table 1) in the core (Fig. 2). The thin aplite dikes are the only facies in the core which contain plentiful K-feldspar. Low temperature, brittle deformation has resulted in numerous fractures, adjacent to which alteration has formed a retrograde, greenschist facies assemblage.

Table 1.
Modal* analyses of samples from the CP14A (Southport) drillcore.

	1785.2**	1707	1779	1860	1850
Plagioclase	51.2	48.0	48.1	50.2	18.6
Quartz	38.0	35.5	21.4	27.6	-
K-feldspar	6.1	0.2	-	0.1	-
Biotite	0.2	7.9	13.4	12.0	3.5
Amphibole	-	7.0	14.4	9.1	70.5
Epidote	0.4	0.2	1.6	0.6	1.9
Chlorite	0.4	tr	tr	tr	5.4
Muscovite	2.6	tr	tr	tr	tr
Accessories	tr	0.4	0.4	0.4	0.1

*Thin section modes basd on 1000 points.
**Samples are labeled according to depth in feet.

The medium-grained, dark gray, tonalitic biotite amphibole-quartz-plagioclase gneiss has accessory K-feldspar, magnetite, titanite, ± zircon, ± apatite, ± allanite. Secondary epidote, chlorite,

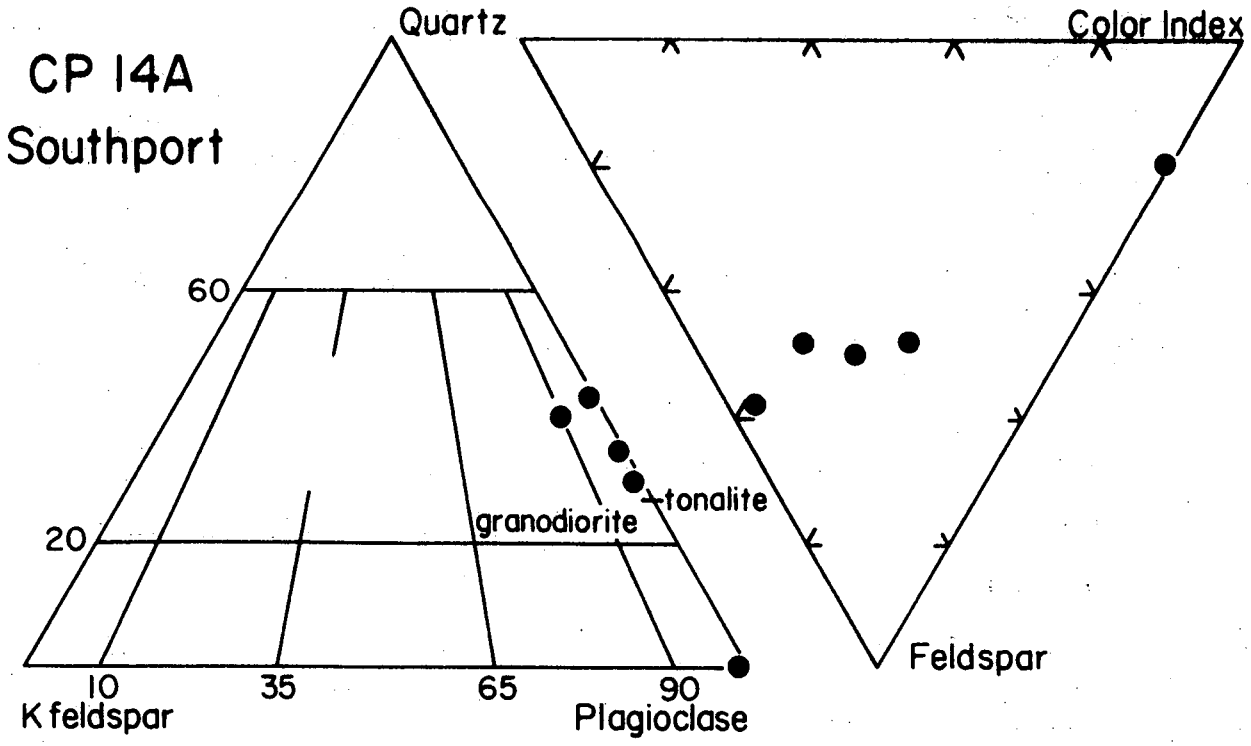

Figure 1. Modal variation of quartz-K feldspar-plagioclase, and quartz-total feldspar-color index in the CP14A (Southport) drillcore. IUGS Subcommission on the Systematics of Igneous Rocks classification.

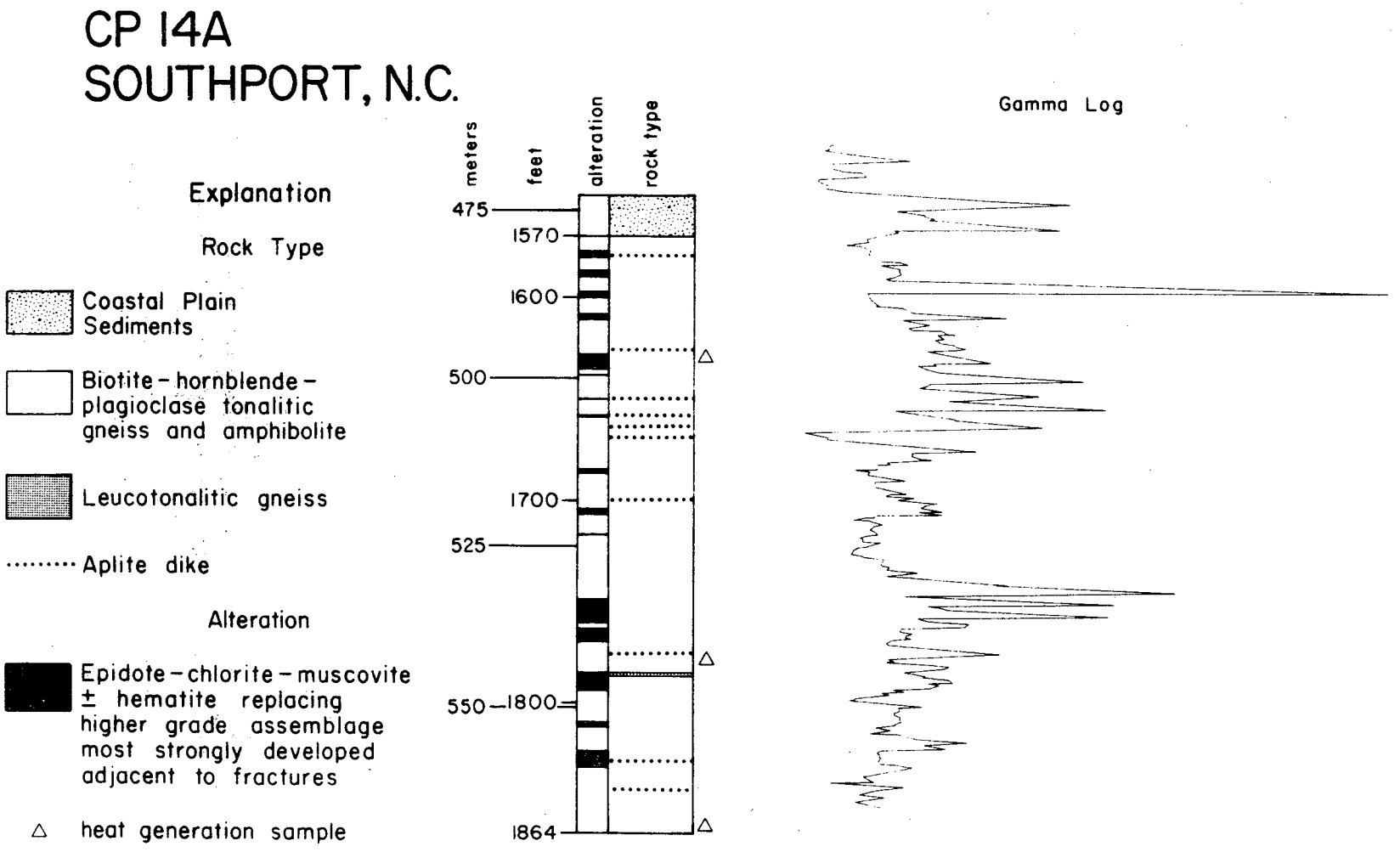

Figure 2. Lithologic and gamma log of the crystalline basement portion of the CP14A (Southport) drillcore.

muscovite, and calcite are present in trace amounts in most of the gneiss.

The fine- to medium-grained, very dark gray, amphibolite gneiss comprises biotite, plagioclase, hornblende, and accessory pyrite, magnetite(?), and apatite. Secondary minerals include muscovite, epidote, chlorite and calcite.

The fine-grained, inequigranular, leucotonalite dike has more K-feldspar than the major tonalitic gneiss, little biotite, and no amphibole (sample 1785.2, Table 1). Accessory minerals include opaque oxides, apatite, and zircon. Secondary minerals include epidote, chlorite, and muscovite. K-feldspar is restricted to the groundmass around the coarser plagioclase.

The thin, fine-grained, aplite dikes consist of plagioclase, quartz, and K-feldspar with accessory biotite, opaque oxide, titanite, allanite, and secondary chlorite, epidote, and muscovite. This and all other facies of the core are foliated.

Zones of alteration occur adjacent to fractures in the core. Within these zones there is nearly complete alteration of the preexisting assemblage to chlorite + epidote + quartz + calcite.

Heat generation in the tonalitic gneiss is uniformly low (Table 2). The gamma log of this core (Fig. 2) varies because of the amphibolite layers which have even lower heat generation than the tonalite gneiss. There are also several positive gamma log spikes, some of which correlate to the thin aplite dikes, others of which are not explained by the lithologic log.

Table 2.
Heat generation.

Depth in feet	U, ppm	Th, ppm	K, wt %	Heat generation x 10^{-13} cal/cm^3 sec
1630	1.5	6.4	1.4	2.3
1778	0.9	5.2	1.3	1.7
1859	0.6	3.7	1.1	1.2

Mineralogy

Plagioclase. Plagioclase compositions in the CP14A core are highly variable between samples, but relatively constant within a single sample (Table 3). Plagioclase from unaltered tonalitic gneiss (1707, An_{40-42}) and unaltered amphibolite (1850, An_{64-70}) are highly calcic, which is typical of amphibolite grade for these rock compositions. Plagioclase from the greenschist grade assemblages of the altered zones of the core are albites (1753.5 and 1825, An_1).

TABLE 3. PLAGIOCLASE ANALYSES FOR THE CP14A CORE

	1	2	3	4	5	6	7
SIO2	56.36	57.00	57.65	67.76	67.82	51.24	49.44
TIO2	0.14	0.11	0.10	0.22	0.17	0.15	0.11
A2O3	25.75	26.15	26.17	19.74	19.02	29.85	30.90
FEO	0.03	0.06	0.10	0.0	0.0	0.07	0.10
MGO	0.02	0.0	0.0	0.0	0.0	0.03	0.0
MNO	0.0	0.0	0.0	0.0	0.0	0.0	0.0
CAO	8.48	7.89	8.07	0.10	0.16	13.11	14.13
NA2O	6.35	6.44	6.21	11.44	11.02	3.97	3.40
K2O	0.17	0.23	0.28	0.01	0.07	0.06	0.03
SUM	97.30	97.88	98.58	99.27	98.26	98.48	98.11
SI	2.593 *	2.601 *	2.611 *	2.979 *	3.007 *	2.362 *	2.297 *
AL	1.396 3.989	1.406 4.008	1.397 4.007	1.023 4.002	0.994 4.001	1.622 3.984	1.691 3.988
CA	0.418 *	0.386 *	0.392 *	0.005 *	0.008 *	0.648 *	0.703 *
NA	0.566 *	0.570 *	0.545 *	0.975 *	0.947 *	0.355 *	0.306 *
K	0.010 *	0.013 *	0.016 *	0.001 *	0.004 *	0.004 *	0.002 *
FE	0.001 *	0.002 *	0.004 *	0.0 *	0.0 *	0.003 *	0.004 *
TI	0.005 *	0.004 *	0.003 *	0.007 *	0.006 *	0.005 *	0.004 *
MG	0.001 *	0.0 *	0.0 *	0.0 *	0.0 *	0.002 *	0.0 *
MN	0.0 1.002	0.0 0.975	0.0 0.960	0.0 0.988	0.0 0.965	0.0 1.016	0.0 1.019
O	8.000 *	8.000 *	8.000 *	8.000 *	8.000 *	8.000 *	8.000 *
AN	42.04	39.81	41.09	0.48	0.79	64.37	69.54
AB	56.96	58.81	57.22	99.46	98.79	35.28	30.28
OR	1.00	1.38	1.70	0.06	0.41	0.35	0.18
F/M	0.842	0.0	0.0	0.0	0.0	1.309	0.0
F/FM	0.457	0.0	0.0	0.0	0.0	0.567	0.0

1 CP14A 1707 PLAG 1
2 CP14A 1707 ZONED PLAG MID
3 CP14A 1707 ZONED PLAG CORE
4 CP14A 1753.5 PLAG 1
5 CP14A 1825 PLAG 2
6 CP14A 1850 PLAG 1
7 CP14A 1850 PLAG 2

Amphibole. Amphibole, which is a plentiful phase in both the tonalitic gneiss and amphibolite, is pleochroic X = yellow-green, Y = olive-green, Z = blue-green. Amphibole of the tonalitic gneiss has Fe/(Fe+Mg) = 0.44-0.49 (samples 1707 and 1753.5, Table 4). Amphibole of the amphibolite has Fe/(Fe+Mg) = 0.32-0.35 (Sample 1850,Table 4). Both of these amphiboles are tschermakitic hornblende according to the classification of Leake (1978).

Biotite. Biotite in the CP14A core is of intermediate composition, with a distinct break between that of the amphibolite and that of the tonalitic gneiss (Table 5). Biotite of the tonalitic gneiss has Fe/(Fe+Mg) = 0.47-0.49 and tetrahedral Al between 2.44 and 2.45. Biotite of the amphibolite is more magnesian and aluminous, with Fe/(Fe+Mg) = 0.32 and tetrahedral Al = 2.57. Biotite in both facies is pleochroic tan to brown.

Chlorite. Chlorite occurs as a minor secondary phase throughout the CP14A core, and it is very plentiful in the altered zones adjacent to fractures. Chlorite in most cases replaces biotite, but in the more altered zones it also replaces amphibole. As is true of the amphibole and biotite, the chlorite is most magnesian in the amphibolite (Fe/(Fe+Mg) = 0.29-0.31, sample 1850, Table 6) and more iron-rich in the tonalitic gneiss (Fe/(Fe+Mg) = 0.36-0.43, other samples, Table 6). The chlorites are pycnochlorite and ripidolite according to the classification of Hey (1954).

Epidote. Epidote occurs as a secondary phase in the CP14A core, and is very plentiful adjacent to fractures in the core. The epidote is 23 to 32 percent pistacite and has a very minor picmontite component (Table 7).

Discussion

The CP14A drillhole encountered a relatively mafic rock of probable igneous origin which has a tectonic foliation which was formed under amphibolite grade conditions. A later, low-temperature deformation caused fracturing, with the introduction of fluids which resulted in the greenschist grade alteration of the rock adjacent to these fractures.

References

Hey, M. H., 1954, A new review of the chlorites: Mineral. Mag., 30, 277-292.

Leake, B. E., 1978, Nomenclature of amphiboles: Am. Mineral., 63, 1023-1052.

TABLE 4. AMPHIBOLE ANALYSES FOR THE CP14A CORE

	1	2	3	4	5	6	7
SIO2	42.58	42.78	43.91	45.39	45.08	44.97	45.67
TIO2	1.62	1.38	1.21	1.18	1.54	1.36	1.12
A2O3	9.91	9.82	9.54	8.59	9.82	10.25	9.34
FEO	17.20	16.84	16.59	15.81	12.53	12.26	11.76
MGO	10.20	10.55	10.84	11.90	13.35	13.67	14.16
MNO	0.29	0.43	0.48	0.49	0.13	0.18	0.20
CAO	11.89	11.93	12.14	12.04	12.07	11.85	12.12
NA2O	1.21	0.99	0.91	0.82	1.34	1.29	1.26
K2O	1.04	1.04	0.91	0.79	0.59	0.50	0.46
H2O	2.04	2.04	2.06	2.09	2.11	2.11	2.11
SUM	97.98	97.80	98.59	99.10	98.56	98.44	98.20
SI	6.265 *	6.292 *	6.380 *	6.513 *	6.401 *	6.376 *	6.476 *
AL	1.718 7.983	1.702 7.994	1.620 8.000	1.452 7.966	1.599 8.000	1.624 8.000	1.524 8.000
AL	0.0 *	0.0 *	0.013 *	0.0 *	0.044 *	0.089 *	0.037 *
TI	0.179 *	0.153 *	0.132 *	0.127 *	0.164 *	0.145 *	0.119 *
FE	2.116 *	2.071 *	2.016 *	1.897 *	1.488 *	1.454 *	1.395 *
MN	0.036 *	0.054 *	0.059 *	0.060 *	0.016 *	0.022 *	0.024 *
MG	2.237 4.569	2.313 4.590	2.348 4.568	2.545 4.629	2.825 4.538	2.889 4.599	2.993 4.567
CA	1.874 *	1.880 *	1.890 *	1.851 *	1.836 *	1.800 *	1.841 *
NA	0.345 *	0.282 *	0.256 *	0.228 *	0.369 *	0.355 *	0.346 *
K	0.195 2.415	0.195 2.357	0.169 2.315	0.145 2.224	0.107 2.312	0.090 2.245	0.083 2.271
H	2.000 2.000	2.000 2.000	2.000 2.000	2.000 2.000	2.000 2.000	2.000 2.000	2.000 2.000
O	23.000 *	23.000 *	23.000 *	23.000 *	23.000 *	23.000 *	23.000 *
F/M	0.962	0.919	0.884	0.769	0.532	0.511	0.474
F/FM	0.490	0.479	0.469	0.435	0.347	0.338	0.322

1 CP14A 1707 HBD 1
2 CP14A 1707 HBD 2
3 CP14A 1753.5 HBD 1
4 CP14A 1753.5 HBD 2

5 CP14A 1850 AMPH 1
6 CP14A 1850 AMPH 2
7 CP14A 1850 AMPH 3

TABLE 5. BIOTITE ANALYSES FOR THE CP14A CORE

	1		2		3		4	
SIO2	36.09		36.02		36.19		36.06	
TIO2	2.86		2.76		2.93		2.96	
A2O3	16.09		15.59		15.39		16.58	
FEO	17.55		18.05		19.19		13.30	
MGO	11.35		11.70		11.29		15.67	
MNO	0.28		0.29		0.18		0.06	
CAO	0.03		0.0		0.06		0.06	
NA2O	0.08		0.05		0.11		0.05	
K2O	9.82		9.57		9.44		8.62	
H2O	3.90		3.89		3.90		3.98	
SUM	98.05		97.92		98.68		97.34	
SI	5.547	*	5.553	*	5.559	*	5.433	*
AL	2.453	8.000	2.447	8.000	2.441	8.000	2.567	8.000
AL	0.461	*	0.386	*	0.345	*	0.376	*
TI	0.331	*	0.320	*	0.338	*	0.335	*
FE	2.256	*	2.327	*	2.465	*	1.676	*
MN	0.036	*	0.038	*	0.023	*	0.008	*
MG	2.600	5.684	2.689	5.760	2.585	5.757	3.519	5.913
CA	0.005	*	0.0	*	0.010	*	0.010	*
NA	0.024	*	0.015	*	0.033	*	0.015	*
K	1.925	1.954	1.882	1.897	1.850	1.892	1.656	1.681
H	4.000	4.000	4.000	4.000	4.000	4.000	4.000	4.000
O	24.000	*	24.000	*	24.000	*	24.000	*
F/M		0.882		0.880		0.963		0.478
F/FM		0.469		0.468		0.491		0.324

1 CP14A 1707 BIO 1
2 CP14A 1707 BIO2
3 CP14A 1707 BIO 2
4 CP14A 1850 BIO 1

TABLE 6. CHLORITE ANALYSES FOR THE CP14A CORE

	1	2	3	4	5	6	7
SIO2	27.92	27.10	27.91	26.36	25.90	26.95	30.67
TIO2	0.22	0.21	0.13	0.18	0.13	0.23	1.11
A2O3	19.13	18.87	18.15	20.67	20.11	19.37	18.40
FEO	19.98	22.65	20.41	19.04	21.13	15.35	15.84
MGO	18.58	17.51	19.72	19.44	17.54	21.17	19.59
MNO	0.38	0.47	0.50	0.37	0.24	0.22	0.10
CAO	0.01	0.08	0.03	0.01	0.03	0.01	0.13
NA2O	0.0	0.02	0.01	0.01	0.03	0.03	0.05
K2O	0.13	0.0	0.01	0.01	0.03	0.16	1.89
H2O	11.54	11.42	11.56	11.54	11.27	11.40	11.94
SUM	97.89	98.33	98.43	97.63	96.38	94.89	99.72
SI	2.899 *	2.844 *	2.893 *	2.738 *	2.755 *	2.832 *	3.079 *
AL	1.101 4.000	1.156 4.000	1.107 4.000	1.262 4.000	1.245 4.000	1.168 4.000	0.921 4.000
AL	1.240 *	1.177 *	1.111 *	1.268 *	1.275 *	1.231 *	1.255 *
TI	0.017 *	0.017 *	0.010 *	0.014 *	0.010 *	0.018 *	0.084 *
FE	1.735 *	1.988 *	1.770 *	1.654 *	1.879 *	1.349 *	1.330 *
MN	0.033 *	0.042 *	0.044 *	0.033 *	0.022 *	0.020 *	0.009 *
MG	2.876 *	2.738 *	3.047 *	3.010 *	2.781 *	3.316 *	2.931 *
CA	0.0 5.920	0.0 5.974	0.0 5.988	0.0 5.983	0.0 5.977	0.0 5.963	0.0 5.874
NA	0.0 *	0.004 *	0.002 *	0.002 *	0.006 *	0.006 *	0.010 *
K	0.017 5.920	0.0 5.974	0.001 5.988	0.001 5.983	0.0 5.977	0.021 5.963	0.242 5.874
H	8.000 8.000	8.000 8.000	8.000 8.000	8.000 8.000	8.000 8.000	8.000 8.000	8.000 8.000
O	18.000 *	18.000 *	18.000 *	18.000 *	18.000 *	18.000 *	18.000 *
F/M	0.615	0.741	0.595	0.560	0.684	0.413	0.457
F/FM	0.381	0.426	0.373	0.359	0.406	0.292	0.313

1 CP14A 1707 CHLOR 1
2 CP14A 1753.5 CHLOR 1
3 CP14A 1753.5 CHLOR 2
4 CP14A 1825 CHLOR 1
5 CP14A 1825 CHLOR 2
6 CP14A 1850 CHLOR 1
7 CP14A 1850 CHLOR 2

TABLE 7. EPIDOTE ANALYSES FOR THE CP14A CORE

	1	2	3	4	5
SIO2	37.69	35.88	36.89	38.12	37.64
TIO2	0.36	0.19	0.29	0.23	2.18
A2O3	21.07	21.46	24.82	22.93	21.55
FEO	13.92	13.58	10.62	12.28	12.30
MGO	0.07	0.07	0.05	0.01	0.10
MNO	0.25	0.28	0.05	0.16	0.0
CAO	22.67	22.78	23.59	23.19	23.59
NA2O	0.01	0.04	0.01	0.0	0.01
K2O	0.01	0.01	0.01	0.01	0.03
H2O	1.79	1.75	1.83	1.83	1.83
SUM	97.84	96.04	98.16	98.76	99.23

SI	3.153	*	3.069	*	3.026	*	3.127	*	3.087	*
AL	0.0	3.153	0.0	3.069	0.0	3.026	0.0	3.127	0.0	3.087
AL	2.077	*	2.163	*	2.399	*	2.216	*	2.083	*
TI	0.023	*	0.012	*	0.018	*	0.014	*	0.134	*
MG	0.009	*	0.009	*	0.006	*	0.001	*	0.012	*
FE	0.974	*	0.971	*	0.729	*	0.842	*	0.844	*
MN	0.018	3.100	0.020	3.176	0.003	3.155	0.011	3.085	0.0	3.073
CA	2.032	*	2.088	*	2.073	*	2.038	*	2.073	*
K	0.001	*	0.001	*	0.001	*	0.001	*	0.003	*
NA	0.002	2.034	0.007	2.095	0.002	2.076	0.0	2.039	0.002	2.078
H	1.000	1.000	1.000	1.000	1.000	1.000	1.000	1.000	1.000	1.000
O	13.000	*	13.000	*	13.000	*	13.000	*	13.000	*
PS		31.74		30.79		23.27		27.44		28.83
CZ		67.69		68.56		76.62		72.20		71.17
PD		0.58		0.64		0.11		0.36		0.0
F/M		113.603		111.122		119.741		698.092		69.012
F/FM		0.991		0.991		0.992		0.999		0.986

1 CP14A 1753.5 EPID 1
2 CP14A 1753.5 EPID 2
3 CP14A 1825 EPID 1
4 CP14A 1825 EPID 2
5 CP14A 1850 EPID 1

Rb-Sr Isotopic Study of Granitic Core from Portsmouth, Virginia

by
Gail S. Russell and C. Winston Russell
Orogenic Studies Laboratory

A coarse-grained non-megacrystic biotite granite similar to many of the post-metamorphic granites of the southeast (Speer et al., 1980) was encountered in drillhole CP-25A at Portsmouth, Virginia. Six samples of the 1-1/2 inch diameter core, weighing about 1 kg each, were selected for Rb-Sr whole rock analysis. The number and size of samples were limited by the requirement that they be free of fractures and mineralized zones. Details of the analyses are at the end of this section.

The results are listed in Table 1 and plotted on Figure 1. The whole rock isochron age is 263 $\pm$ 24 m.y. (2σ - MSRS = 0.8186). The initial $^{87}Sr/^{86}Sr$ composition of 0.7076 $\pm$ 0.0012 is not low enough to rule out some residence of components of the granitoid in the upper crust.

Some later veins and disseminations of muscovite + fluorite + carbonate are present; however, petrography and mineral chemistry suggest that these represent reaction of a late-stage aqueous fluid with previously crystallized minerals during cooling of the magma (Speer, pers. comm.). There is no petrographic evidence for a post-crystallization thermal event which might have disturbed the isotopic system.

Biotites separated from whole rock samples from 1848' and 1956' yield identical biotite/whole rock ages of 267 m.y. in spite of a very large difference in the Rb/Sr ratios. This age, with the calculated initial ratio of 0.7073, is indistinguishable from the whole rock age of 263 $\pm$ 24 m.y. and indicates that the Portsmouth granitoid cooled rapidly past the blocking temperature of biotite.

The date is interpreted as the age of crystallization of a magma intruding relatively cool or rapidly cooling country rock. Zircon data will be obtained to confirm this.

The Portsmouth granitoid, which is petrographically similar to the post-metamorphic intrusives in the exposed Piedmont in the southern Appalachians (Speer et al., 1980), falls within the 265-325 m.y. range of Rb-Sr ages reported by Fullagar (1971), Jones and Walker (1973), and Fullagar and Butler (1979). However, it is younger than all except the Siloam granite in Georgia and supports the hypothesis of eastward younging of plutonism across the southern Appalachians (Glover et al., 1978).

Analytical Methods

All analyses were made on the Nuclide 6-inch radius of curvature, 60° magnetic sector, thermionic source mass spectrometer installed in the Orogenic Studies Laboratory at VPI & SU in April 1979. It is interfaced to a model 9825A Hewlett Packard programmable calculator (Nuclide's PC/SIM-1 automated system) for magnetic peak stepping and data reduction.

Fourteen analyses of SRM 987 standard carbonate during this study have an $^{87}Sr/^{86}Sr$ isotopic composition of 0.71022 $\pm$ 0.00016 (2σ). All

Table 1.

Rb and Sr data for whole rock samples from drillhole CP25-A at Portsmouth, VA.

Depth	Rb (ppm)	Sr (ppm)	$^{87}Rb/^{86}Sr$	$^{87}Sr/^{86}Sr$
1848'	253	209	3.507	0.72064
1853'	231	220	3.033	0.71907
1916'	246	228	3.130	0.71935
1919'	296	190	4.500	0.72435
1942'	268	199	3.890	0.72244
1956'	255	222	3.335	0.71993

Table 2.

Rb and Sr data for whole rock/biotite pairs from Portsmouth, VA drillhole.

Depth	Rb (ppm)	Sr (ppm)	$^{87}Rb/^{86}Sr$	$^{87}Sr/^{86}Sr$
1848'				
WR	253	209	3.507	0.72064
Biot	551	36.7	44.127	0.87465
1956'				
WR	255	222	3.335	0.71993
Biot	1.240	14.5	268.24	1.72538

Depth	Biotite/Whole Rock Age	Calculated $(^{87}Sr/^{86}Sr)_{initial}$
1848'	267 $\pm$ 7 m.y.	0.7073 $\pm$ 0.0016
1956'	267 $\pm$ 5 m.y.	0.7073 $\pm$ 0.0015

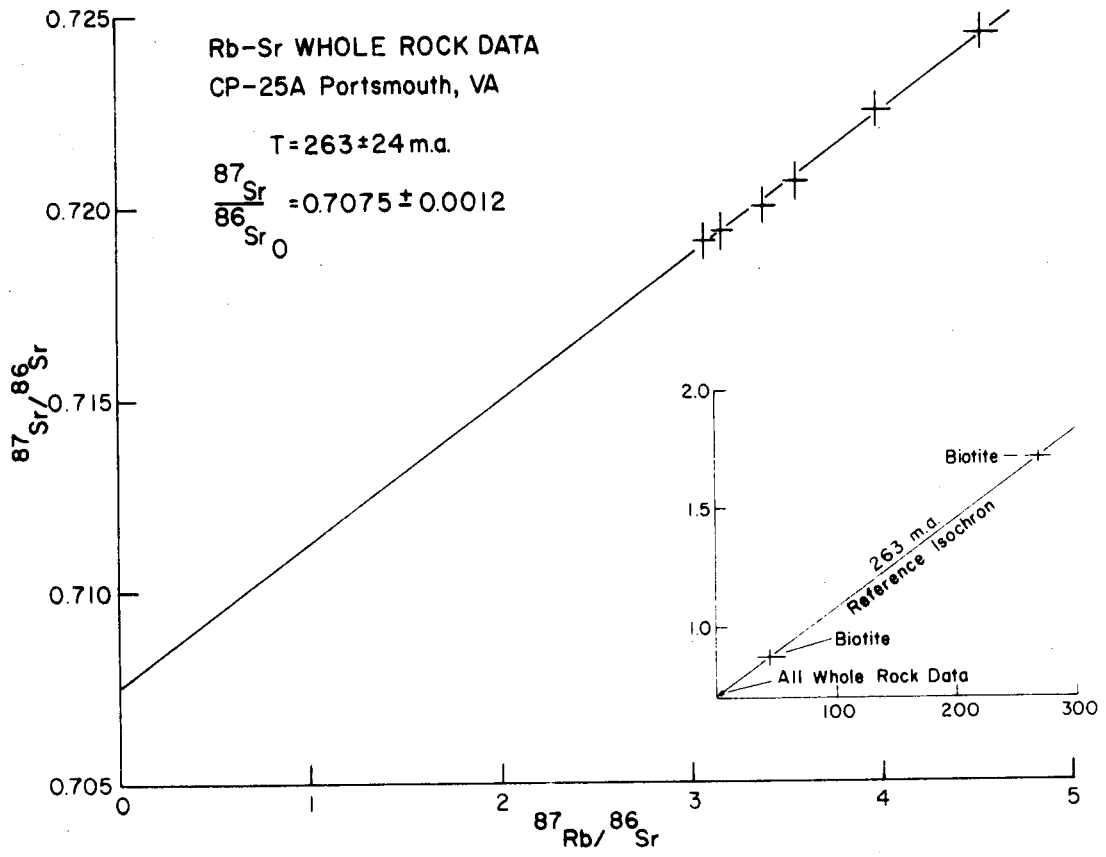

Figure 1. Rb-Sr isochron plot for whole rock samples from drill-hole CP-25A at Portsmouth, Virginia. Inset shows the relation of two biotite separates to the extension of the whole rock isochron.

strontium isotopic analyses have been normalized to $^{86}Sr/^{88}Sr$ = 0.1194. The precision of individual strontium analyses are routinely less than 0.04% (2σ). In this initial year of operation, each whole rock sample has been processed in duplicate. The differences between the $^{87}Sr/^{86}Sr$ compositions measured in duplicate samples have usually been less than 0.01% and always 0.02% or less. Rubidium and strontium concentrations were determined by isotope dilution using ^{84}Sr spike prepared by the National Bureau of Standards (SRM 988) and ^{87}Rb prepared at Oak Ridge National Laboratories. An analytical error of ±2% (2σ) is estimated for the $^{87}Rb/^{86}Sr$ ratio.

Ages and initial ratios are calculated using the York model II equation (York, 1969). All errors are given at the 2σ confidence level. As a measure of the goodness of fit of the data to an isochron, the weighted sum of the residuals squared (MSRS - analogous to MSWD of the McIntyre (1966) program) are given for each isochron.

Standard dissolution and ion exchange techniques were used. High purity water was obtained by tandem distillation of deionized water in quartz and teflon sub-boiling stills. HCl was purified with the quartz sub-boiling still; other acids by the two-bottle teflon still described by Mattinson (1972). All procedures are carried out in 100+ clean air. Blanks for both rubidium and strontium are less than 200 picograms.

References

Fullagar, P. D., 1971, Age and origin of plutonic intrusions in the Piedmont of the Southeastern Appalachians: Geol. Soc. America Bull., v. 82, p. 2845-2862.

Fullagar, P. D. and J. R. Butler, 1979, 325 to 265 m.y.-old granitic plutons in the Piedmont of the southeastern Appalachians: Amer. Jour. Sci., v. 279, p. 161-185.

Glover, L. G., III, J. K. Costain, and A. K. Sinha, 1978, Project proposal to U. S. Geological Survey.

Jones, L. M. and R. L. Walker, 1973, Rb-Sr whole-rock age of the Siloam Granite, Georgia: A Permian intrusive in the southern Appalachians: Geol. Soc. America Bull., v. 84, p. 3653-3658.

Mattinson, J. M., 1972, Preparation of hydrofluoric, hydrochloric and nitric acids at ultralow lead levels: Anal. Chem., v. 44, p. 1715-1716.

McIntyre, G. A., C. Brooks, W. Compston, and A. Turek, 1966, The statistical assessment of Rb-Sr isochrons: Jour. Geophys. Res., v. 71, p. 5459-5468.

Speer, J. A., S. W. Becker, and S. S. Farrar, 1980, Field relations and petrology of the post-metamorphic, coarse-grained granitoids and associated rocks of the southeastern Appalachian Piedmont: in D. R. Wones (ed.), The Caledonides in the USA, VPI & SU Memoir no. 2, p. 137-148.

York, D., 1969, Least squares fitting of a straight line with correlated errors: Earth Planet. Sci. Letters, v. 5, p. 320-324.

Structure Contour Map of Basement Beneath the Atlantic Coastal Plain

by
Richard J. Gleason
Orogenic Studies Laboratory

Knowledge of the depth to basement beneath the Atlantic Coastal Plain is a fundamental requirement for the evaluation of the geothermal resource potential at any particular location. The sediment thickness overlying a basement heat source must be known in order to determine the insulating capability of the blanketing sediments and to extrapolate shallow, measured temperature gradients to the base of the Coastal Plain sequence. The depth to basement at any given site is also an important factor in the planning of deep drilling and in the evaluation of the economics of drilling and utilization of a potential geothermal resource.

Structure contour maps of basement beneath the North Carolina and Georgia Coastal Plains were presented in a previous report (VPI&SU-5648-5). The definition of "basement" used in the current report follows that presented previously.

Basement structure contour maps for the Northern Atlantic Coastal Plain and the South Carolina Coastal Plain are presented in this report as Figures 1 and 2, respectively. These maps were prepared from all available drillhole and seismic data obtained through a review of literature, state survey files, and in a few cases, holes drilled as part of the VPI & SU geothermal program. This compilation includes 176 drillholes in the Virginia Coastal Plain, 79 in Maryland, 45 in Delaware, 87 in New Jersey, and 37 in South Carolina. As is true in other parts of the Coastal Plain, the overwhelming majority of these basement drill holes are concentrated along the western edge of the Coastal Plain. This phenomenon is not apparent on the South Carolina map (Fig. 2) because shallow water well data were not readily available for this state.

Drill hole data were augmented by seismic refraction data, including 42 points in South Carolina (Bonini and Woollard, 1960), 12 points in Virginia (Ewing et al., 1937), one point in Maryland (Hansen, 1978), and 18 points in New Jersey (Ewing et al., 1939, 1940). In the Maryland Coastal Plain, there is a considerable wealth of seismic reflection data including those of Jacobeen (1972), Hansen (1978), and those obtained by Geophysical Services, Inc. for the VPI & SU program in preparation for the 1979 deep test at Crisfield.

The two maps presented as Figures 1 and 2 differ somewhat from earlier published versions. Figure 1 of the Northern Atlantic Coastal Plain is considerably more refined than that of Maher (1971) or Flawn (1967) but is only subtly different than that of Brown et al. (1972). With the inclusion of more recent drilling and seismic data, this present map is the most complete, updated version available.

Figure 2, of the South Carolina Coastal Plain, differs significantly from several earlier published maps. Maher (1971) indicated basement contours parallel to the coastline, while Figure 2 indicates that basement contours strike obliquely to the coastline. The basement contour map presented by Bonini and Woollard (1960) is a generalized partial map of the northeastern part of South Carolina and pre-

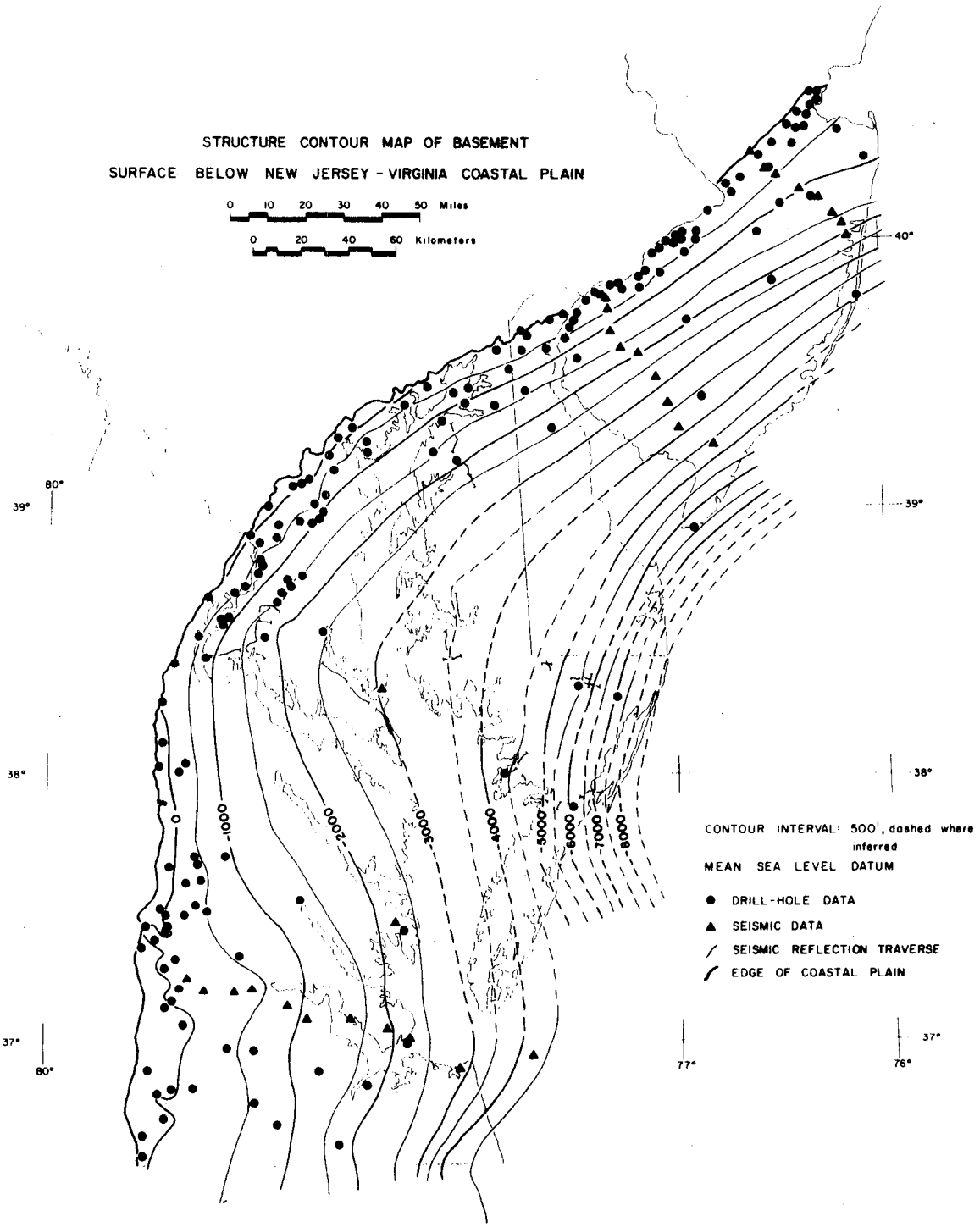

Figure 1. Structure contour map of the basement surface below Northern Atlantic Coastal Plain.

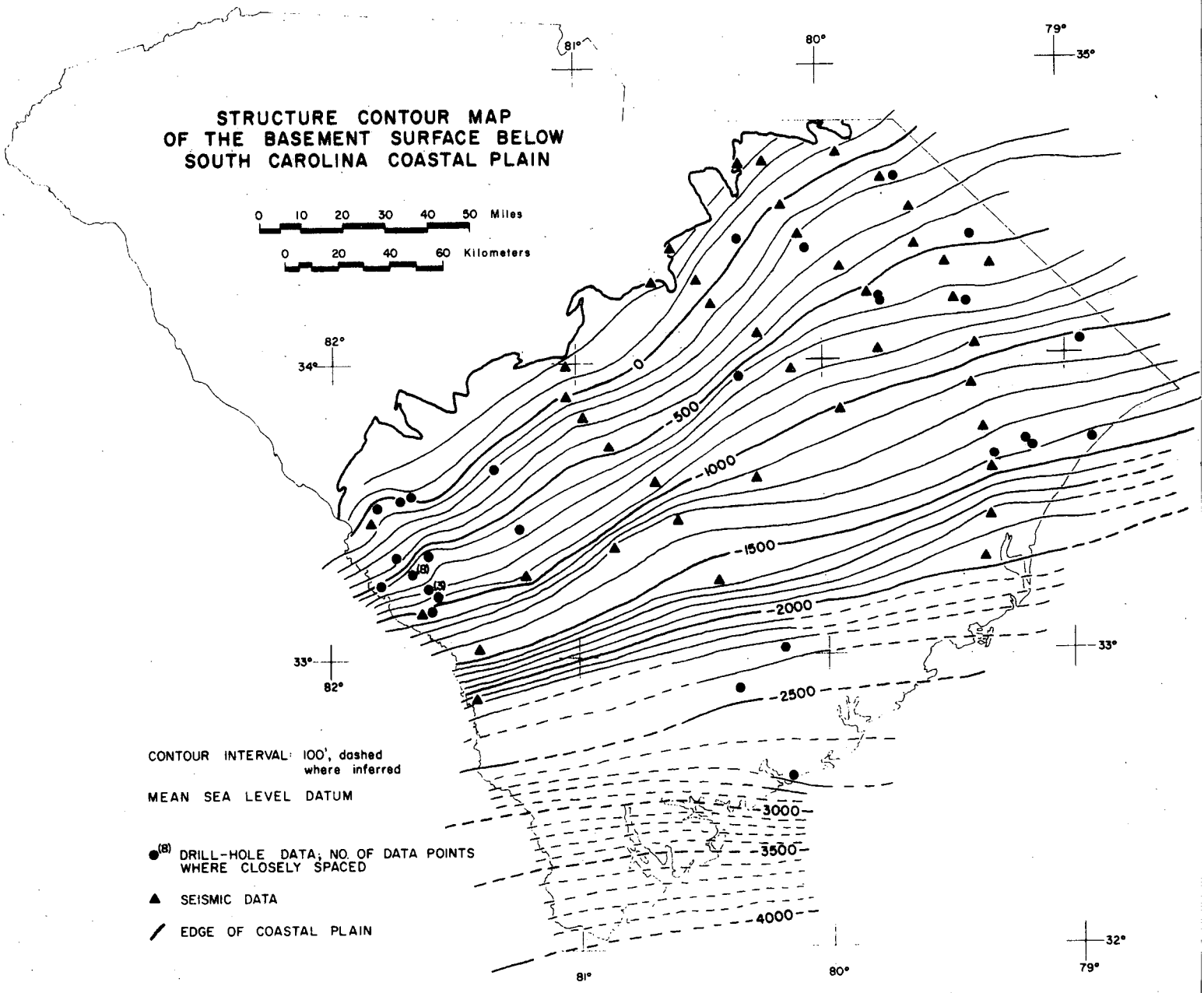

Figure 2. Structure contour map of the basement surface below South Carolina Coastal Plain.

sents no data for the southwestern part of the state. Figure 2 is also more detailed and refined than that of Flawn (1967). The basement contour map presented by Siple (1959) is most nearly identical to that presented here, although the general basement surface dip indicated is slightly steeper (.4°) on Siple's map than in Figure 2 (.35°).

The basement contour maps presented in this report, when combined with those presented previously, provide complete depth-to-basement coverage for the entire Atlantic Coastal Plain from New Jersey to Georgia. This coverage will allow us to estimate depths to basement for upcoming heat flow/temperature gradient holes in the VPI & SU program. In addition, depths obtained from these maps will assist us in providing estimates of basement temperatures in areas of future potential geothermal interest.

References

Bonini, W. E. and Woollard, G. P., 1960, Subsurface geology of North Carolina-South Carolina Coastal Plain from seismic data, Amer. Assoc. Petrol. Geol. Bull., v. 44, p. 298-315.

Brown, P. M., Miller, J. A., and Swain, F. M., 1972, Structural and stratigraphic framework, and spatial distribution of permeability of the Atlantic Coastal Plain, North Carolina to New York, U. S. Geol. Survey, Prof. Paper 796, 79 p.

Ewing, M., Crary, A. P., and Rutherford, H. M., 1937, Geophysical investigations in the emerged and submerged Atlantic Coastal Plain, Part 1: Methods and results, Geol. Soc. Amer. Bull., v. 48, p. 753-802.

Ewing, M., Woollard, G. P., and Vine, A. C., 1939, Geophysical investigations in the emerged and submerged Atlantic Coastal Plain, Part III: Barnegat Bay, New Jersey, section, Geol. Soc. Amer. Bull., v. 50, p. 257-296.

Ewing, M., Woollard, G. P., and Vine, A. C., 1940, Geophysical investigations in the emerged and submerged Atlantic Coastal Plain, Part IV: Cape May, New Jersey, section, Geol. Soc. Amer. Bull., v. 51, p. 1821-1840.

Flawn, P. T., 1967, Basement map of North America, Amer. Assoc. Petrol. Geol., U. S. Geol. Survey.

Hansen, H. J., 1978, Upper Cretaceous (Senonian) and Paleocene (Danian) pinchouts on the south flank of the Salisbury embayment, Maryland, and their relationship to antecedent basement structures, Maryland Geol. Survey, Rep. of Inves. #29, 36 p.

Jacobeen, F. H., Jr., 1972, Seismic evidence for high angle reverse faulting in the coastal plain of Prince Georges and Charles County, Maryland, Maryland Geol. Survey, Info. Circular #13, 21 p.

Maher, J. C., 1971, Geologic framework and petroleum potential of the Atlantic Coastal Plain and Continental Shelf, U. S. Geol. Survey, Prof. Paper 659, 98 p.

Siple, G. E., 1959, Guidebook for the South Carolina Coastal Plain field trip of the Carolina Geological Society, South Carolina State Development Board, Div. of Geology, Bull. #24, 27 p.

STRATIGRAPHIC AND STRUCTURAL FRAMEWORK OF THE VIRGINIA COASTAL PLAIN: REVIEW AND ASSESSMENT, June, 1980

by
Robert L. McConnell
Orogenic Studies Laboratory

Introduction

The central Atlantic Coastal Plain is an eastward dipping wedge of largely clastic sediments, resting on a pre-Cretaceous "basement". Recent geophysical studies coupled with drill data confirm the similarlity of basement rocks to those of the rocks exposed in the Piedmont Physiographic Province immediately to the west. The latter consist of late Precambrian and Paleozoic metasedimentary and metavolcanic rocks, intrusive rocks of mainly Paleozoic age, and westward- and eastward inclined N and NE trending faults, bounding graben filled with Triassic and (?)Lower Jurassic dominantly fluvial and lacustrine sediments, and lava flows and sills. Drilling records indicate that buried Triassic-Jurassic(?) basins underlie portions of the Atlantic Coastal Plain throughout its length. As these basins are fault-bounded, faults in the Coastal Plain could be localized by reactivation of these fractures. Unpublished studies by geologists at the Virginia Division of Mineral Resources (Rader, E. K., ms) show oversteepening of structure-contours on Cretaceous through Eocene sediments north of Richmond, Virginia, over the eastern margin of one such buried Triassic basin.

Geophysical studies of the Virginia portion of the Coastal Plain (Figs. 1,2) show conspicuous trends in aeromagnetic and gravity highs and lows oriented north to northeast. By analogy with such trends in the Piedmont, where rocks are exposed, it is inferred that these trends represent bands of acidic and mafic crystalline rocks. The boundaries between such "bands", because rocks on either side would have significantly different density and rigidity, would be areas or zones where stress might tend to be concentrated, thus resulting in earthquake activity and potential zones of surface faulting. Reilly, Glover, and Robinson (1980) have reinterpreted the positive gravity anomaly that trends NNE under the Coastal Plain from northwest of Richmond, Virginia. By potential field modelling of geologic structure, they interpret the anomaly to be an anticlinal structure containing a widespread layer of amphibolite. The top of the mantle is also upwarped below the anticline and contributes to the anomaly (Reilly and others, 1980, Fig. 9).

Although surface faults are rare in the Virginia Coastal Plain, a plot of recently described fault zones suggests, by referral to Figures 1 and 2, that faulting has been controlled by inferred rigidity contrasts in the basement (Fig. 3). Moreover, at least one such fault is associated with surface "lineaments" (Dischinger, 1979), in this case an alteration in the course of the Appommattox River, west of Hopewell, Virginia. Another possible "lineament", identified by the writer in the Tunstall and King William 7.59 quadrangles, appears to truncate terraces along the Pamunkey River (Fig. 4).

Figure 1. Aeromagnetic map of a portion of the Virginia Coastal Plain.

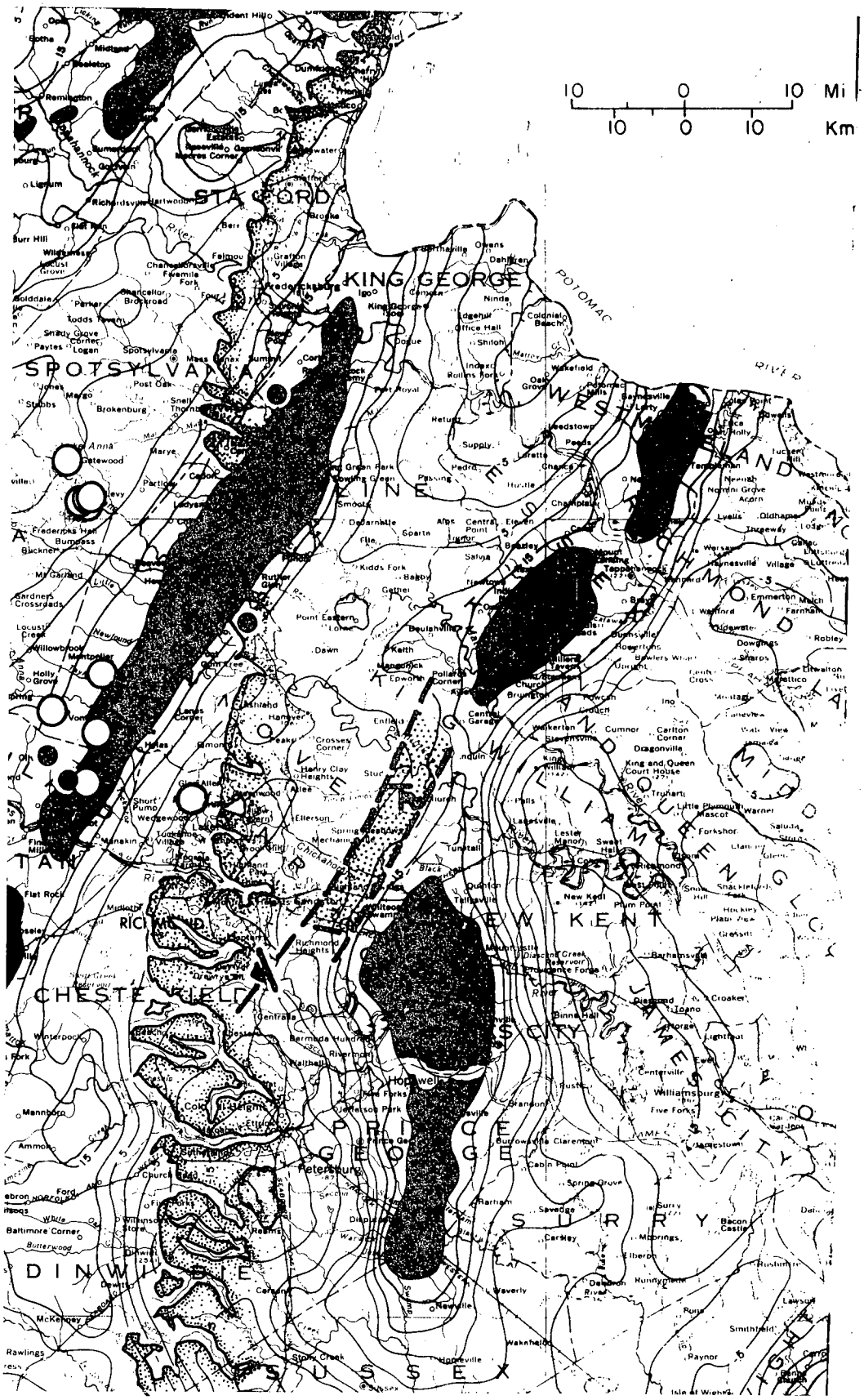

Figure 2. Gravity map of a portion of the Virginia Coastal Plain. Circles and dots mark locations of earthquake epicenters. Stippled pattern through Richmond traces western margin of the Coastal Plain.

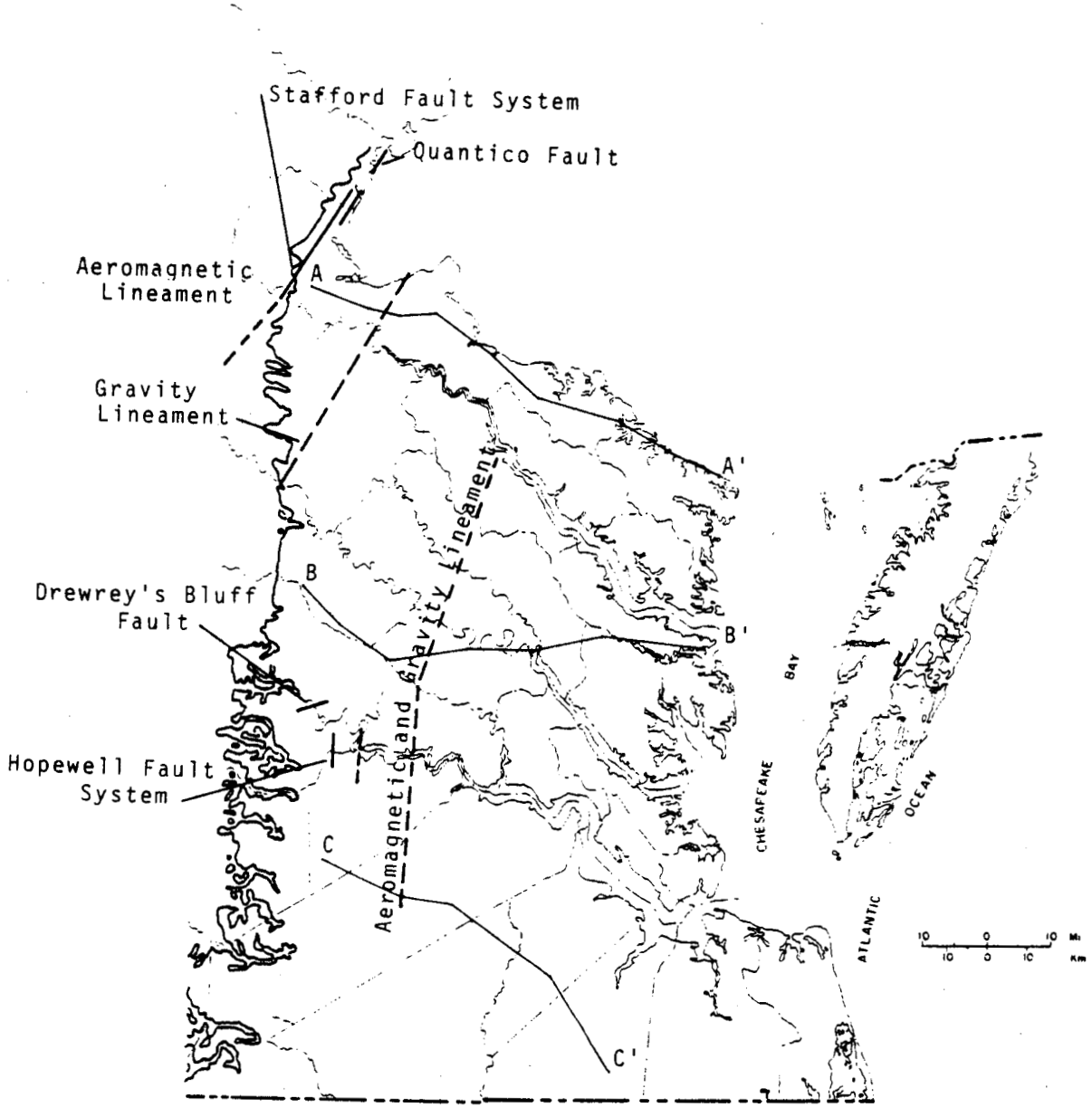

Figure 3. Location of faults and fault trends in the Virginia Coastal Plain. AA', BB', CC' refer to cross-sections in Figure 8. Dashed NS line in Hopewell Fault system is position of inferred fault on the basis of structure-contour mapping by Dischinger (1979).

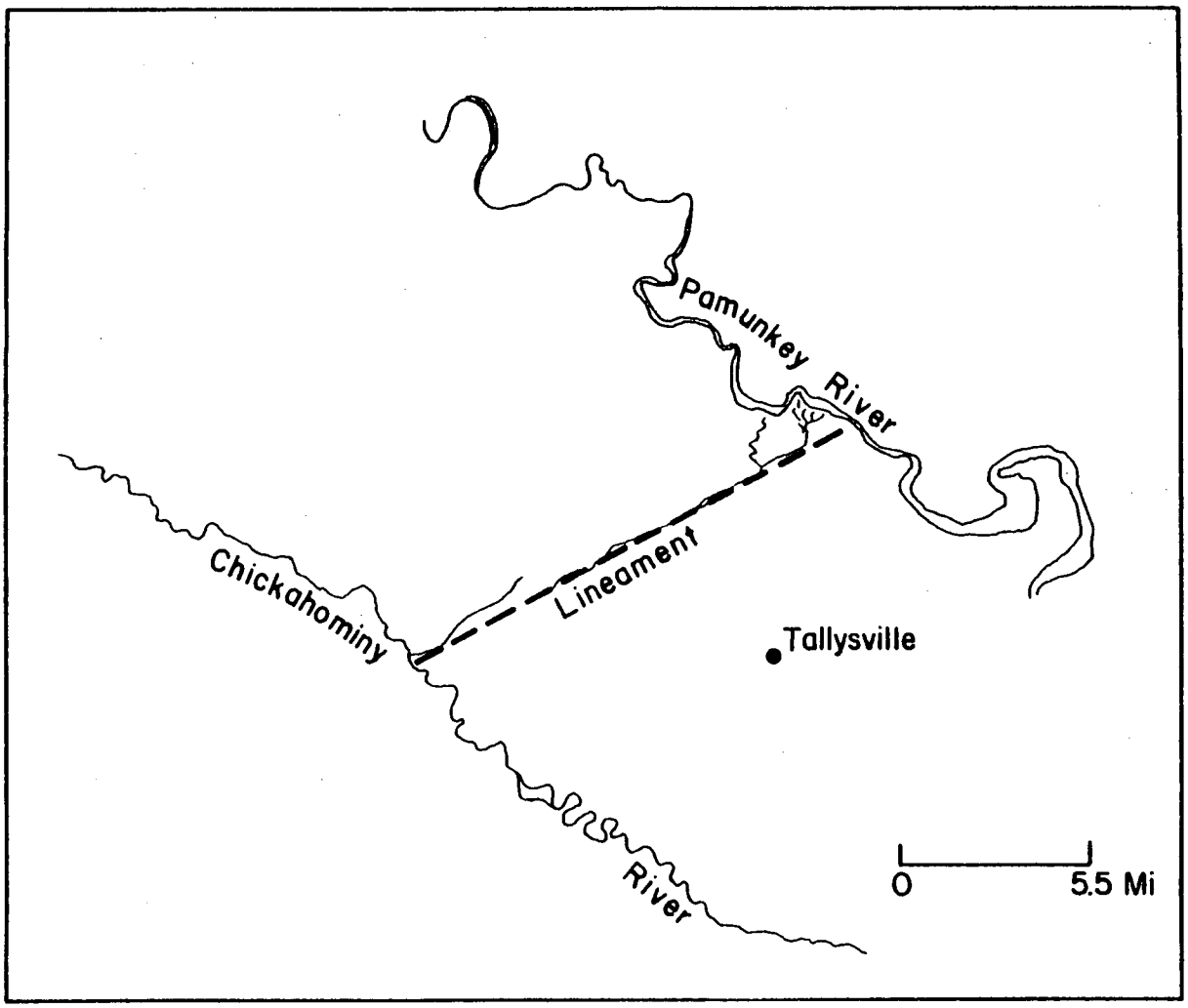

Figure 4. Surface lineament, Tunstall quadrangle.

Lithologically, the sediments of the Virginia Coastal Plain and nearby areas may be characterized as an eastward-thickening wedge of post-Triassic, mainly clastic, deposits which are dominated in thickness by deposits of Cretaceous age (Fig. 5). The sediment package is over 400 m thick at Hog Island, on the James River across from Williamsburg, 1.3 km thick at Virginia Beach, 2 km thick in the Delmarva Peninsula, and thickens offshore under the waters of the continental shelf. Recent wells drilled offshore in the Baltimore Canyon area penetrate 5 km of sediments without encountering crystalline basement (Oil and Gas Journal, May 16, 1980, p 40-41).

Two areas of very thick sedimentary accumulations have been referred to as the Salisbury "Embayment" (Delmarva Peninsula) and the Albemarle "Embayment" (SE Va., NE N.C.) by Owens (1969). In these areas in the subsurface, the thickness of Cretaceous sands, silts, and clays exceeds 700 m (Albemarle) and 1200 m (Salisbury) (Anderson, 1948, in Owens, 1969). These sediments commonly contain large volumes of water under artesian conditions. Usually it is not potable, with salinities generally exceeding 1,000 mg/l. These areas are underlain by basement rocks of relatively low gravity and aeromagnetic values. These are interpreted as granitic plutons because of gravity patterns, by analogy with Piedmont rocks. At Crisfield, Maryland, metavolcanic rocks have been encountered beneath Cretaceous sediments. Granites generate heat by decay of radioactive elements. This heat may be trapped in Cretaceous aquifers below a blanket of low-thermal-conductivity pelitic rocks and glauconitic fine sands. Further details of sedimentation will be considered below.

Purpose of the present investigation is as follows:

To determine structural controls on deposition of sediments in the Virginia Coastal Plain, with particular reference to Cretaceous clastics.

To identify zones of post-Triassic faulting that may affect distribution and geometry of aquifers in Virginia, using the following methods:

1. Detailed mapping across surface lineaments.
2. Detailed strip-mapping of sediments across gravity and aeromagnetic gradients, where faulting is expected to be localized.
3. Study of river-terrace deposits for offset where such deposits cross gravity and aeromagnetic gradients.
4. Integration of surface mapping with subsurface samples obtained by power-auger traverses, constructing structure-contour and isopach maps on pre-Pliocene sediments, in order to identify zones of oversteepening, indicative of deformation.
5. Identify sites for VIBROSEIS traverses to determine patterns and history of faulting.

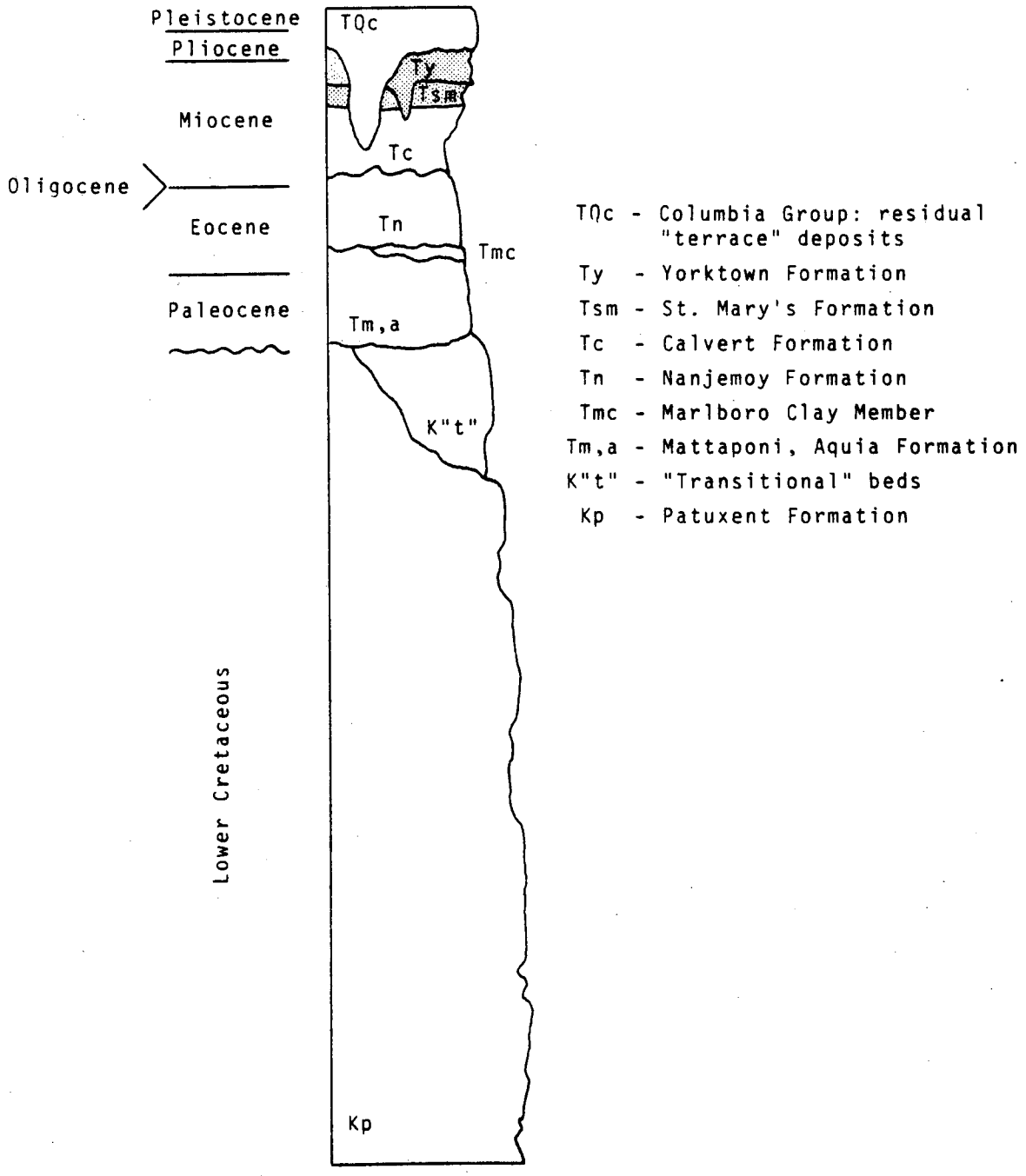

Figure 5. Schematic stratigraphic column of strata of central Virginia Coastal Plain.

To identify zones of potentially low thermal conductivity in post-Cretaceous sediments.

Stratigraphy

Triassic Basins in the Coastal Plain - general considerations.

As mentioned earlier, wells penetrating "basement" in the Virginia Coastal Plain are rare - therefore, knowledge of the nature of the basement is still relatively rudimentary. In at least four areas, Triassic basins have been interpreted in the basement by analysis of well cuttings: one northeast of Richmond is penetrated by several wells (for inferred position see Fig. 2), a second has been penetrated in easternmost King William County, a third penetrated in southeastern City of Suffolk (the former Nansemond County, approximately 7 km north of the North Carolina state line), and a fourth near Petersburg in southern Prince George County. Where mapped at the surface, in the Piedmont Province, Triassic basins are found to be bounded on the east or west by a normal fault or faults. Thus, the presence of buried Triassic basins indicates areas where post-Triassic faulting may have been localized, by reactivation of faults of Triassic-Jurassic(?) age.

Lower Cretaceaous

Patuxent Formation

The Patuxent Formation is exposed intermittently along the western margin of the Virginia Coastal Plain, from the Petersburg-Richmond area north to Stafford County on the south side of the Potomac. It thickens rapidly eastward, reaching thicknesses of 300 m or greater at Hog Island, Surry County (State Water Control Board Well W-4880 drilled in 1977 penetrates 920 ft. of Patuxent before bottoming at 1240 ft., without reaching basement). Although published isopach maps of the Patuxent in Virginia do not exist due to paucity of well data, examination of well cuttings by the writer, and others, and projections of depth to basement by Teifke (1973) and geologists of the Geothermal Project at Virginia Polytechnic Institute and State University, allow a crude estimate of thickness trends in the Patuxent to be made. Such estimates, coupled with lithofacies analyses (in progress), are of value because:

1. The Patuxent is the greatest potential source of ground water in Virginia, though quality of water is variable, and chloride content increases rapidly (and greatly exceeds drinking water standards) east of the City of Suffolk (State Water Control Board, 1970, in McConnell, 1977).
2. Semi-quantitative estimates of permeability and thermal conductivity for the Patuxent are of significance, as the Patuxent generally directly overlies basement, which is the source of radiogenically-produced heat.

Figure 6 is a structure-contour map on the top of the Patuxent compiled by Teifke (1973) from well data in Virginia. It is suggested

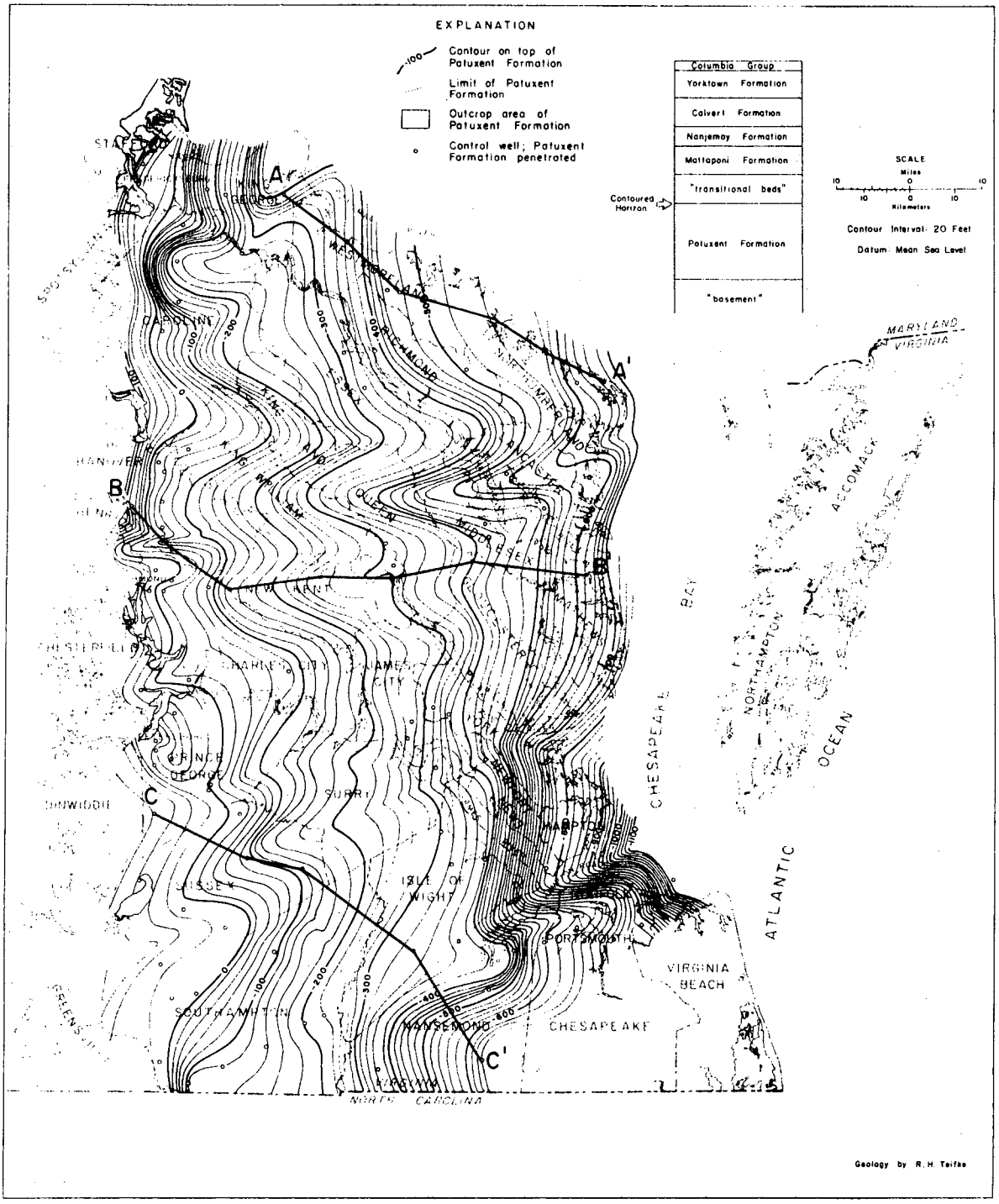

STRUCTURE-CONTOUR MAP OF THE PATUXENT FORMATION
COASTAL PLAIN OF VIRGINIA
1973

Figure 6. Structure-contour map on the Patuxent Formation (Teifke, 1973).

that a hinge line of sorts existed in lower Cretaceous time, and downwarping of a portion of the Coastal Plain occurred along roughly line A-A' (Fig. 6). Two major deflections in the structure contours (BB' and CC') appear: Both are nearly normal to trends of gravity and aeromagnetic gradients (Figs. 1,2). It may be noted that these features persist into Paleocene-Eocene time (Figs. 8-11) but seem to be inactive by post-Eocene time.

Post-Patuxent strata reach thicknesses in excess of 300 m immediately offshore under Chesapeake Bay. In the same area, structure contours on "basement" reach depths of 1 km, indicating thicknesses of Patuxent of 700 m here. In the vicinity of Hog Island (Surry County, Virginia) as mentioned previously, nearly 300 m of Patuxent is encountered without penetrating basement. Because outcrop exposures are rare except along the western margin of the Coastal Plain, where thickness of the Patuxent is generally less than 30 m, and where the lithology is dominantly piedmont alluvial gravels, descriptions of Patuxent lithology are mainly from drill cuttings examined by the writer, with supplementary data from unpublished descriptions by Dischinger (1979) and published summaries by Teifke (1973) and Brown and others (1972).

Figure 7 is a columnar section of the Patuxent Formation compiled by the writer from W-4880 at Hog Island. Over all, the Patuxent is characterized by medium- to coarse-grained sand. Glauconite in concentrations of more than a few percent of the sand-sized fractions occurrs only near the contact with the Mattaponi, and in an isolated 3 m zone near the middle of the drilled section. Overall permeability depends, among other things, on amount of clay, which is generally present, presumably as interstitial fill. While clay is an important constituent, pebble and granule-sized particles are minor in abundance. Fossils are rare; foraminifera including Bulimina, Nonion, Siphogenerina, Textulania, Nodosacia, Robulus, are found scattered through the unit, while Guttulina(?), Globulina(?), Robulus, Bolivina, Textularia, Globigrina and Marginulina are concentrated in the upper 10 m, below the Mattaponi (foram identification by M. T. Currie, Virginia Division of Geology). Many of these forms are also common to the overlying glauconitic sand units. Occasional gastropods and ostracods were noted.

Farther to the east, in James City County, near the community of Five Forks, where a well penetratees the upper 60 m of Patuxent, sand and gravel is dominant. To the west, as far as the Fall Line, the Patuxent, though much thinned, is coarser, and gravels are common in the section.

To the north, in Westmoreland County, several wells penetrate as much as 130 m of the Patuxent. Here the upper 25 m is generally sandy clay, grading downward into the claey coarse sands typical of Patuxent in the south.

Representative cross-sections of the Virginia Coastal Plain from Stafford to Northumberland Counties on the north (A-A'), and from Han-

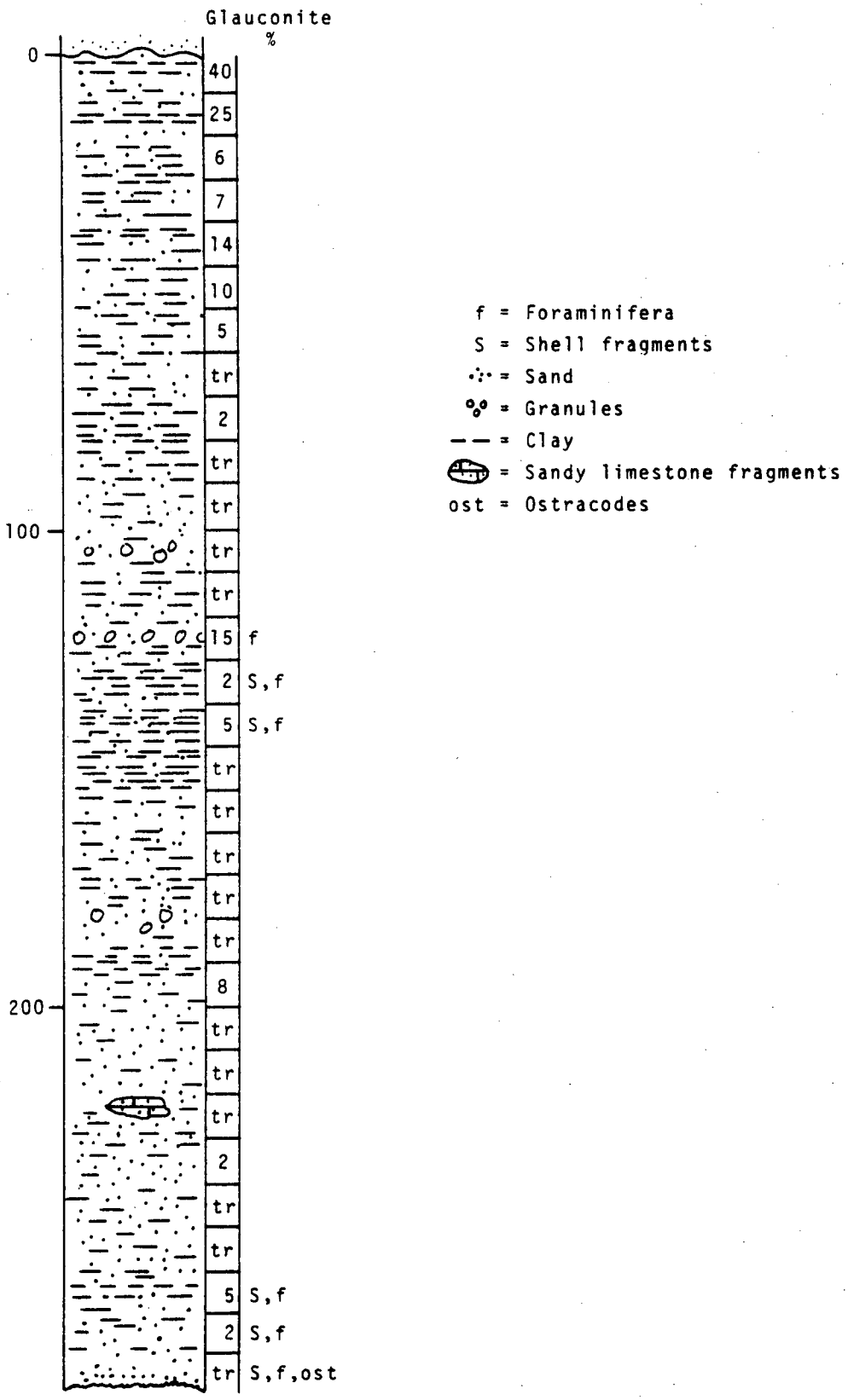

Figure 7. Columnar section of the Patuxent formation, compiled by R. L. McConnell from well-cutting log of well W#4880, Hog Island, Virginia. Unwashed samples were used in descriptions, but fines present in the samples probably represent minimum amount originally in sediment, due to "washing" effect of drilling activity, which tends to remove fines.

over/Henrico County boundary north of Richmond to Middlesex County on the east (B-B') (Teifke, 1973), are presented in Figure 8. These sections were compiled from well cuttings at the Virginia Division of Mineral Resources well repository in Charlottesville. Section C-C', a shortened cross-section from Prince George County to City of Suffolk, shows the rapid thickening of the Cretaceous section in a southeasterly direction.

Lower Cretaceous

"Transitional beds"

Glauconitic varicolored sands, silts, and clays underlie the Mattaponi in the subsurface in two areas of the Virginia Coastal Plain (Fig. 9), with presumably unconformable contact. These units are informally referred to as "transitional beds" by Teifke (1973) as a result of the supposed transitional nature between the dominantly glauconitic fine sands of the Mattaponi/Aquia, and the gravels and sands of the upper Patuxent. These sediments reach a thickness of a minimum of 100 m (and are probably much thicker) in Chesapeake County, southeastern Virginia, and perhaps 80 m in King George County, northern Virginia. The "transitional beds" are not equivalents of Upper Cretaceous rocks of Maryland, as they contain a fauna (mainly foraminifera - Teifke, 1973) of Early Cretaceous age.

These units, in some cases, are highly pelitic, with discrete layers of sandy, gravelly, or silty clay reaching 15 m thick. The clays are themselves glauconitic, and the glauconite is considered autochthonous due to the absence of abrasion (Teifke, 1973). Isopachs of the "transitional beds" imply an increase in thickness to the southeast of Chesapeake County, Virginia, into northeasternmost North Carolina, again, completely in the subsurface. Farther to the southeast, at Cape Hatteras, North Carolina, the Lower Cretaceous section as a whole reaches 1100 m in thickness (Heezen and others, 1959) which includes "transitional beds" and Patuxent equivalents. At Cape Hatteras, however, the units are sands and carbonates.

Paleocene-Eocene

Mattaponi-Aquia-Nanjemoy Formations

The formations are considered as a single unit for the following reasons:

1. They are all glauconitic sands.
2. Use of the terms "Aquia" and "Mattaponi" is in dispute among various workers.
3. Where the Marlboro Clay, a distinctive "pinkish-orange" clay zone generally found at the base of the Nanjemoy, is missing, the units are difficult to distinguish.

Areas of maximum accumulation of these units are (1) the mouth of the James, near Hampton in the southeastern Coastal Plain, and (2) King George County and vicinity. In both areas, over 100 m are present in the subsurface (Fig. 10,11). For convenience, these units are

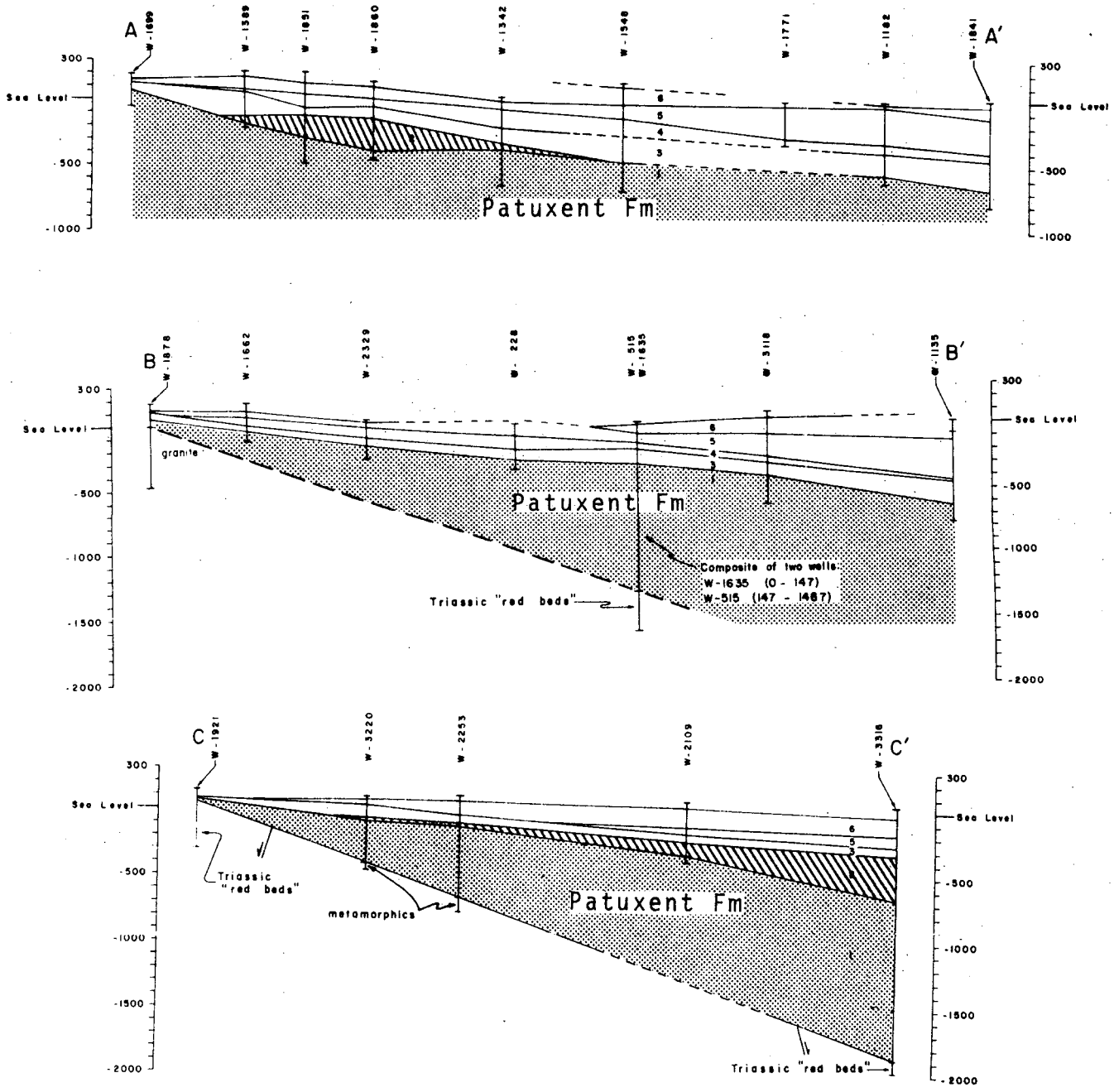

Figure 8. Representative cross-section of the Coastal Plain modified from Teifke (1973). For location, see Figure 3.

COMMONWEALTH OF VIRGINIA
DEPARTMENT OF CONSERVATION AND ECONOMIC DEVELOPMENT
DIVISION OF MINERAL RESOURCES
James L. Calver
Commissioner of Mineral Resources and State Geologist

BULLETIN 83
PLATE 7

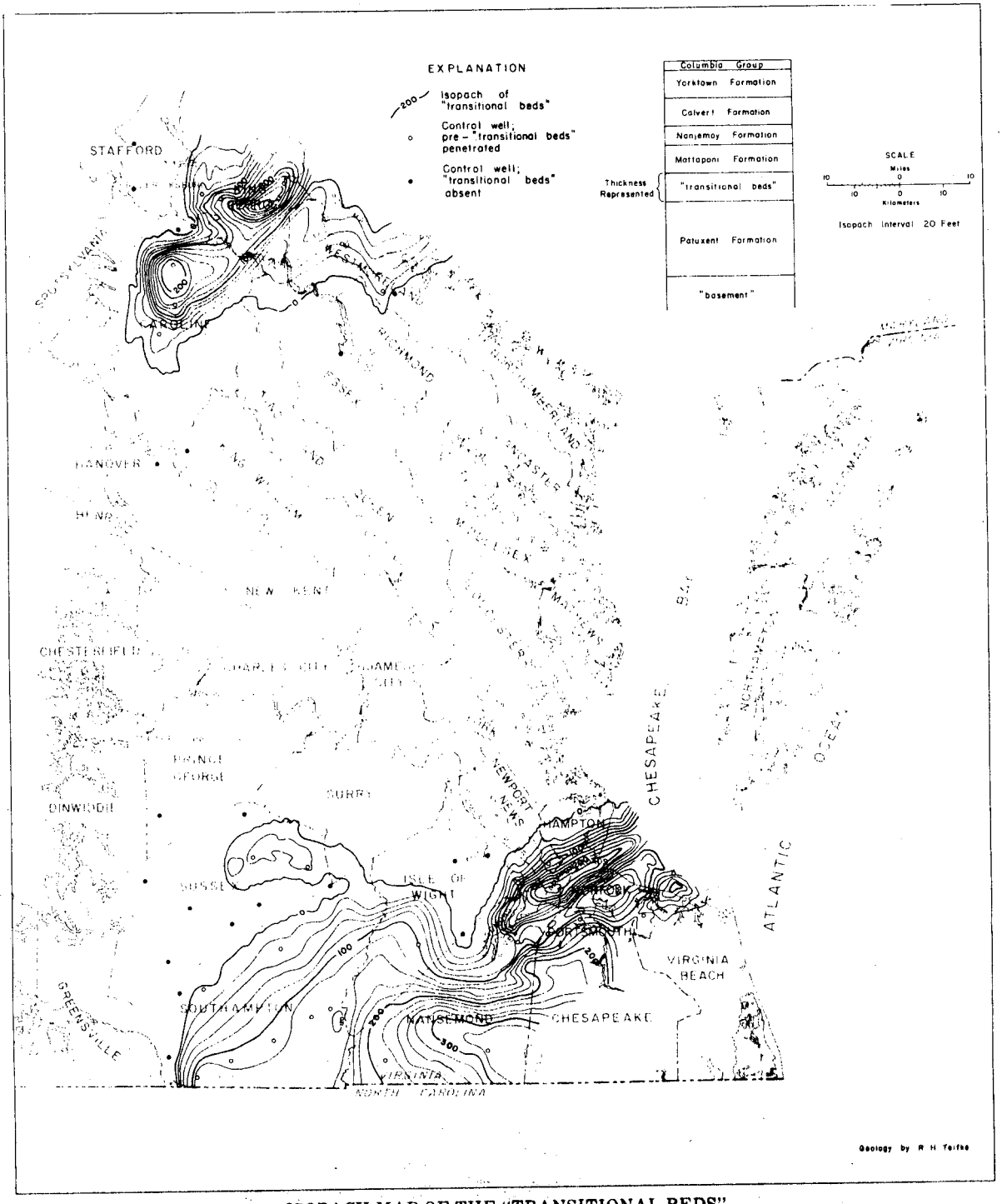

ISOPACH MAP OF THE "TRANSITIONAL BEDS"
COASTAL PLAIN OF VIRGINIA
1973

Figure 9. Isopach map of the Lower Cretaceous ""Transitional Beds"" (Teifke, 1973).

COMMONWEALTH OF VIRGINIA
DEPARTMENT OF CONSERVATION AND ECONOMIC DEVELOPMENT
DIVISION OF MINERAL RESOURCES
James L. Calver
Commissioner of Mineral Resources and State Geologist

BULLETIN 83
PLATE 9

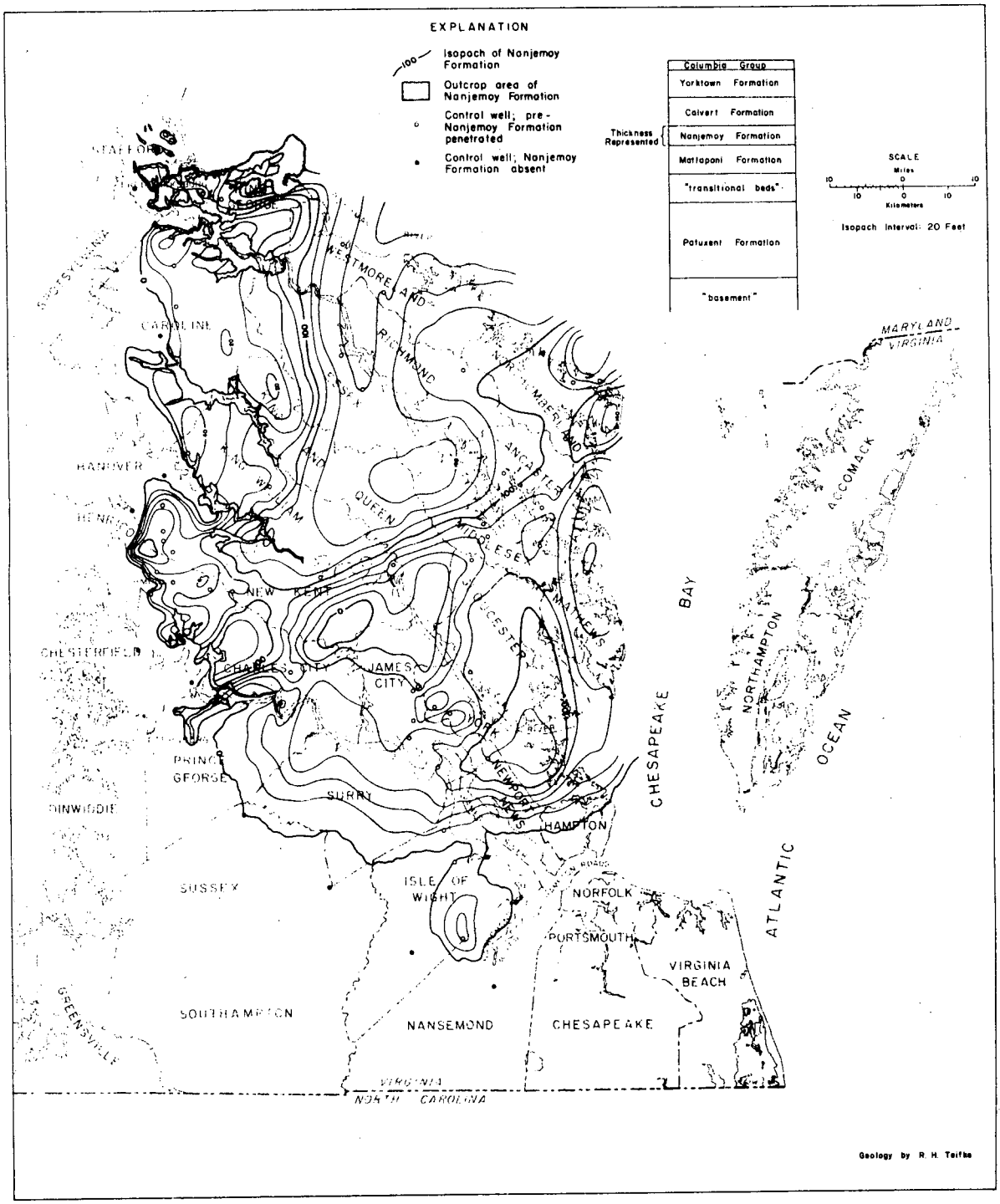

ISOPACH MAP OF THE NANJEMOY FORMATION
COASTAL PLAIN OF VIRGINIA
1973

Figure 10. Isopach map of the Nanjemoy Formation (Teifke, 1973).

COMMONWEALTH OF VIRGINIA
DEPARTMENT OF CONSERVATION AND ECONOMIC DEVELOPMENT
DIVISION OF MINERAL RESOURCES
James L. Calver
Commissioner of Mineral Resources and State Geologist

BULLETIN 83
PLATE 8

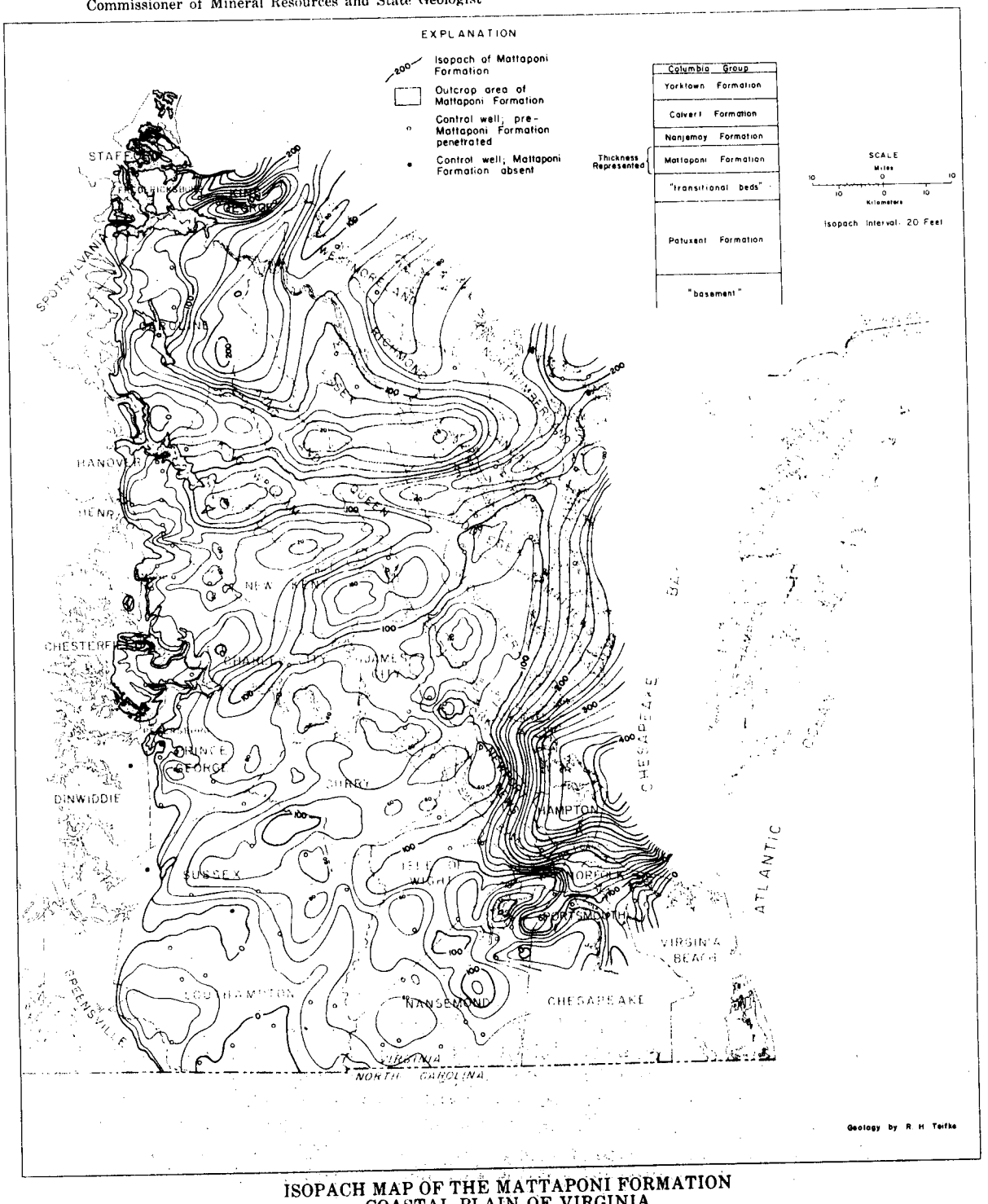

ISOPACH MAP OF THE MATTAPONI FORMATION
COASTAL PLAIN OF VIRGINIA
1973

Figure 11. Isopach map of the Mattaponi Formation (Teifke, 1973).

referred to as the Glauconite Sands, lower unit (Mattaponi-Aquia) and upper unit (Nanjemoy).

In well cuttings the uppper and lower units are practically indistinguishable. Individual 3-5 m thick units contain 50-80% glauconite in the sand-sized fraction, with varying amounts of silt and clay, the latter seeming on a qualitative basis to be more abundant in the lower unit. Feldspar is rare. Shell hash, mostly pelecypods, is common to dominant over 10 m intervals in the lower unit. Muscovite is often a major component of the silt-sized fraction. To the east, in Gloucester County, clay increases in the lower unit, coupled with rapid increase in thickness of the lower unit as a whole. In this area, the thick (25 m) clay units and glauconitic sands might provide a zone of relatively low thermal conductivity. The lower unit serves as an important aquifer for industrial uses in southeastern Virginia, although water quality is generally relatively low (Virginia Division of Water Resources, 1970, in McConnell, 1977).

Coincident with the lower James River (around Hampton Roads) is a zone of relatively abrupt thickening in the lower unit. To the northwest along the James River, however, no alteration of isopachs is noted; as mentioned previously, however, data points were few.

Miocene

Calvert Formation

The Calvert persists over the entire northern and southeastern Coastal Plain, reaching thicknesses in excess of 100 m in the Virginia Beach area (Teifke, 1973). It is intermittently exposed over a wide area of the westernmost Coastal Plain, from Richmond/Henrico County to Stafford and King George Counties, on the south side of the Potomac. To the south and west of this area it has been eroded. Isopach maps on few data points show no oversteepening in the Calvert across the James, site of the postulated Hampton Roads fault of Cedarstrom, nor across any buried gravity or aeromagnetic gradient (Fig. 12).

The Calvert typically consists of green to drab greenish brown clays, and clayey silts and sands. The lower portions are generally diatomaceous, and above a gravelly basal unit, a Siphogenerina zone is found over much of the central Coastal Plain. The Calvert is sparsely fossiliferous, with layers of dominantly mollusc (pelecypods and gastopods) shells not uncommon in the upper sandy and silty unit. The three-ribbed gastropod Ecphora is indicative of the unit in the northern Coastal Plain (Mixon and Newell, 1978) and is found intermittently in the southern outcrop portions (Henrico, King William Counties) as well. Contact is unconformable with the underlying Nanjemoy.

COMMONWEALTH OF VIRGINIA
DEPARTMENT OF CONSERVATION AND ECONOMIC DEVELOPMENT
DIVISION OF MINERAL RESOURCES
James L. Calver
Commissioner of Mineral Resources and State Geologist

BULLETIN 83
PLATE 10

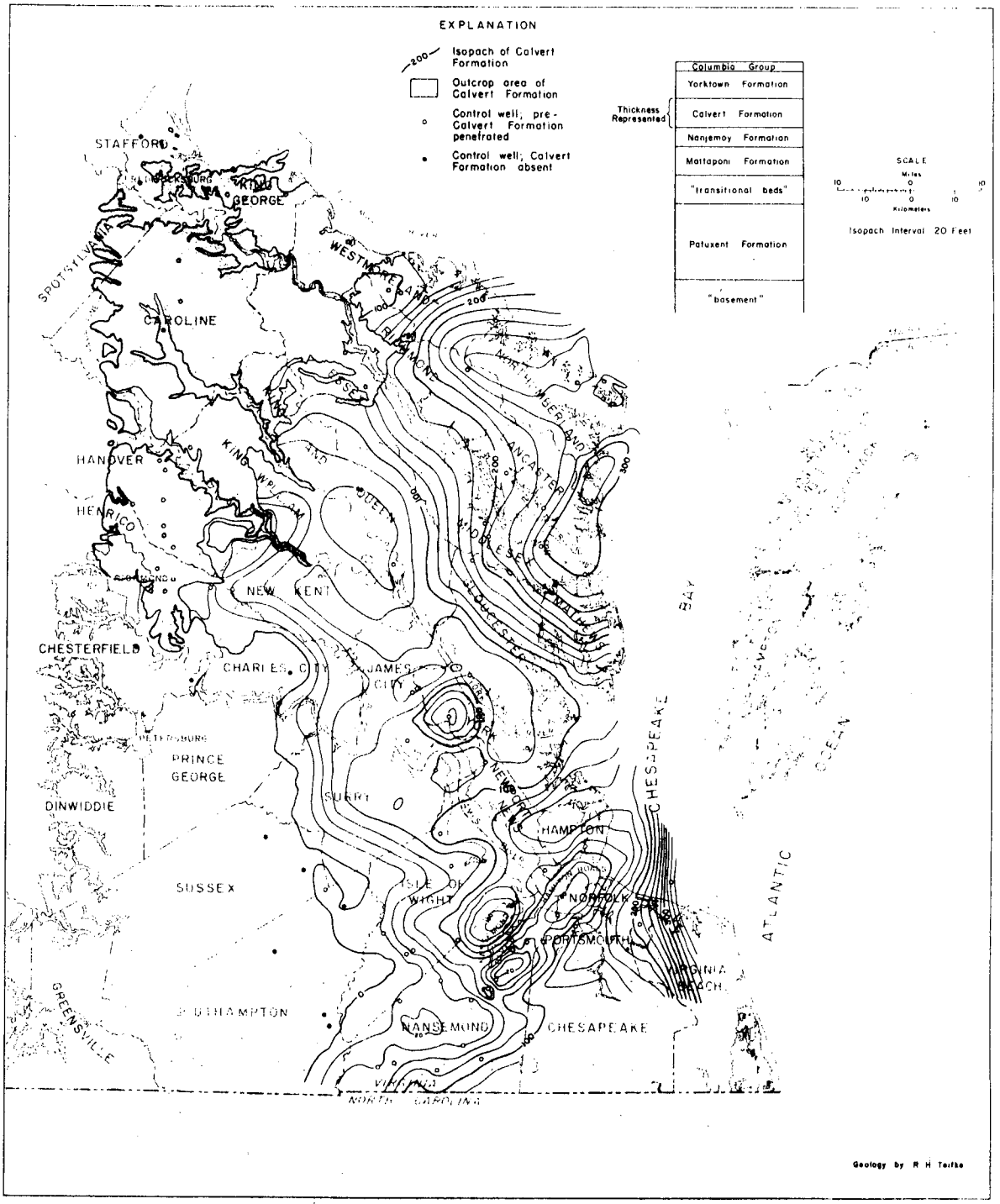

ISOPACH MAP OF THE CALVERT FORMATION
COASTAL PLAIN OF VIRGINIA
1973

Figure 12. Isopach map of the Calvert Formation(Teifke, 1973).

Miocene

St. Mary's Formation

In southeastern Virginia, the clam Pecten clintonius is diagnostic of the basal Yorktown (Bick and Coch, 1969), while Spisula rappahannockensis and Isognomon maxillata are characteristic of the underlying unit, the Virginia-St. Mary's Formation. S. rappahannockensis is more common as a guide fossil in central Virginia.

The St. Mary's in central Virginia is a generally thin (10-15 m) fine grained, locally fossiliferous marine sand. To the southeast (south of Williamsburg and in the York-James Peninsula), it reachees thicknesses of nearly 50 m in the subsurface and is composed of interbedded fine sand and coquina (Bick and Coch, 1969).

Miocene-Pliocene

Yorktown Formation

Described first in bluffs along the York River, the Yorktown Formation in the type area is dominantly marine, with layers of coquina alternating with fossiliferous sands. Farther to the west, estuarine and fluvial components become more important. In thickness, the Yorktown, which in some areas is missing due to post-depositional erosion, reaches 110 m near the mouth of the James River (Teifke, 1973) and thins rapidly to the area east of Richmond, where 15-20 m is representative. Contact with underlying units is generally thought to be unconformable (Teifke, 1973), with up to a meter of relief reported on the underlying Nanjemoy in the Hopewell area (Dischinger, 1979).

The Yorktown in some areas is glauconitic and locally contains abundant foraminifera, gastropods, pelecypods and echinoid spines.

The Yorktown has a major fluvial component in the central and northern Coastal Plain (Fig. 13). Interbedded with fluvial sand and gravel layers are fossiliferous glauconitic fine sands, mainly in the lower Yorktown. The sands often grade up from a fossil-rich layer into fine glauconitic sands and into fine silts and clays. The Yorktown was deposited under marine, estuarine and fluvial conditions. Paleontological data on the Yorktown may be found in Dischinger (1979), Bick and Coch (1969), McLean (1966), and Gardner (1943), among others.

Cenozoic

Pliocene-Holocene

"Columbia Group"

The Columbia Group is a term applied to deposits of variable thickness (usually <20 m) which accumulated mainly along major drainageways (York, James, Rappahannock and Potomac) during several per-

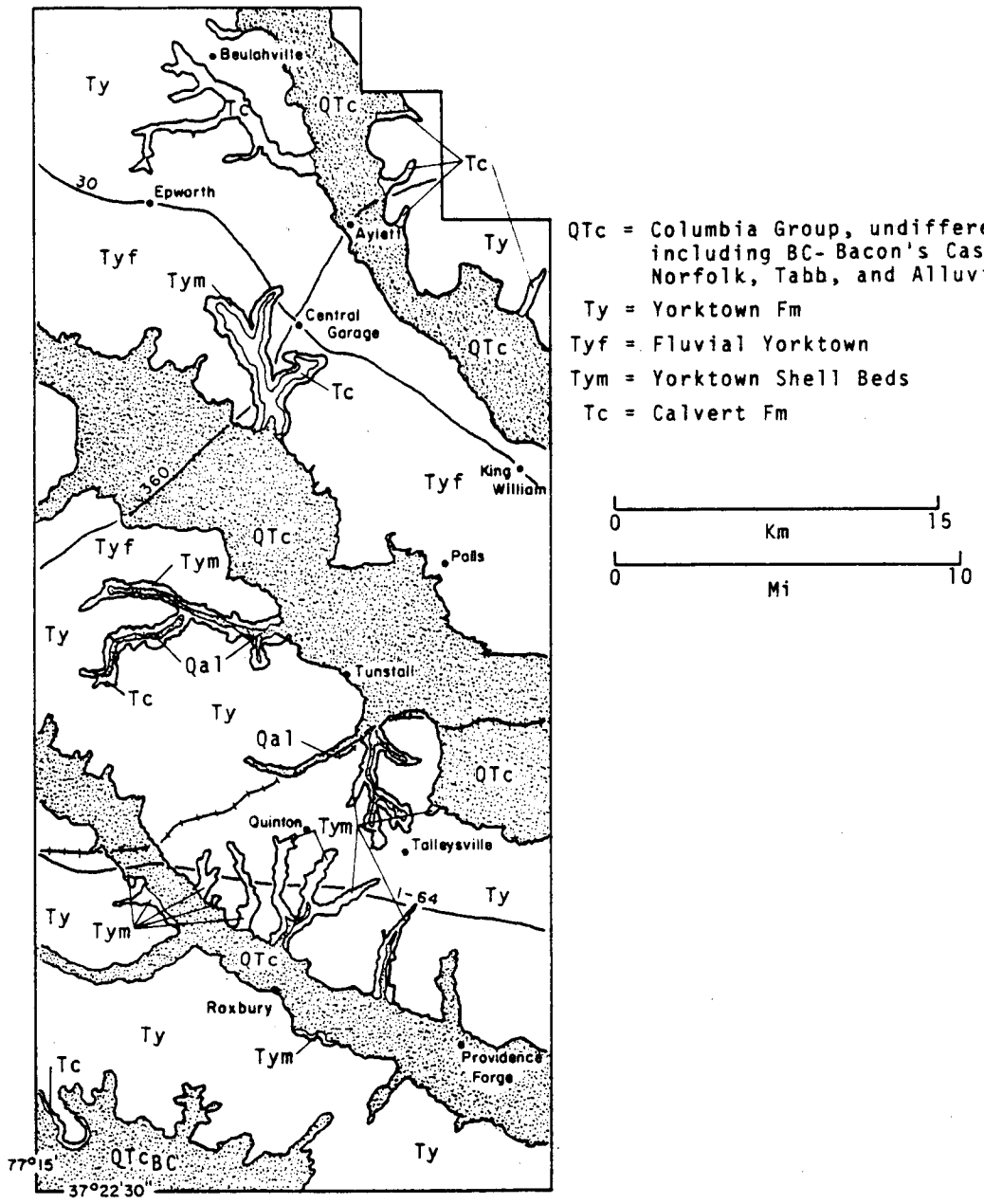

Figure 13. Reconnaissance geologic map of a portion of the central Coastal Plain, by R. L. McConnell, October, 1979-May, 1980.

iods, from Late Pliocene through Pleistocene time, when the sea stood at higher levels than at present. Advances and retreats of the sea resulted in geomorphic features called by various workers "terraces" or "plains" (Coch, 1968), and scarps. The oldest of these "plains" stands the highest, the youngest is nearest sea level. The various plains are underlain by sediments generally of an estuarine character, which may however grade into nearshore marine (becoming more pronounced to the east) and fluvial (more dominant to the west). The plain surfaces and sediments which make up the plains are presently referred to, in ascending order, as the Tabb, Norfolk, and Bacon's Castle (Coch, 1968; Bick and Coch, 1969). These sediments are referred to as formations and may be found at predictable levels along major drainageways. Figure 14 is a schematic representation of plain and scarp topography, and stratigraphy, longitudinal and traverse to a major drainageway.

Faulting in the Virginia Coastal Plain

Previous Work

Examples of post-Triassic faulting are rare in Virginia and known to exist in the Virginia Coastal Plain only along the western margin. Recent work by Mixon and Newell (1977, 1978) and Dischinger (1979) has located surface faults associated with geomorphic lineations such as truncated terraces and altered stream courses, and gravity and aeromagnetic gradients in basement crystalline rocks. Mixon and Newell (1977, 1978) have defined the Stafford fault system trending SW from near Woodbridge, Virginia, through Fredericksburg to north of Spotsylvania (Fig. 3). The Stafford system trends parallel to a pronounced aeromagnetic lineament. Presumably rigidity contrasts in rocks across the gradient, or old faults, localized stresses which resulted in the largely high-angle reverse faults of the Stafford fault system. Mixon and Newell (1977) further note that the Brandywine fault system of Maryland trends SSW from just north of the Potomac under the Coastal Plain, coinciding with a gravity gradient in northern Virginia. To the southwest along this gradient is found the fault-bounded Richmond Triassic basin. Maximum displacement on the Stafford system ranges to 50 m, and deformation took place during Cretaceous-Middle Tertiary time. The faults have been traced for up to 13 km (Mixon and Newell, 1977).

Dischinger (1979) in an unpublished M.S. thesis, has identified zones of post-Triassic faulting in the vicinity of Hopewell, Virginia. Figure 15, a structure-contour map on the base of the Aquia Formation, based largely on power-auger traverses, documents offsets along two north-trending zones (Dischinger, 1979) and suggests graben-horst structures. Moreover, at least portions of the course of the James and Appommattox Rivers seem to be affected by the fracture systems. These faults, as well as the Stafford fault system of Mixon and Newell (1975, 1978) can be seen to parallel gravity gradients in the subsurface, further documenting possible controls on faulting in the Coastal Plain.

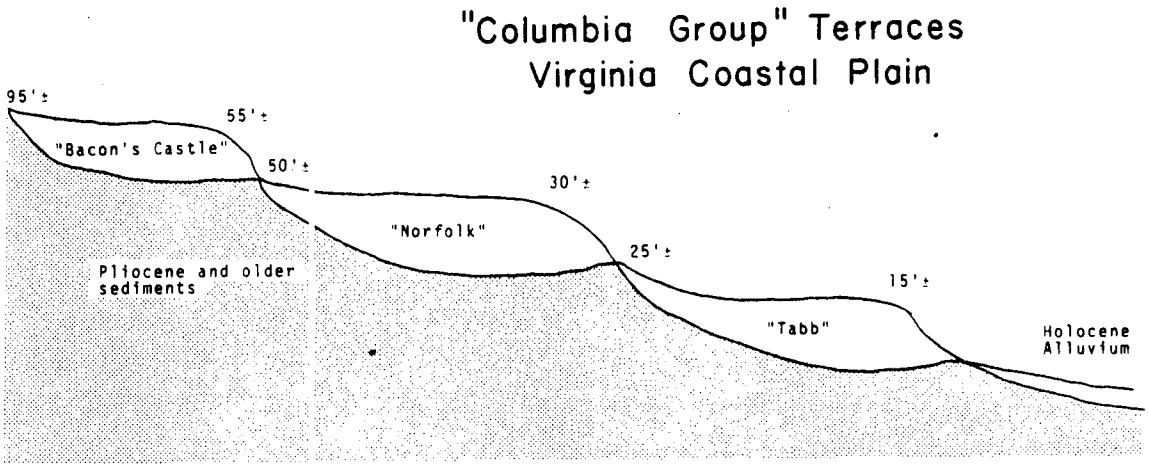

Figure 14. Schematic representation of Columbia Group terrace deposits along a major drainageway in the central Coastal Plain. The Bacon's Castle may reach elevations of over 100 ft. in the study area.

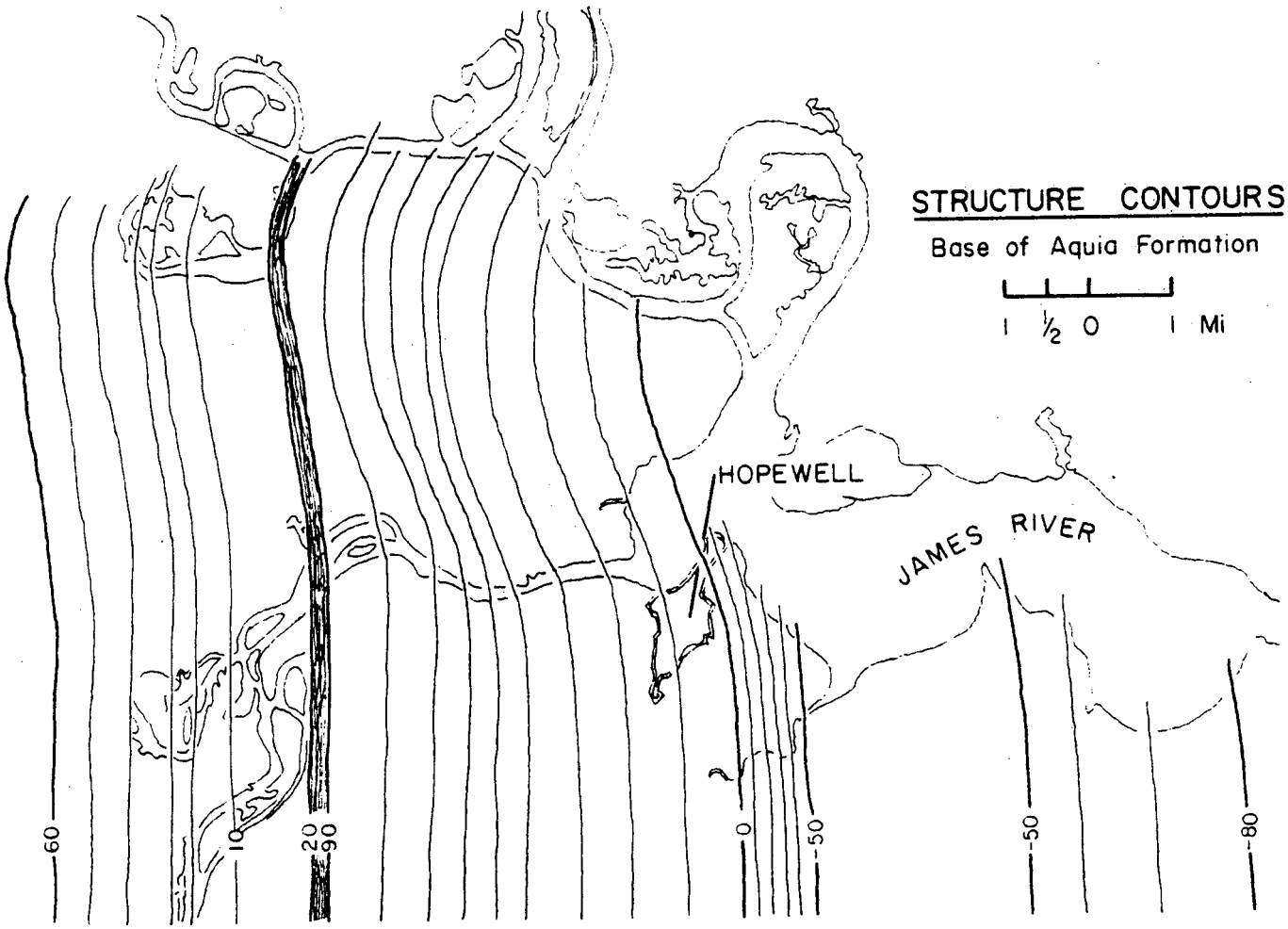

Figure 15. Structure-contours on the base of the Aquia Formation, Hopewell area, Virginia (after Dischinger, 1979). Note oversteepening at left and center of map.

Cederstrom (1945), on the basis of well-log data which indicated significantly greater thickness of Eocene sediments north of the James than south, postulated a fault system occupying the southeastern present river course and extending as far west as James City County which he named the Hampton Roads Fault. Though uncertainty on formation boundaries has led more recent workers to question the magnitude of the difference in thickness of Eocene sediments, the possibility exists that a major structural zone exists in that region. Drilling and geophysical studies would be necessary to verify the existence of such a structure.

Present Research

The present study centers on portions of nine quadrangles in the central Virginia Coastal Plain (Fig. 13). By reference to geophysical maps (Figs. 1,2), it is apparent that strong N and NE trending aeromagnetic and gravity gradients exist across these quadrangles. By comparison to areas previously mentioned, along the Coastal Plain margin, faulting, if present, should tend to be localized parallel to such gradients. With this in mind, investigation of all borrow pits, quarries and large man-made excavations in this nine-quadrangle area was carried out. Such work had a dual purpose: to search for evidence of surface faulting, and to aid in understanding of sedimentary and stratigraphic framework of Columbia Group and Yorktown beds.

Further work involved reconnaissance geologic mapping over the study area and adjacent areas, which has taken approximately 7-8 field weeks to date. Recognition of the nature and extent of surface units is essential in determining position of Columbia Group terrace deposits which usually have truncated some stratigraphic section beneath them. In addition, presence or absence of units such as the Virginia St. Mary's may be important in positioning power auger traverses. Geologic mapping is continuing in the study area.

All well samples in the study area on file with the Division of Mineral Resources in Charlottesville have been petrographically studied as an aid in projection of geologic units in the field, and as an aid in lithofacies analysis. Cuttings from approximately two dozen wells have been studied.

Furthermore, cores intersecting basement throughout the Coastal Plain have been studied to determine depth to basement, and depth of key horizons such as the top of the Patuxent Formation. Lithofacies analysis of the Patuxent has begun with analysis of the 300 m incomplete section at Hog Island, Surry County, and analysis of the upper 10-100 meters of the Patuxent exposed in wells from Westmoreland and Northumberland Counties on the NE to Middlesex, Gloucester, James City and York Counties along the east coast, on the west side of Chesapeake Bay, through the study area to the western margin of the Coastal Plain (Chesterfield and Caroline Counties) where the Patuxent is relatively thin. Such studies are continuing and will be expanded to the southeastern Coastal Plain, where the Patuxent thickens and fines considerably (Fig. 8).

A potential lineament has been identified in the Tunstall and King William quadrangles by analysis of Landsat imagery and air photos. The feature seems to truncate a terrace deposit along the Pamunkey River. Although reconnaissance mapping has not indicated evidence of surface faulting, detailed mapping and power-auger traverses will be carried out to determine the nature of this feature.

Further efforts to be undertaken include:

Power auger traverses across the inferred buried Triassic basin in the Studley 7.5 minute quadrangle are in progress to determine nature and age of any offset, by construction of structure-contour maps on key horizons, such as the top of the Nanjemoy Formation.

Investigation of bluffs and terraces along the Pamunkey and Mattaponi Rivers in the study area, where these rivers intersect subsurface gravity and aeromagnetic gradients, will be undertaken by boat. A fault in one such bluff along the James River at Drewrey's Bluff (Cederstrom, 1945; York and Oliver, 1976) south of Richmond has been described, and Dischinger (1979) has trenched the aforementioned fault along a bluff of the James and Appomattox Rivers, near Hopewell (see above).

Selection of potential sites for VIBROSEIS traverses. Two such sites have been tentatively suggested: normal to the James River in the southern portion of the Westover quadrangle; and roughly parallel to State Highway 30, in the Beulahville quadrangle, where the road cuts nearly at right angles to the gravity gradient. Further sites will be selected on the basis of detailed mapping and power-auger traverses.

Lithofacies analysis of the Patuxent Formation will be carried out to determine likely areas where thick (†700 m) sections of the Patuxent may contain appreciable quantities of water under favorable conditions of high heat flow and low thermal conductivity. Semi-quantitative estimates of thermal conductivity and permeability will be undertaken on the basis of sediment characteristics from study of well cuttings, and published literature.

Finally, sample preparation is underway to conduct analyses of heavy mineral suites from sediments of the terrace deposits of the Columbia Group to aid in provenance determination and evaluate this method of relative age determination in the field. Scanning electron microscopy is planned on the quartz grains of the same units to determine if abrasion can serve as a qualitative guide to relative ages, effects of transport, and solution.

References

Bick, K. F. and N. K. Coch, 1968, Geology of the Williamsburg, Hog Island and Bacon's Castle Quadrangles, Virginia: Va. Div. Min. Res. Rep. Inv. 18.

Brown, P. M., J. A. Miller and F. M. Swain, 1972, Structural and stratigraphic framework and spatial distribution of permeability of the Atlantic Coastal Plain, North Carolina to New York: U. S. Geol. Surv. Prof. Paper 796.

Cederstrom, D. J., 1945, Geology and Ground-Water Resources of the Coastal Plain in Southeastern Virginia: Va. Geol. Surv. Bull. 63.

Coch, N. K., 1966, Geology of the Benn's Church, Smithfield, Windsor and Chuckatuck Quadrangles, Virginia: Va. Div. Min. Res., Rep. of Inv. 17.

Dischinger, J. D., 1979, Late Mesozoic and Cenozoic stratigraphic and structural framework near Hopewell, Virginia: unpublished M.S. thesis, Univ. of North Carolina, Chapel Hill.

Gardner, J., 1943, Mollusca from the Miocene and lower Pliocene of Virginia and North Carolina: U. S. Geol. Surv. Prof. Pap. 199-A.

McConnell, R. L., 1977, Environmental report on ERDA-funded geothermal drilling activity - Coastal Plain and Piedmont Provinces - Virginia and adjacent states: U. S. Energy Research and Development Administration, unpublished report.

McLean, J. D., 1966, Miocene and Pleistocene foraminifera and ostracoda in southeastern Virginia: Va. Div. Min. Res. Rep. Inv. 9.

Mixon, R. B. and W. L. Newell, 1977, Stafford fault system; structures documenting Cretaceous and Tertiary deformation along the Fall Line in northeastern Virginia: Geology, 5, 437-440.

_____, 1978, The Faulted Coastal Plain Margin at Fredericksburg, Virginia: Guidebook, 10th Annual Virginia Geology Field Conference.

Owens, J. P., 1969, Post-Triassic tectonic movements in the central and southern Appalachians as recorded by sediments of the Atlantic Coastal Plain: Ch. 28 in Studies in Appalachian Geology: Central and Southern, G. W. Fisher, F. J. Pettijohn, J. C. Reed and K. N. Weaver, eds., Interscience Publ., 417-427.

Reilly, J. M., L. Glover, III, and E. S. Robinson, 1980, A geologic and potential field investigation of part of the central Virginia Piedmont with reference to the geologic framework of current seismicity: Quarterly Report to the U.S. Nuclear Regulatory Commission, February, 1980.

Teifke, R. H., 1973, Stratigraphic units of the lower Cretaceous through Miocene series: in Geologic Studies, Coastal Plain of Virginia, Va. Div. Min. Res., Bull. 83, pt. 1, 1-78.

York, J. G. and J. E. Oliver, 1976, Cretaceous and Cenozoic faulting in eastern North America: Geol. Soc. Am. Bull., 87, 1105-1114.

B. Geophysics

Stratigraphic Correlation of the Crisfield Test Hole (DGT-1) To Other Deep Holes

M. Svetlichny and J. J. Lambiase
Regional Geophysics Laboratory

A regional lithostratigraphic correlation can be made from DGT-1 to other basement holes in the Eastern Shore of Maryland and Virginia. The three basement holes included for correlation are the Taylor No. 1 test hole near Temperanceville, Virginia, the Hammond Well No. 1, Salisbury, Maryland and the Bethards Well No. 1 located near Berlin, Maryland (Fig. 1). In addition, any lithologic contrasts between DGT-1 and the Janes Island Well, Crisfield, Maryland are mentioned. Whenever the classification systems of Maryland and Virginia disagree, the chronostratigraphic units proposed by Brown and others (1972) were used to correlate time equivalent formations.

The structural configuration of the basement in the vicinity of the deep holes includes 1) the axial zone of the Salisbury Embayment, 2) the southern flank of the Salisbury Embayment and the extension to the Norfolk Arch, 3) a pronounced change in strike of the basement surface north and south of the axial zone and 4) an increased slope of the basement surface east of longitude 75°30'. These structures are described in greater detail by Brown and others (1972) and Hansen (1978). The Taylor hole and DGT-1 are located approximately 0°30' south of the axial zone on the southern flank of the Embayment and within that portion of the Coastal Plain beneath which the basement rock surface has a dip of 10 to 14 m per km. The predominant strike direction of the basement complex is south to south-southeast for these two holes. The Hammond and Bethards holes are located near latitude 38°20'; this latitude coincides with the axial zone of the Salisbury Embayment. Farther west, in Dorchester and Calvert counties, the axial zone is centered at latitude 38°30', and the axis trends in a west-northwest direction. The Hammond hole also marks the approximate boundary between the two regions of different basement slope. About 30 km to the east, the Bethards hole is within the area where basement rocks dip from 17 m to 28 m per km, or roughly twice the slope of the basement surface west of longitude 75°30'.

These major structural features of the basement complex were the primary controls for determining the areal extent of depositional environments throughout the Cretaceous and Tertiary Periods. Vertical readjustment to stress within the area including the Salisbury Embayment and the Norfolk Arch is directly associated with stratigraphic pinchouts that were initiated in the Upper Cretaceous Epoch and continued into the Paleocene Epoch.

The basal Coastal Plain sediments occurring in the four basement holes are of Late Jurassic-Early Cretaceous Age and are designated as Unit-H. Rocks of Unit-G, also Early Cretaceous in age, display a similar areal distribution to Unit-H and together they comprise the Patuxent Formation. Underlying the Patuxent in DGT-1 in the depth interval 1286.9 - 1362.2 m (4222 - 4469 ft) are consolidated sediments

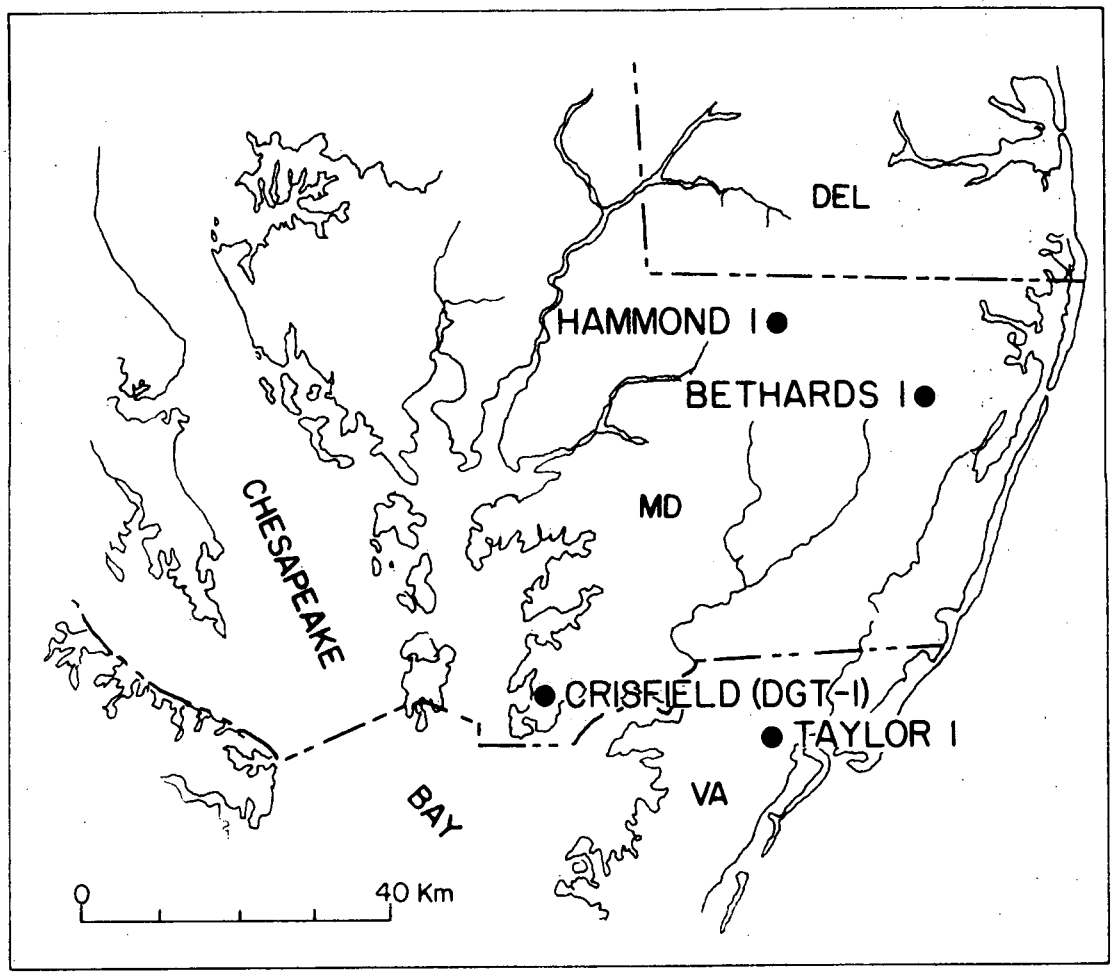

Figure 1. Location of the Crisfield (DGT-1), Taylor #1, Hammond #1, and Bethards #1 wells.

of an undetermined formation. Red beds and arkosic sands of uncertain age underlie the Patuxent in the Hammond, Bethards, and Taylor holes (Robbins and others, 1975). The regional dip for the top of the Patuxent east of longitude 75°30' and between the Hammond and Bethards holes is about 20 m per km, but the average regional dip west of this longitude in the Eastern Shore is less than 8 m per km (pl. 8, Brown and others, 1972). Electric log correlation from DGT-1 to the Taylor hole suggests that the top of the Patuxent is at 993.6m (3260 ft) in the latter. Below this depth, the electric log indicates the first appreciable bodies of sand typical of the Patuxent. The formation increases in thickness from 466.3 m (1530 ft) in DGT-1 to 861.4 m (2826 ft) in the Taylor hole. In the Hammond and Bethards holes the upper limit of the Patuxent has not been defined, but was assigned by Robbins and others (1975) to the Potomac Group.

In the Delmarva Peninsula, Units H and G are chiefly nonmarine, and consist primarily of fine to very coarse, gravelly, arkosic and quartz sands interbedded with thinner layers of shale and sandy shale. The gravels are more highly concentrated in the basal portion, but are locally common throughout the section. Layers of clean sand occur but are subordinate to sand beds mixed with minor amounts of shale. The sands generally become less arkosic and finer grained upward. The shales are frequently mottled in shades of red-brown, maroon and gray, and to a lesser extent in shades of yellow and green.

The uppermost beds of Lower Cretaceous Age (stratigraphic Unit-F) are represented by the Patapsco-Arundel group in Maryland. The areal distribution of this unit also is similar to that of Units H and G, but structure contours for the top of Unit-F indicate that east of the Hammond hole the slope has decreased to approximately 10 m per km. West of the Hammond and Taylor holes, throughout Wicomico, Somerset, and Accomack counties, the average regional dip is close to 5 m per km (Brown and others, 1972). According to Anderson (1948) sediments from the Patapsco-Arundel group were encountered from 705.0 - 1348.4 m (2313-4424 ft) in the Hammond hole and from 844.3 - 1486.3 m (2770 - 4876 ft) in the Bethards holes; however, Robbins and others (1975) prefer to leave this section within the Potomac Group. In DGT-1, sediments from the Patapsco-Arundel group extend from 564.5 - 820.5 m (1852 - 2692 ft), while in Taylor #1 the equivalent section ranges from 475.5 - 993.6?m (1560 - 3260? ft).

Although beds in this region are generally nonmarine, marine sections have been recognized in the Hammond and Bethards holes (Brown and others, 1972). The differentiation of the Patapsco-Arundel group into distinct formations by lithology alone is possible only where clays characteristic to the Arundel are present (Glaser, 1969). In DGT-1 at a depth of 701.6 m (2302 ft), a lithologic change from predominantly dark gray shales in the lower portion to an alternating sand and shale section above determines the contact between these two formations. Overall, Unit-F is represented by thick white sands but contains thicker shale and sandy shale beds than the underlying Units H and G.

At the base of the Upper Cretaceous Epoch and continuing into the Paleocene Epoch, much of the Eastern Shore of Maryland and Virginia was an environment of erosion and/or nondeposition. During this time the Norfolk Arch was a tectonically positive feature with respect to the Embayment area, causing sediments advancing southward to thin and eventually terminate (Hansen, 1978). Structure contour maps (pls. 10,11, Brown and others, 1972) for the top of Units E and D (Raritan Formation) indicate that the sediments have pinched out throughout most of the Eastern Shore except for the eastern half of Worcester County; however, the updip limit of strata for these units is farther south and west than shown because Raritan sediments occur in DGT-1, the Janes Island and Hammond holes. According to Anderson (1948) the Raritan ranges from 484.0 - 705.0 m (1588 - 2313 ft) in the Hammond hole, while Robbins and others (1975) place all pre-Magothy beds below 466.3 in the Potomac Group. In DGT-1 and the Taylor hole, the top of the Raritan is at 360.3 m (1182 ft) and at 438.9 m (1440 ft) respectively with the surface beds dipping at 2.5 m per km.

Unit-E is nonmarine in Maryland and marginal marine in southeast Virginia, while Unit-D is generally nonmarine to marginal marine in both areas (Brown and others, 1972). The lithology of the sediments in Hammond #1 and Bethards #1 is similar to that of DGT-1, consisting mostly of intercalated thin sands and clay-shales. The sands are generally very-fine to medium grained and micaceous. The clay-shales are colored in shades of red, brown, gray, and are commonly lignitic. In DGT-1, the sands from the top of the formation to 429.8 m (1410 ft) are mostly fine to medium grained. Coarse grains are common from 429.8 m (1410 ft) to 360.3 m (1182 ft). In Hammond #1, the sands are generally finer, without coarse grains, and shale is more abundant than in DGT-1.

The distribution of beds in the overlying Unit-C (Magothy Formation) also is determined largely by the structural effect of the Norfolk Arch which causes a continuous stratigraphic pinchout zone extending from southern Maryland to the Virginia-North Carolina border. The exact updip limit in the subsurface is not delineated due to a lack of data from sparse wells in the Chesapeake Bay area, but the Magothy was encountered in DGT-1 from 338.9 m (1112 ft) to 360.3 m (1182 ft) and in the Janes Island hole from 338.3 m (1110 ft) to 349.0 m (1145 ft). In the Hammond hole, fine sand and clay beds ranging from 451.1 - 466.3 m (1480 - 1530 ft) were assigned to the Magothy while electric log data restricted this formation to the depth interval 568.4 - 576.1 m (1865 - 1890 ft) in the Bethards hole (Robbins and others, 1975).

Lithologically, the Magothy Formation contains more quartzose sand in DGT-1 than in Hammond #1. Clay-shales interlaminated with very fine sands predominate in both the Hammond and Bethards holes, but fine to medium sands and thinner clay stringers occur in DGT-1. Carbonaceous matter and lignite are common in each hole but reworked fossil fragments occur only in the Hammond and Bethards holes. The gradual fining of the sediments and the presence of shell fragments downdip indicate a facies change progressing from a marginal marine to a marine condition.

Overlying the Magothy and correlated with the Matawan and Monmouth Formations in Maryland are Units B and A respectively. These two units represent the uppermost beds of the Upper Cretaceous Series and were deposited under more marine conditions than Unit-C. The updip limit of Units B and A is similar to Unit-C, although their occurrence in DGT-1 and the Janes Island hole is questionable due to lithologic similarity with the overlying Paleocene Series. Directly above the Magothy in DGT-1 and extending from 326.1 - 338.9 m (1070 - 1112 ft) are alternating beds of clayey, gray, fine to medium quartz sand and thinner beds of fine sandy clay, both slightly glauconitic. The lack of abundant glauconite and a poor resemblance to the characteristic lithology of the Matawan and Monmouth Formations suggests that the entire interval from 259.7 - 338.9 m (852 - 1112 ft) is represented by rocks of Midway Age. The Matawan is marine in the Eastern Shore and consists of lead gray glauconitic clay in Hammond #1 and glauconitic sandy clay in Bethards #1 (Anderson, 1948). The Monmouth, also marine, contains dark green argillaceous, glauconitic sand; the sand is generally coarser than in the Matawan. For the Hammond hole, Robbins and others (1975) assigned the Monmouth to the depth interval 411.5 - 424.6 m (1350 - 1393 ft) and the underlying 26.5 m (87 ft) was assigned to the Matawan. In the Taylor hole, 18.3 m (60 ft) of Cretaceous sediments above the pre-Magothy unconformity 420.6 m (1380 ft) were left undivided.

Toward the end of the Paleocene Epoch, marine sediments were deposited throughout the entire Eastern Shore and most of the Virginia Peninsula (pl. 15, Brown and others, 1972). Rocks of Midway Age in the Janes Island well and in DGT-1 are alternating beds of gray clay and fine to medium quartz sand with varying amounts of glauconite. Farther east in the Hammond and Bethards holes, sand is not as abundant and the Paleocene sections consist almost entirely of dull brown glauconitic clay and sandy clay. The top of the Paleocene Series in DGT-1 is placed at 259.7 m (852 ft). In the Taylor hole, the Paleocene-Eocene contact is at 463.3 m (1520 ft). This gives a regional dip between the two holes of 6.2 m per km.

The Lower Eocene Series (Rocks of Sabine Age) is absent from Somerset and Worcester Counties southward to the Virginia-North Carolina border. In Taylor #1, 76.2 m (250 ft) of the Nanjemoy Formation (Rocks of Claiborne Age) were encountered from 387.1 - 463.3 m (1270 - 1520 ft). In this hole, marginal marine sediments consist of dark gray, medium to coarse quartz sand that is commonly glauconitic (Onuschak, 1972). Glauconite is diagnostic in the Nanjemoy from Hammond #1 341.4 - 356.6 m (1120 - 1170 ft), but the sands generally are finer grained and contain interbeds of gray-brown clay. The section ranges from 396.2 - 425.8 m (1300 - 1397 ft) in the Bethards hole with a similar lithology of glauconitic sandy clay. The Piney Point Formation of Jackson Age is the uppermost Eocene unit and occurs in each of the four holes in Maryland. It is generally a thin shallow marine formation ranging from 21.3 m (70 ft) thick in DGT-1, to 30.5 m (100 ft) thick in Hammond #1, and approximately 61.0 m (200 ft) thick in Bethards #1. In DGT-1 and the Janes Island well, the sediments are gray fine to coarse quartzose sand and glauconitic sand in a green,

clayey matrix (Hansen, 1967). In the Hammond and Bethards holes, a brown silty clay predominates with only a minor amount of fine sand.

The Calvert Formation (Rocks of Middle Miocene Age) unconformably overlies the Piney Point in the four holes in Maryland and overlies the Nanjemoy in Taylor #1. This formation represents a major marine transgression with sediments overstepping progressively older strata to the west, so that in Maryland the Calvert may overlie units as old as Midway Age and in Virginia it directly overlies units as old as Lower Cretaceous Age (Hansen, 1978). A continuous cover of these beds overlies that portion of the Coastal Plain that was previously affected by stratigraphic pinchouts. The structural surface map (pl. 20, Brown and others, 1972) indicates a relatively small dip at the end of Middle Miocene time, averaging 1 m per km. The top of the Calvert in DGT-1 is at 131.7 m (432 ft) and it is 106.7 m (350 ft) thick. Farther east in Taylor #1, the Calvert ranges from 240.8 - 387.1 m (790 - 1270 ft). According to these depths, the regional dip between DGT-1 and Taylor #1 is close to 3.4 m per km.

The diagnostic lithology of the Calvert is its abundant diatomaceous clay and silt, mainly dark gray, green, and brown with minor amounts of fine sand. Macrofossils are scarce throughout, but in DGT-1, Janes Island, and Hammond #1 shell fragments become common towards the upper contact. The sand fraction is generally restricted to the basal sediments, but in DGT-1 and Hammond #1, fine sand also occurs in the upper 18.3 m (60 ft). The lithology of the Calvert in Taylor #1 is different from the other holes in that the clays contain a fair amount of medium sand, with coarse sand common in the bottom quarter of the interval (Onuschak, 1972).

The Choptank, St. Marys and Yorktown Formations are correlated with the Late-Miocene stage in Maryland. In Virginia Late Miocene beds are not lithologically distinct, and are referred to as the Yorktown Formation. However, the proximity of the Taylor hole to the state of Maryland makes it possible to subdivide the Yorktown by comparison of the electric logs between Taylor #1 and the Crisfield holes. The structure-contour map (pl. 21, Brown and others, 1972) indicate an average dip of .4 m per km for the top of Late-Miocene beds. Between Crisfield and Taylor #1, this slope is closer to 1.1 m per km as the top of the Late Miocene section deepens from 12.2 - 48.8 m (40 - 160 ft). The areal distribution of Late Miocene beds is similar to the distribution of the Calvert although the updip limit is farther to the east because several marine regressions occurred during the close of the Miocene Epoch.

The Choptank in the Eastern Shore of Maryland is recognized by clayey, gray, fine to medium grained sands and shell beds. In the Crisfield holes and Taylor #1, the Calvert clays grade into the basal sediments of the Late Miocene stage. The electric log from 189.0 - 240.8 m (620 - 790 ft) in Taylor #1 resembles the log pattern for the Choptank in DGT-1 106.7 - 134.1 m (350 - 440 ft). In Hammond #1, the Choptank ranges from 157.0 - 195.1 m (515 - 640 ft) and consists of pearl gray to white marl and medium-grained sand with macrofossils (Anderson, 1948).

Overlying the Choptank is the St. Marys Formation, a predominantly fine sandy clay and silt unit with shell fragments. The electric log from 121.9 - 189.0 m (400 - 620 ft) in Taylor #1 indicates clay, and on this basis the interval may be correlated with the St. Marys in DGT-1 76.2 - 106.7 m (250-350 ft) and the Janes Island well 70.1 - 94.5 m (230-310 ft). In Hammond #1, the St. Marys 100.6 - 157.0 m (330 - 515 ft) consists mainly of fine to medium grained sand and does not correlate lithologically with the other holes.

The Yorktown Formation represents the uppermost section of the Late Miocene stage in Maryland, and also can be distinguished in Taylor #1 by correlating the electric log with DGT-1. It is characterized by medium to coarse sands, granules, and gravels in gray clay and silt. Fragments of macrofossils occur in each hole except Hammond #1 39.6 - 100.6 m (130 - 330 ft) and are occasionally abundant in the Janes Island well. The Yorktown ranges in depth from 12.2 - 70.1 m (40 - 230 ft) in the Janes Island well and from 48.8 - 88.4 m (160 - 290 ft) in Taylor #1, with the surface beds dipping as 1.1 m per km.

The correlation presented above generally conforms well with prior regional stratigraphic correlations. However, there are discrepencies, but these are mainly due to modifications that were made as a result of the addition of new data. Correlation of DGT-1 to other holes in Maryland and Virginia also improves the continuity of lithologic data across the state line.

References

Anderson, J. L., 1948, Cretaceous and Tertiary subsurface geology: Maryland Department of Geology, Mines, and Water Resources Bull. 2, 441 p.

Brown, P. M., Miller, J. A., and Swain, F. M., 1972, Structural and stratigraphic framework and spatial distribution of permeability of the Atlantic Coastal Plain, North Carolina to New York: U.S. Geol. Survey Prof. Paper 796, 79 p.

Glaser, J. D., 1969, Petrology and origin of Potomac and Magothy (Cretaceous) sediments, Middle Atlantic Coastal Plain: Maryland Geological Survey, Report of Investigations No. 11, 101 p.

Hansen, H. J., 1967, Hydrogeologic data from the Janes Island State Park test well (1514 feet): Maryland Geological Survey Basic Data Report No. 3, 24 p.

Hansen, H. J., 1978, Upper Cretaceous (Senonian) and Paleocene (Danian) pinchouts on the south flank of the Salisbury Embayment, Maryland, and their relationships to antecedent basement structures: Maryland Geological Survey Report of Investigations No. 29, 34 p.

Onuschak, E. Jr., February 1972, Deep test in Accomack County, Virginia: Virginia Minerals Vol 18, No. 1, p. 1 - 4.

Robbins, E. I., Perry, W. J., Jr., and Doyle, J. A., 1975, Palynological and stratigraphic investigations of four deep test wells in the Salisbury Embayment of the Atlantic Coastal Plain: U.S.G.S. Open File Report, 120 p.

Stratigraphic Correlation of Atlantic Coastal Plain Sediments in Southeast Virginia

Micheal Svetlichny
Regional Geophysics Laboratory

Introduction

During the period September - December 1978, seven heat flow determination holes (five holes approximately 300 m deep and two "basement" holes) were drilled in the Atlantic Coastal Plain of Southeastern Virginia and the York-James Peninsula. These holes were drilled as part of our ongoing program to evaluate geothermal resource beneath the Atlantic Coastal Plain. One hole was drilled in Isle of Wight County (No. 26), and in the cities of Suffolk (No. 25A), and Norfolk (No. 24). Two holes were drilled in the cities of Hampton (Nos. 27 and 60) and Virginia Beach (Nos. 23 and 22). Holes 26 and 25A penetrate the top of the crystalline basement at depths of 423 m and 547 m respectively. Figure 1 shows the location and total depth of each hole.

This report presents a correlation of lithostratigraphic units in the Coastal Plain of the seven holes. Because of poor sampling techniques by drilling company personnel, drill cuttings were found to be unreliable for correlation of formation boundaries; however, gamma log correlation proved to be effective. In addition, a deep test well at Norfolk (TW-1, 786 m T.D.) is centrally located with respect to the seven holes, and the gamma log from TW-1 provides a base for correlating the stratigraphic boundaries in the seven research holes. A gamma log correlation for the eight holes in presented in Figure 2. In this paper, the stratigraphic nomenclature with age relationships of the Tertiary and Cretaceous formations will be the same as that used by Teifke (1973). Additional data used in support of gamma log correlation includes the structure-contour maps of Brown and others (1972), Teifke (1973), and Oak and Coch (1973).

Stratigraphy

In the two basement holes, thick intervals of indurated sediments were encountered beneath the Patuxent Formation and above the basement surface. In Hole 26, the indurated section is 64 m thick and occurs from 359 m to approximately 423 m. The drill cuttings are a mixture of siltstone, shale, feldspathic and quartz sands with a reddish color, although there may be some contamination from the overlying Patuxent sands and gravels. The basement beneath the indurated section consists of granite and greenstone. In Hole 25A, the indurated section is slightly thicker (76 m), and occurs from 472 m to 547 m. Lithologically, the sediments resemble those from Hole 26, but there are two minor intervals within the indurated section that consist of unconsolidated sediments. The basement rock below 547 m is granite. In the deep test at Norfolk, the basement rock was not reached and the hole bottomed in silt and clay (Brown, 1968). The indurated section is likely to occur in a deeper interval considering the thickness of this section approximately 20 km southwest in Hole 25A.

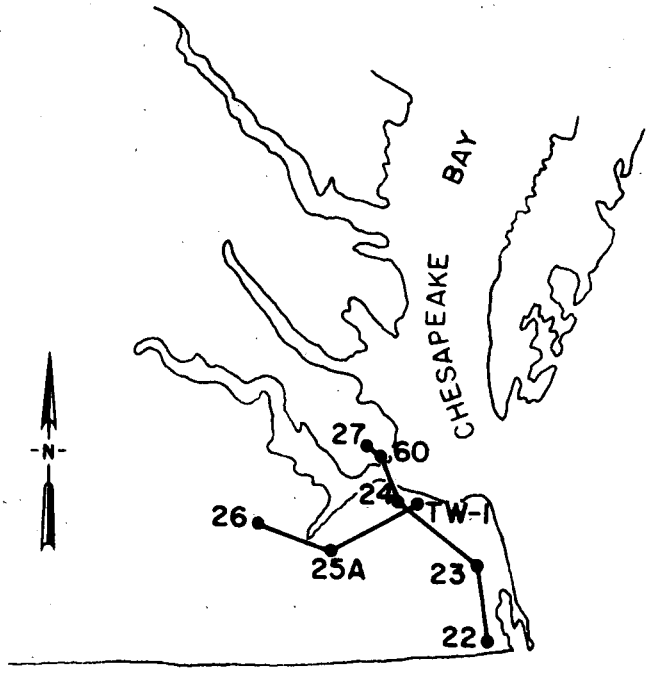

Figure 1. Location of eight drill holes in southeastern Virginia and locations of transects for gamma log correlation.

Figure 2. Gamma log correlation along the transects shown in Figure 1.

ELEV 1.5 M
27
HAMPTON

ELEV 3.0 M
60
HAMPTON

ELEV 1.5 M
24
NORFOLK

ELEV 4.6 M
23
VIRGINIA BEACH

ELEV 1.5M
22
VIRGINIA BEACH

METERS

0
50
100
150
200
250
300
350
400

POST MIO. — COLUMBIA GROUP

LATE MIOCENE — YORKTOWN

LATE EOCENE – MID MIOCENE — CALVERT

UPPER CRETACEOUS — MATTAPONI

LOWER CRETACEOUS — "transitional beds"

?

?

GAMMA LOG CORRELATIONS

HEATFLOW HOLES, TW-1 – SOUTHEAST VIRGINIA

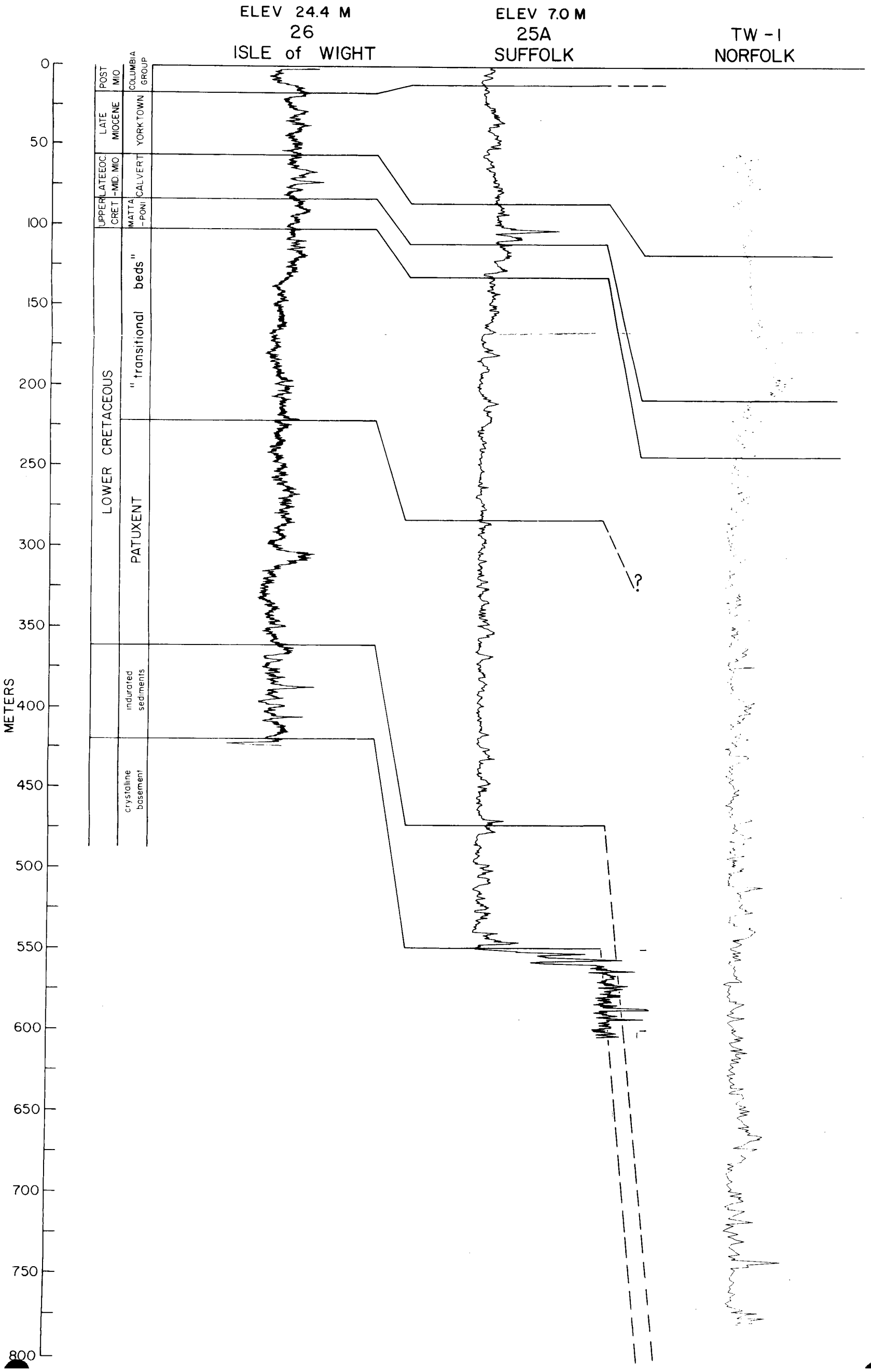

The Lower Cretaceous Patuxent Formation was penetrated fully only in Holes 26 and 25A. This unit is distinguished from the overlying "transitional beds" by coarser grained sands which are typically more feldspathic in composition, by the presence of fine gravels, and by a smaller percentage of silts and clays (Teifke, 1973). The Patuxent and the "terrestrial beds" are often gradational in lithology near the contact and cannot be readily distinguished by gamma logs.

According to Teifke (1973), the top of the Patuxent in Hole 26 is directly overlain by sediments from the Upper Cretaceous Mattaponi Formation at a depth of 123 m. Brown and others' (1972) structure map indicates the top of the Patuxent at approximately 291 m, overlain by 126 m of the Lower Cretaceous "transitional beds". This would place the top of the "transitional beds" at 105 m, reasonably close to a major break in the gamma log at 102 m that effectively defines the "transitional beds" - Mattaponi contact. It is possible that Teifke has left the Lower Cretaceous Series undivided in the area near Hole 26 and has assigned all sediments below 123 m to the Patuxent. At 220 m, the gamma log exhibits a major break. This rapid deflection in the gamma curve below 220 m may be due to the sudden increase in feldspar content typically found in the Patuxent sands. On this basis, the Lower Cretaceous section in Hole 26 is 196 m thick ranging from 102 m to 359 m, with the Patuxent-"transitional beds" contact at 220 m.

For Hole 25A, the "transitional beds" occur between 129 m and 168 m according to Teifke and from 148 m to 299 m according to Brown and others. A break in the gamma log similar to the one in Hole 26 at 220 m, occurs at 283 m, approximately 16 m above the "transitional beds"-Patuxent boundary derived from Brown and others' structure map. At 129 m, a characteristic break occurs in the gamma log such as the one that marks the "transitional beds"-Mattaponi contact in Hole 26; this agrees almost exactly with Teifke's depth. The combined thickness of the two Lower Cretaceous units is 342 m and the top of the Patuxent is at 283 m. In Holes 27, 60, and 24, the top of the Patuxent Formation was not penetrated. In these holes drilling stopped within the "transitional beds". The regional dip of the Patuxent surface derived from Brown and others' structure map is about 8 m per km, but due to the configuration of the basement surface, the formation thickens at a higher rate in an easterly direction. On a line between Hampton (Holes 27,60), Norfolk (Hole 24) and extending to Hole 22 near the southeast corner of Virginia, the total thickness remains nearly constant. Isopach thickness indicates approximately 334 m of Patuxent sediments along that line. Eastward from Norfolk to Cape Henry, the thickness increases by close to 67 m. The "transitional beds" dip to the southeast at a rate of approximately 6 m per km and thicken in the same direction. This unit is expected to be around 198 m in total thickness near Holes 27, 60, and 24 and close to 300 m at Holes 23 and 22.

A pronounced lithologic change marks the boundary between the "transitional beds" and the Mattaponi Formation. The fine-grained clastics of the "transitional beds" are succeeded by the glauconite to quartz-glauconite sands and glauconite-bearing clays of the Mattaponi.

The formation contact is reflected in the gamma logs by a steady and low gamma response in the upper segment of the "transitional beds" to a substantially higher gamma response with frequent peaks in the Mattaponi. In each hole, except for the two in the City of Virginia Beach (Nos. 23 and 22), this boundary was penetrated by drilling. In the latter two holes, drilling stopped within the Mattaponi.

Breaks in the gamma logs that define the "transitional beds"-Mattaponi contact in Holes 26 and 25A also are evident in Holes 27, 60, 24, and TW-1. The thickest section drilled within the Mattaponi is in the southeast tip of the York-James Peninsula, (No. 27) where 91 m (from 155 m to 246 m) was encountered. In the other Hampton hole, No. 60, there are 67 m between 178 m to 245 m. South of the James River at Norfolk, the Mattaponi in Holes 24 and TW-1 is represented by only 38 m (201 m - 239 m) and 33 m (207 m - 240 m) respectively. Structure maps by Teifke are in accord with both the upper and lower boundaries of this formation. Downdip, in Holes 23 and 22, the unit is undoubtedly thicker, where 54 m and 61 m were penetrated respectively, although the basal contact with the "transitional beds" was not reached in either hole. The Mattaponi generally thickens in a southeasterly direction and as much as 143 m of the unit may occur in Hole 22 (Brown and others, 1972). Westward, 20 m (109 - 129 m) was penetrated in Hole 25A and 18 m (84 - 102 m) in Hole 26.

Throughout most of the study area, the Mattaponi is overlain by the Late Eocene-Mid Miocene Calvert Formation. As outlined in Teifke's structure map, the Early Eocene Nanjemoy Formation may occur as a featheredge above the Mattaponi in the northeastern corner of the Isle of Wight county and in the northern half of the City of Hampton. Holes 26 and 27 are within these regions but the Nanjemoy is difficult to delineate because of its thinness (less than 6 m in each hole) and due to its lithologic similarity with the Mattaponi.

The basal member of the Calvert consists mainly of phosphoritic quartz sands and minor lenses of clay (Teifke, 1973). The presence of phosphate accounts for a very high rate of gamma activity and also provides an excellent marker for the Mattaponi-Calvert boundary. Upwards, the Calvert is dominated by clays and silty clays colored in shades of gray and bluish-gray.

Sediments of the overlying Late Miocene Yorktown Formation were deposited under a regressive cycle through Late Miocene time. The basal Yorktown is characterized by an influx of coarser grained clastics. Fine to coarse quartz sands and fine-grained gravels interbedded with shell beds and clay generally define the Yorktown north of the James River, whereas south of the river, the Yorktown consists of quartz-glauconite sands overlain by a sequence of bioclastic sands (Teifke, 1973). Southward, the Yorktown becomes increasingly clayey and tends to obscure the Calvert-Yorktown contact which otherwise would be evident in the gamma logs. This contact was difficult to locate in Holes 22, 23, 24, 25, and 26. For these holes, approximate depth of the contact was assigned from Brown and others' structure map. In Holes 27 and 60 in Hampton, this contact is made evident by a

lower gamma activity in the basal Yorktown, reflecting an influx of coarser sediments.

The Calvert is a relatively thin unit in Holes 26 (56 - 84 m) and 25A (85 - 109 m), but increases substantially in thickness north of the James River in Hampton, where 65 m and 76 m occur in Holes 27 (90 - 155 m) and 60 (102 - 178 m) respectively. In Norfolk, the section is slightly thicker, with 90 m at both TW-1 (118 - 207 m) and 24 (111 - 201 m). The maximum thickness is found at Hole 22 near the town of Creeds, where 94 m of Calvert sediments were penetrated (from 155 m to 249 m). In Hole 23, located at the Oceana Naval Air Station, the Calvert is 85 m thick (161 - 246 m). Throughout the entire study area, the top of the Calvert dips to the east at a uniform rate of approximately 2 m per km.

In Holes 26, 25A, 27, and 60, there are distinct inflections in the gamma logs that correspond well with Brown and others' depths for the Yorktown-Columbia Group contact. In Holes 23 and 22, the depths of these inflections are in accord with the cross sections of the Columbia Group for southeast Virginia by Oaks and Coch (1973). In Hole 24, this contact is not easily recognizable in the gamma logs and the approximate depth from Brown and others' structure map was used. The Yorktown increases in thickness in an east-southeast direction. The minimum thickness penetrated is 40 m in Hole 26 (17 - 56 m); this increases to 76 m in Hole 25A (9 - 85 m). In the Hampton-Norfolk area, the thickness varies from 68 m in Hole 27 (21 - 90 m) to 76 m in Hole 60 (26 - 102 m) and 38 m in Hole 24 (23 - 111 m). In the City of Virginia Beach, the unit increases to 140 m in Hole 23 (21 - 161 m) and it is 137 m thick in Hole 22 (92 - 155 m).

References

Brown, D. L., 1968, Memorandum report on test drilling at Norfolk, Virginia: U.S.G.S. Open File Report, 28 p.

Brown, P. M., Miller, J. A., and Swain, F. M., 1972, Structural and stratigraphic framework and spatial distribution of permeability of the Atlantic Coastal Plain, North Carolina to New York: U.S. Geol. Survey Prof. Paper 796, 79 p.

Oaks, R. Q., Jr., and Coch, N. K., 1973, Post-Miocene stratigraphy and morphology, Southeastern Virginia: Virginia Division of Mineral Resources Bull. 82, 135 p.

Teifke, R. H., 1973, Stratigraphic units of the Lower Cretaceous through Miocene Series, in Geologic Studies, Coastal Plain of Virginia: Virginia Division of Mineral Resources Bull. 83, Pt. 1, 101 p.

Lithology of the Southern Atlantic Coastal Plain With Reference to Thermal Conductivity and Temperature Prediction

Joseph J. Lambiase
Regional Geophysics Laboratory

Introduction

Until recently, geothermal exploration efforts have concentrated on the northern Atlantic Coastal Plain; that is, north of, and over, the Cape Fear Arch in southern North Carolina. Virtually all sediments in that region are clastics, almost all of which are unconsolidated. There is a marked change in the character of Coastal Plain sediments south of the arch in that carbonates are abundant. Overall thermal conductivity of southern Coastal Plain sediments may be significantly different from thermal conductivity in the northern Coastal Plain so that geothermal gradients also may be different and, therefore, temperatures at depth. However, the spatial distribution of carbonates and clastics in the southern Coastal Plain needs to be considered because this effects the accuracy with which temperatures at depth can be estimated from shallow (300 m) geothermal gradients.

Southern Coastal Plain Lithology

An analysis of the general trends in the lithology of the southern Coastal Plain indicates that most carbonate rocks are of Tertiary age, and that most Cretaceous rocks are clastics. A generalized stratigraphic column would have Cretaceous sands and clays underlying a thick sequence of Tertiary limestone that is capped by a thin sequence of late Tertiary and Quaternary sands.

Rocks of Lower Cretaceous age occur in Georgia, and are mostly sandstone and shaley sandstone with some shales. A thick Upper Cretaceous sequence occurs in South Carolina and Georgia; it is mostly sands with some clays (Richards, 1967).

Most of the Tertiary rocks in South Carolina and Georgia are carbonates. They range in composition from limestone and sands to calcareous clays and sands. In addition to the carbonates, there are thinner clastic units, chiefly sands with some clays, of Eocene and Miocene age. Pleistocene and Holocene sediments are mostly sands with minor amounts of silt, clay, and gravel (Cooke, 1936; Cramer, 1974).

Comparison to the Northern Atlantic Coastal Plain

Generally, the Cretaceous sediments of the southern Atlantic Coastal Plain are very similar to their northern counterparts. In fact, the same lithologic units comprise the Cretaceous section throughout most of the Coastal Plain (Brown and others, 1972).

The major difference between the northern and southern Coastal Plain occurs in the Tertiary section. As noted earlier, the Tertiary

of the southern Atlantic Coastal Plain is composed primarily of carbonates. In the northern Coastal Plain, Tertiary sediments are all clastic, and a high proportion of them are more fine-grained than the underlying Cretaceous sediments (Brown and others, 1972).

Thus, both the northern and southern section of the Atlantic Coastal Plain have a coarse, clastic Cretaceous section. In the south, this is overlain by a predominantly carbonate Tertiary section while in the north relatively fine-grained clastics overlie the Cretaceous sediments.

Thermal Conductivity and Temperature Prediction

The average thermal conductivity of the southern Atlantic Coastal Plain probably is higher than that of the northern Coastal Plain because of lithologic differences. The Cretaceous units are expected to have similar thermal conductivities to their northern counterparts, but the southern carbonates should have a higher thermal conductivity than the fine-grained northern sediments because calcium carbonate has a much higher thermal conductivity than clay.

There are factors that cause the thermal conductivity of carbonate sediments to vary. Obviously, the amount of calcium carbonate relative to clastic impurities is important. Probably the most important factor is porosity. Carbonates can have very low porosities if they are well cemented. Conversely, primary porosity can be high if the unit is an unconsolidated carbonate sand. Secondary porosity from dissolution and/or fracturing also can increase porosity substantially. The effect of porosity on thermal conductivity is that it controls water content. Because water has a very low thermal conductivity, water content is a very important control on bulk thermal conductivity.

It is expected that porosity, and therefore thermal conductivity, of the southern Atlantic Coastal Plain carbonates will be quite variable. There are numerous wells that produce large quantities of water from porous limestones (Thomson and others, 1956; Siple, 1975) as well as well-cemented, low porosity carbonate units. Thermal conductivity of a given lithologic unit may vary regionally depending upon water content as a result of the development of secondary porosity. Average thermal conductivity of the Tertiary carbonates probably varies from place to place, but generally it is expected to be higher than that of the fine-grained Tertiary sediments of the northern Coastal Plain.

Regional trends in thermal conductivity as a result of lithology will effect the accuracy of temperature prediction based on shallow geothermal gradient holes. Very few of the shallow (300 m) holes that were drilled in the northern Coastal Plain penetrated a substantial amount of Cretaceous sediments. Thus, the geothermal gradients that were determined in those holes are from the relatively fine-grained, low thermal conductivity Tertiary sediments, and consequently the gradients are higher than the average gradient for the entire sedimentary section. This makes prediction of temperature at depth difficult,

because it is impossible to determine exactly how much the gradient will decrease with depth due to increased thermal conductivity in the Cretaceous sediments.

Prediction of temperature at depth from shallow gradients probably will be more accurate for the southern Atlantic Coastal Plain than it is for the north. The Tertiary carbonates in the south should have a thermal conductivity that is much more similar to the underlying Cretaceous sediments than the conductivity of the fine-grained northern Tertiary sediments. Geothermal gradients determined in shallow (300 m) holes are expected to be much closer to the average gradient for the entire sedimentary section. There probably is an increase in thermal conductivity with depth, but it should not be a large increase. Also, thermal conductivity values from the deeper holes that have penetrated Cretaceous sediments in the north will help to better estimate thermal conductivity at depth. Thus, more representative shallow gradients, and better estimates of thermal conductivity at depth, should allow more accurate prediction of temperature at depth. As an example, at Jesup, Georgia, the temperature predicted at 1.3 km (basement) based on the gradient over the upper 300 m was 50 °C. The actual temperature measured at the base of the sedimentary section (1.3 km) was 50 °C.

Conclusions

There is a major lithologic difference between the southern and northern Atlantic Coastal Plain. Both regions have a thick sequence of coarse clastic Cretaceous sediments. In the south, this is overlain by Tertiary carbonates, while relatively fine-grained clastics comprise the Tertiary section in the north.

The thermal conductivity of the southern Tertiary sediments should be higher than that of their northern counterparts. However, primary and secondary porosity will strongly effect thermal conductivity. Shallow geothermal gradients determined from carbonate sediments should be close to the average gradient for the complete sedimentary section. As a result, accurate prediction of temperature at depth from shallow gradients should be more accurate in the southern Atlantic Coastal Plain than it is in the north.

References

Brown, P. M., Miller, J. A., and Swain, F. M., 1972. Structural and stratigraphic framework, and spatial distribution of permeability of the Atlantic Coastal plain, North Carolina to New York. U.S. Geol. Surv. Prof. Paper 796, 79 p.

Cooke, C. W., 1936. Geology of the Coastal Plain of South Carolina. U.S. Geol. Surv. Bull., 867, 196 p.

Cramer, H. R., 1974. Isopach and lithofacies analysis of the Cretaceous and Cenozoic rocks of the Coastal Plain of Georgia. In Symposium on the Petroleum Geology of the Georgia Coastal Plain, Stafford, L. P. (ed.), Georgia Geol. Surv. Bull., 87, 21-43.

Richards, H. G., 1967. Stratigraphy of the Atlantic Coastal Plain between Long Island and George -- a review. Amer. Assoc. Petroleum Geol. Bull., 51, 2400-2429.

Siple, G. E., 1975. Ground-water resources of Orangeburg County, South Carolina. South Carolina State Devel. Bd., Div. of Geol. Bull., 36, 59 p.

Thomson, M. T., Herrick, S. M., Brown, E. and others, 1956. The availability and use of water in Georgia. Georgia Dept. of Mines, Mining, and Geol., Bull. 65, 329 p.

VPI & SU Drilling Program:
Heat Flow and Gradient Holes
by
Richard J. Gleason
Orogenic Studies Laboratory

The heat flow/gradient test drilling program is presently mid-way through the schedule for the present fiscal year. Approximately six weeks were spent modifying our Longyear model #38 drill to an upgraded model #44 drill. The new drill is more powerful and is more capable at deeper drilling that its predecessor.

Presently completed are hole 16B, near Kinston, NC, and hole 26, at Isle of Wight, VA. Both of these holes were extensions of previously drilled and cased holes, and 300 feet of basement core were obtained from each location along with equilibrium gradient data. Our drillers recently completed gradient hole #13A at Myrtle Beach, SC. This is to date the deepest continuous hole we have drilled, having penetrated basement at 1575'. Hole caving and drill-string problems prevented acquisition of basement core, however. After completion of hole #13A, we will commence drilling hole #10, a 1000' gradient hole at Charleston, SC.

Representatives of the Division of Geothermal Energy of DOE and staff members of the Geothermal Project at VPI&SU have agreed to substitute gradient test holes at Kings Bay, GA and Cove Point, MD for previously scheduled hole #9s 23 (Virginia Beach), 12B (Georgetown), and 7A (Savannah, GA/SC area). Permitting and leasing activities have been initiated for these two new holes, and drilling may commence by September 1980. Prior to this drilling, it is anticipated that gradient hole #10 and perhaps #44 (Savannah, GA) will have been completed. Hole #59 at Smith Point, VA, has been postponed until the Fall of 1980, due to lease limitations prohibiting drilling activity on the particular property during the peak summertime marina activity.

Temperature Logs of Observation Wells in The Coastal Plain of Georgia

Wilson S. McClung
Regional Geophysics Laboratory

A survey was made of existing USGS observation wells in the Coastal Plain of Georgia (the existing observation wells of NJ, DE, MD, VA, NC, and SC have been reported on in previous reports). Geothermal gradients were determined for ten of these wells, the locations of which are shown in Figure 1. The temperature profiles of these wells are shown in Figure 2 and least square gradients range from 15.8 °C/km in TW2 to 29.3 °C/km in 12F36 and 30.6 °C/km in JE2A. Refer to Table 1 for complete well data.

The temperature profiles of five of these wells contain a disturbed monotemperature zone caused by the effect of the Ocala Formation. The Ocala Formation is composed of a highly porous and permeable cavernous limestone and is the chief fresh water aquifer in the Coastal Plain of Georgia. The monotemperature zones seen in JE2A (251-267 m), 11L2 (25-100 m), 18H16 (65-135 m), 27E4 (157-183 m), and 33M4 (166-205 m) represent the convection of water within the Ocala Formation.

Temperature Logs of Three Gas Wells In Washington County, Georgia

Temperature logs have been obtained from three gas exploration holes in Washington County, GA. Two of these holes penetrate the buried Riddleville Triassic basin beneath the Coastal Plain sequence (TRT1 and MCC1). The third hole is located a few miles further to the north off the basin and penetrates basement beneath the Coastal Plain (S791). Refer to Figure 1 for hole locations.

Hole S791 enters basement at 340 m (1115 ft) and bottoms within basement at 750 m (2460 ft). The gradient is 17.4 °C/km within Coastal Plain sediments and 14.0 °C/km within basement (Figure 3). This hole was logged approximately six months after drilling and testing procedures were completed and, therefore, had essentially reached thermal equilibrium.

Hole TRT1 was logged to a total depth of 1125 m (3691 ft). Triassic was encountered at 335 m (1100 ft). The gradient within the Triassic is 14.5 °C/km while the Coastal Plain gradient is 18.4 °C/km (Figure 4). This hole was logged approximately one year after drilling and testing procedures were completed.

Hole MCC1 was drilled to a total depth of 2860 m (9383 ft) encountering Triassic at 350 m (1148 ft) and crystalline basement at 2530 (8300 ft); however, it was temperature logged only to 2115 m (6939 m) due to the depth capacity of the VPI&SU logging system. Gradients are 15.7 °C/km within the overlying Coastal Plain and 16.0

HOLE NUMBER AND LOCATION	LATITUDE	LONGITUDE	DATE LOGGED	HOLE DEPTH (METERS)	DEPTH INTERVAL (METERS)	GRADIENT (°C/Km)
JE2 Gardi, GA	31°32.329	81°43.949	3/27/80	509.7	30.2-499.5	30.6
18H16 Adel, GA	31° 8.239	83°26.079	3/14/80	264.7	125.0-264.7	26.6
TW1 Albany, GA	31°30.149	84°6.729	3/12/80	432.6	21.4-432.6	20.4
TW2 Tarversville, GA	32°33.019	83°26.629	3/21/80	366.5	99.0-364.1	15.8
TW27 Brunswick, GA	31°16.569	81°32.669	3/27/80	533.0	13.2-518	28.5
27E4 Billy's Island, GA	30°49.719	82°21.619	3/24/80	206.6	84.3-206.6	20.4
11L2 Pretoria, GA	31°35.539	84°20.559	3/11/80	203.6	106.0-203.6	20.2
12F36 Cairo, GA	30°52.629	84°12.879	3/13/80	147.6	55.3-147.6	29.3
30L3 Jesup, GA	31°37.089	81°54.579	3/26/80	177.2	24.7-177.2	19.5
33M4 Ludowici, GA	31°38.989	81°36.099	3/26/80	264.6	43.0-264.6	26.0

Table 1. Summary of Georgia Coastal Plain observation well data.

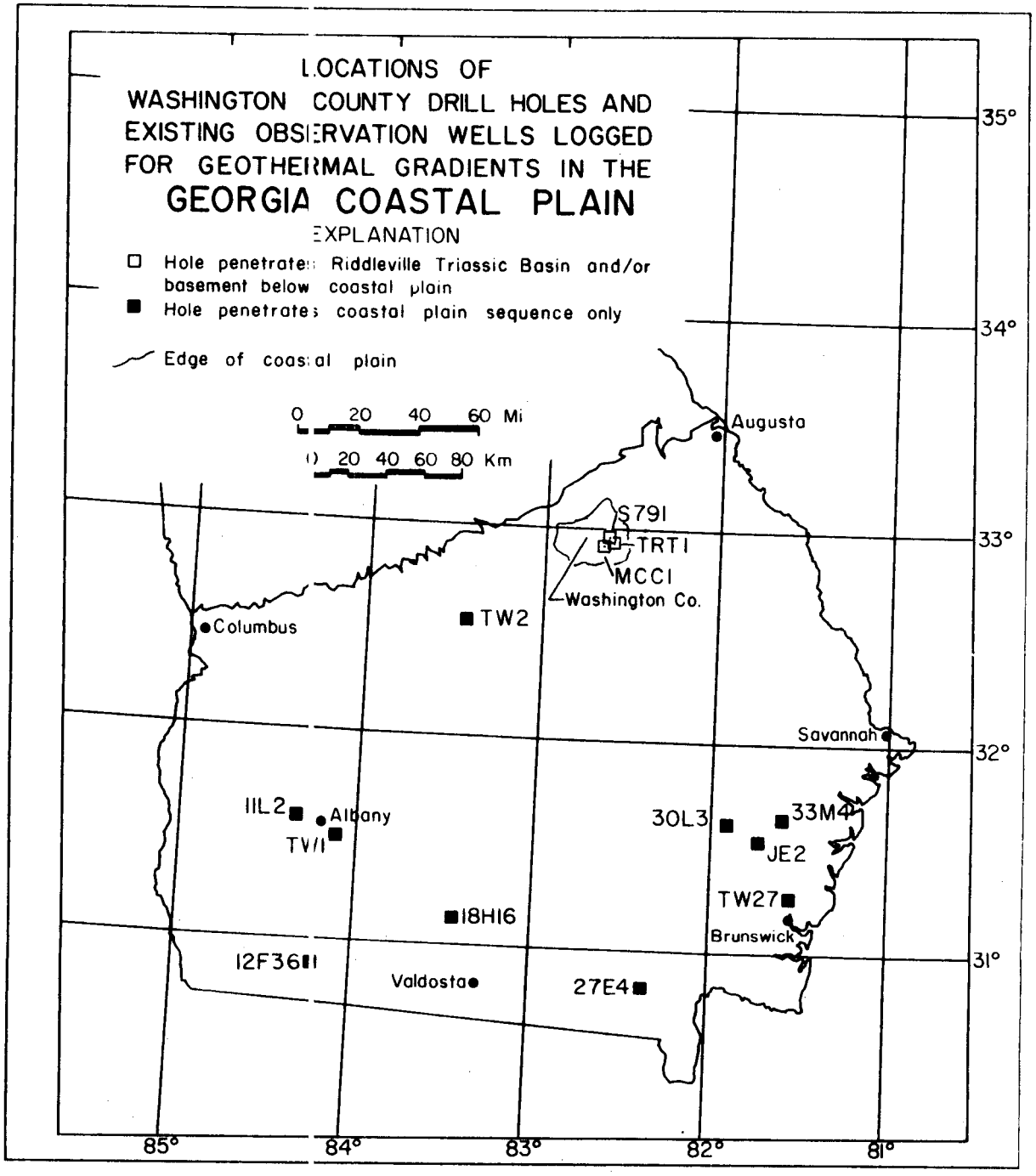

Figure 1. Locations of Washington County gas exploration holes and USGS observation wells logged for geothermal gradients in the Georgia Coastal Plain.

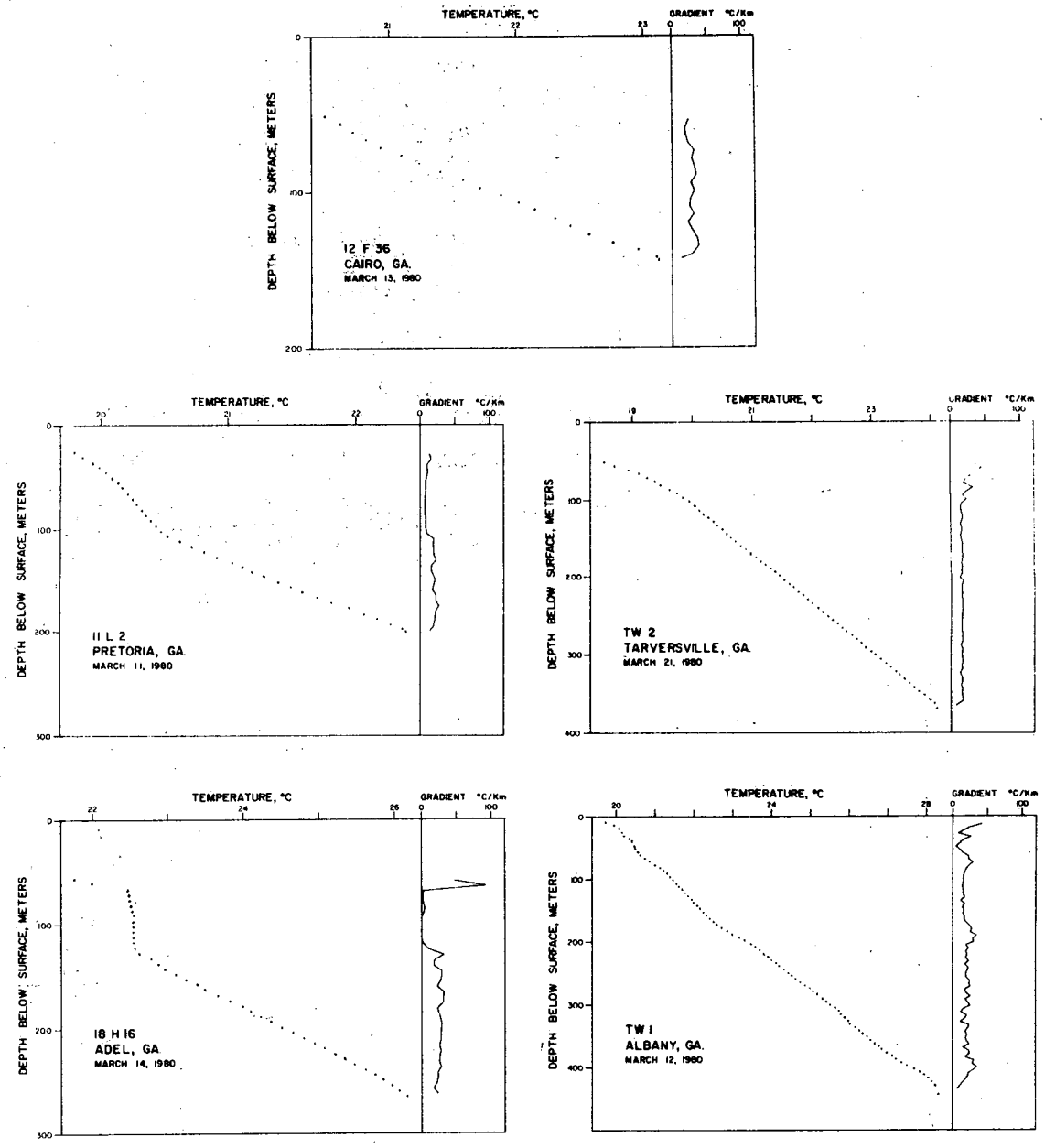

Figure 2: Temperature profiles of Georgia Coastal Plain observation wells.

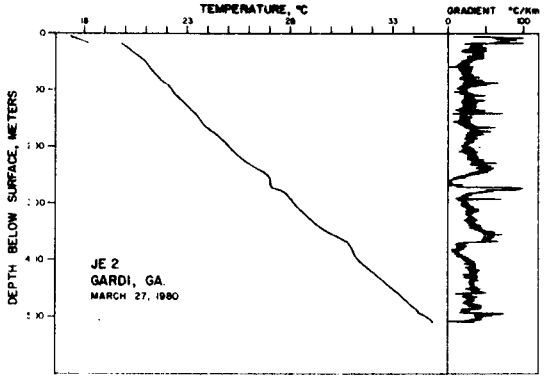
TEMPERATURE, °C
GRADIENT °C/Km
DEPTH BELOW SURFACE, METERS
JE 2
GARDI, GA.
MARCH 27, 1980

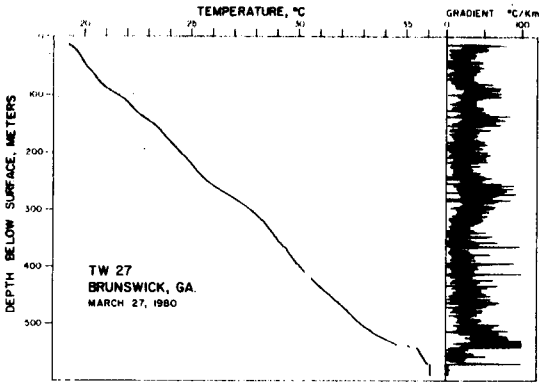
TEMPERATURE, °C
GRADIENT °C/Km
DEPTH BELOW SURFACE, METERS
TW 27
BRUNSWICK, GA.
MARCH 27, 1980

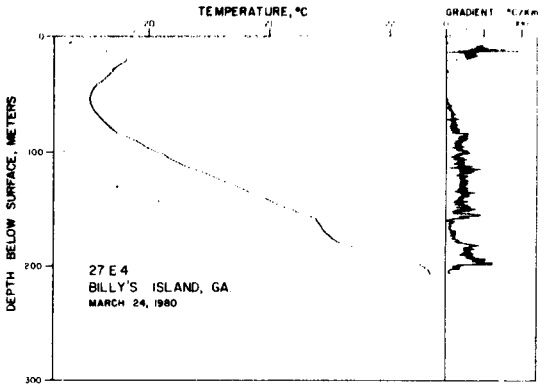
TEMPERATURE, °C
GRADIENT °C/Km
DEPTH BELOW SURFACE, METERS
27 E 4
BILLY'S ISLAND, GA.
MARCH 24, 1980

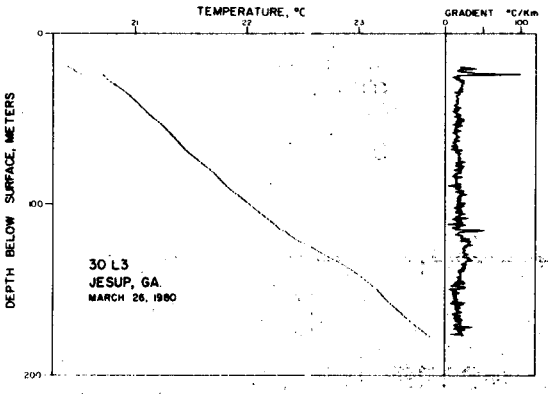
TEMPERATURE, °C
GRADIENT °C/Km
DEPTH BELOW SURFACE, METERS
30 L3
JESUP, GA.
MARCH 26, 1980

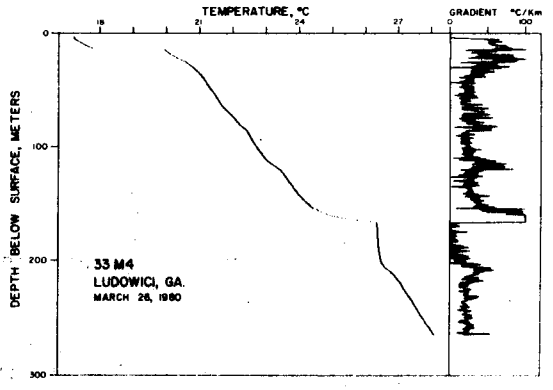
TEMPERATURE, °C
GRADIENT °C/Km
DEPTH BELOW SURFACE, METERS
33 M4
LUDOWICI, GA.
MARCH 26, 1980

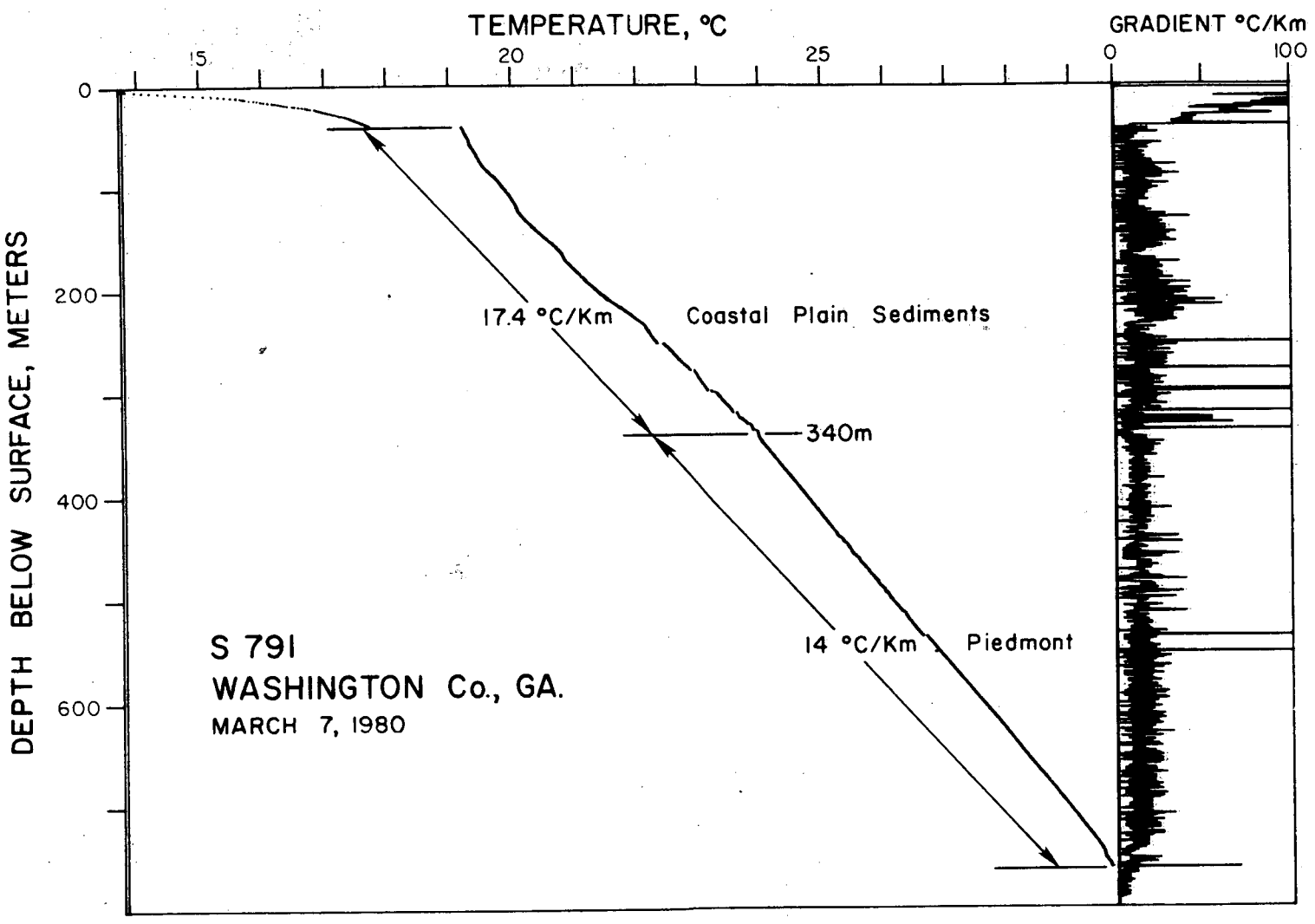

Figure 3: Temperature profile of gas exploration well S791 in Washington County, Georgia

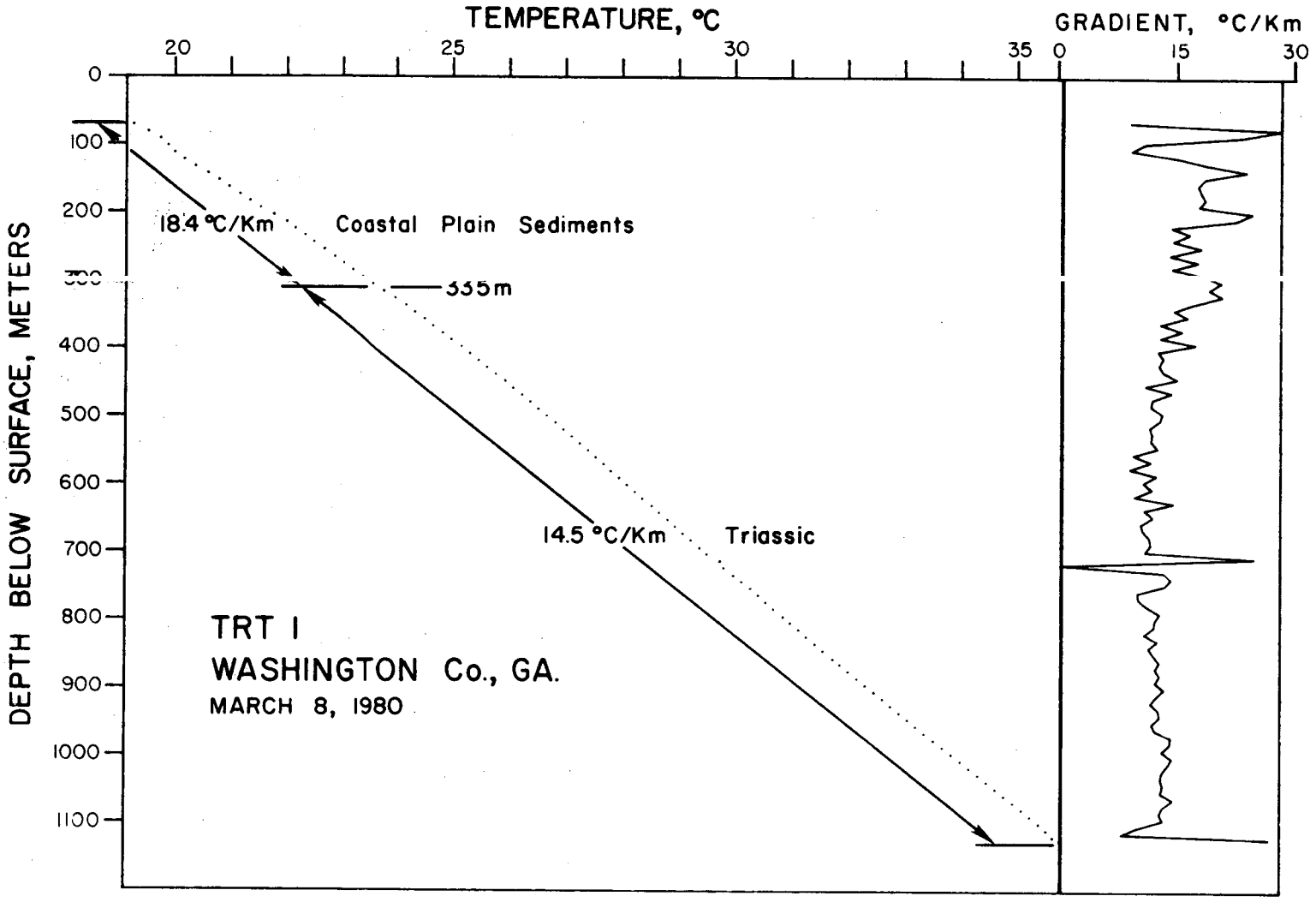

Figure 4: Temperature profile of gas exploration well TRT1 in Washington County, Georgia

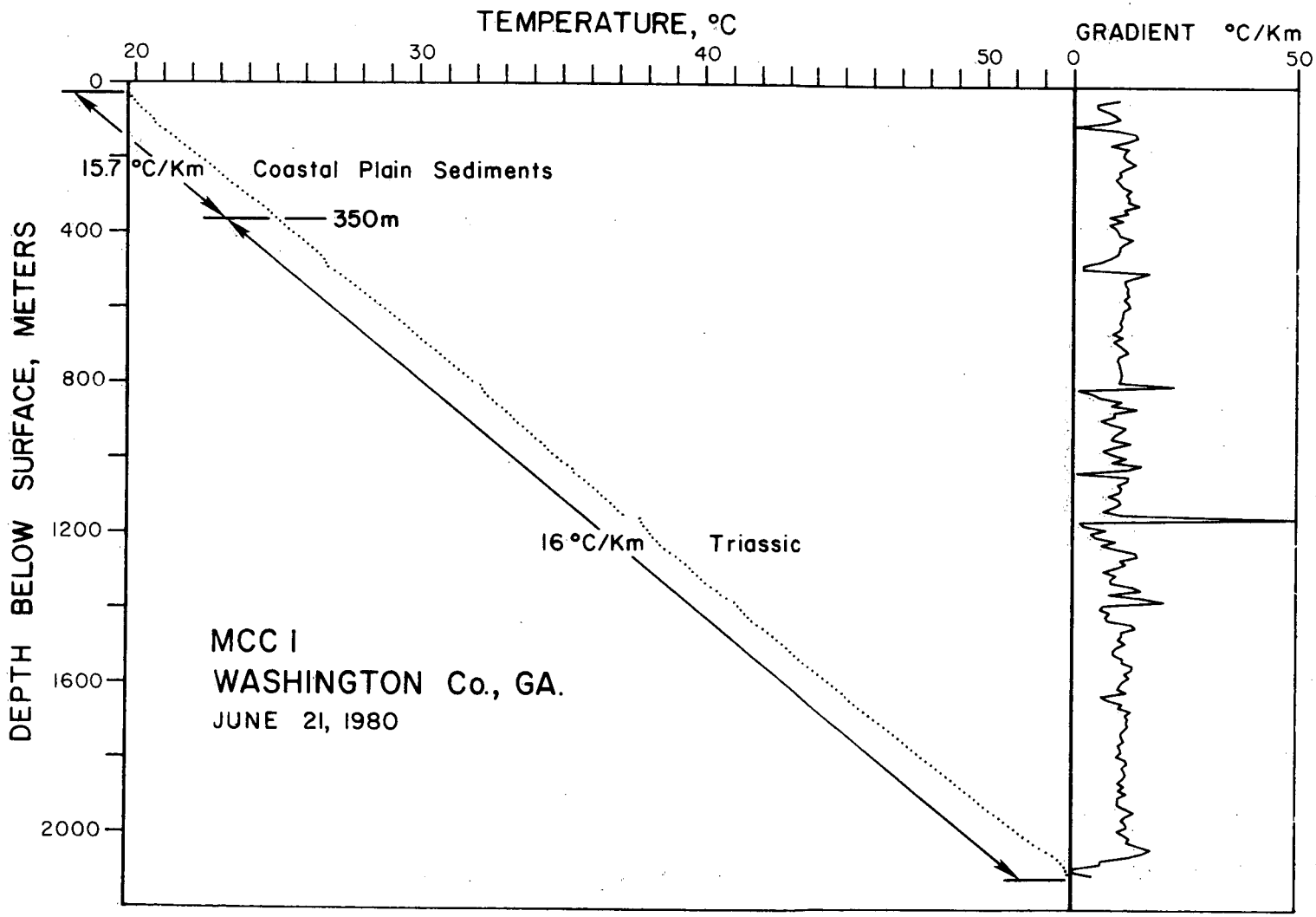

Figure 5: Temperature profile of gas exploration well MCC1 in Washington County, Georgia

°C/km within the Triassic (Figure 5). Unfortunately, no temperature profile is available of the lower section of the Triassic and the underlying basement; however, a Schlumberger maximum temperature thermometer recorded a temperature of 63.9 °C (147 °F) at 2853 m (9360 ft) approximately 6 hours post circulation. The VPI&SU temperature log was run two months post circulation.

ANALYSIS OF THE RELATIONSHIP BETWEEN ENERGY OUTPUT AND WELL SPACING IN A TYPICAL ATLANTIC COASTAL PLAIN GEOTHERMAL DOUBLET SYSTEM

by
Randell J. Laczniak
Regional Geophysics Laboratory

INTRODUCTION

The topic of geothermal energy in the southeastern United States is being discussed seriously. This interest in geothermal energy is due to the increase in price of conventional fuels and improved heat pump technology. Current technology is optimal for the western United States where liquid-dominated high-temperature systems (i.e. temperatures between 90 and 150°C) and vapor-dominated systems (i.e. temperatures of about 240°C) are prevalent. The geothermal resources of the southeastern United States are classified as liquid-dominated low-temperature systems. This type of system is defined by temperatures less than 90°C (White and Williams, 1975). The development of an efficient method of obtaining energy from the lower temperature systems requires an in-depth description and study of each unique system.

Major problems facing the utilization of geothermal energy in the southeastern United States are land subsidence, aquifer collapse, and the disposal of large quantities of highly saline waters. One solution is the reinjection of water back into the aquifer. This maintains piezometric pressures, and thus prevents subsidence and insures a continuous supply of water. At the present time, the practice of reinjection is banned by most states in the southeastern United States because of the possibility of adverse chemical and physical reactions caused by the injected fluid within the aquifer. With proper state authorization and under strict state supervision, the legalization of reinjection should present little, if any, problem.

Two basic but different methods for reinjection exist: 1) the forward and return flow method and 2) the flow-through method (Ingenjorsbyran, 1978). The first method consists of a single pumping-injection well. Water is pumped, stored, and later reinjected by way of a single well. Numerous authors have investigated the thermal and fluid response of a geothermal reservoir to this single well design (e.g., Lippmann et al., 1977; Claesson et al., 1978).

In the flow-through method, separate pumping and injection wells comprise a sink-source or doublet system. The energy which is extracted from the system is directly proportional to the temperature of the water at the production well. A usable form of energy is obtained by running the "hot" water through a heat exchanger.

Doublet systems have an increasing energy output and enhancement of the thermal life-span with increasing well spacing. However, as well spacing increases, the cost of a piping network connecting the injection well to the production well increases. Land acquisition may become more difficult and the costs associated with acquiring the land

may rise with an increase in well spacing. A greater spacing distance requires a pump with a greater lift capacity. The cost and amount of energy needed to power a pump is proportional to it's lift specification. The economics are crucial to the success of a geothermal heat extraction system; therefore, well spacing should be minimized for a desired energy output. The topic of well spacing has been discussed by Gringarten and Sauty (1975) for the Dogger aquifer near Paris, France, where the optimum well spacing was found to be 900 meters.

With more hydrologic and geothermal data now available for the aquifers of the Atlantic Coastal Plain, it is possible to investigate, through modeling, the relationship between the energy extracted and the distance between the source and sink well in a doublet. This relationship can aid in the evaluation of a particular doublet system by defining such limiting characteristics as the thermal life-span of the system and the determination of the optimal well spacing for the specific energy needs of a region.

The thesis of this investigation is the relationship between well spacing and the amount of energy extracted from a "typical" Atlantic Coastal Plain geothermal system. Various well spacings, permeabilities, and pumping-injection rates are considered in the simulations over a period of 15 years. The research employs a numerical model developed at Lawrence Berkeley Laboratories (Lippmann et al., 1977). The numerical model is used to calculate the thermal and fluid-flow fields for a 3-dimensional rectangular liquid-dominated low-temperature system.

THE NUMERICAL MODEL

CCC (Conduction-Convection-Consolidation) is a computer code employing a numerical modelling technique which solves the heat and mass flow equations. It was developed at Lawrence Berkeley Laboratories and is a modification-combination of the SHAFF (Sorey, 1975) and TRUST (Narasimhan, 1975) programs. Documentation of the program itself is still incomplete; however, a basic understanding of the workings of the program can be obtained from some prelimimary notes (Lippmann and Mangold, 1977) and from the discussion of the forerunner program, entitled TRUMP (Edwards, 1972).

The source code of the CCC program was written in FORTRAN IV for execution on the CDC 6700 system at Lawerence Berkeley Laboratories and contains numerous colloquial FORTRAN statements. The code was modified by the investigator to execute on the VPI&SU IBM 370. The program employs what is referred to as the integral finite difference method (IFDM). This method was used as early as 1953 (MacNeal, 1953) and has since been applied to studying groundwater systems (Todd,1959; Tyson and Weber, 1964; Cooley, 1971; Narasimhan and Witherspoon, 1976).

The Integrated Finite Difference Method

The IFDM is a numerical approach used to solve the equations governing heat and mass flow. The two equations are coupled by interlacing them in the time domain. In this section a mathematical derivation of the method as applied to the mass flow equation will be discussed. The heat flow equation is solved in a similar manner and the derivation is therefore omitted from the discussion. A complete and detailed discussion of the derivations are found in papers by Narasimhan and Witherspoon (1976 and 1978) and Sorey (1975). For a description of the variables the reader is referred to the section on Nomenclature.

The partial differential equation governing confined transient groundwater flow can be written as:

$$(1) \qquad \text{div}(K \text{ grad } h) + q = S_p \frac{\partial h}{\partial t}$$

Equation (1) integrated over any number of small finite volumes, V, in the flow region is:

$$(2) \qquad \int_v \{\text{div}(K \text{ grad } h) + q\} dV = \frac{\partial}{\partial t} \int_v (S_p h) dV$$

Using the divergence theorem and assuming q is an average value over subregion V on the left-hand side of equation (2) and assuming that Sp and h are average values over subregion V on the right-hand side, equation (2) is:

$$(3) \qquad \int_s (K \text{ grad } h \cdot N) dS + qV = S_p V \frac{\partial h}{\partial t}$$

The surface integral on the left-hand side of equation (3) physically describes the summation of fluxes over a surface, S.

The basic concept of the IFDM is similar to other numerical techniques in use to solve potential field problems. The region is discretized into a number of smaller subregions (see Figure 1). The model thus becomes a distributive parameter model, by providing the necessary control of the parameters within the system. A general finite difference approximation of equation (3) can now be written to describe each element in the system as:

$$(4) \qquad \sum_n K_{m,n} \left(\frac{h_n - h_m}{D_{m,n}}\right) A_{m,n} + q_m V_m = S_p V_m \frac{\Delta h_m}{\Delta t}$$

Here, if subregion m and n have different material properties, Km,n is the harmonic mean permeability.

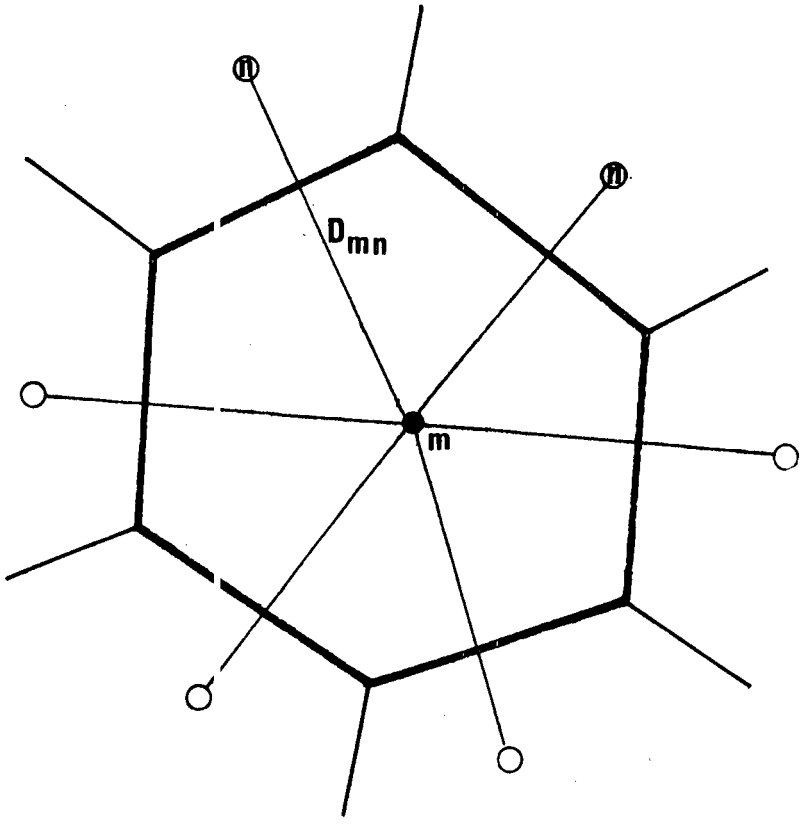

Figure 1: Illustrative representation of a descretized region showing a typical nodal element, m, and typical neighboring nodal element, n.

By rewriting equation (4) in terms of the intrinsic permeability and multiplying each term by the fluid density, the following equation is obtained:

$$(5) \qquad \sum_n \rho \frac{k\rho g}{\mu} \left(\frac{h_n - h_m}{Dm,n}\right) A_{m,n} + Q_m = M_{c,m} \frac{\Delta h_m}{\Delta t}$$

For convenience equation (5) is simplified by combining terms to obtain the conductance of the interface between elements. The conductance, Um,n, physically describes the flux across interface m, n due to a unit difference in the hydraulic head between the corresponding nodes. Equation (5) then becomes:

$$(6) \qquad \sum_n U_{m,n}(h_n - h_m) + Q_m = M_{c,m} \frac{\Delta h_m}{\Delta t}$$

If in Equation (6), h_n and h_m are initial known values at the beginning of the interval (Δt). An explicit solution for Δh is:

$$(7) \qquad \Delta H_{m,exp} = \frac{\Delta t}{M_{c,m}} \left\{\sum_n U_{m,n}(h_n^0 - h_m^0) + Q_m\right\}$$

A more general solution for equation (7) encompassing the case where nodal element m partially coincides with the boundary of the flow region can be expressed as:

$$(8) \quad \Delta h_{m,exp} = \frac{\Delta t}{M_{c,m}} \left\{\sum_b U_{m,b}(h_b - h_m^0) + \sum_n U_{m,n}(h_n^0 - h_m^0) + Q_m\right\}$$

The primary disadvantage of the explicit solution is one of instability (O'Brien, 1951; Narasimhan, 1975). Accordingly, this solution is limited to the time constraint:

$$(9) \qquad \Delta t < \frac{M_{c,m}}{\sum_n U_{m,n}}$$

If Δt exceeds this limit, the accuracy of the solution diminishes in the vicinity of the element m.

To overcome this time constraint and progress more rapidly in the time domain, equation (5) is written in a special explicit-implicit form where,

$$h_m = h_m^0 + \lambda \Delta h_m \tag{10a}$$

$$h_n = h_n^0 + \lambda \Delta h_n \tag{10b}$$

to obtain:

$$\Delta h_m = \frac{\Delta t}{M_{c,m}} \{\sum_b U_{m,b}[h_b - (h_m^0 + \lambda \Delta h_m)] + \sum_n U_{m,n}(h_n^0 + \lambda \Delta h_n) - (h_m^0 - \lambda \Delta h_m) + Q_m\} \tag{11}$$

Equation (11) can now be separated into an explicit and implicit component by collecting terms.

$$\Delta h_m = \Delta h_{m,exp} + \frac{\lambda \Delta t}{M_{c,m}} \{- \sum_b U_{m,b} \Delta h_m + \sum_n U_{m,n}(\Delta h_n - \Delta h_m)\} \tag{12}$$

Considering the local nature of stability (Richtmeyer and Morton, 1967) $\Delta h_{m,exp}$ can be calculated first for the entire system of nodal points in the flow region. Then in those elements where t exceeds the stability limit, an implicit correction could be computed. This explicit-implicit scheme is the basis for program CCC. Edwards was the first to take advantage of the local nature of stability in his program TRUMP (Edwards, 1972).

The partial differential equation governing heat flow through a porous media can be expressed as (from Mercer, 1973):

$$(\rho c)_M \frac{\partial T}{\partial t} = \text{div}(K_e \text{ grad } T) - \rho v_d c \cdot \text{grad } T + q_e \tag{13}$$

Applying the divergence theorem to equation (13), the energy equation can be written in integral form as:

$$\frac{\partial}{\partial t} \int_v [(\rho c)_M T] dV = \int_s (K_e \text{ grad } T \cdot N) ds - \int_s (\rho c \delta T \, v_d \cdot N) dS + \int_v q_e dV \tag{14}$$

Equation (14) is solved by the IFDM in a manner similar to that previously used to solve the mass flow equation. The resulting special explicit-implicit difference equation is:

$$(15) \quad V_m(\rho c)_M \frac{\Delta T_m}{\Delta t} = \sum_n (K_e A)_{m,n} \frac{T_n - T_m}{D_{m,n}} + (\rho v_d c A)_{m,n} + \lambda\{(K_e A)_{m,n} \frac{\Delta T_n - \Delta T_m}{D_{m,n}} + (\rho v_d c A)_{m,n} \Delta T_{m,n}\} + q_e v_m$$

GENERAL HYDROGEOLOGY OF THE ATLANTIC COASTAL PLAIN

The Atlantic Coastal Plain consists of a seaward thickening wedge of interbedded sands and clays deposited by fluvial, deltaic, and marine processes. Hydrogeologically, these sediments represent a vertical sequence of moderate to highly productive aquifers resting on a pre-Cretaceous basement complex. The sands serve as a permeable medium and comprise the main water bearing units. The less permeable clays act as confining units and subdivide the system into numerous semi-independent aquifer systems with minimally dependent values of hydraulic head.

The Atlantic Coastal Plain is divided into three general subsystems according to geologic age: 1) the Quaternary system, 2) the Tertiary system, and 3) the Cretaceous system. The Quaternary system is the uppermost hydrologic unit and lies above the first major clay layer. Hydrogeologically, it is classified as a water-table or unconfined aquifer. Production is low to moderate. Thus, these aquifers are seldom tapped for anything other than domestic purposes (i.e., individual household needs). Thickness of the aquifer is generally less then 30 meters.

The Tertiary and Cretaceous systems lie beneath the Quaternary system. Hydrogeologically, these systems are described as a series of confined and semi-confined aquifers. Both are moderate to highly productive and serve as domestic and industrial sources of water. The thickness of the aquifers within these systems ranges from about 30 to 120 meters (Cedarstrom, 1945).

The source of regional recharge is direct precipitation and runoff. Regional recharge to the underlying aquifers occurs east of the major groundwater divide (Appalachian Mountains) through surface outcrops. A more localized form of recharge is direct vertical leakage from precipitation. The rate of recharge due to natural vertical leakage to any particular aquifer is controlled by the vertical permeability of the upper sediments. The low permeability of the clay layers present in the Tertiary and Cretaceous systems retard vertical permeability; therefore, without reinjection the potential yield of the aquifers is limited.

The water quality is dependent on the mineral constituents and the chemical properties of the host formation. These vary with location. One general trend is the presence of high concentrations of total dissolved solids along the eastern shore; for example, concentrations of total dissolved solids were measured at 72,039 ppm in a deep test well near Crisfield, Maryland (Hartsock, 1979).

DESCRIPTION AND DISCUSSION OF A "TYPICAL" ATLANTIC COASTAL PLAIN GEOTHERMAL SYSTEM

The characteristics of a "typical" Atlantic Coastal Plain geothermal system are taken from data and information obtained from the Crisfield, Md. geothermal test well drilled during June, 1979 (Dashevsky and McClung, 1979) and supplemented with information found in the literature (Brown and Silvey, 1972 ; Cedarstrom, 1945; and U. S. Geological Survey, 1967). A schematic diagram of the system is shown in Figure 2.

A homogeneous aquifer is bounded on top by an aquitard. The aquitard consists of a semi-impermeable group of sands, clays, and shales. This unit is overlain by another aquifer. The bottom of the main aquifer is bounded by an aquiclude, representing some relatively impermeable material, either well-consolidated sediments or crystalline basement. In the horizontal direction the system is unbounded in one direction (i.e., horizontally infinite) and bounded in the other by some relatively impermeable material. The aquifer has a vertical thickness of 50 meters.

The hydraulic operation of the system is kept simple. Water is pumped out of the aquifer at the production well where it is run through a heat exchanger. Reinjection of the thermally spent cooler water takes place through an injection well located at a distance, d, from the production well.

Water entering the aquifer at the injection well flows at a rate, v_d, toward the production well. Heat is transferred by forced and natural convective and conductive processes. Cooler water flowing in the direction of the production well gains heat due to the higher ambient temperatures in conjuction with the heat flow through the system. The surrounding temperatures are lowered due to the loss of heat to the cooler injected fluid.

The point in time when the injected water begins to noticeably lower the temperature at the production well (by $\approx 1°C$) is called "breakthrough". Breakthrough is dependent on the well spacing and the pumping-injection rate. At some distance, d, and some pumping-injection rate, Qp, the temperature of the injected water will totally recover and thus inhibit breakthrough. In this special case the geothermal resource is classified as a <u>totally renewable</u> resource.

The system is located at a depth centered around 1,375 meters. The system is artesian with an initial total hydraulic head producing a

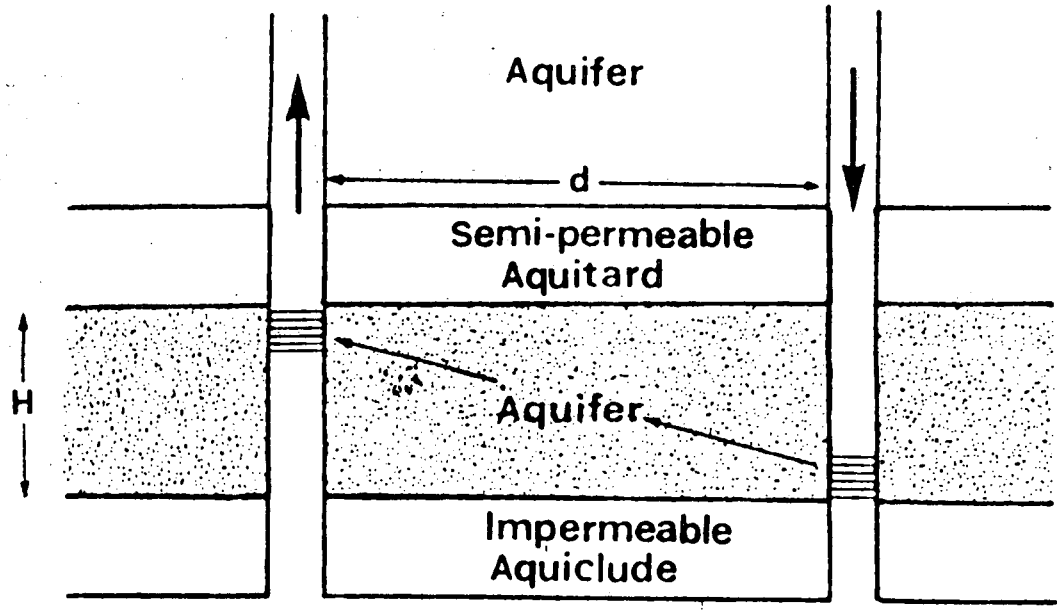

Figure 2: Schematic diagram of the doublet geothermal system used in the simulations. Hatched region shows perforated (pumping-injection) zones.

slight flow at the surface in a well tapping the reservoir. The blanketing sediments are assumed to have an average thermal gradient of 40°C/km. These values for thermal gradient and depth determine the temperature of the system to be in the vicinity of 55°C. The overall terrestrial heat flow in the system, a function of both the thermal conductivity and thermal gradient is 75.38 mW/m^2.

The amount of energy extracted from a geothermal system using a heat pump is dependent on the thermal output and the pumping rate. Energy output in Btu's per hour is calculated using equation (16) (from Paddison et al., 1978).

$$(16) \qquad \frac{\text{Btu's}}{\text{hr}} = Qp \times 907.2 \times \Delta T$$

Here, Qp is in gallons per minute.

A geothermal system which is pumped at 500 gpm, has an output temperature of 55°C, and an input temperature of 43°C (T= 12°C.) produces 5,443,200 Btu's per hour. The amount of energy extracted from the geothermal water could be raised considerably by inputting enough electrical energy to power a special type of heat pump known as a temperature amplifier (Neiss, 1979; Westinghouse Electric Corporation, 1979).

DESCRIPTION AND DEVELOPMENT OF THE SIMULATION MODEL

A general simulation model was constructed to simulate the pressure and temperature fields in a "typical" Atlantic Coastal Plain geothermal system. The integrated finite difference method was employed to solve the mass and heat flow equations. The model makes use of the symmetry present in a doublet system by modelling one-half of the whole system.

Mesh Design

The model consists of a 3-dimensional layered rectangular mesh (see Figure 3). The mesh contains 1,342 three-dimensional elements each defined by a nodal point. The nodal elements are interconnected via 4,172 element interfaces. Temperatures and pressures are obtained at the nodal points during the simulations.

The mesh design subdivides the geothermal system into three hydrologic units based upon the geology. The upper and lower hydrologic units each consist of one grid layer and have a vertical thickness of 25 meters. The upper grid layer represents a semi-permeable unit and the lower grid layer a confining unit. The main reservoir is represented by the central five grid layers, each grid layer having a thickness of 10 meters.

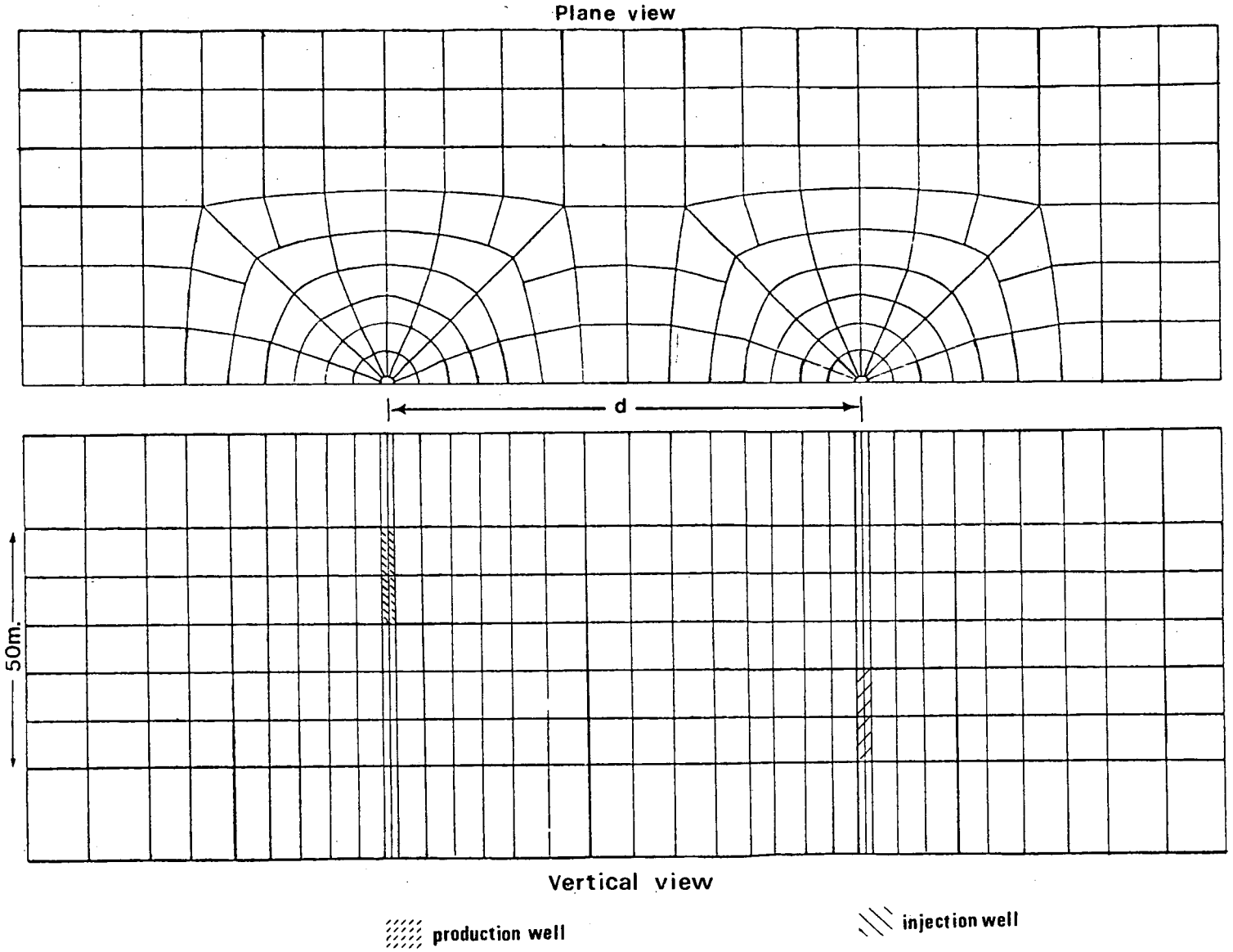

Figure 3: Mesh design to simulate a "typical" Atlantic Coastal Plain geothermal system. Distance, d, represents the desired well spacing.

Table 1 - Material properties used to simulate a "typical" Atlantic Coastal Plain geothermal system. The first entry for each property is in the units used by the program and the second is in cgs units.

PROPERTIES	AQUITARD	AQUIFER	AQUICLUDE
Heat Capacity			
($j\ kg^{-1}\ °C^{-1}$)	$.921x10^{+3}$	$.103x10^{+4}$	$.803x10^{+3}$
(cgs units)	.220	.246	.192
Density			
($kg\ m^{-3}$)	$2.60x.0^{+3}$	$2.65x10^{+3}$	$2.60x10^{+3}$
(cgs units)	2.60	2.65	2.60
Th. Cond.			
(j/m day °C)	$1.63x10^{+5}$	$2.60x10^{+5}$	$2.17x10^{+5}$
(cgs units)	$4.50x10^{-3}$	$7.20x10^{-3}$	$6.00x10^{-3}$
Temp. Grad.			
($°C\ km^{-1}$)	40	25	30
(cgs units)	.0004	.00025	.0003
Permeability			
(m^2)	$Kx10^{-4}$	K	$Kx10^{-25}$
(cgs units)	K	$Kx10^{+4}$	$Kx10^{-21}$
Porosity	.20	.15	.20
Sp. Storage			
(m^{-1})	$3.00x10^{-5}$	$1.50x10^{-4}$	$4.00x10^{-5}$
(cgs units)	$3.00x10^{-7}$	$1.50x10^{-6}$	$4.00x10^{-7}$

Table 2 - Fluid properties used to simulate a "typical" Atlantic Coastal Plain geothermal system. The first entry for each property is in the units used by the program and the second is in cgs units.

FLUID PROPERTIES

Compressibility	
(m^2 N^{-1})	5.000×10^{-10}
(cgs units)	5.000×10^{-11}
Th. Expansivity	
($°C^{-1}$)	3.170×10^{-4}
Reference density	
(kg m^{-3})	1003.17
(cgs units)	1.00317
Reference Temp.	
(°C)	40
** Viscosity	
(Pa sec)	6.750×10^{-4}
(cgs units)	$6.-5 \times 10^{-3}$
** Specific Heat	
(j kg^{-1} $°C^{-1}$)	$4.115 \times 10^{+3}$
(cgs units)	.983

** Value varies linearly with temperature

Table 3 - Equations approximating physical properties of brines using properties of pure water (Wahl, 1977).

Density

$$\rho = \rho_w + .00073(w_t)$$

Specific Heat

$$H_c = H_{c,w}(1 - \frac{w_t}{100})$$

Viscosity

$$\mu = \mu_w(1 + .021w_t + .00027w_t^2)$$

The design utilizes the natural convection present within the geothermal system due to water density and viscosity variations with temperature (Lippmann et al., 1977). Thus, the production well is located in the upper portion of the reservoir with the injection well located in the lower portion of the reservoir.

The horizontal dimensions are scaled according to the horizontal distance, d, between the production and injection wells. Well spacings of 100, 250, 500, and 1000 meters are tested in the simulations.

Fluid and Material Properties

Fluid and material properties used in the simulation model are chosen to describe a "typical" Atlantic Coastal Plain geothermal system. Values for these properties are obtained from the Crisfield geothermal test well (Dashevsky and McClung, 1979) and from literature pertaining to deeper wells in the Atlantic Coastal Plain (Brown and Silvey, 1972; Cedarstrom, 1945; U. S. Geological Survey, 1967).

Material properties used in the simulation model are found in Table 1. The model consists of a caprock, a bedrock, and an aquifer defining an aquitard, an aquiclude, and a reservoir, respectively. Permeabilities are varied in the test simulations from 9.862×10^{-15} to 9.862×10^{-13} m^2 (10 to 1000 millidarcys).

The fluid properties (see Table 2) are based on a total dissolved solid content of 15,000 ppm. Fluid properties of the salt water are estimated from those of pure water using the equations developed by Wahl (1977) and are listed in Table 3.

The values for density, specific heat, and viscosity are functions of temperature and are calculated by the program. Density varies with temperature according to equation (17):

$$\rho = \rho_o\{1 - \gamma(T-T_o) - (T-T_o)^2\} \qquad (17)$$

Variations with temperature in specific heat and viscosity are determined linearly from upper and lower limits inputted by the investigator.

Initial and Boundary Conditions

The initial and boundary conditions are determined using geothermal and hydrologic data obtained from the Crisfield well site (Dashevsky and McClung, 1979; Hartsock, 1979). The conditions are based on the system being located at an average depth of 1.375 kilometers. Initial values for fluid pressures and temperature are shown in Figure 4.

Fluid pressures are chosen to simulate an artesian system. Initially water is assumed to be under sufficient pressures to cause the piezometric surface to be located at ground level in a well tapping the aquifer. Initial pressure gradients describe a dead system where

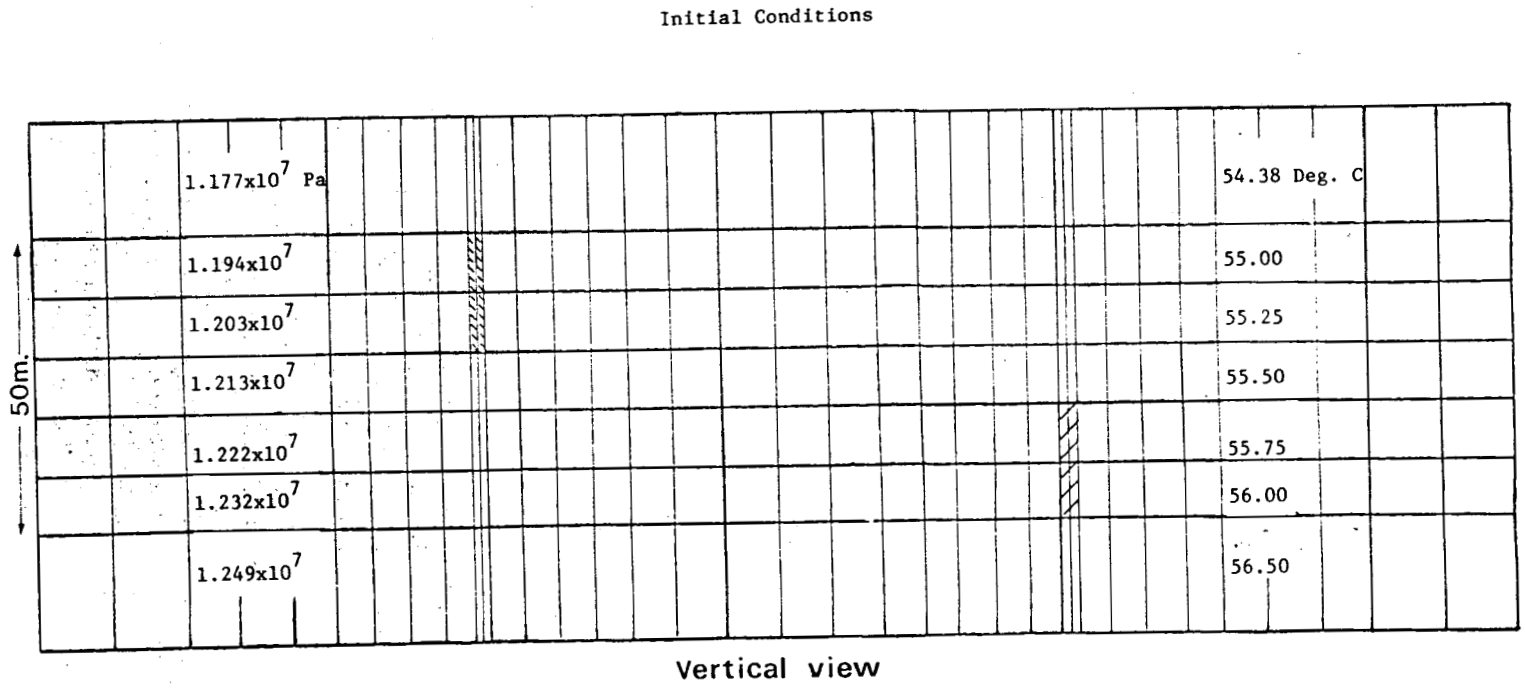

Figure 4: Initial pressure and temperature conditions used in the simulations. Values shown are input at the nodal points throughout the entire length of the grid layer. Nodal points are located in the center of the nodal elements.

ground water velocities are zero because the value of hydraulic head is constant throughout the system. The initial temperature at the upper boundary is determined using a thermal gradient of 40°C/km for the overlying sediments. The initial temperatures within the system are determined using the thermal gradients listed in Table 1. The initial temperature gradients are chosen in conjunction with the thermal conductivities of each hydrologic unit to produce a heat flow of 75.38 mW/m^2 (1.8×10^{-6} cal/cm^2 sec).

The criterion used to determine the location of the upper and lower boundary nodes relative to the rest of the system is that no more than a 10% change in heat flow should take place through the lower boundary-system interface. This criterion was satisfied in all simulations with the greatest change in heat flow being +7.2%. The boundaries enclosing all sides of the system are placed at a distance two times the distance between the production and injection wells. The boundary conditions used are:

a) the upper and lower boundaries are constant pressure (11648852.0 and 12608247.0 Pa, respectively) and constant temperature (53.875 and 56.875°C, respectively) boundaries,
b) the vertical boundaries along the caprock and bedrock are adiabatic and impermeable,
c) the reservoir boundaries along the vertical sides perpendicular to distance, d (well spacing), are constant pressure and temperature boundaries equal to the initial conditions defined for each respective layer,
d) the reservoir boundary along the vertical sides parallel to distance, d, are impermeable and isothermal with values defined by the initial conditions.

The upper constant pressure boundary simulates an overlying system of aquifers and serves as the source for recharge by leakage through the semi-confining unit. Leakage is induced only when pumping induces a hydraulic gradient across this interface. The constant pressure boundaries along the vertical sides of the reservoir perpendicular to distance, d, act as a line source or sink depending on the hydraulic gradients across these interfaces. There is no flow through the lower boundary-system interface because of the low permeability of the material and the initial zero hydraulic gradient across the interface.

DISCUSSION OF THE SIMULATION PROCEDURE

Well spacings of 100, 250, 500, and 1000 meters are compared. Each individual well spacing is modelled using intrinsic permeabilities of 9.862×10^{-15}, 9.862×10^{-14}, and 9.862×10^{-13} m^2 (10, 100, and 1000 millidarcys, respectively). Pumping and injection rates of 6.31×10^{-03} and 3.153×10^{-02} m^3/sec (100 and 500 gallons per minute) are considered. The water injected into the system is at 43.5 °C. Individual doublet systems are pumped for 15 years or until thermal and fluid flow steady-state conditions are reached.

This procedure is used to investigate the relationship between the temperature at the production well (energy output) and well spacing. The results produced by this procedure are also used to evaluate, in detail, a "typical" Atlantic Coastal Plain geothermal system by:

1) analyzing the temperature field to evaluate the thermal life-span of each individual doublet system,
2) analyzing the pressure field to evaluate the ability of each system to supply adequate amounts of water,
3) analyzing the response of the system to different permeabilities,
4) analyzing the pressure and temperature fields under relatively low and high pumping-injection stresses.

A final group of simulations considers the effect of resting on the system. A period of rest is defined as an interval of time in which the system is allowed to recover from previously applied pumping-injection stresses. To mimic heating demands during the winter and summer seasons, six-month periods of production-injection are alternated with six-month periods of rest over a 5 year interval. One well spacing of 100 meters and permeabilities of 100 and 1000 md are considered. A pumpimg-injection stress of 100 gpm with an injection temperature of 43.5 °C. is applied.

RESULTS AND DISCUSSION

Results of the simulations are displayed graphically by contour and time versus temperature plots in the following sections of this chapter. Contours of the pressure and temperature fields are constructed using a contouring package called GPCP, General Purpose Contouring Program (Calcomp, 1973).

Analysis of the Pressure Field

Map views of the final pressure distribution through the center of the reservoir, located between the grid layers containing the source and sink wells are shown in Figures 5-8. The time given under each plot is the time at which the pressure field reached steady-state. Here, steady-state is not used in a strict sense but is defined by the program to be a small change (less then 2.5% of an input maximum allowed pressure change) in the field over a specified number of consecutive time steps.

The sequence of plots includes simulations with permeabilities of 100 and 1000 md and pumping-injection rates of 100 and 500 gpm for all four well spacings. Plots for the 10 md simulation are not shown. In the 10 md simulation execution terminated abnormally because of the occurrence of a negative pressure anomaly in the pumping element. (Negative pressures are physically impossible in a real system and in the model indicate an insufficient supply of water for the hydrologic characteristics describing the system.)

Figure 5: Plan views of the final pressure distribution through the center section of the reservoir for a system with a permeability of 100 md and a pumping-injection rate of 100 gpm. Hydrologic and system characteristics (i.e., well spacing, time, permeability, and pumping-injection rate) are listed alongside each individual plot. Time indicates the time at which steady-state was reached in the fluid-flow field. Crosses represent location of nodal points. Plots are shown for well spacings of: a) 100, b) 250, c) 500, and d) 1000 meters.

PRESSURE MAP (PASCALS / 1000)
CONTOUR INTERVAL-50 (PASCALS / 1000)

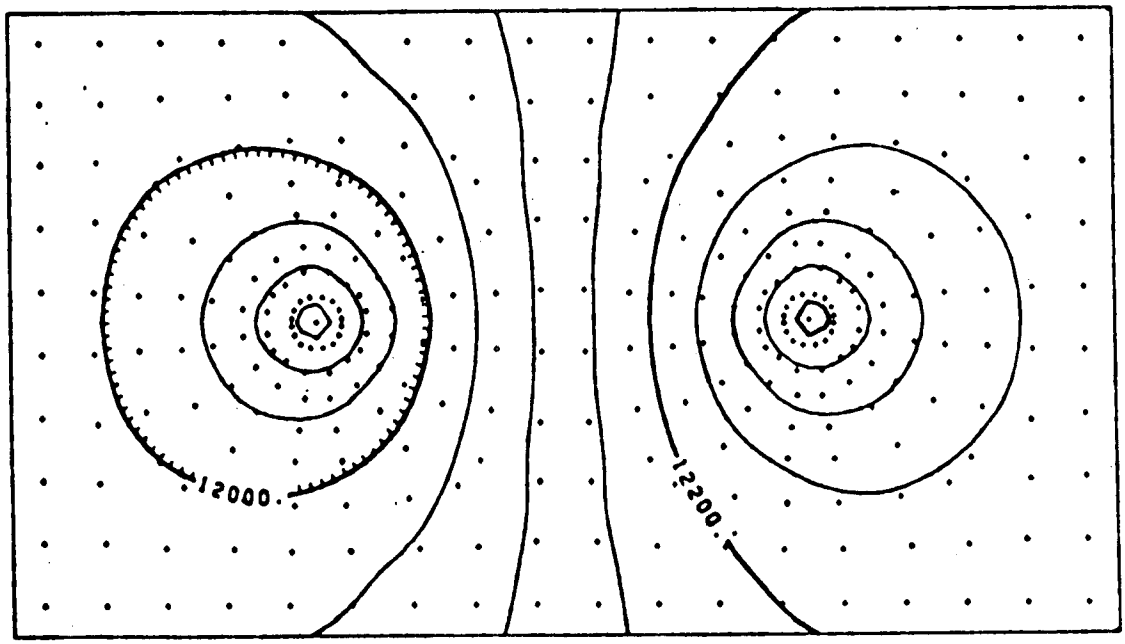

100 M. SEPARATION
TIME= 11.167 DAYS
PERMEABILITY= 100 MD.
PUMPING RATE= 100 GPM.

5a

250 M. SEPARATION
TIME= 64.899 DAYS
PERMEABILITY= 100 MD.
PUMPING RATE= 100 GPM.

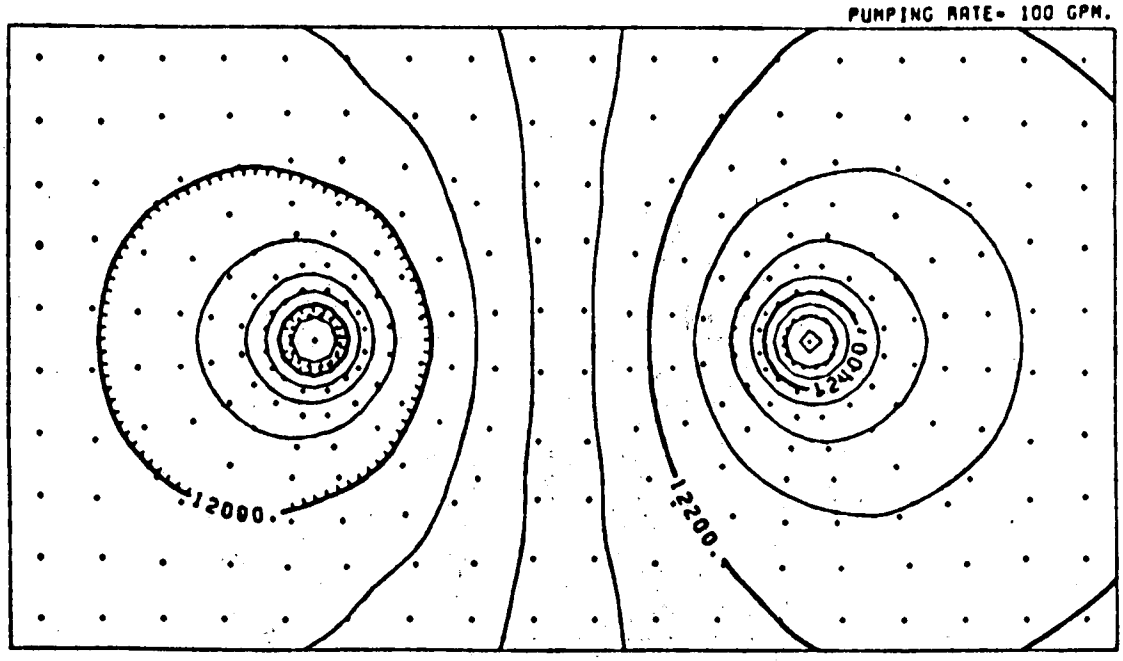

5b

PRESSURE MAP (PASCALS / 1000)
CONTOUR INTERVAL-50 (PASCALS / 1000)

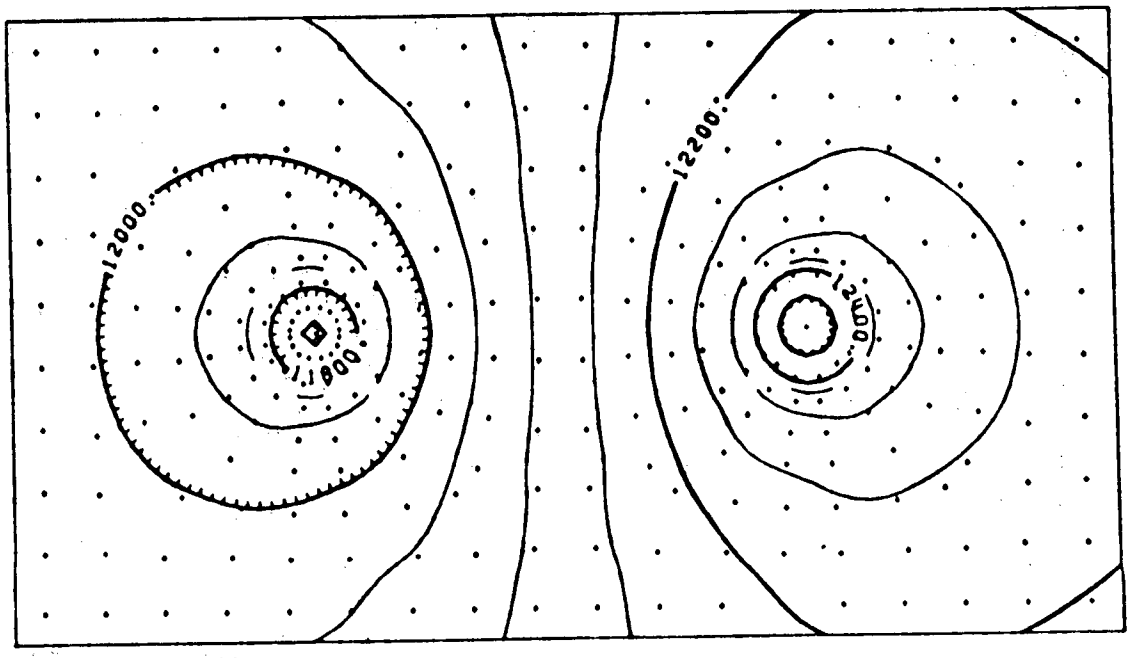

500 M. SEPARATION
TIME= 2341.0 DAYS
PERMEABILITY= 100 MD.
PUMPING RATE= 100 GPM.

5c

1000 M. SEPARATION
TIME= 4164.3 DAYS
PERMEABILITY= 100 MD.
PUMPING RATE= 100 GPM.

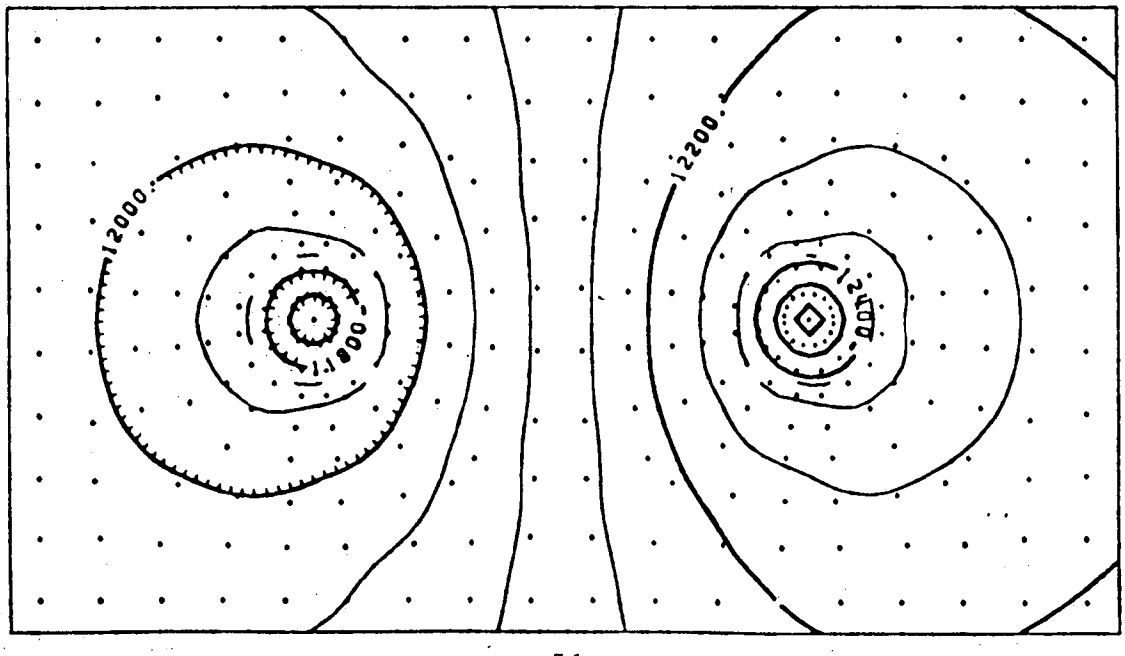

5d

Figure 6: Pressure distribution map as in Figure 5 except the permeability is raised to 1000 md.

PRESSURE MAP (PASCALS / 1000)
CONTOUR INTERVAL-10 (PASCALS / 1000)

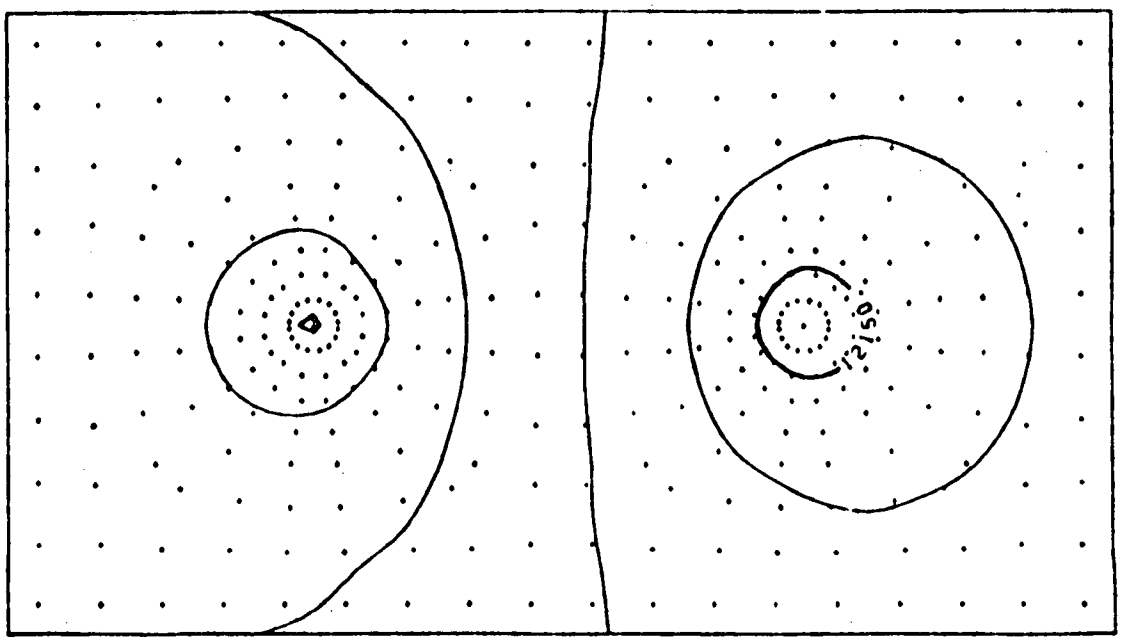

100 M. SEPARATION
TIME= 1.6894 DAYS
PERMEABILITY= 1000 MD.
PUMPING RATE= 100 GPM.

6a

250 M. SEPARATION
TIME= 6.6391 DAYS
PERMEABILITY= 1000 MD.
PUMPING RATE= 100 GPM.

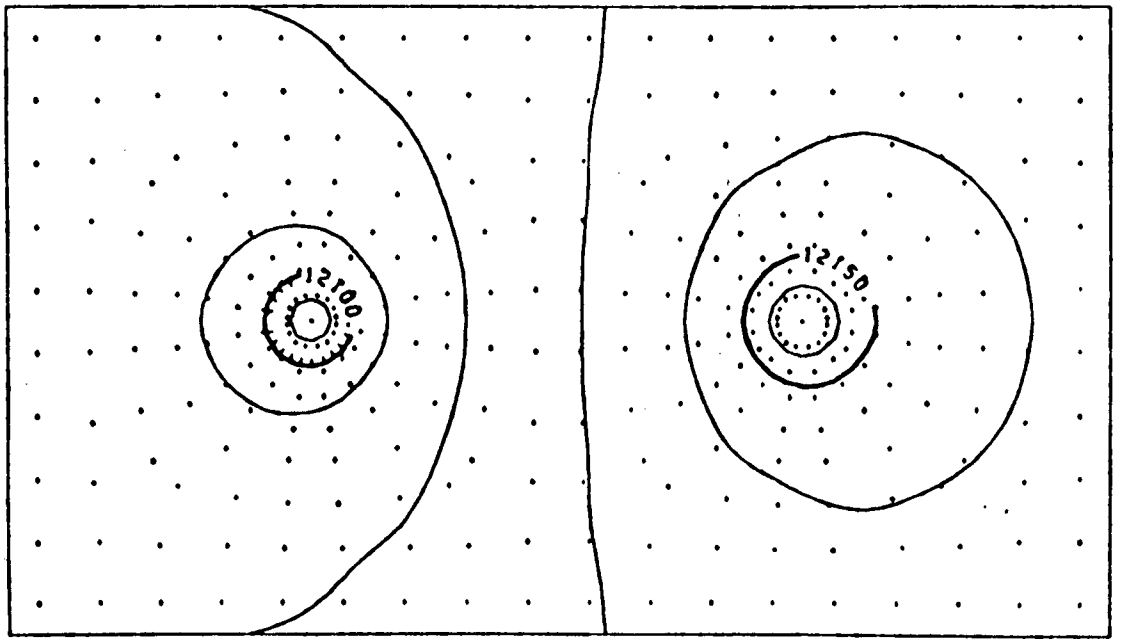

6b

PRESSURE MAP (PASCALS / 1000)
CONTOUR INTERVAL-10 (PASCALS / 1000)

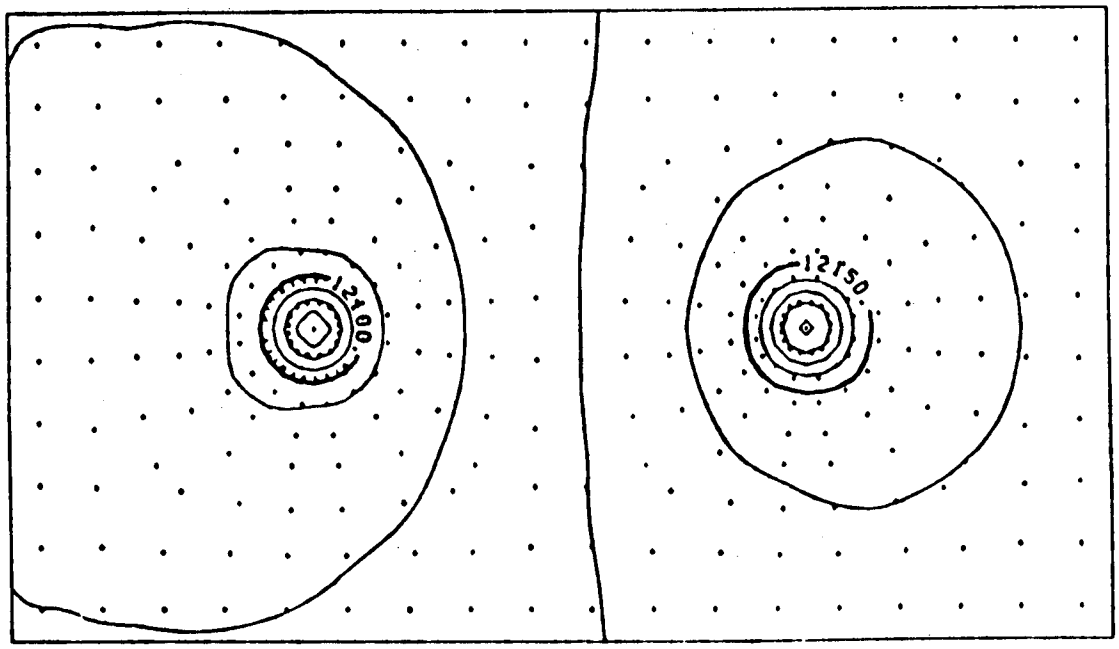

500 M. SEPARATION
TIME= 16.696 DAYS
PERMEABILITY= 1000 MD.
PUMPING RATE= 100 GPM.

6c

1000 M. SEPARATION
TIME= 42.50 DAYS
PERMEABILITY= 1000 MD.
PUMPING RATE= 100 GPM.

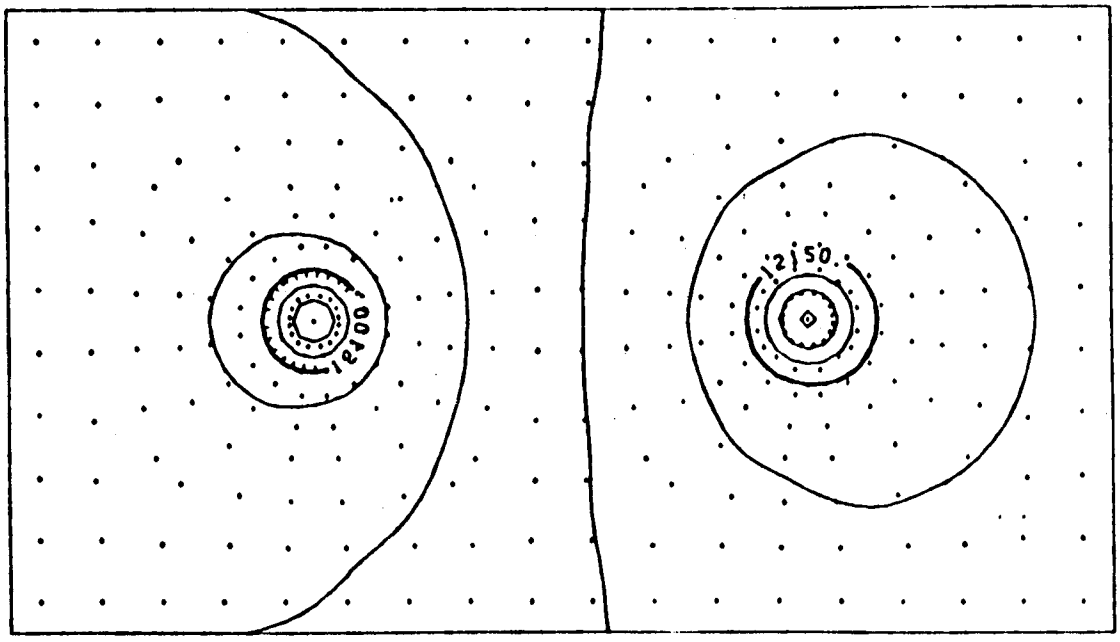

6d

Figure 7: Pressure distribution map as in Figure 5 except the pumping-injection rate is raised to 500 gpm.

PRESSURE MAP (PASCALS / 1000)
CONTOUR INTERVAL-50 (PASCALS / 1000)

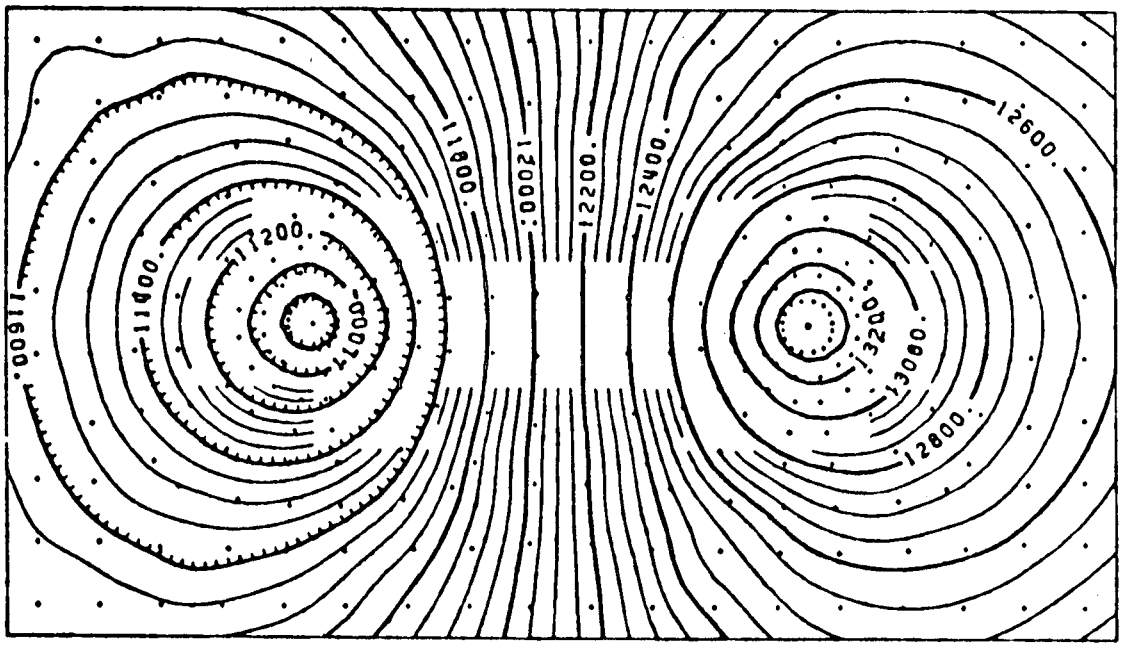

100 M. SEPARATION
TIME= 9.4358 DAYS
PERMEABILITY= 100 MD.
PUMPING RATE= 500 GPM.

7a

250 M. SEPARATION
TIME= 103.33 DAYS
PERMEABILITY= 100 MD.
PUMPING RATE= 500 GPM.

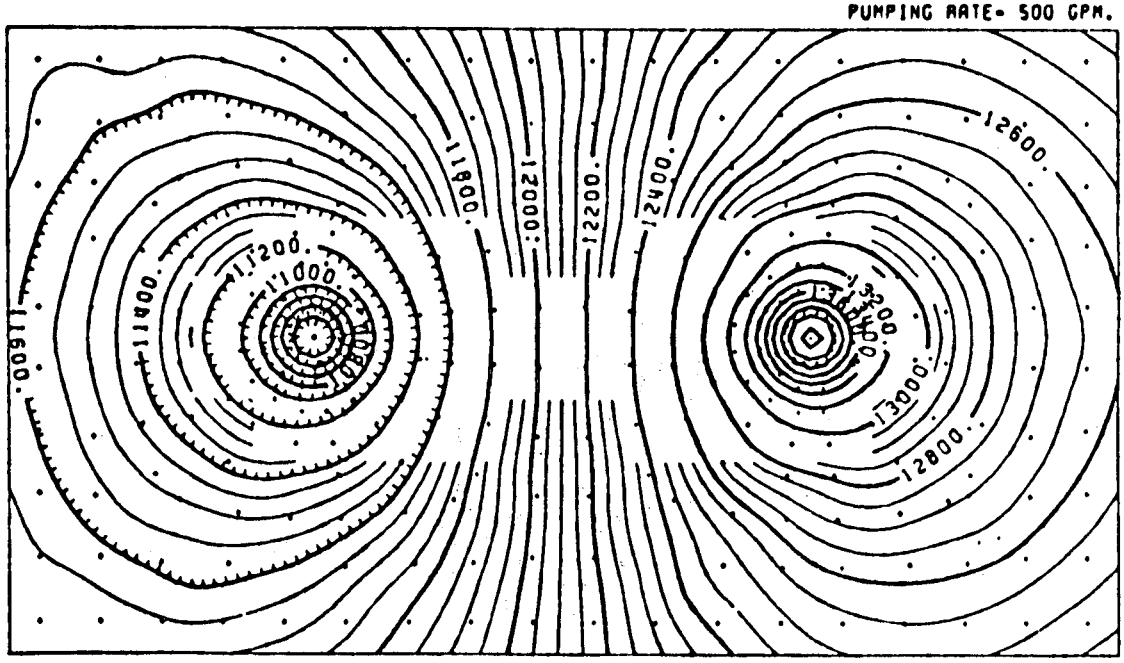

7b

PRESSURE MAP (PASCALS / 1000)
CONTOUR INTERVAL-50 (PASCALS / 1000)

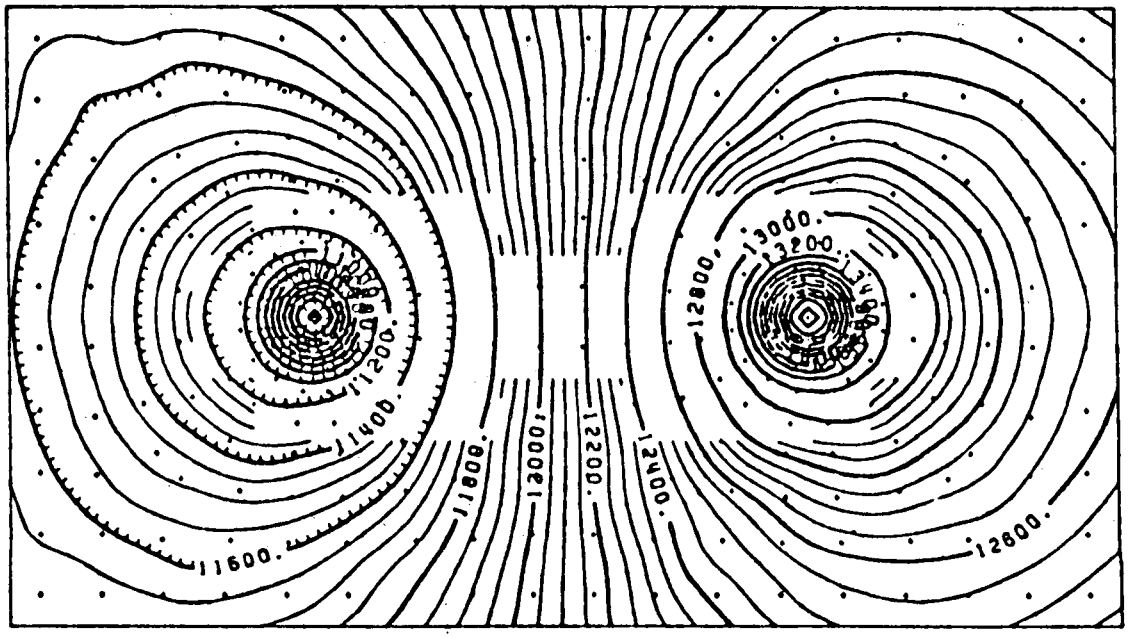

500 M. SEPARATION
TIME- 2334.1 DAYS
PERMEABILITY- 100 MD.
PUMPING RATE- 500 GPM.

7c

1000 M. SEPARATION
TIME- 4396.6 DAYS
PERMEABILITY- 100 MD.
PUMPING RATE- 500 GPM.

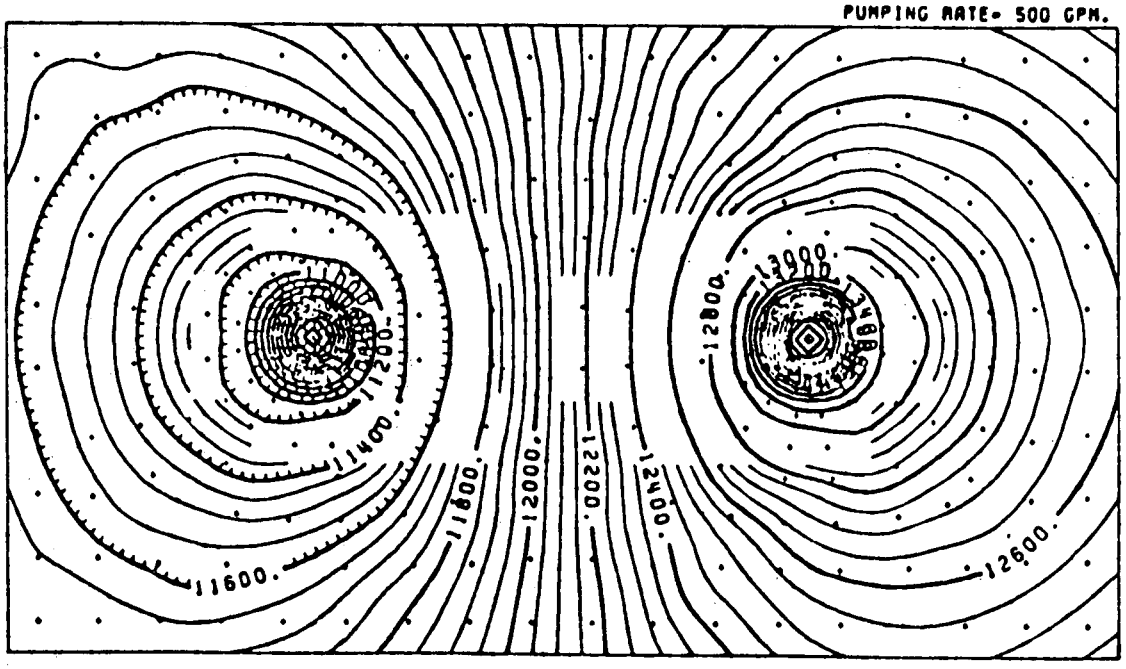

7d

Figure 8: Pressure distribution map as in Figure 5 except the permeability and pumping-injection rate are raised to 1000 md and 500 gpm, respectively.

PRESSURE MAP (PASCALS / 1000)
CONTOUR INTERVAL-50 (PASCALS / 1000)

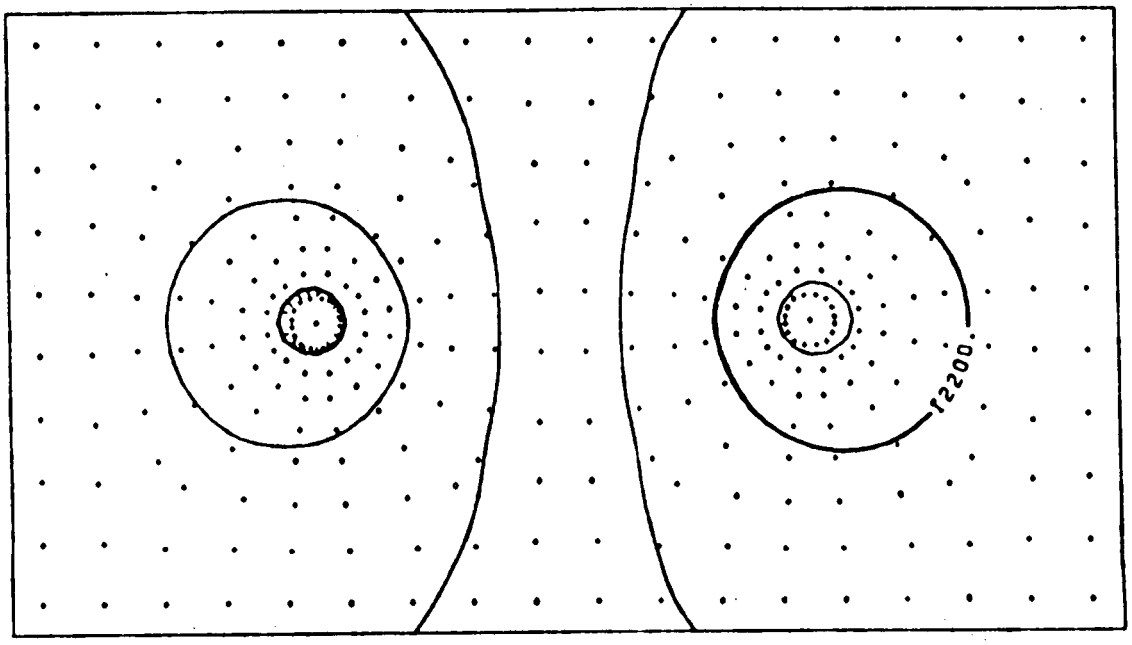

100 M. SEPARATION
TIME= 2.3069 DAYS
PERMEABILITY= 1000 MD.
PUMPING RATE= 500 GPM.

8a

250 M. SEPARATION
TIME= 8.954 DAYS
PERMEABILITY= 1000 MD.
PUMPING RATE= 500 GPM.

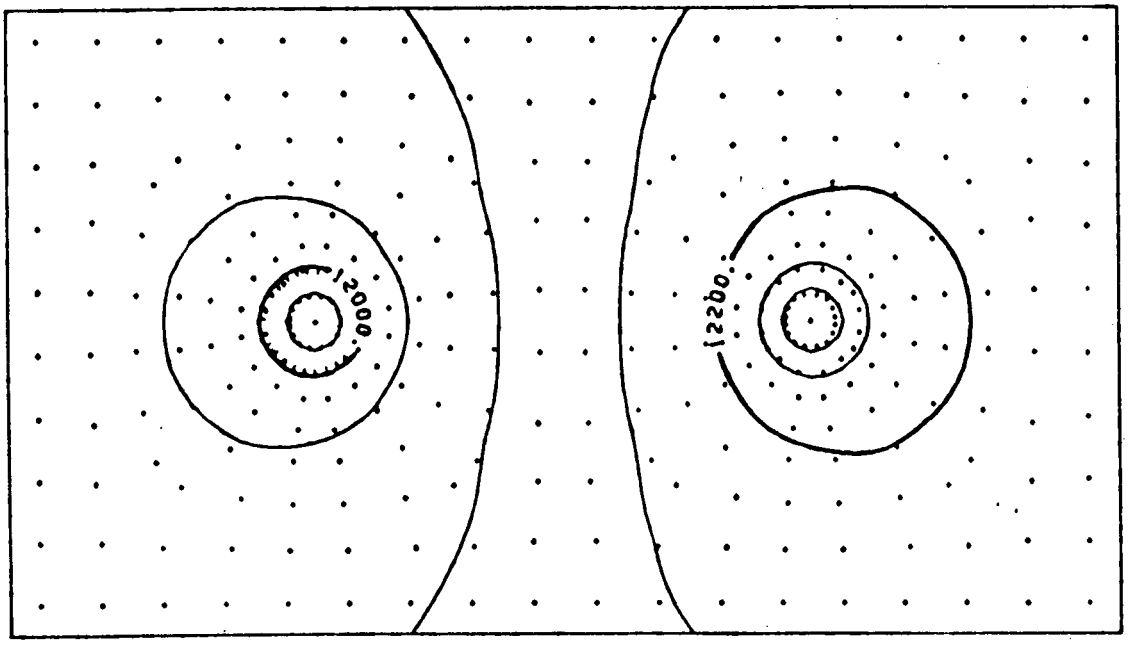

8b

PRESSURE MAP (PASCALS / 1000)
CONTOUR INTERVAL-50 (PASCALS / 1000)

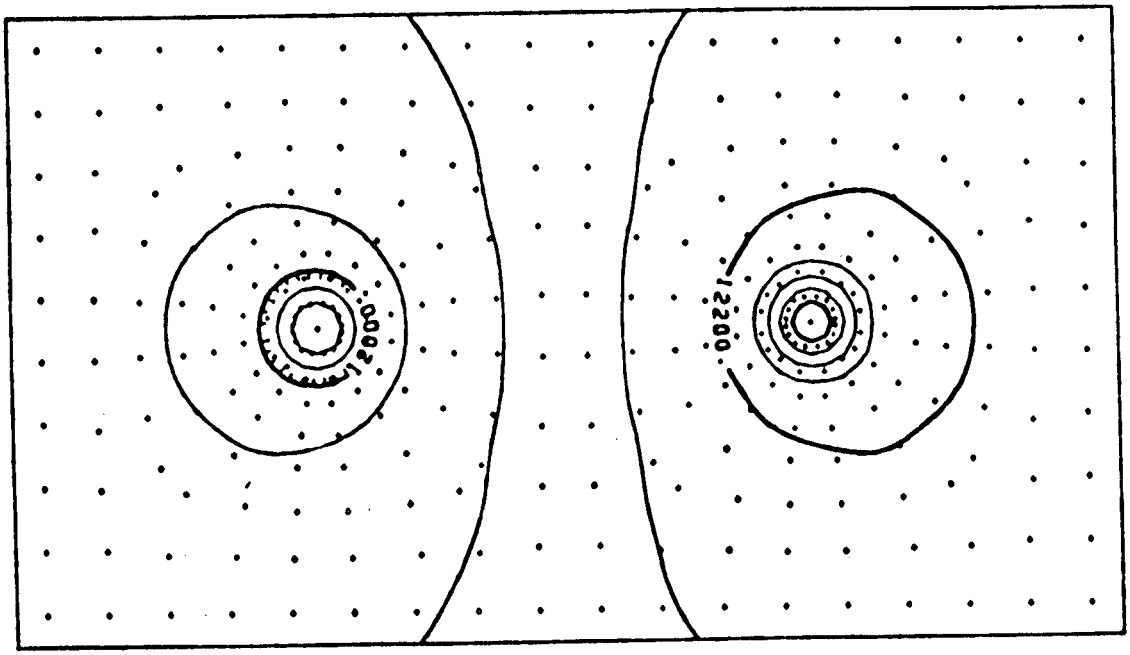

500 M. SEPARATION
TIME= 360.62 DAYS
PERMEABILITY= 1000 MD.
PUMPING RATE= 500 GPM.

8c

1000 M. SEPARATION
TIME= 227.08 DAYS
PERMEABILITY= 1000 MD.
PUMPING RATE= 500 GPM.

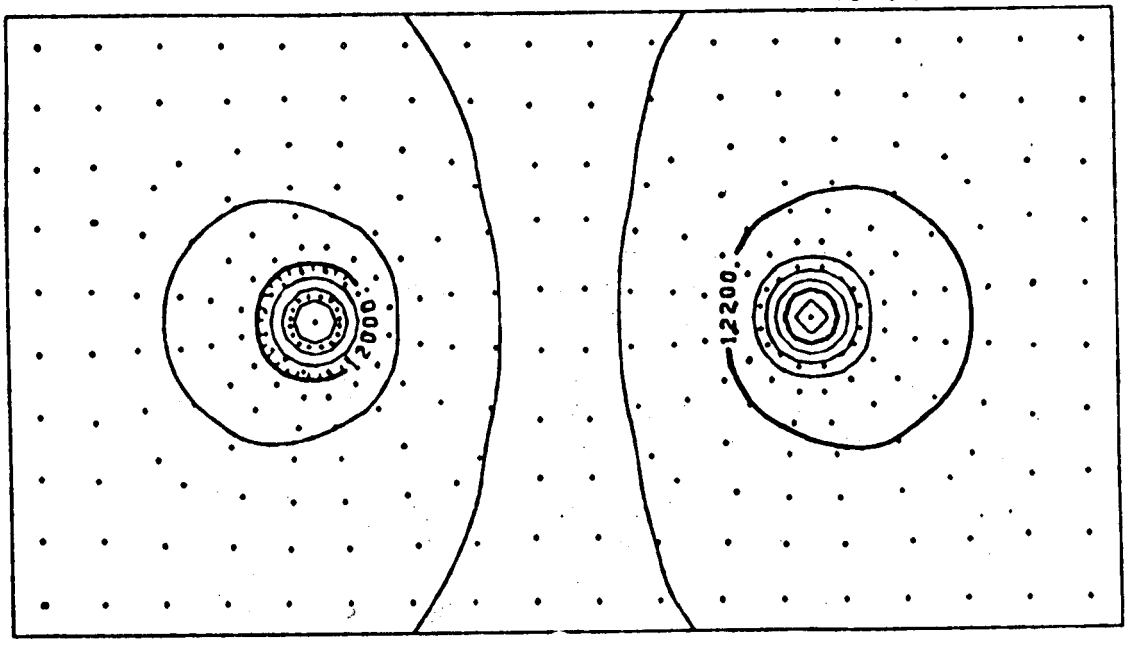

8d

This occurrence of a negative pressure was verified using the Theis-solution for a single pumping well with similar hydrologic characteristics. A simple calculation using the Theis-solution for an aquifer with a permeability of 100 md, a single pumping well being pumped at 500 gpm, and all other hydrologic parameters equal, shows that the drawdown at 55 days would cause a negative hydraulic head. A negative hydraulic head is physically impossible, instead, the result would be a complete dewatering of the aquifer and possible collapse. In the 100 md simulations no negative pressure anomaly occurred, indicating a permeability high enough to allow the injection well to influence the recovery of pressure in the production well. This result indicates the importance of a doublet system in the low permeability aquifers of the Atlantic Coastal Plain. The injection well is needed to maintain sufficient fluid pressure at the production well.

Changes in the pressure distribution with permeability and pumping-injection rate are reflected in the contour plots. As expected, an increase in the pumping-injection rate or a decrease in the permeability produces a greater pressure differential within the system.

A cross-sectional view for all four well spacings of the total head distribution is shown in Figure 9. In this sequence the permeability and the pumping-injection rate are held constant at 100 md and 500 gpm. The influence of the injection well on the production well is displayed by the pattern of the contour lines. The effect is less pronounced in the large separations where there exists a greater independence between the production and injection wells. The location of the equipotential lines indicates that the majority of the flow into the sink and out of the source takes place within the boundaries of the reservoir.

Analysis of the Temperature Field

Map views of the thermal distribution through the center section of the reservoir are shown in Figures 10-13. Results are contoured for 1, 5, 13, and 15 years or until steady-state is reached in the temperature field. The sequence of plots covers permeabilities of 100 and 1000 md and pumping-injection rates of 100 and 500 gpm for all four well spacings. Figure 14 displays a cross-sectional view of the temperature field for all four well spacings in a system with a permeability of 1000 md and a pumping-injection rate of 500 gpm. Figures 15-18 are temperature versus time plots comparing output temperatures (temperature at the production well) in the four well spacings for each combination of permeability and pumping-injection rate.

The figures clearly illustrate the effect of well spacing on the temperature distribution. The general trend present is an increase in the output temperature with an increase in the distance between the production and injection wells. The amount of energy which is extracted from the system assuming no pipe loss is calculated using equation (16). The results are listed in Table 4. The time at which breakthrough occurs is in support of this trend. For all pumping-injection rates and permeablities, breakthrough in the 100 meter spacing

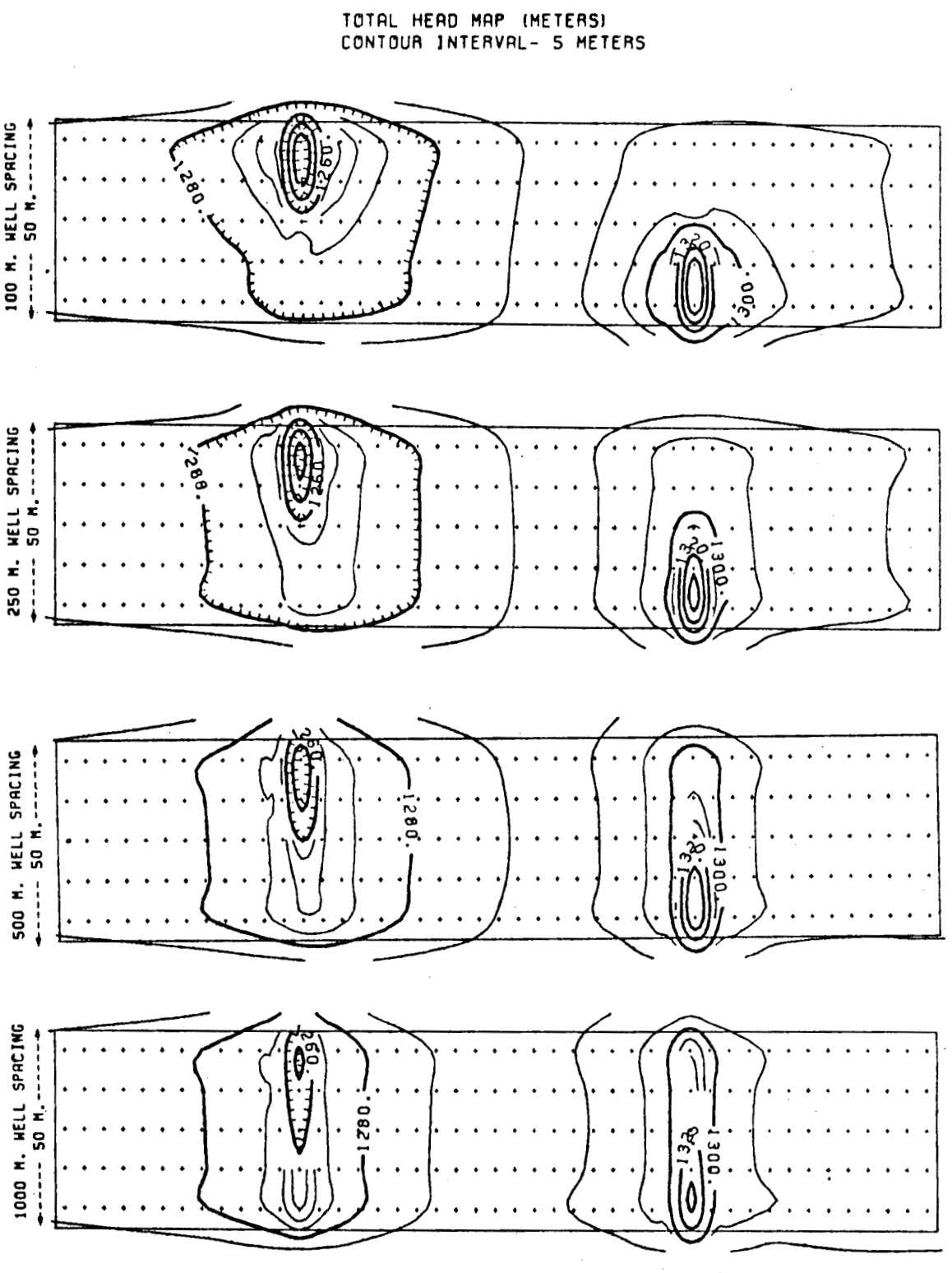

Figure 9: Cross-sectional view of the total head distribution for various well spacings in a system with a permeability of 1000 md and a pumping-injection stress of 500 gpm. Crosses indicate location of nodal points and the values interpolated between the nodal points. Typical flow paths are shown by stream lines (solid black lines with arrows) in the upper and lower sketches.

Figure 10: Time sequence plan view contour plots of the temperature distribution through the center section of the reservoir for a system with a permeability 100 md and a pumping-injection rate of 100 gpm. Temperature distributions are contoured at 1, 5, 10, and 15 years (365, 1825, 3650, and 5475 days) or until steady-state is reached. Hydrologic and system characteristics (i.e., well spacing, time, permeability, pumping-injection rate) are listed alongside each individual plot. Crosses represent location of nodal points. Breakthrough is defined in the sequence as the point in time when the 55°C contour interval intersects the node directly under the production well.

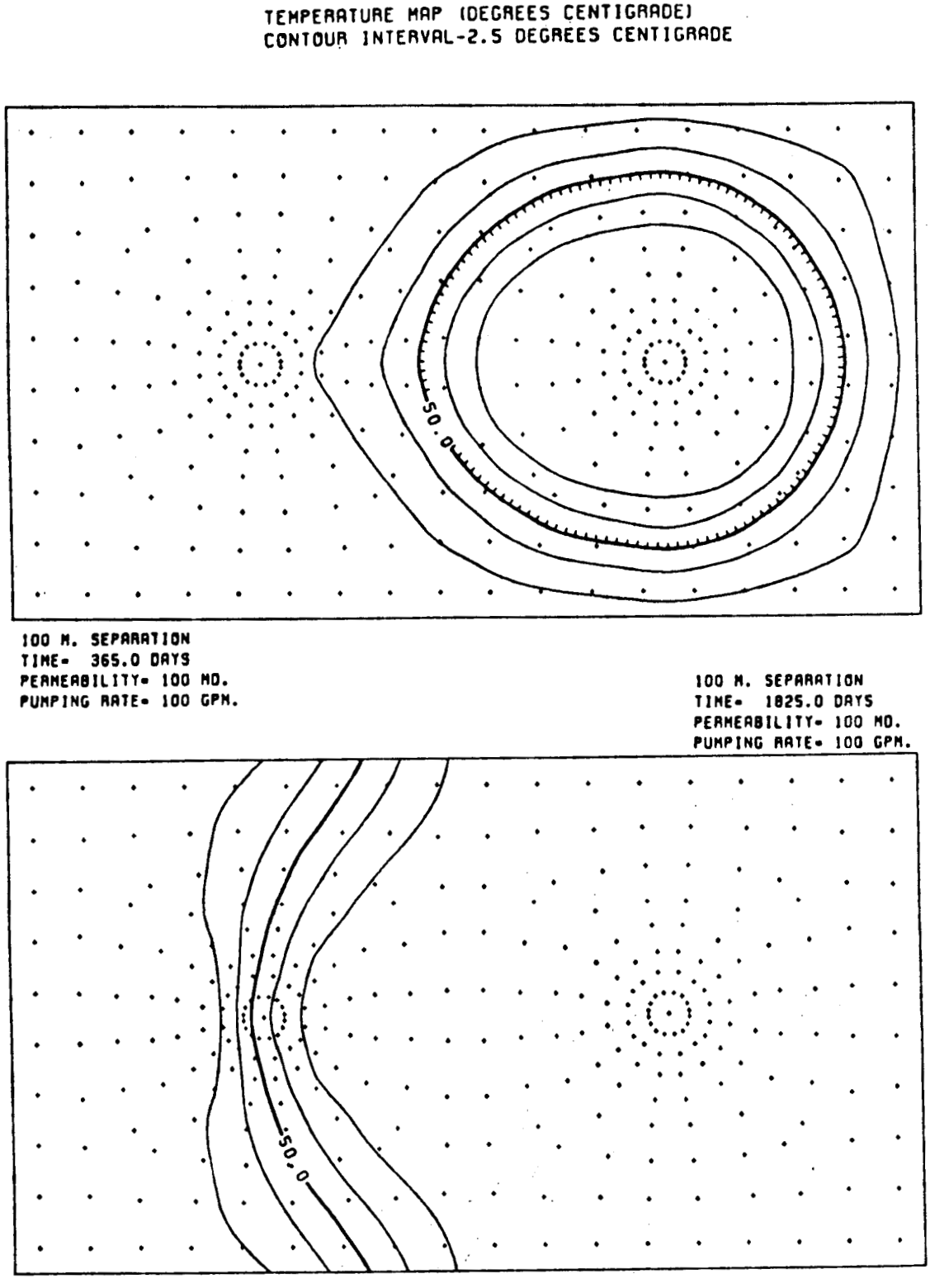

Figure 10a1: Temperature distribution map for a 100 m well spacing at 1 and 5 yrs, upper and lower plots respectively. Note breakthrough occurs prior to 5 yrs.

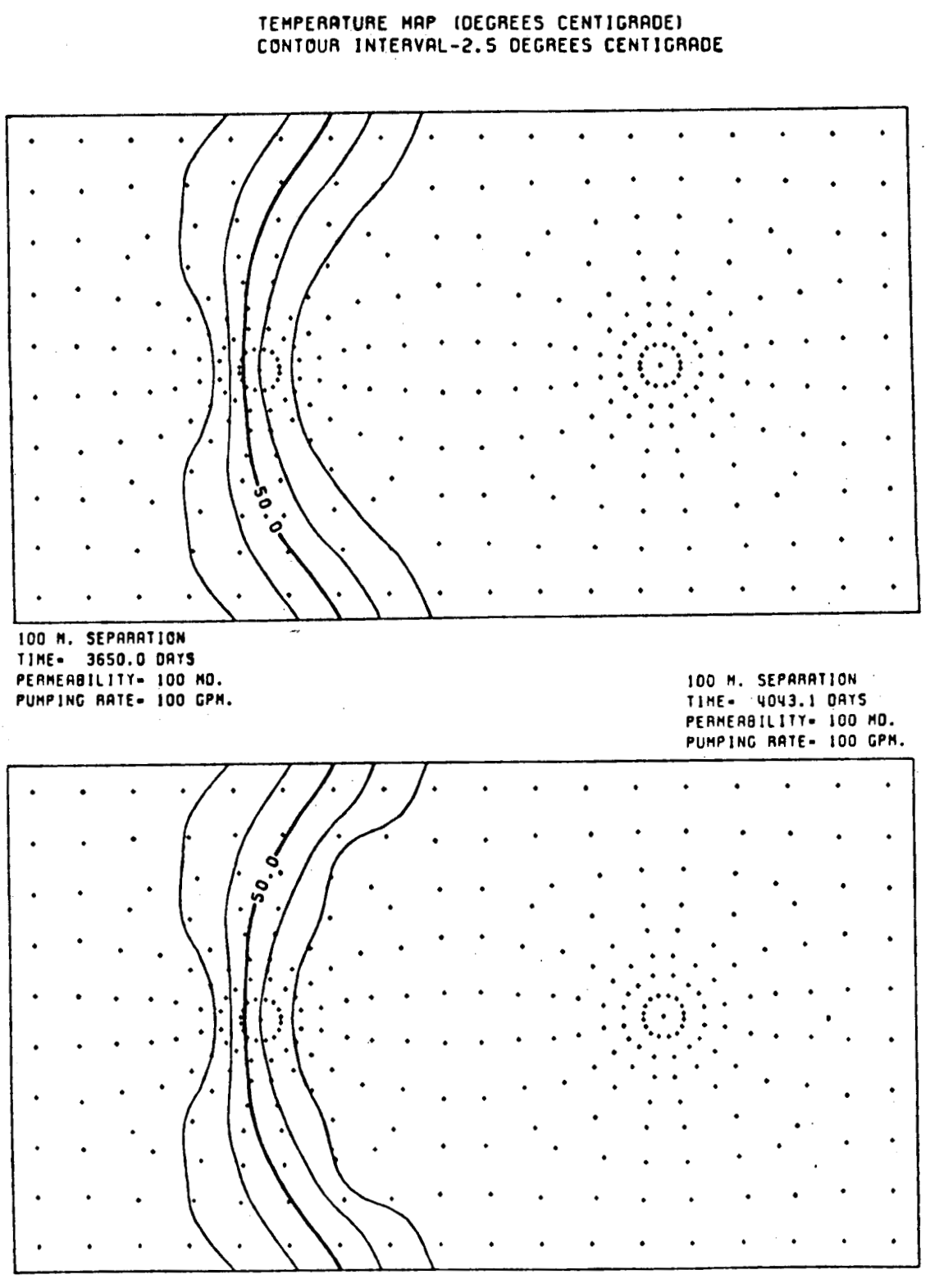

Figure 10a2: Temperature distribution map for a 100 m well spacing at 10 and 11.1 yrs (steady-state), upper and lower plots respectively.
Figure 10b1: Temperature distribution map for a 250 m well spacing at 1 and 5 yrs, upper and lower plots respectively.

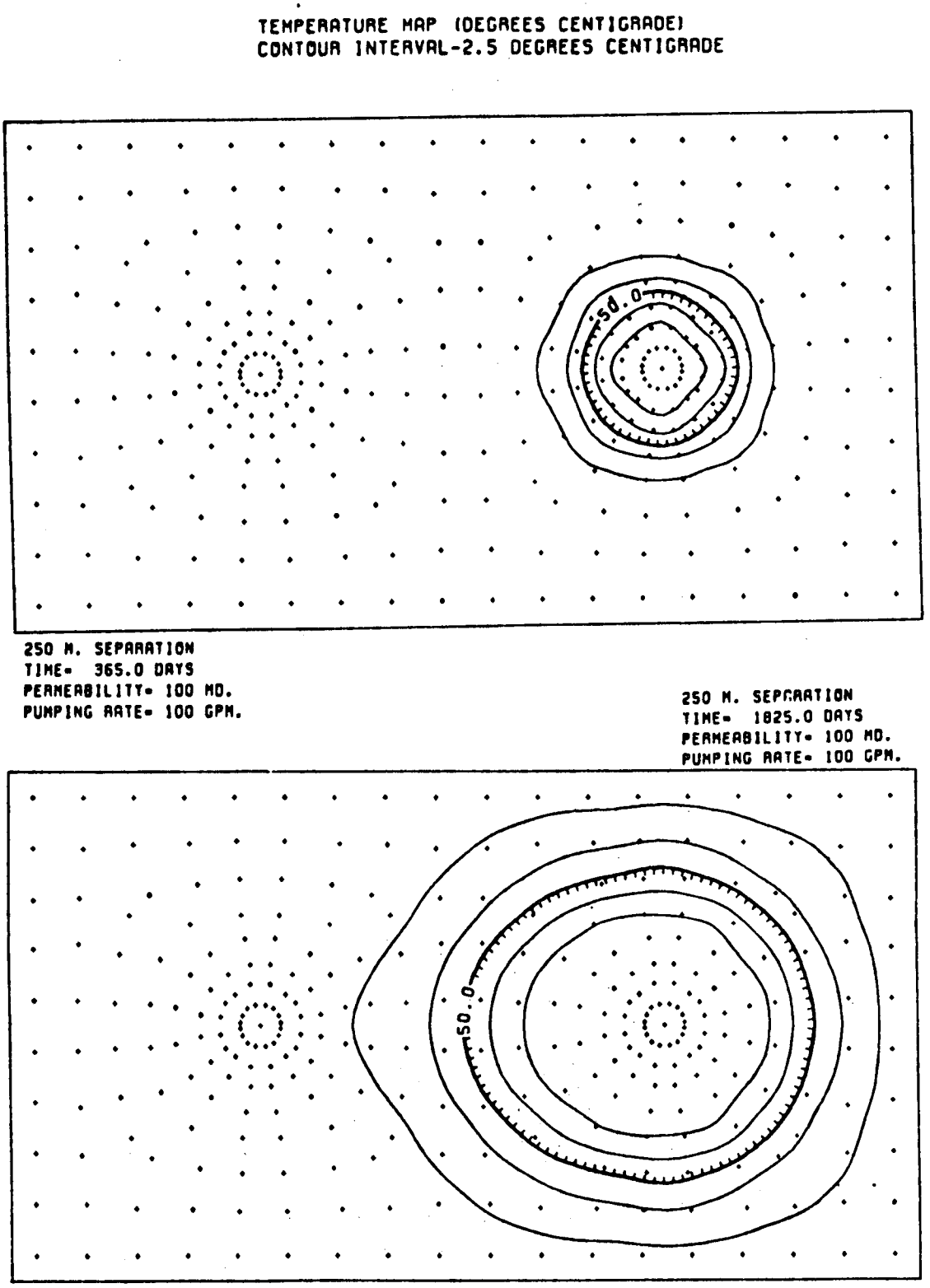

Figure 10b1: Temperature distribution map for a 250 m well spacing at 1 and 5 yrs., upper and lower plots respectively.

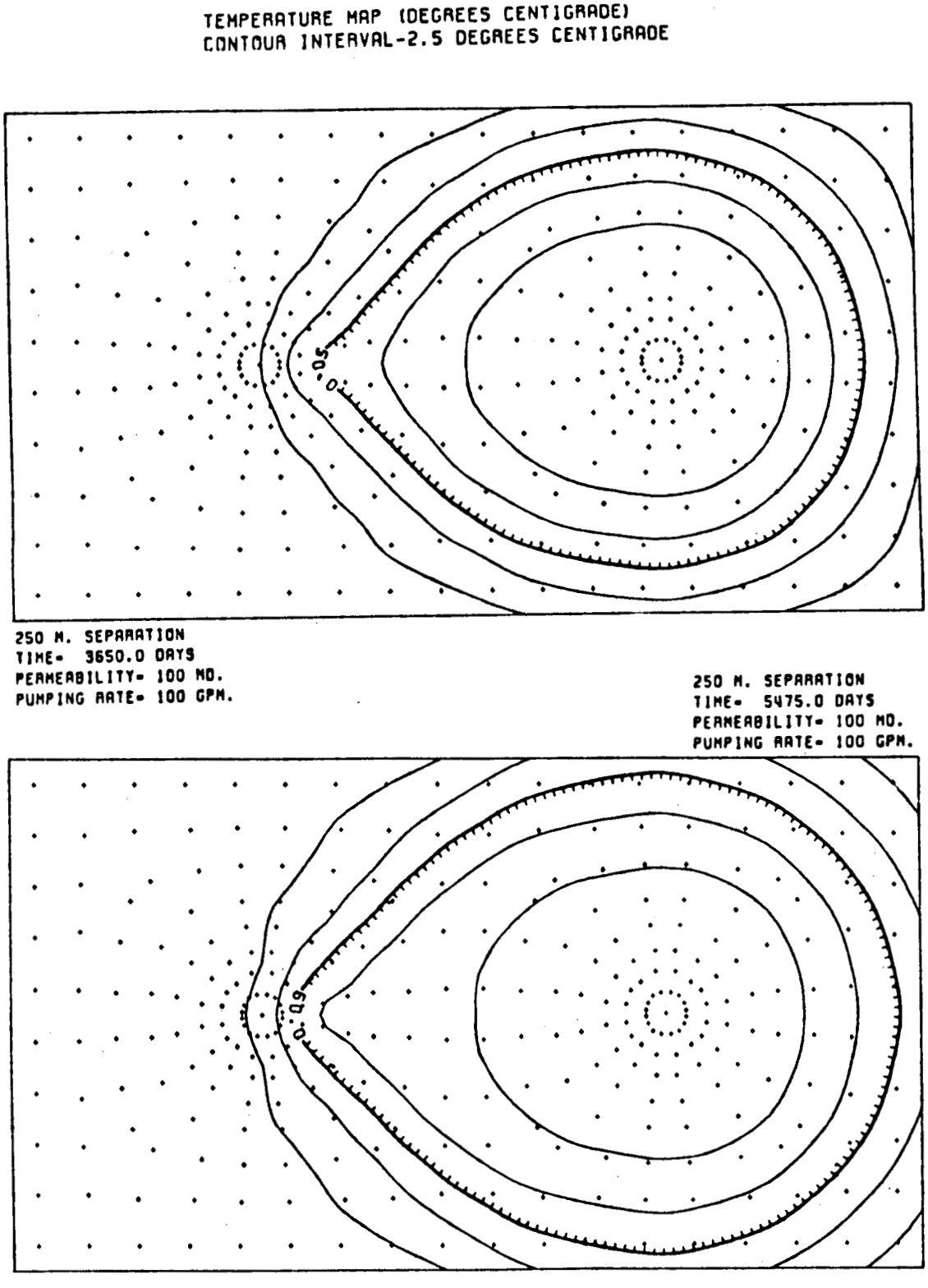

Figure 10b2: Temperature distribution map for a 250 m well spacing at 10 and 15 yrs, upper and lower plots respectively. Note breakthrough occurs at 10 yrs.

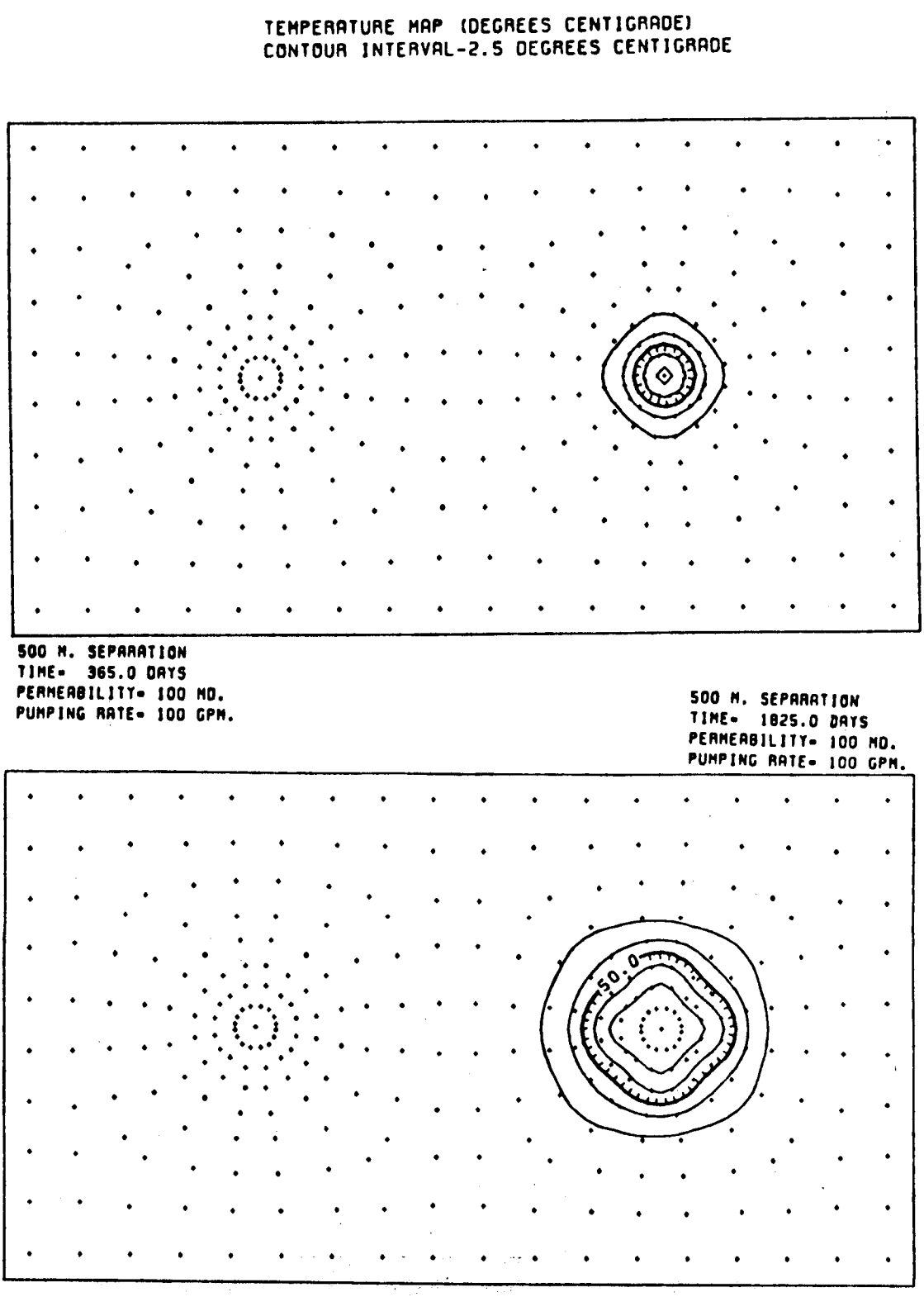

Figure 10c1: Temperature distribution map for a 500 m well spacing at 1 and 5 yrs, upper and lower plots respectively.

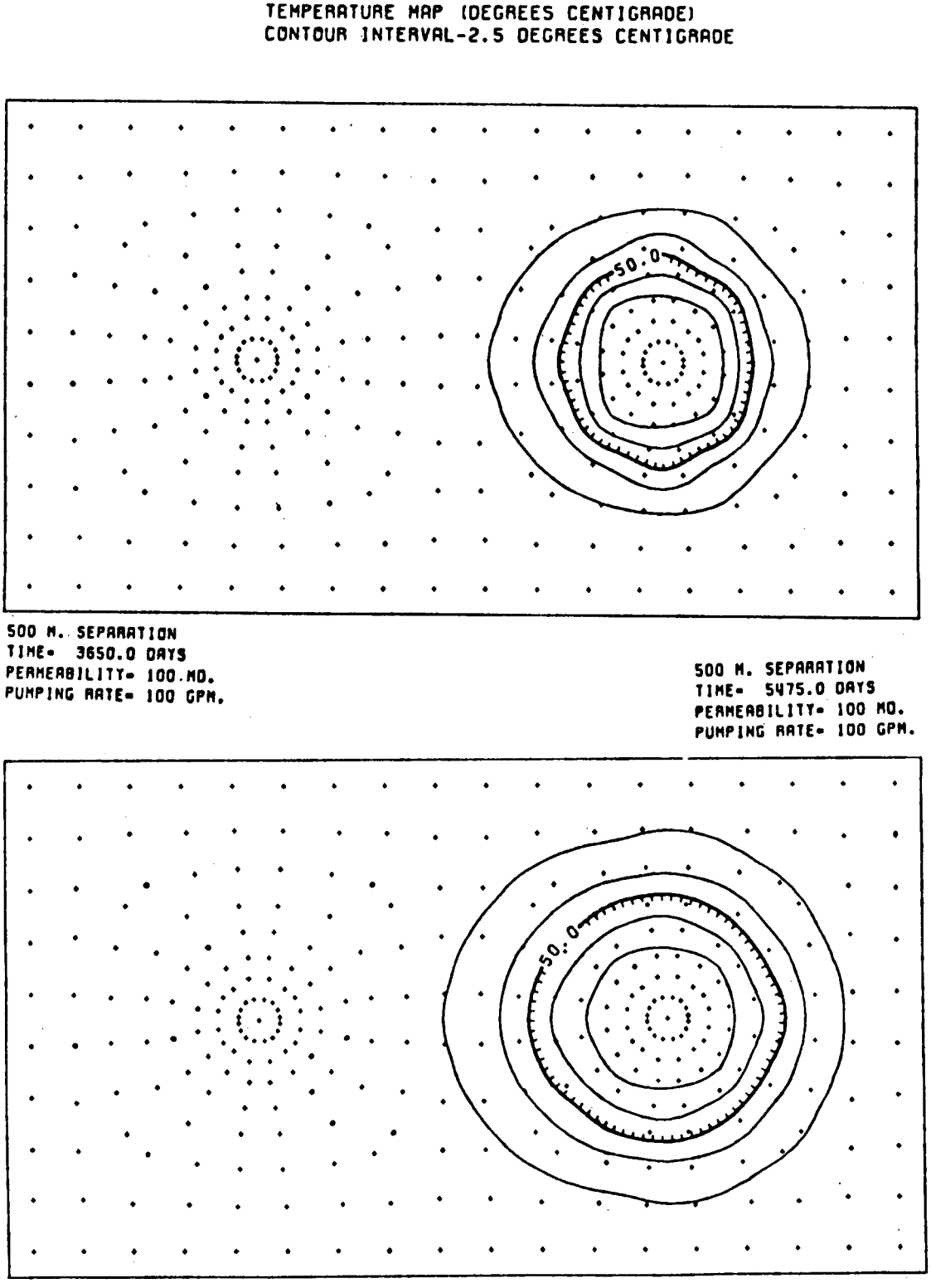

Figure 10c2: Temperature distribution map for a 500 m well spacing at 10 and 15 yrs, upper and lower plots respectively.

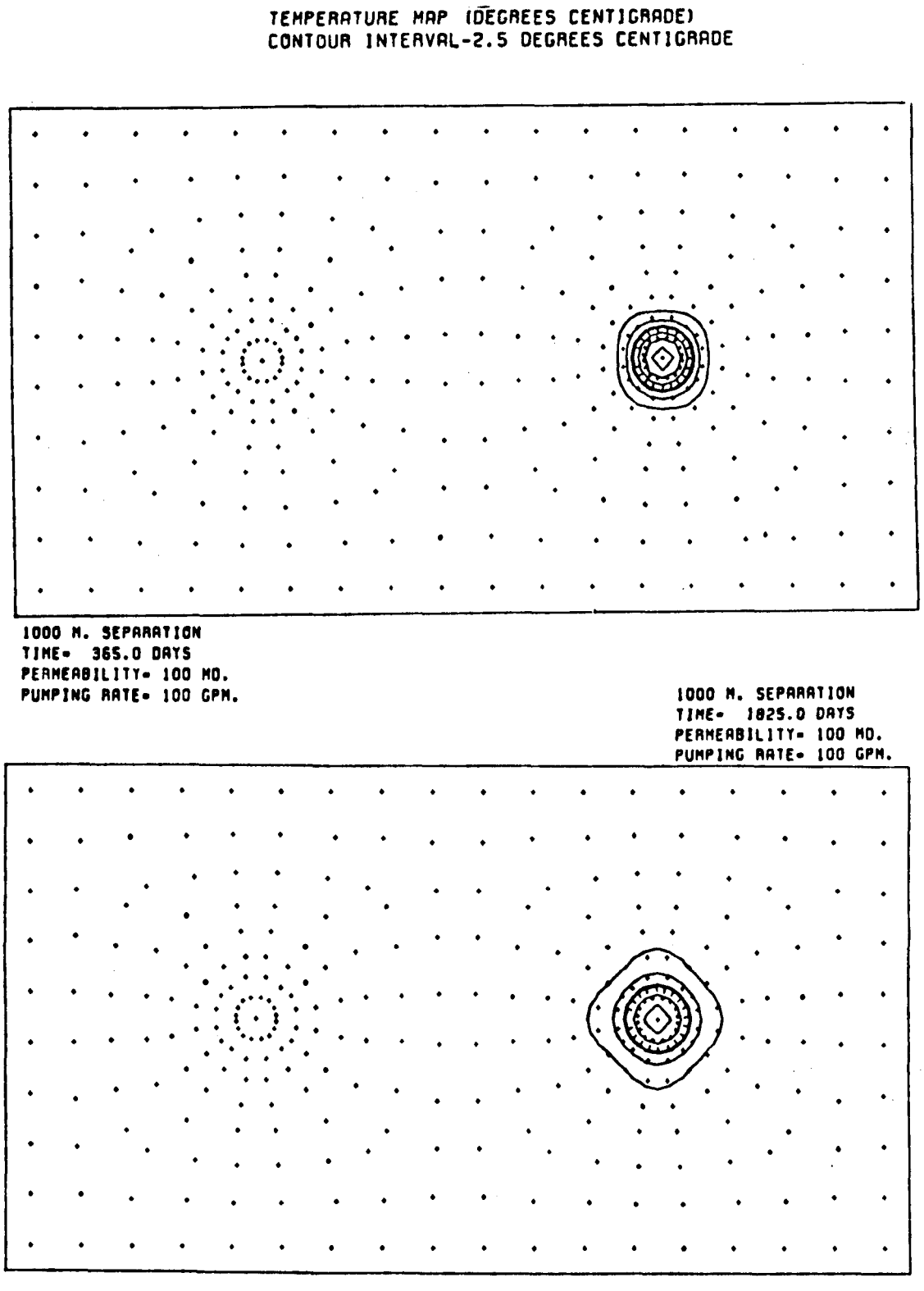

Figure 10d1: Temperature distribution map for a 1000 m well spacing at 1 and 5 yrs, upper and lower plots respectively.

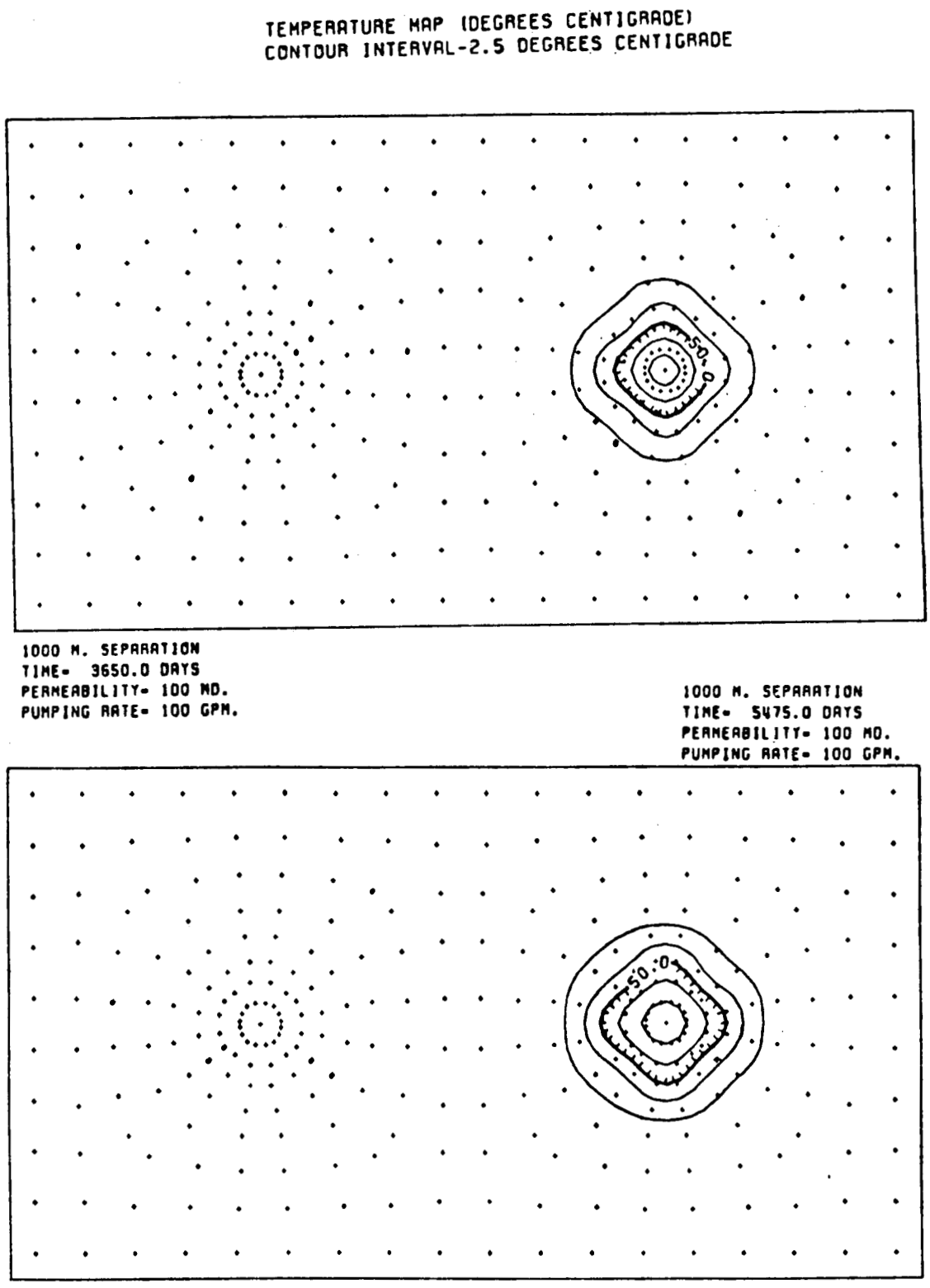

Figure 10d2: Temperature distribution map for a 1000 m well spacing at 10 and 15 yrs, upper and lower plots respectively.

Figure 11: Time sequence plan view contour plots of the temperature distribution as in Figure 10 except the pumping-injection rate is raised to 500 gpm.

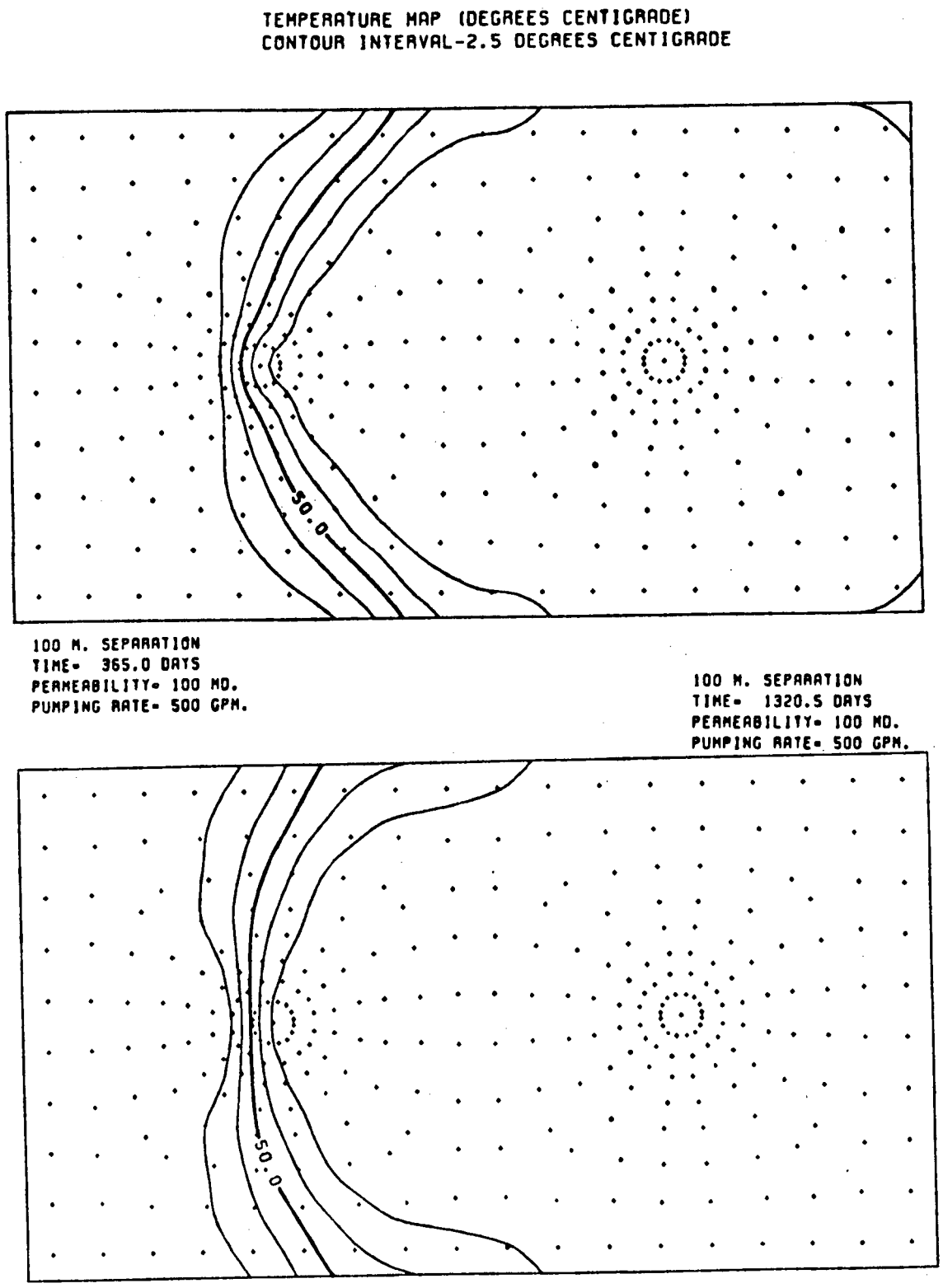

Figure 11a1: Temperature distribution map for a 100 m well spacing at 1 and 3.6 yrs (steady-state), upper and lower plots respectively. Note breakthrough occurred prior to 3.6 yrs.

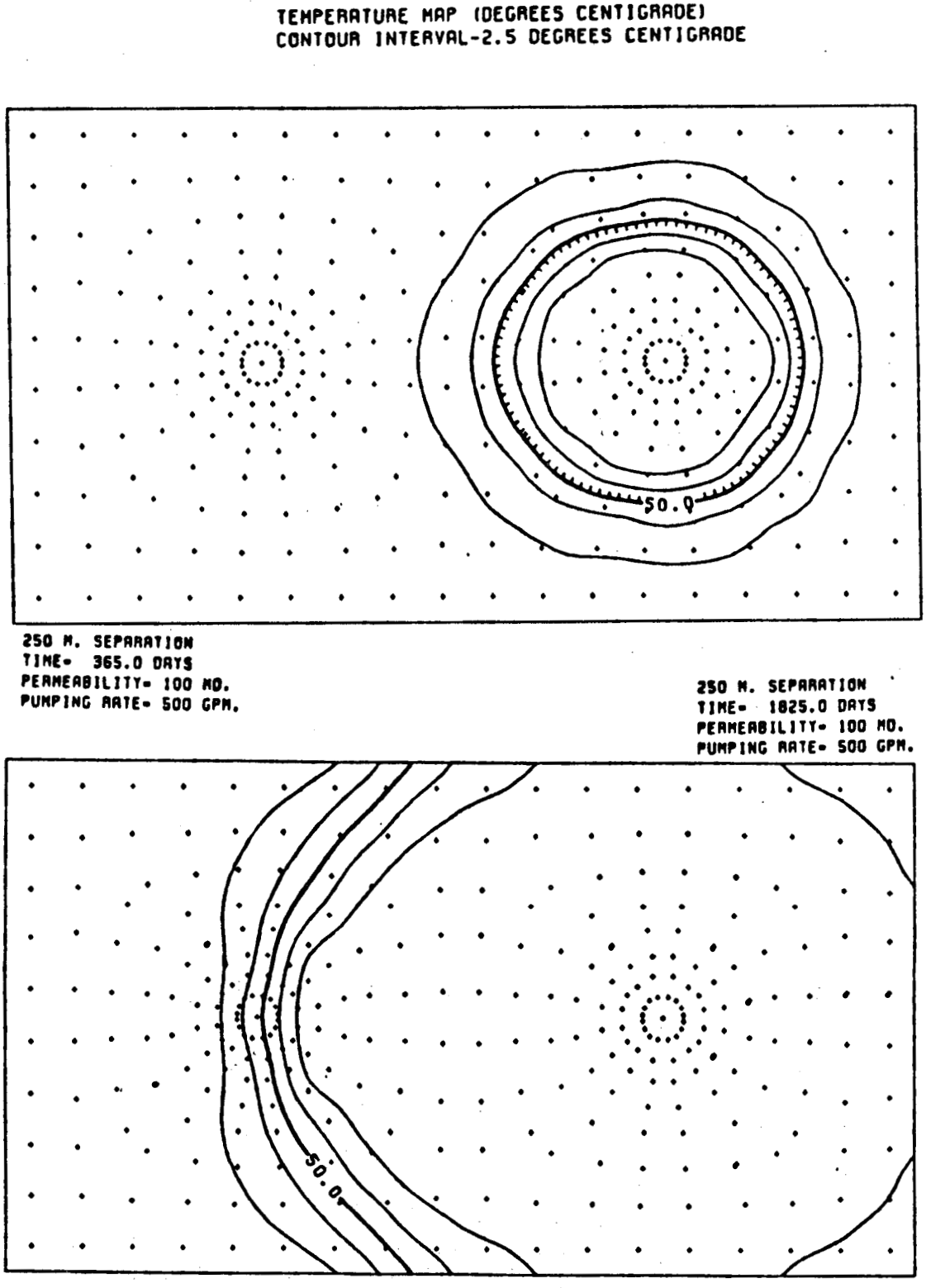

Figure 11b1: Temperature distribution map for a 250 m well spacing at 1 and 5 yrs, upper and lower plots respectively. Note breakthrough occurs prior to 5 yrs.

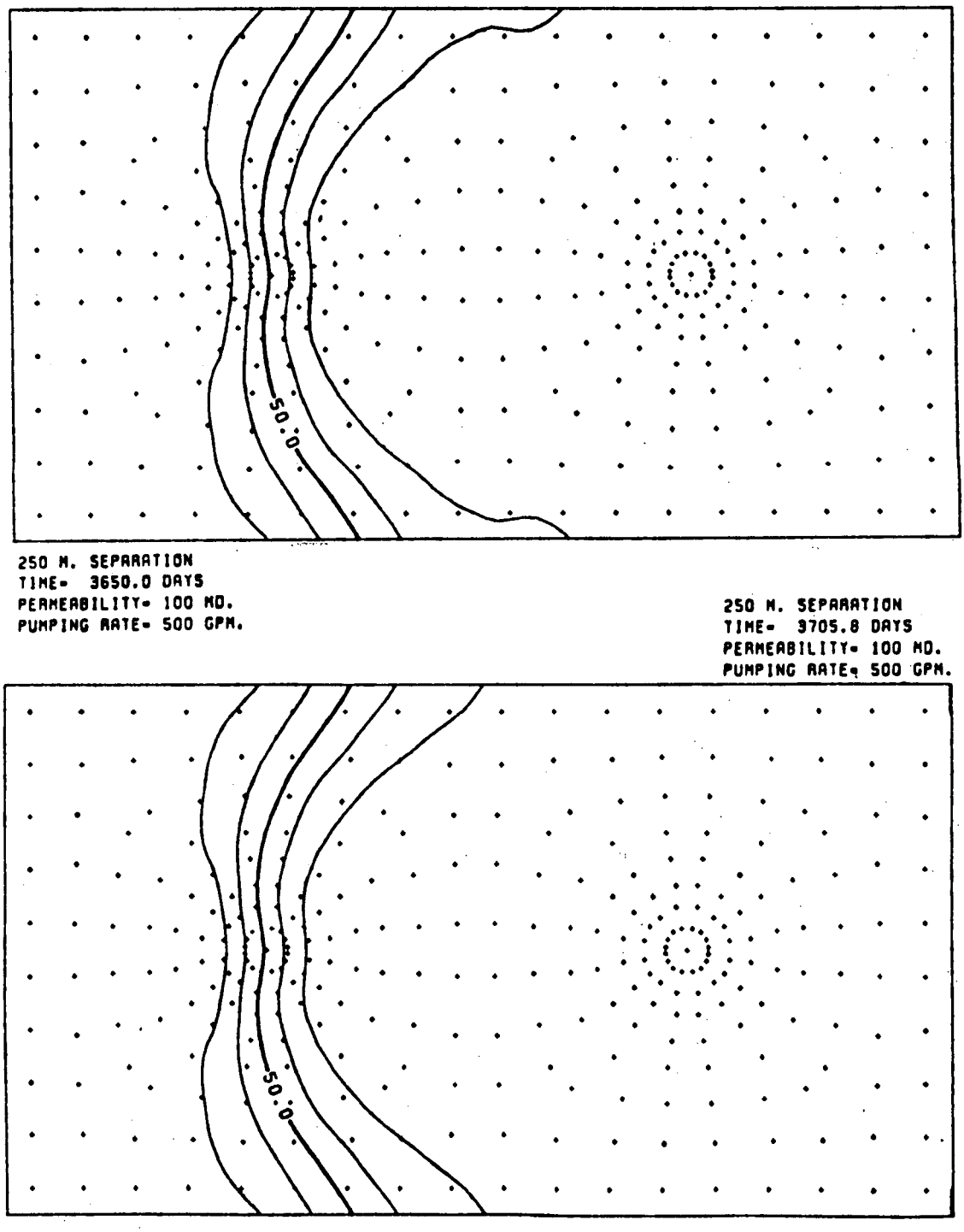

Figure 11b2: Temperature distribution map for a 250 m well spacing at 10 and 10.2 yrs (steady-state), upper and lower plots respectively.

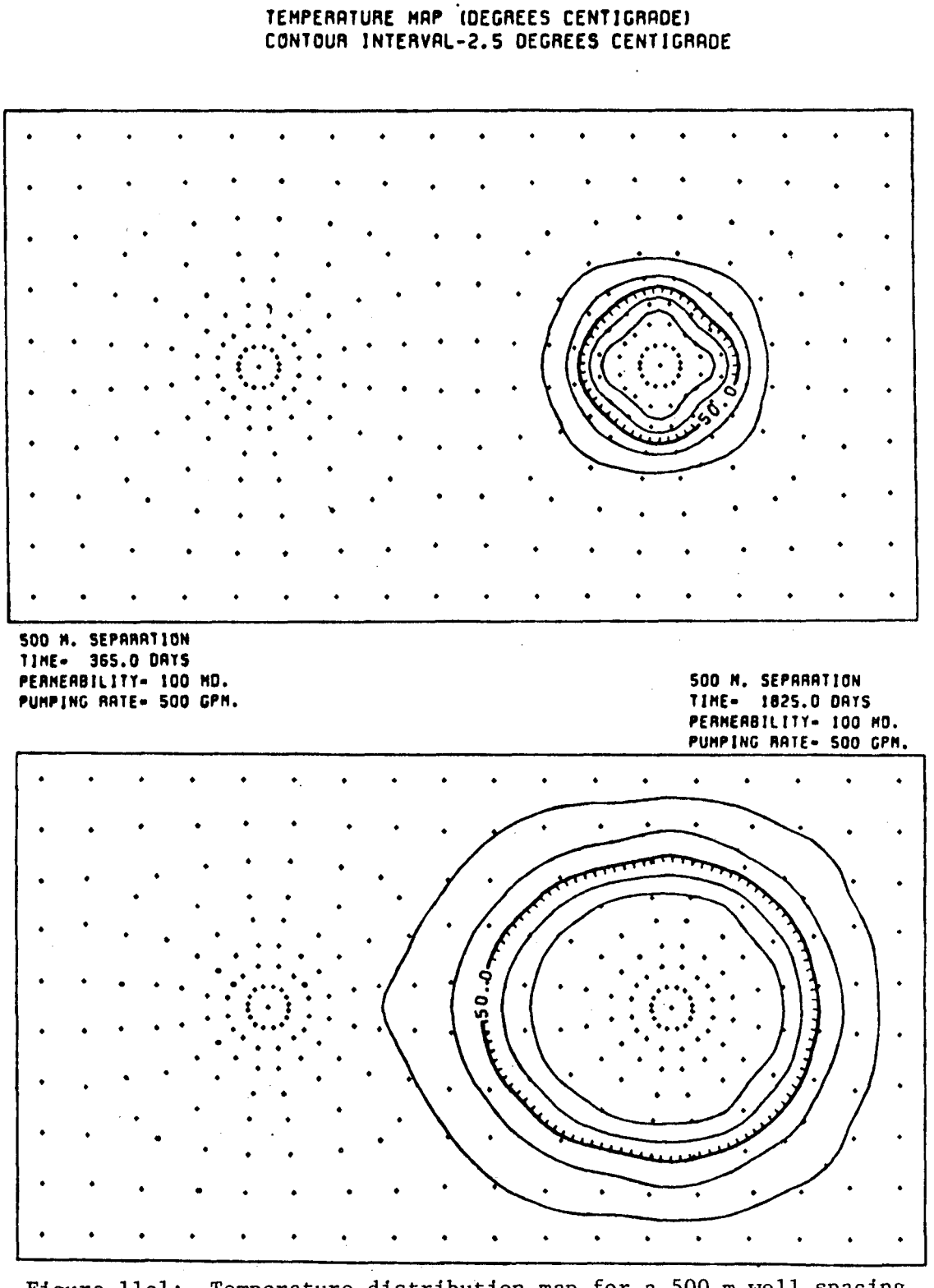

Figure 11c1: Temperature distribution map for a 500 m well spacing at 1 and 5 yrs, upper and lower plots respectively.

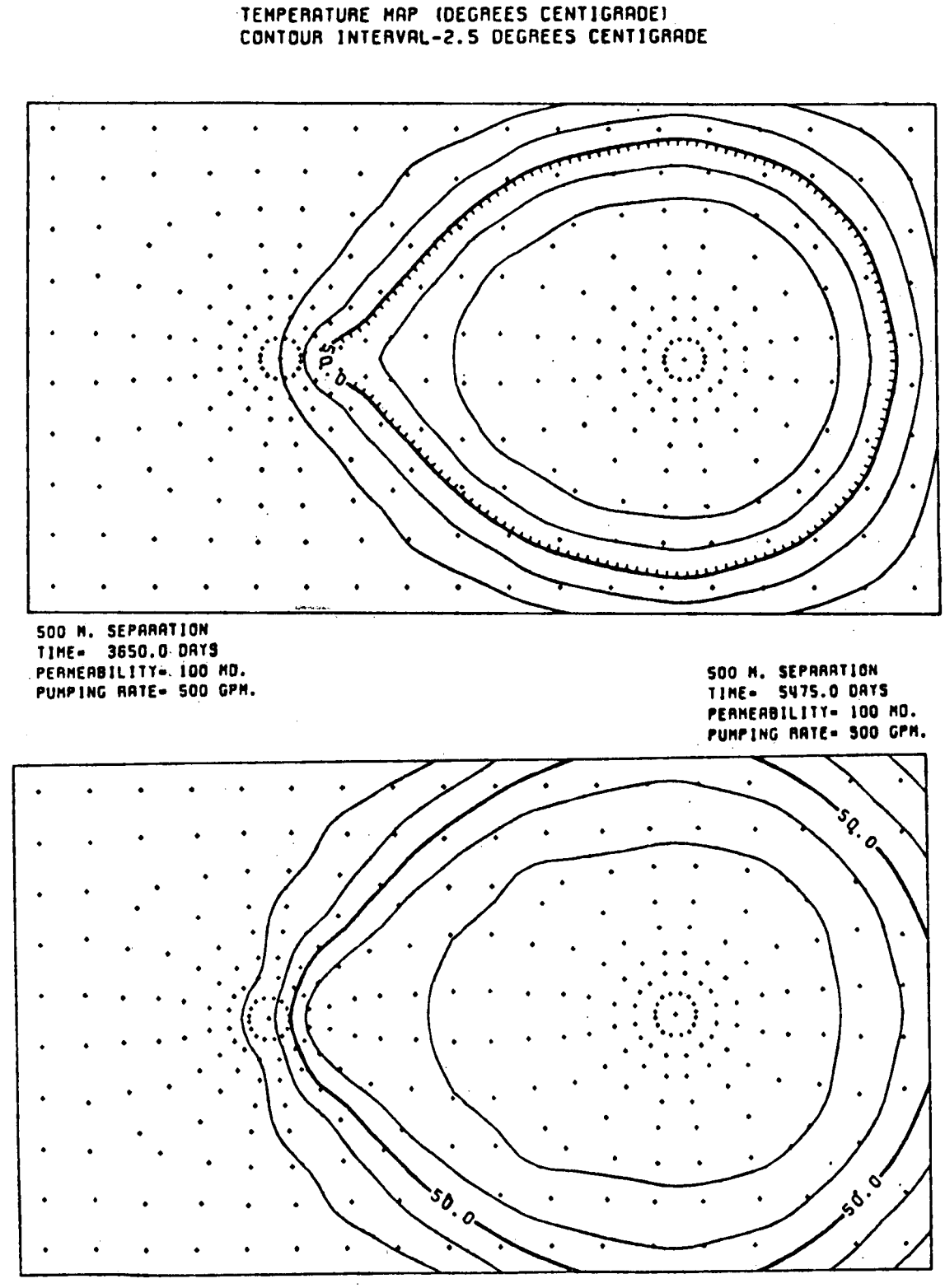

Figure 11c2: Temperature distribution map for a 500 m well spacing at 10 and 15 yrs, upper and lower plots respectively. Note breakthrough occurs at 10 yrs.

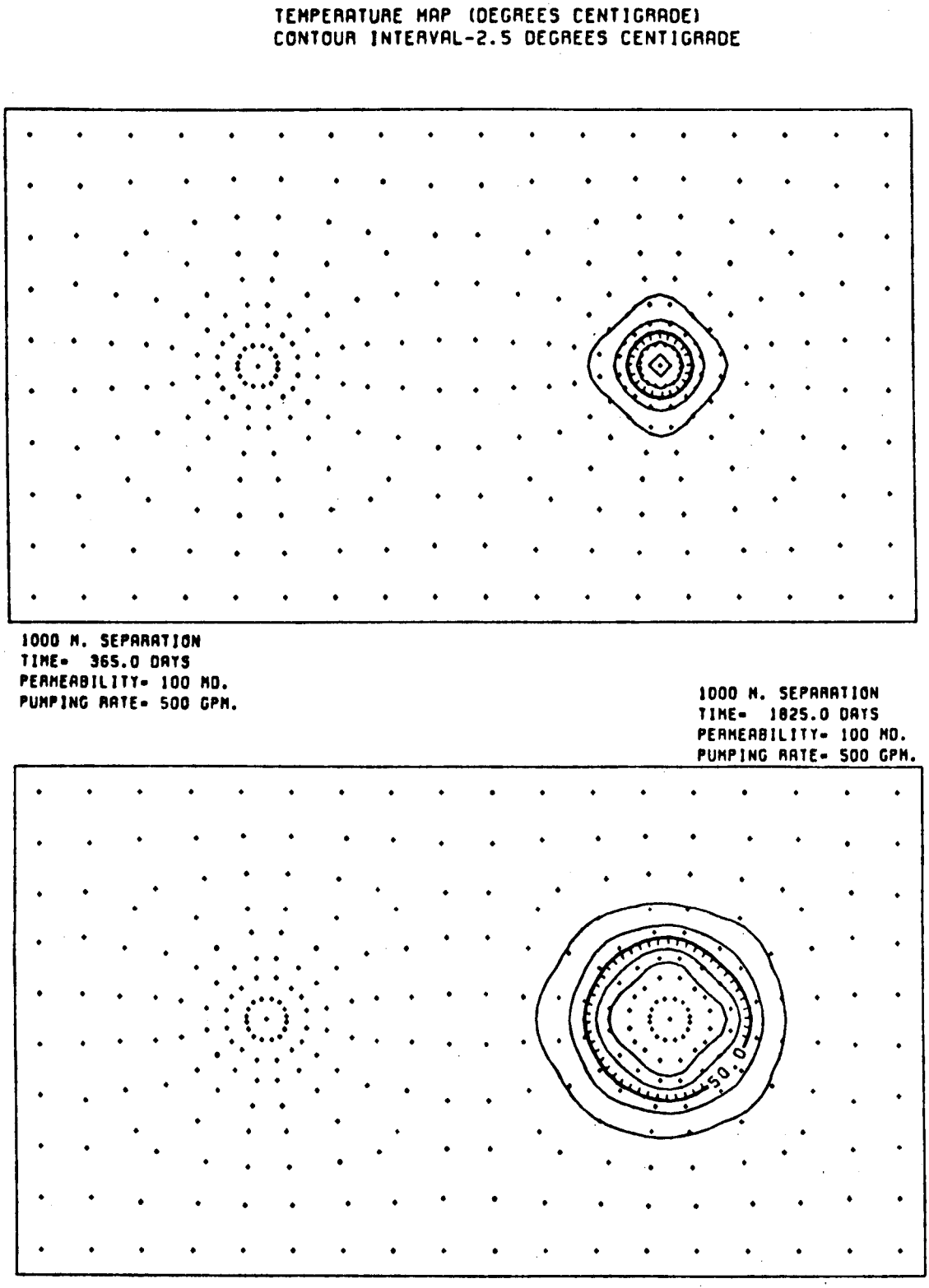

Figure 11d1: Temperature distribution map for a 1000 m well spacing at 1 and 5 yrs, upper and lower plots respectively.

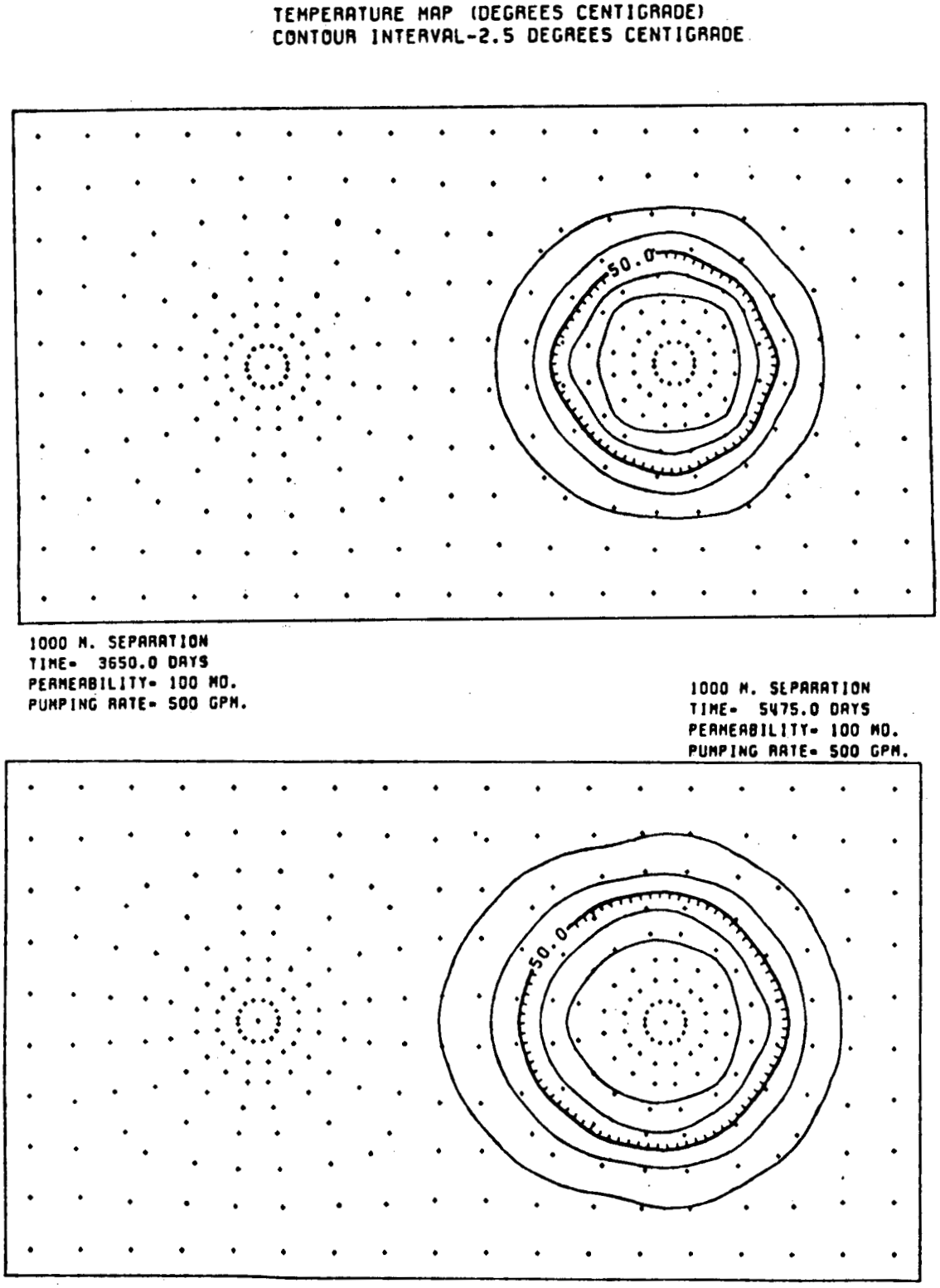

Figure 11d2: Temperature distribution map for a 1000 m well spacing at 10 and 15 yrs, upper and lower plots respectively.

Figure 12: Time sequence plan view contour plots of the temperature distribution as in Figure 10 except the permeability is raised to 1000 md.

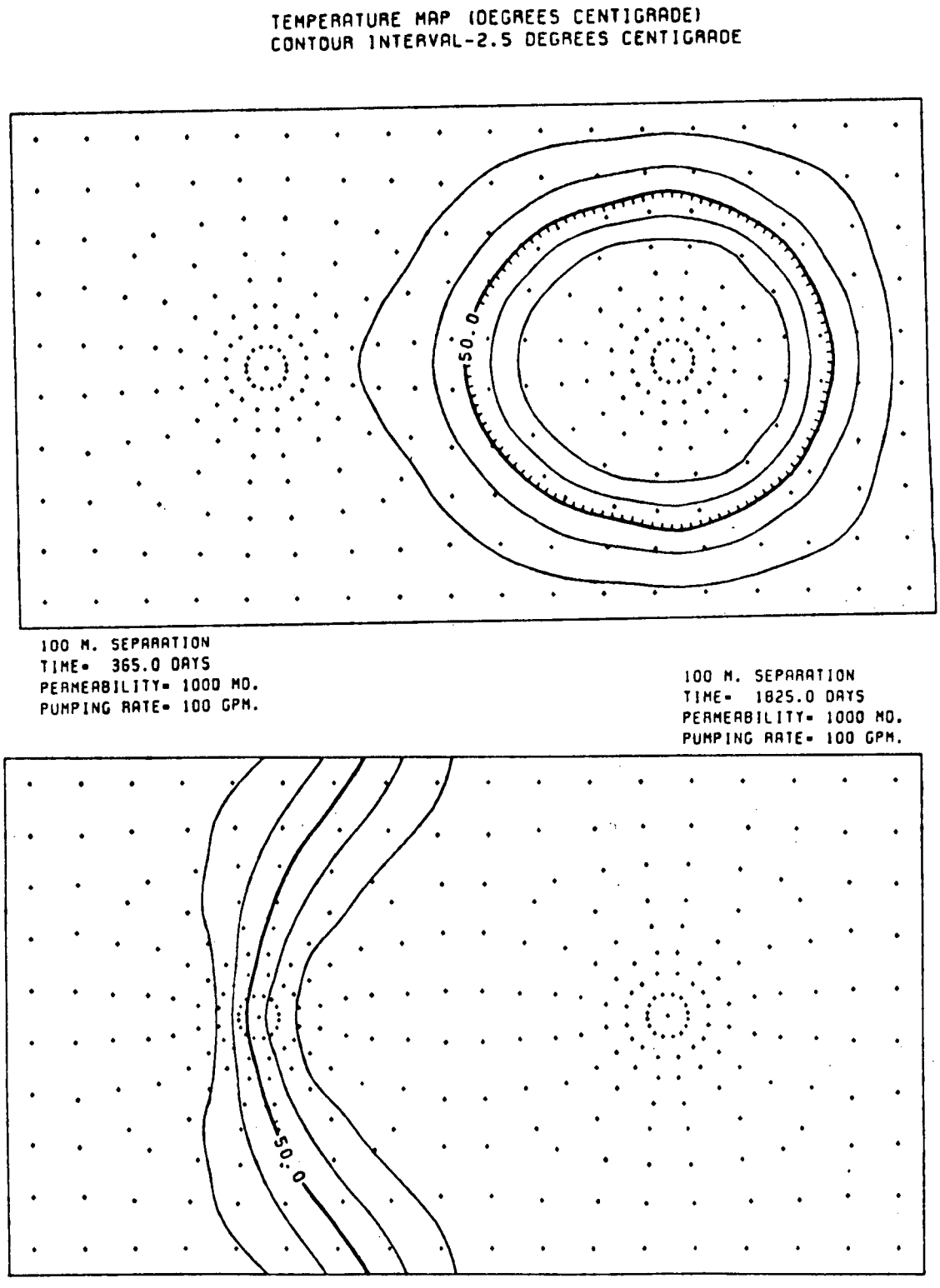

Figure 12a1: Temperature distribution map for a 100 m well spacing at 1 and 5 yrs, upper and lower plots respectively. Note breakthrough occurs prior to 5 yrs.

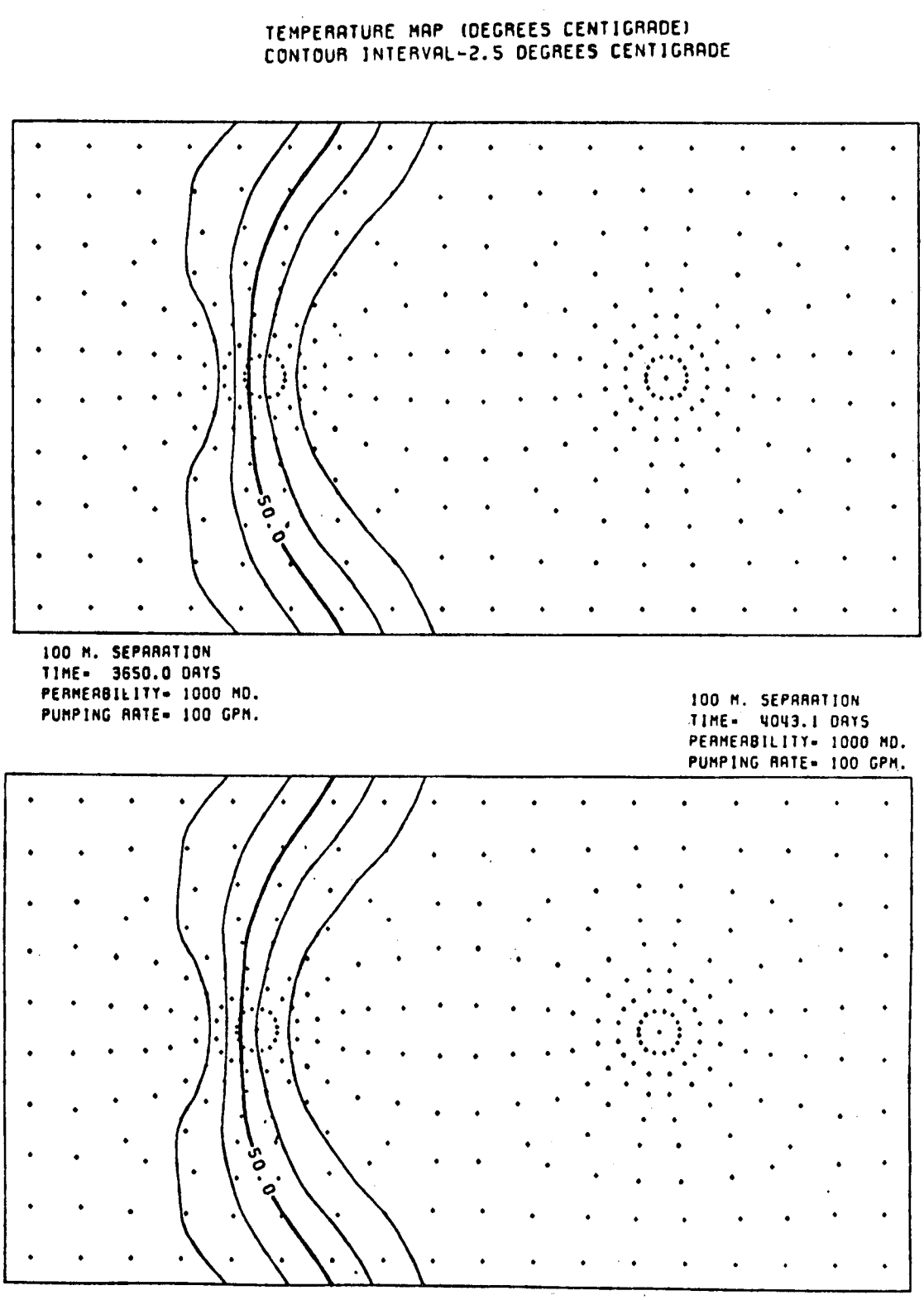

Figure 12a2: Temperature distribution map for a 100 m well spacing at 10 and 11.1 yrs (steady-state), upper and lower plots respectively.

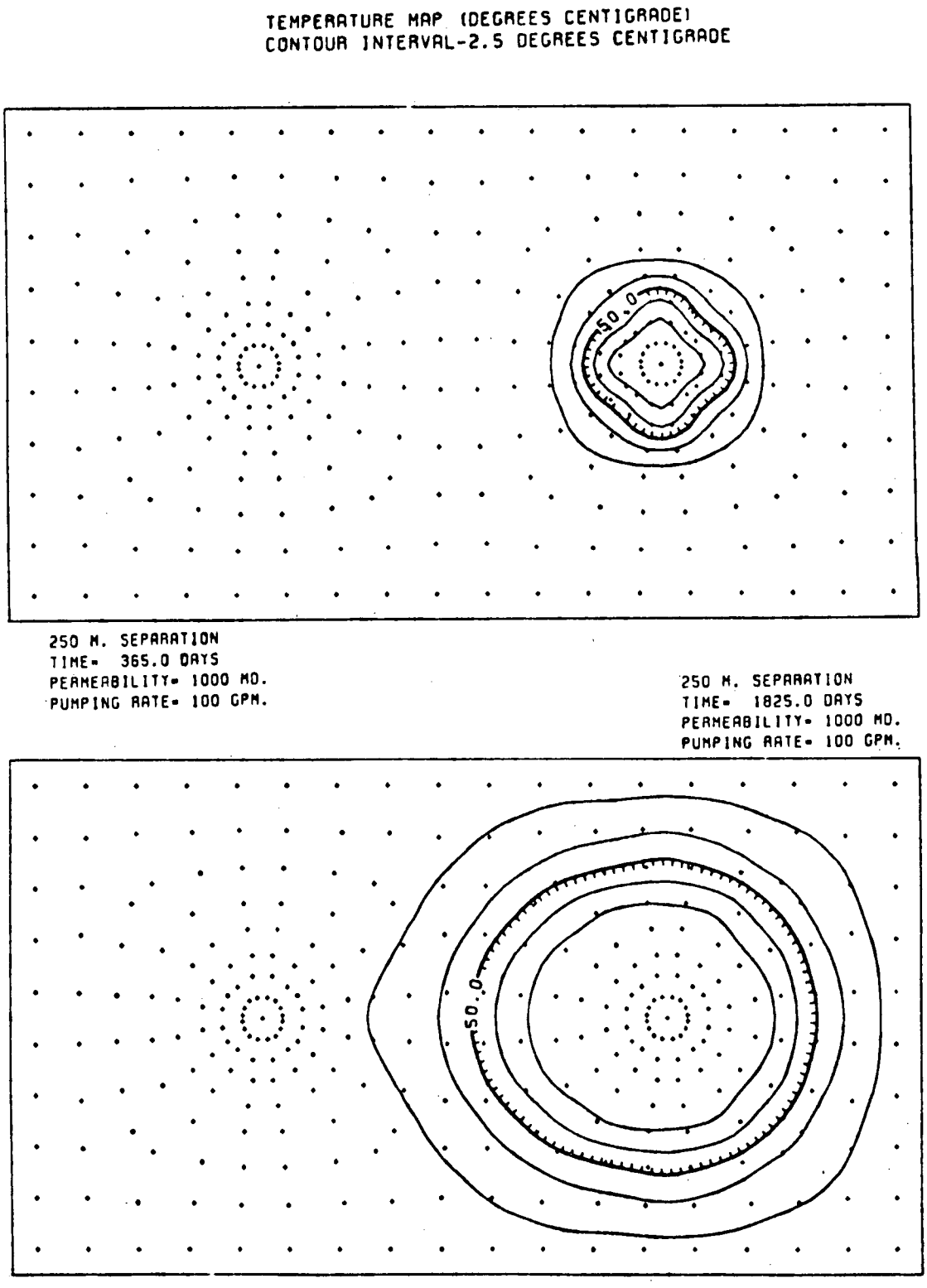

Figure 12b1: Temperature distribution map for a 250 m well spacing at 1 and 5 yrs, upper and lower plots respectively.

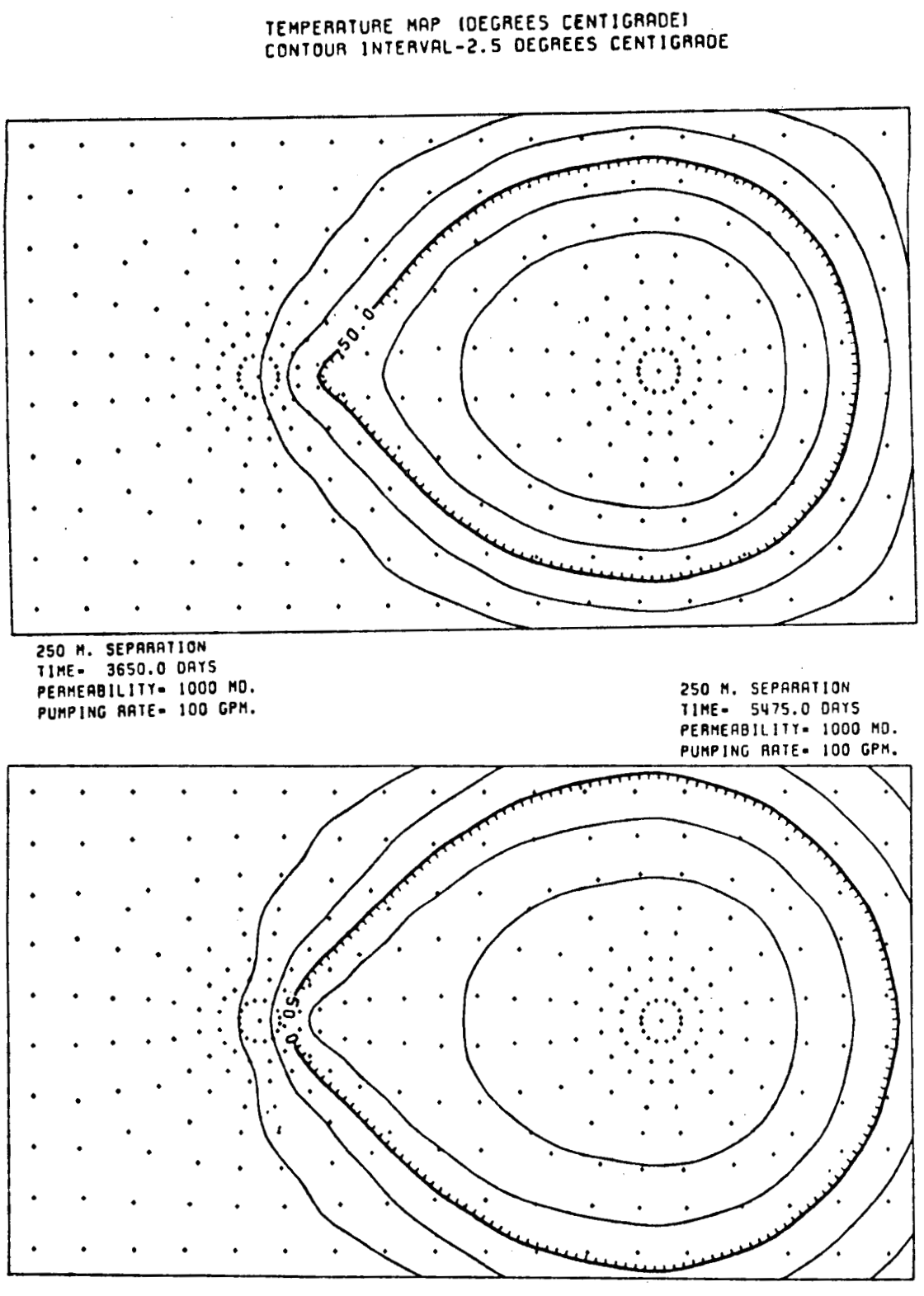

Figure 12b2: Temperature distribution map for a 250 m well spacing at 10 and 15 yrs, upper and lower plots respectively. Note breakthough occurs at 10 yrs.

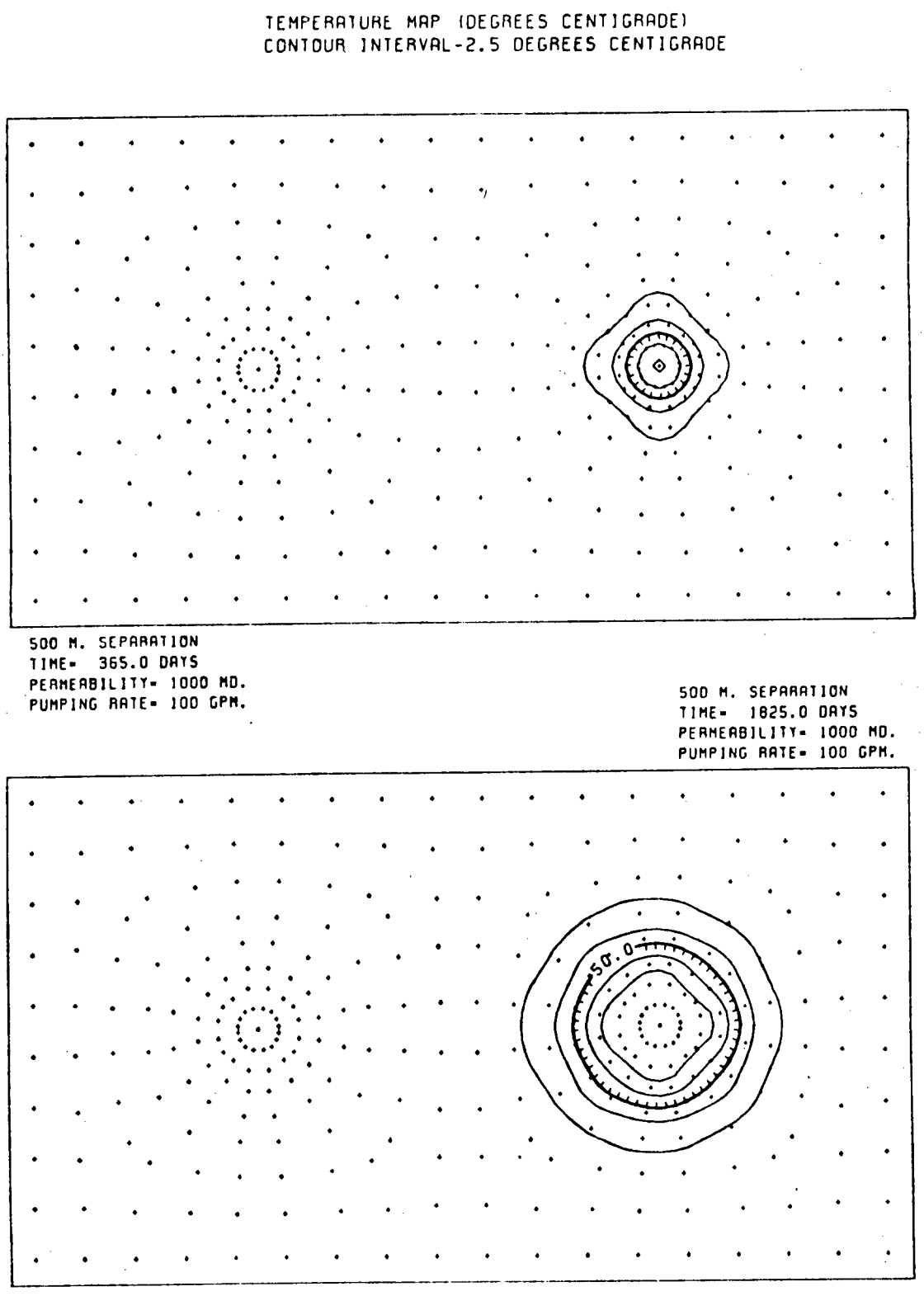

Figure 12c1: Temperature distribution map for a 500 m well spacing at 1 and 5 yrs, upper and lower plots respectively.

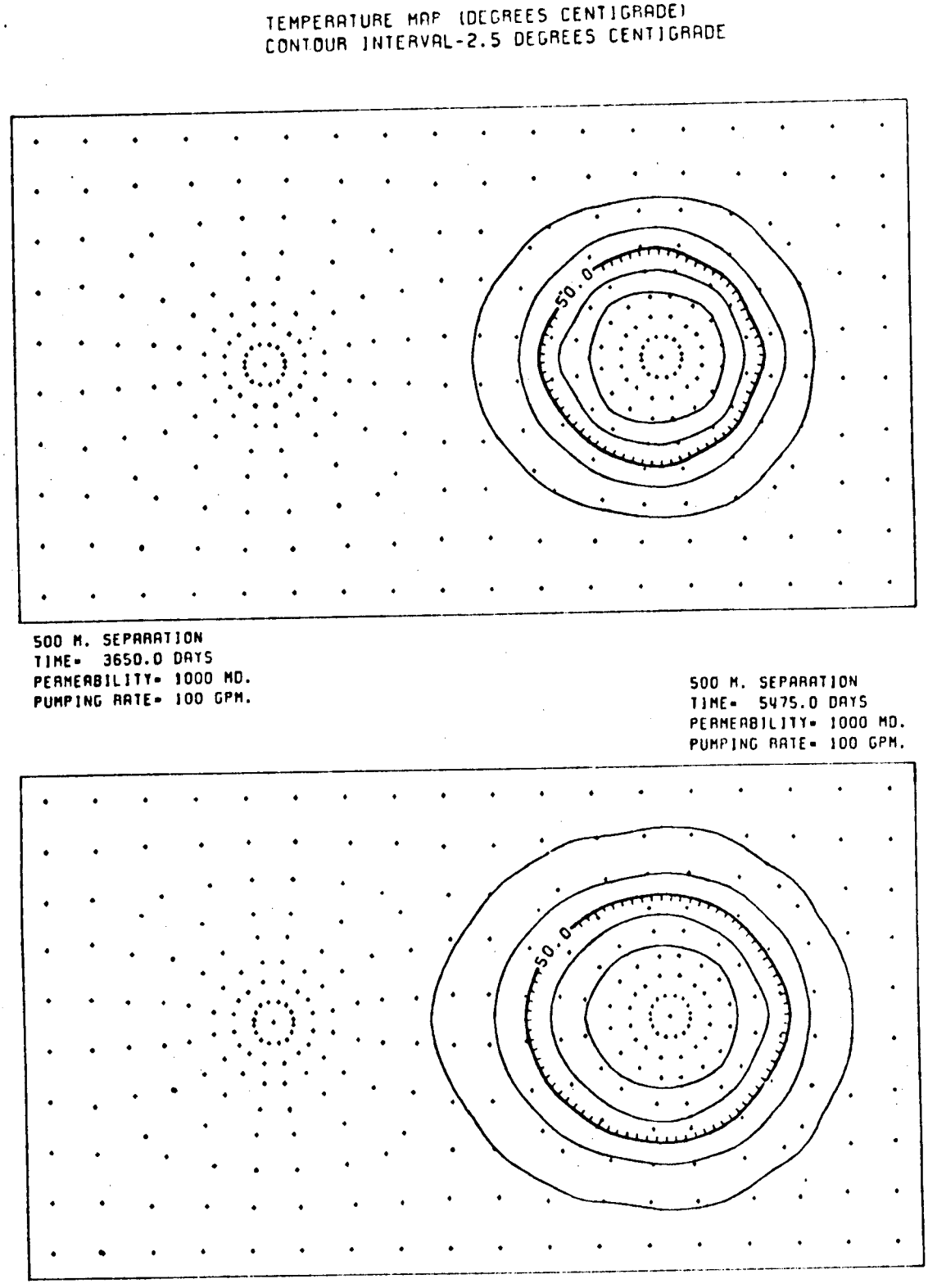

Figure 12c2: Temperature distribution map for a 500 m well spacing at 10 and 15 yrs, upper and lower plots respectively.

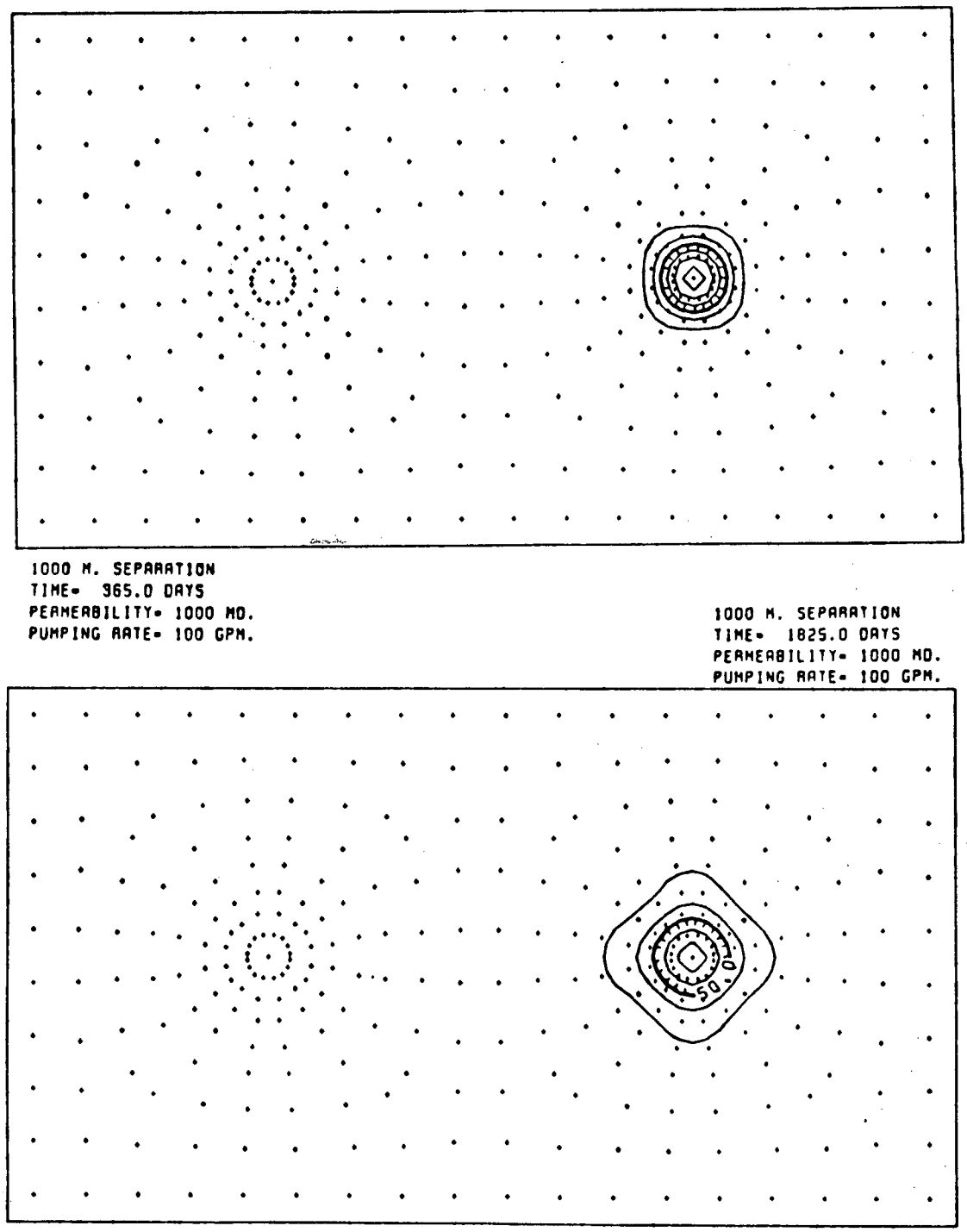

Figure 12d1: Temperature distribution map for a 1000 m well spacing at 1 and 5 yrs, upper and lower plots respectively.

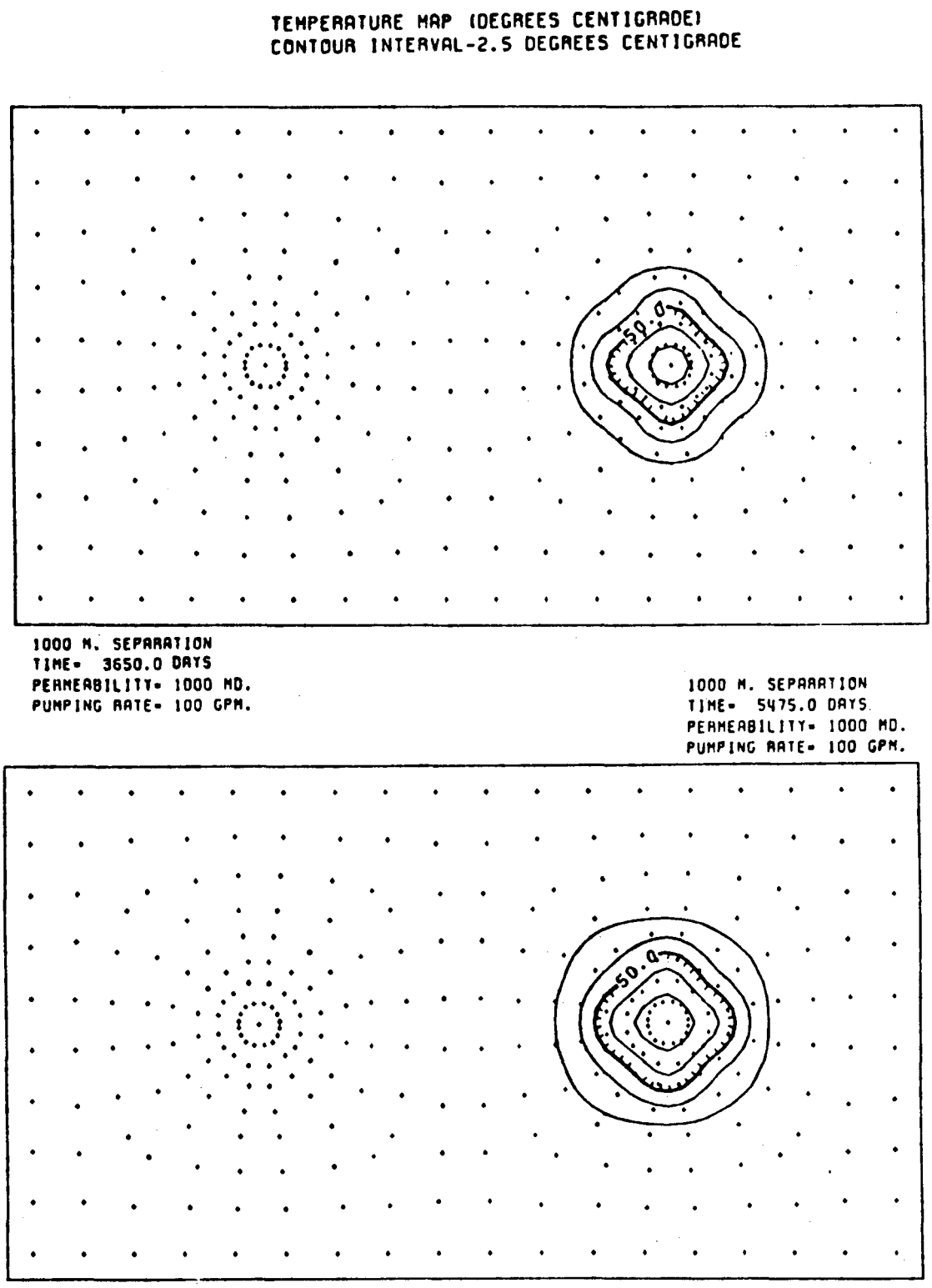

Figure 12d2: Temperature distribution map for a 1000 m well spacing at 10 and 15 yrs, upper and lower plots respectively.

Figure 13: Time sequence plan view contour plots of the temperature distribution as in Figure 10 except the permeability and pumping-injection rate are raised to 1000 md and 500 gpm, respectively.

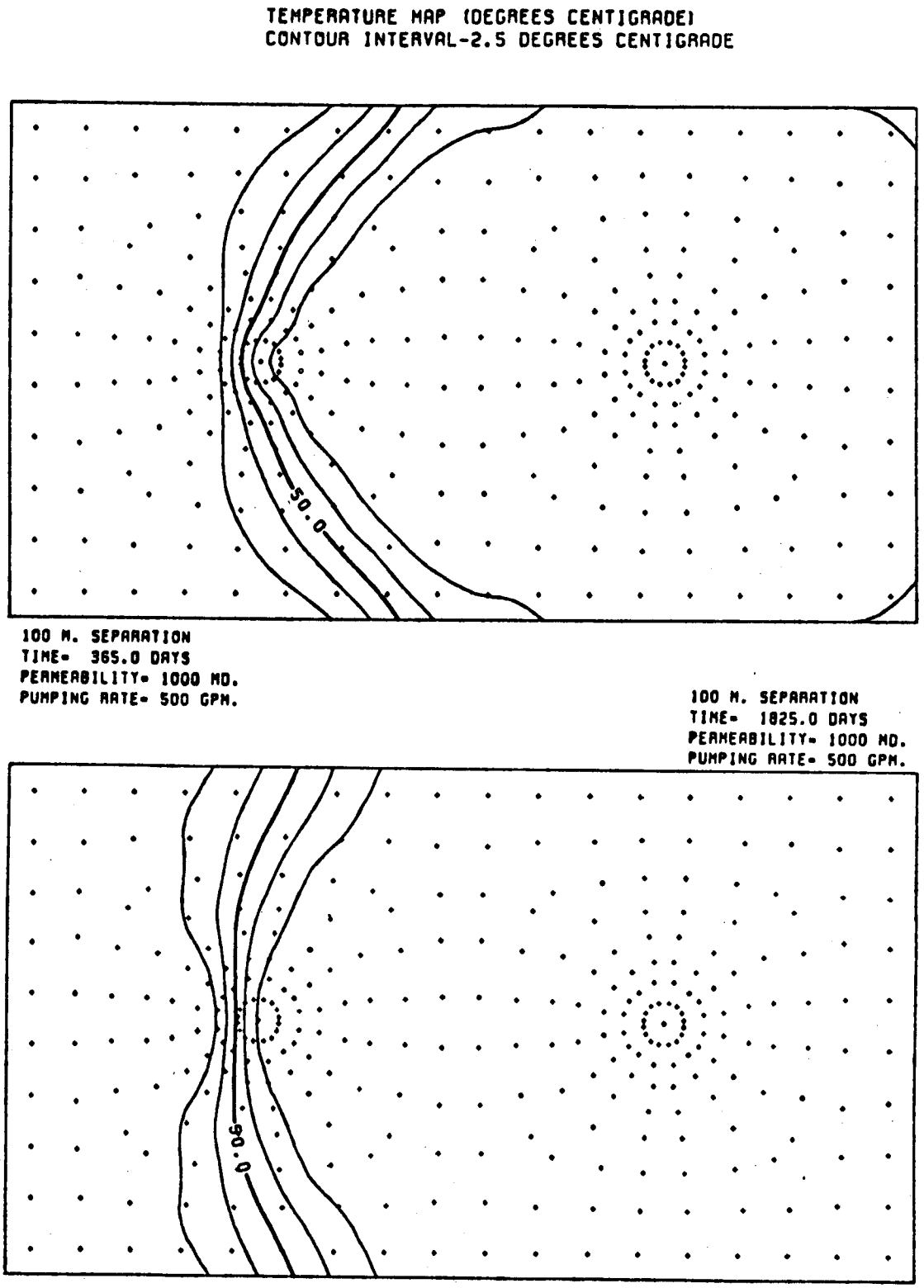

Figure 13a1: Temperature distribution map for a 100 m well spacing at 1 and 5 yrs, upper and lower plots respectively. Note breakthrough occurs prior to 1 yrs.

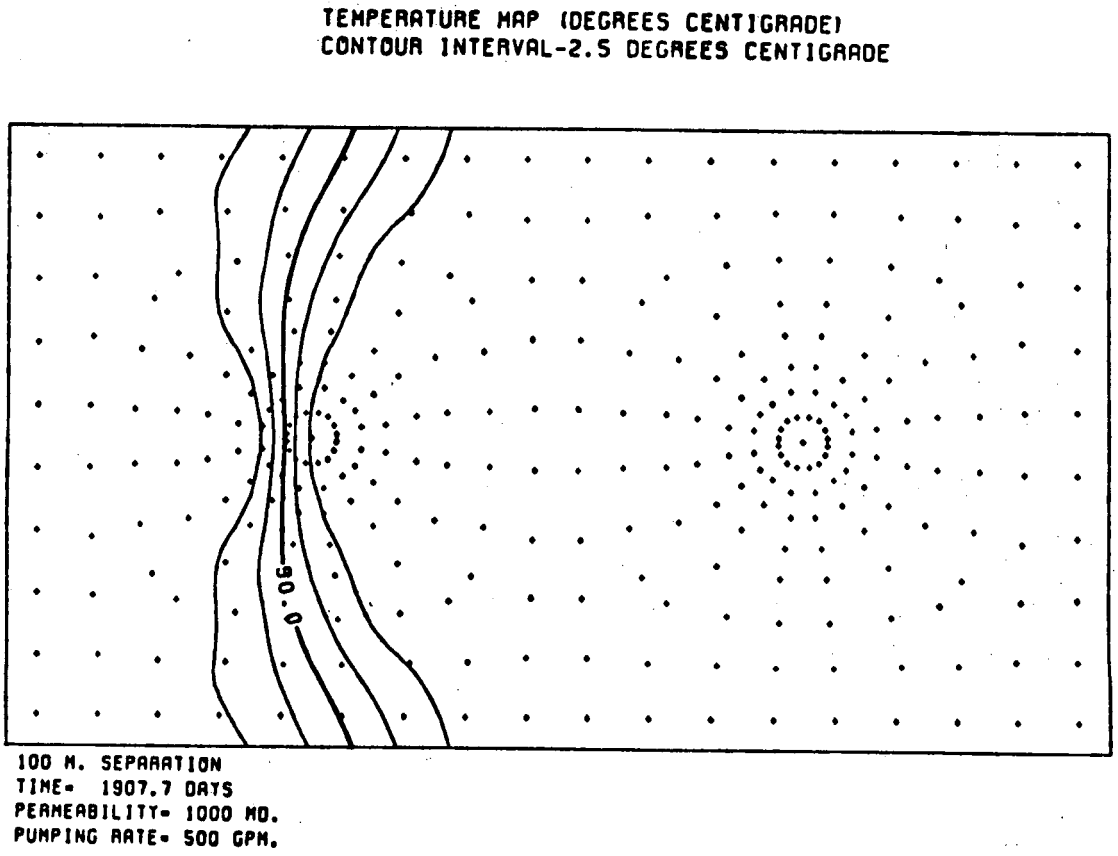

Figure 13a2: Temperature distribution map for a 100 m well spacing at 5.2 yrs (steady-state).

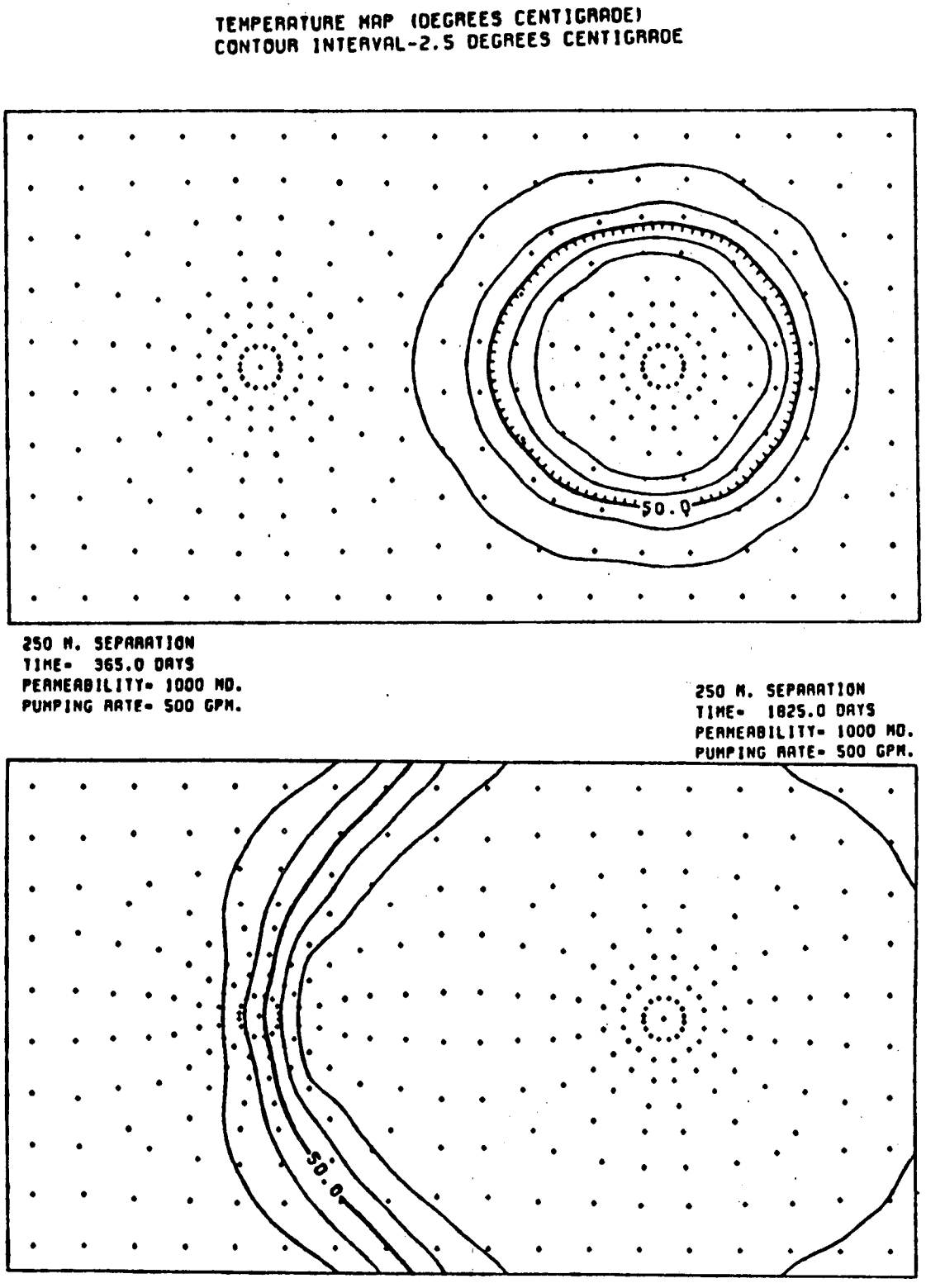

Figure 13b1: Temperature distribution map for a 250 m well spacing at 1 and 5 yrs, upper and lower plots respectively. Note breakthrough occurs prior to 5 yrs.

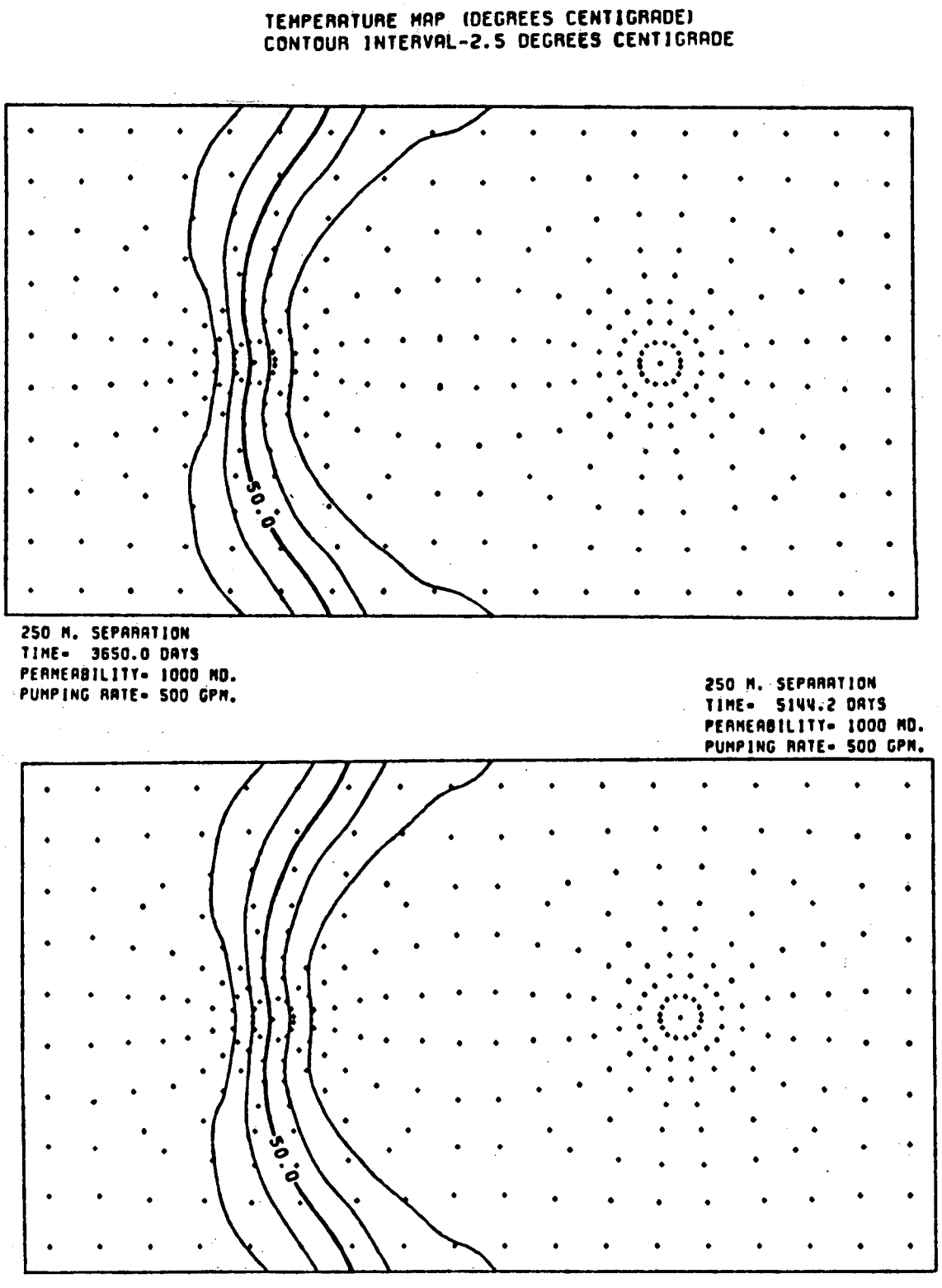

Figure 13b2: Temperature distribution map for a 250 m well spacing at 10 and 14.1 yrs (steady-state), upper and lower plots respectively.

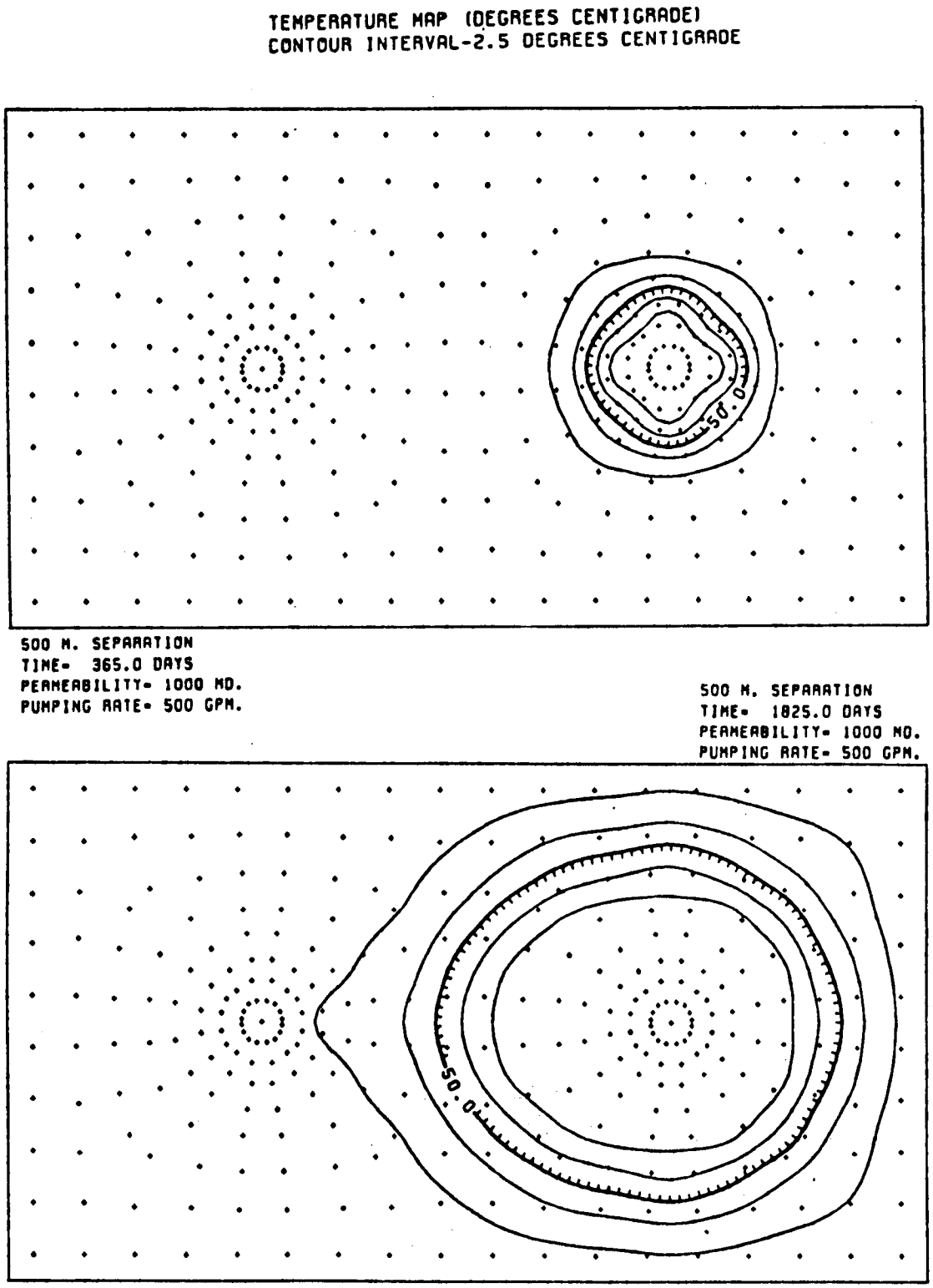

Figure 13c1: Temperature distribution map for a 500 m well spacing at 1 and 5 yrs, upper and lower plots respectively.

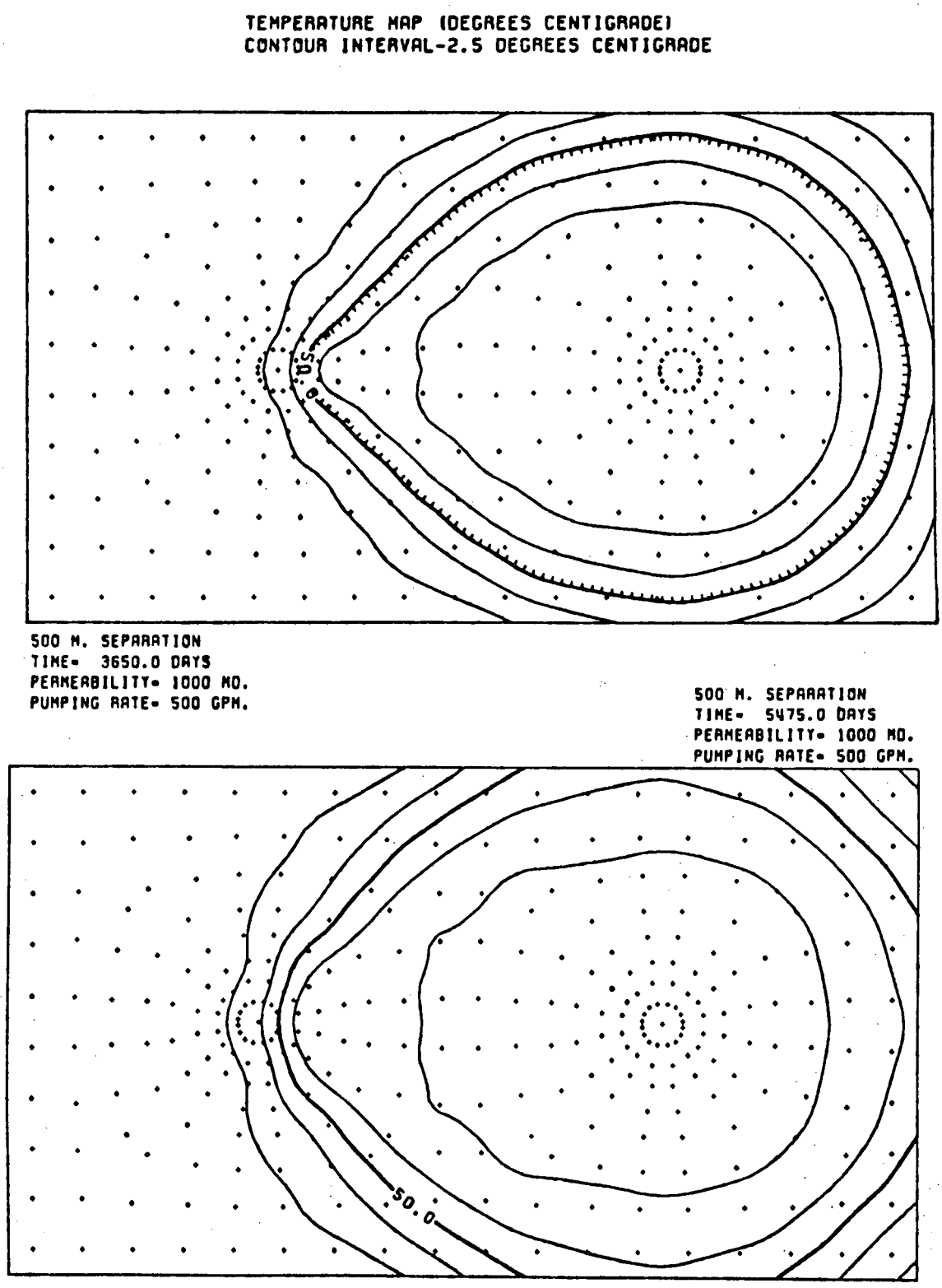

Figure 13c2: Temperature distribution map for a 500 m well spacing at 10 and 15 yrs, upper and lower plots respectively. Note breakthrough occurs prior to 15 yrs.

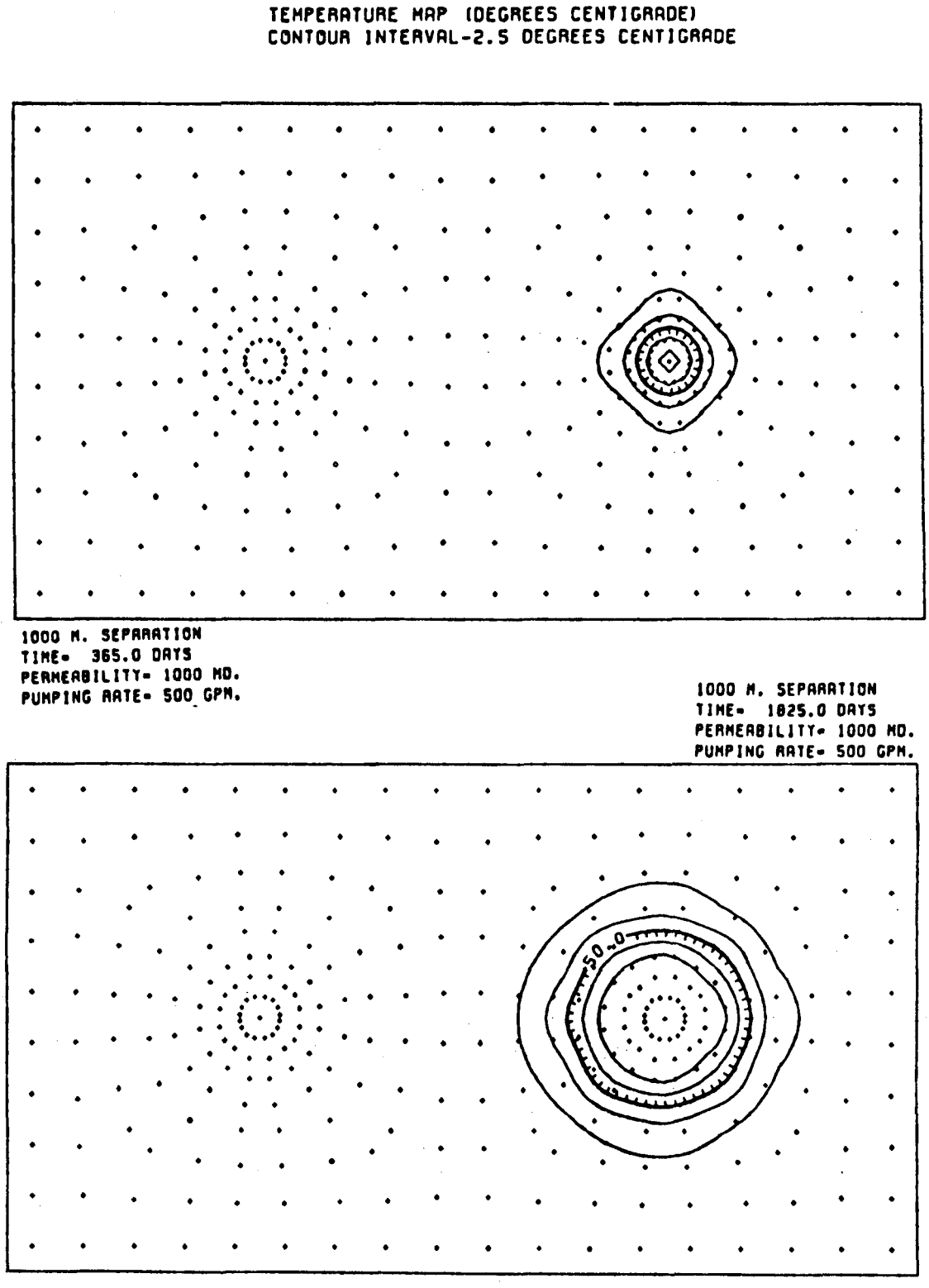

Figure 13d1: Temperature distribution map for a 1000 m well spacing at 1 and 5 yrs, upper and lower plots respectively.

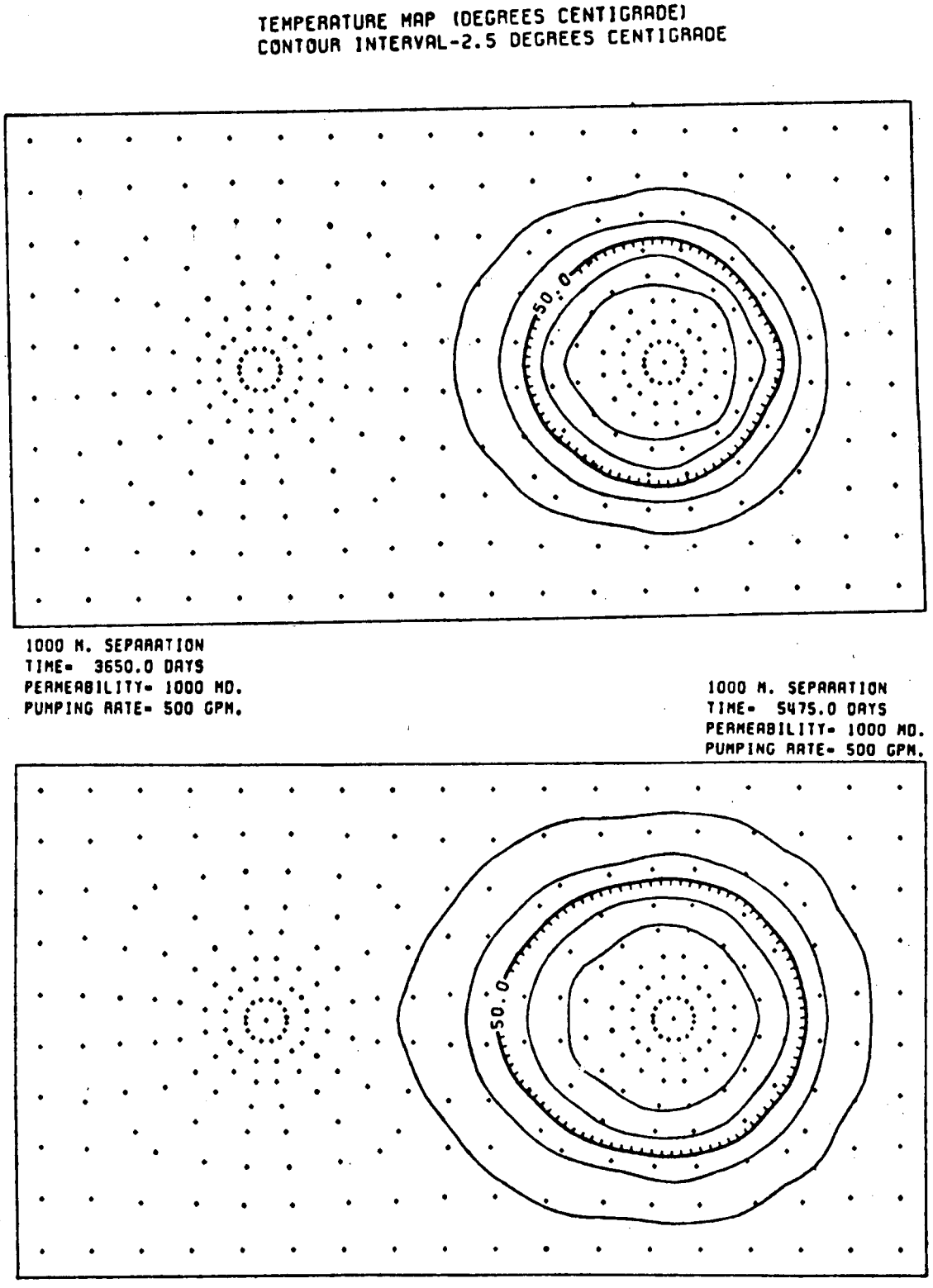

Figure 13d2: Temperature distribution map for a 1000 m well spacing at 10 and 15 yrs, upper and lower plots respectively.

occurs rapidly (less than 2 years) while in the 1000 meter separation breakthrough is altogether absent (see Figures 14-18).

Differences in the pumping-injection rate also affect the temperature distribution and the time of breakthrough within the system. As expected, a greater pumping-injection rate lessens the time it takes for breakthrough to occur. The result is a decrease in the temperature differential between the pumping and injection wells.

The response of the temperature field to different permeabilities is shown through a comparison of the various temperature plots (cf. Figures 10-13 and Figures 15-18). A lowering of the permeability by one order of magnitude results in only a small gain in the final output energy (see Table 4). The slight difference in the occurrence of the breakthrough time is damped out by the end of the simulation. This partial independence between the temperature field and the permeability is understood by analyzing heat transfer in conjuction with Darcy's Law. Heat is transferred by conduction and convection. Conduction is dependent on the physical properties of the materials which are held constant throughout the simulations. Convection is controlled by the fluid velocity field. Darcy's Law states that the velocity is proportional to both the permeability and the hydraulic gradient. Figure 5 reflects a decrease in the hydraulic gradient with an increase in the permeability; therefore, the change in the magnitude of the velocity is small. The combined effect of both conduction and convection produces a similar net heat transfer among systems in which all parameters except permeability are kept constant.

The placement of the pumping and injection well is reinforced by the results of the modelling. Although the pumping well is located in the coolest portion of the reservoir, warmer temperatures migrate quickly to the perforated zone of the production well. This phenomenon is displayed by the initial increase in the temperature at the production well (refer to Figures 15-18) and is due to recharge of warmer waters from the lower portions of the reservoir (refer to Figure 9).

Analysis of the Effect of Resting on the System

Besides a simple doubling of the life span, subjecting the system to alternating six-month periods of continuous pumping and resting produces only negligible changes in the overall temperatures at the injection and production wells. Figure 19 compares the temperatures at the injection well in a rested system to the temperature at the injection well in a continuously pumped system over a period of 5 years. The recovery of heat from terrestrial heat flow at the injection well over the six-month rest period is minimal.

Figure 20 compares temperatures at the production well in a rested system to temperatures in a continuously pumped system. Negligible amounts of heat are recovered from the matrix at the production well over the six-month resting periods. Ignoring periods of recovery in the rested system, comparison of the curves in Figure 14 show only a

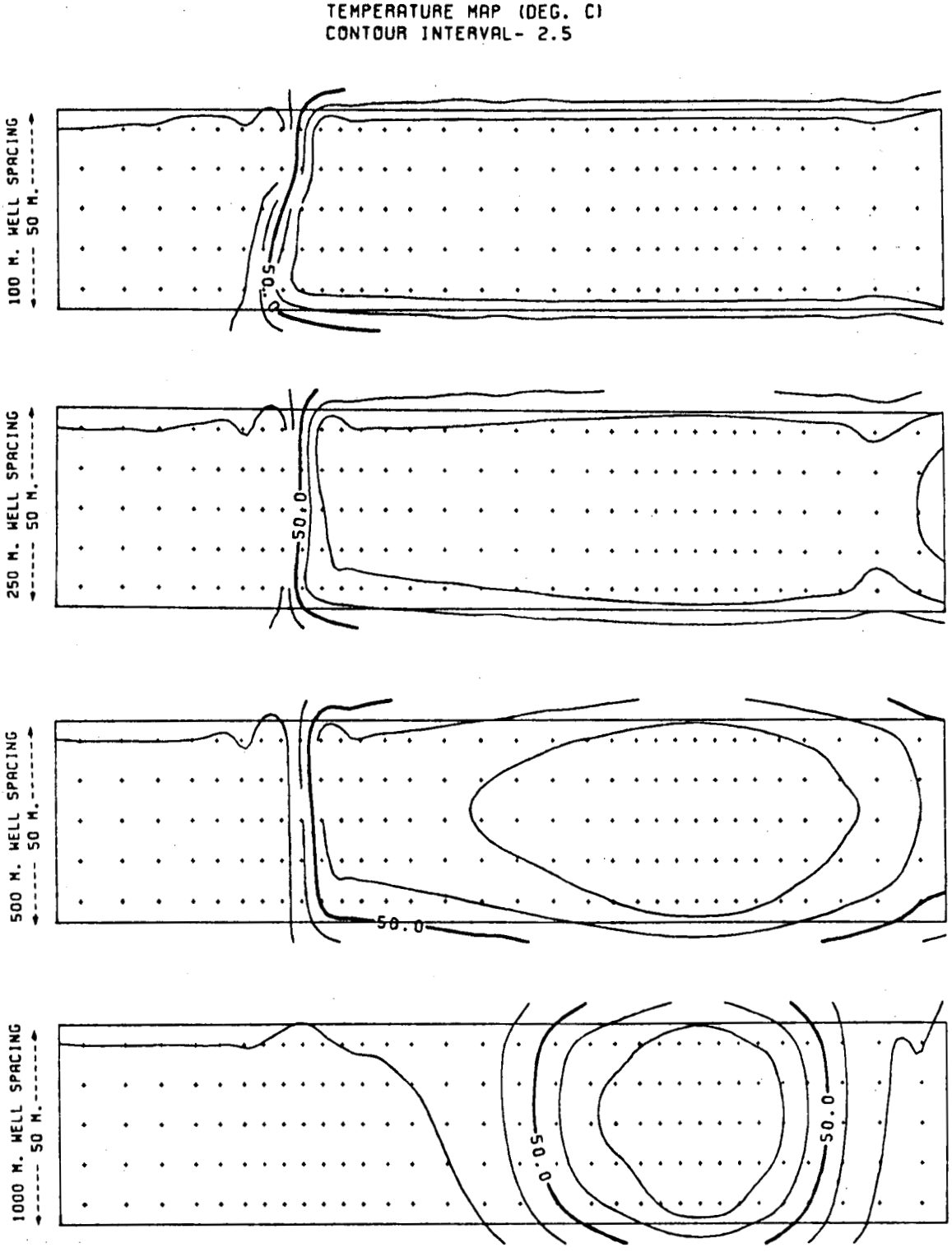

Figure 14: Cross-sectional view of the temperature distribution for various well spacings in a system with a permeability of 1000 md and a pumping-injection stress of 500 gpm. Crosses indicate location of nodal points.

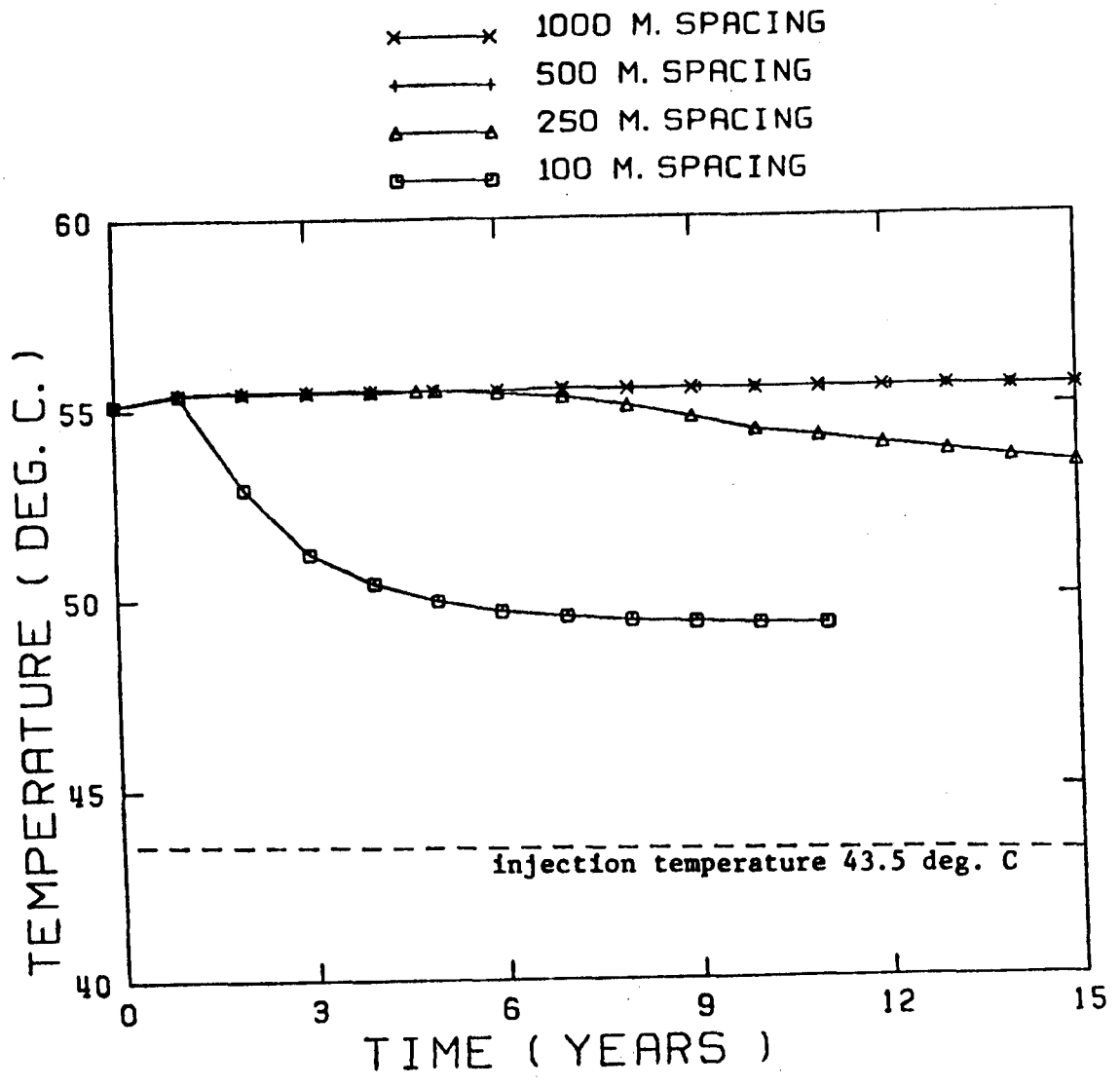

Figure 15: Plot of production temperature versus time for various well spacings in a system with a permeability of 100 md and a pumping-injection stress of 100 gpm. Production temperature is the average of the temperatures recorded at both pumping elements. Note the occurrence of breakthrough, the point in time when the temperature begins to decrease.

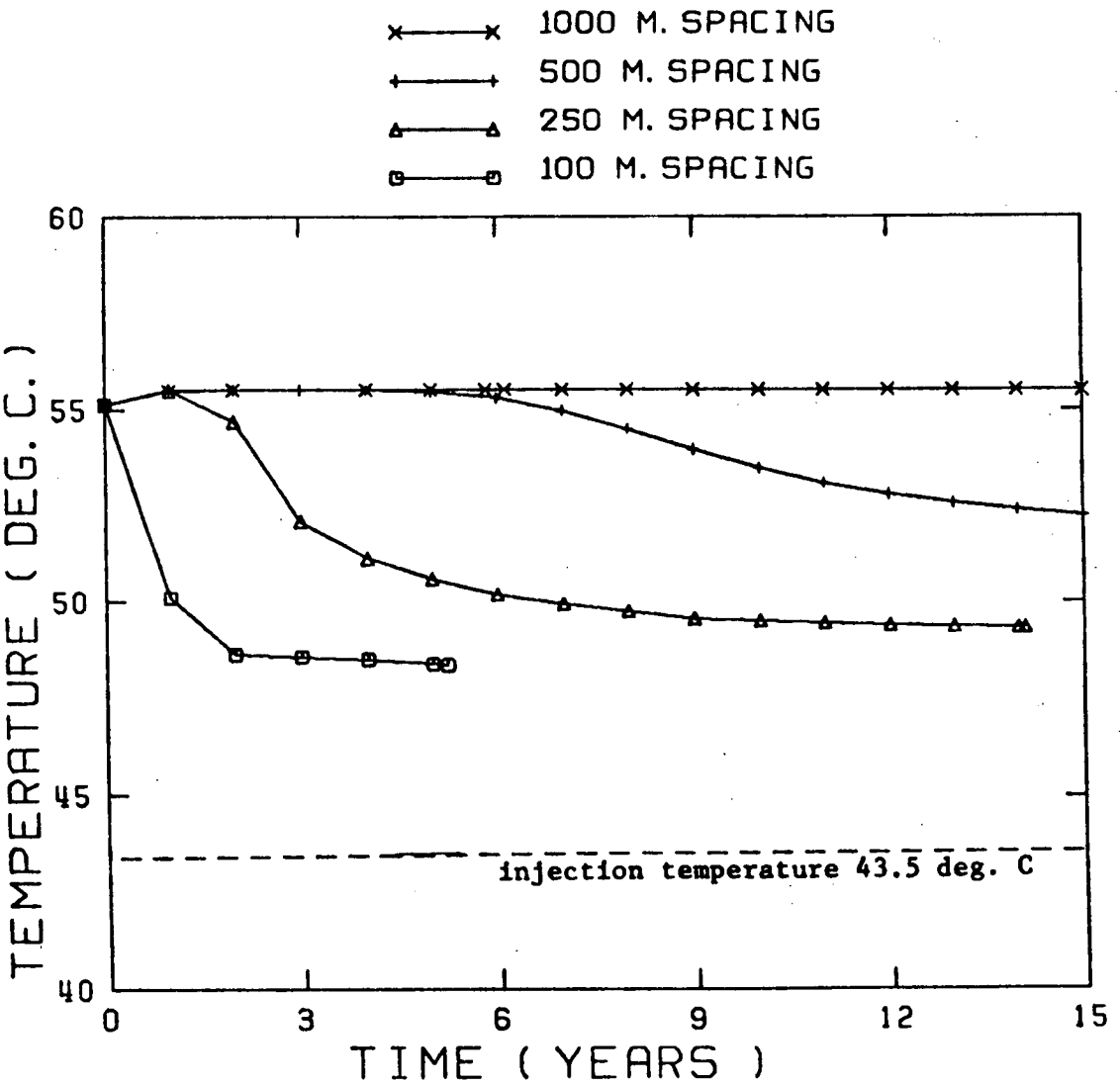

Figure 16: Production temerpature versus time plot as in Figure 12 except the pumping-injection rate is raised to 500 gpm.

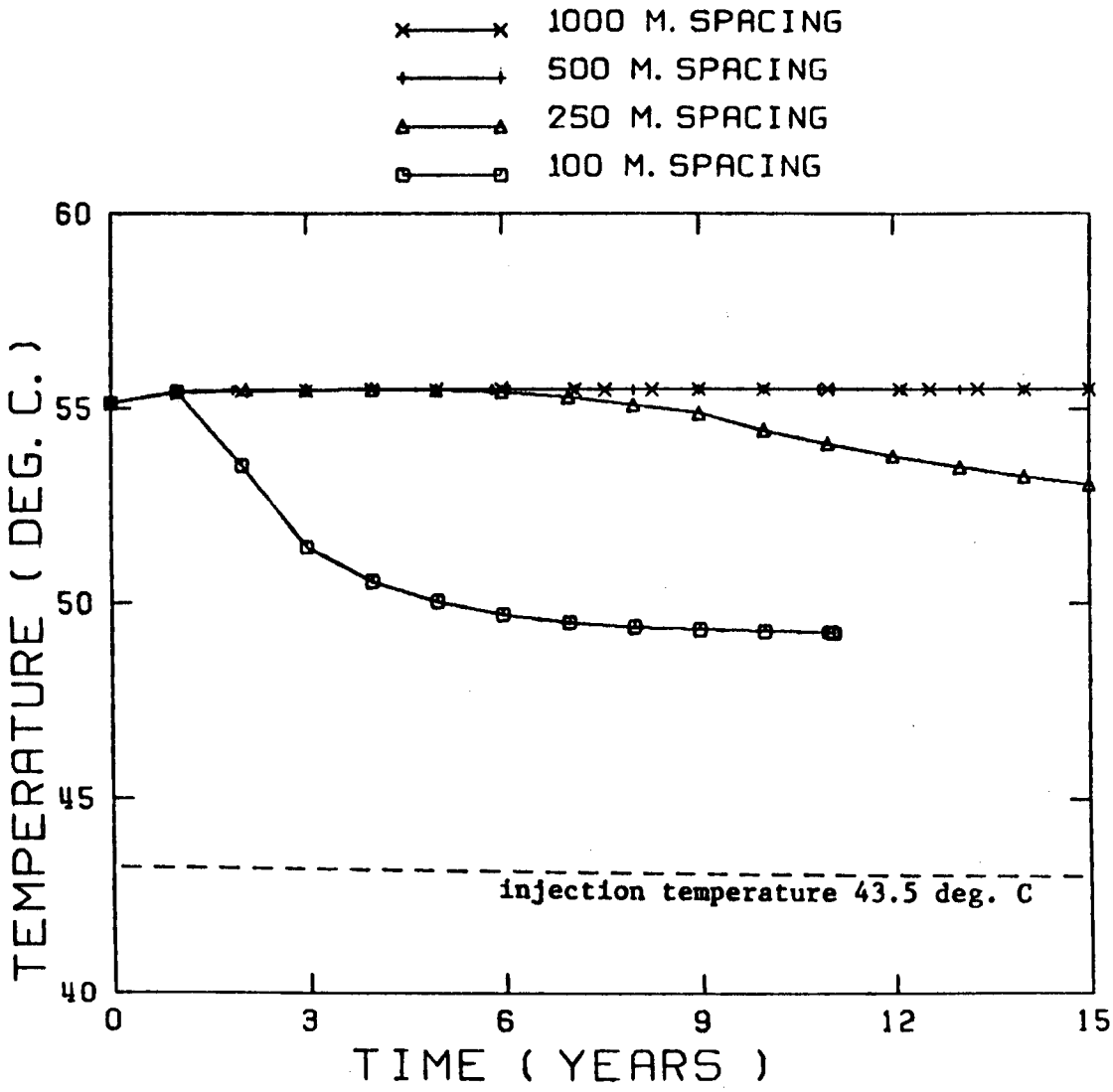

Figure 17: Production temperature versus time plot as in Figure 12 except the permeability raised to 1000 md.

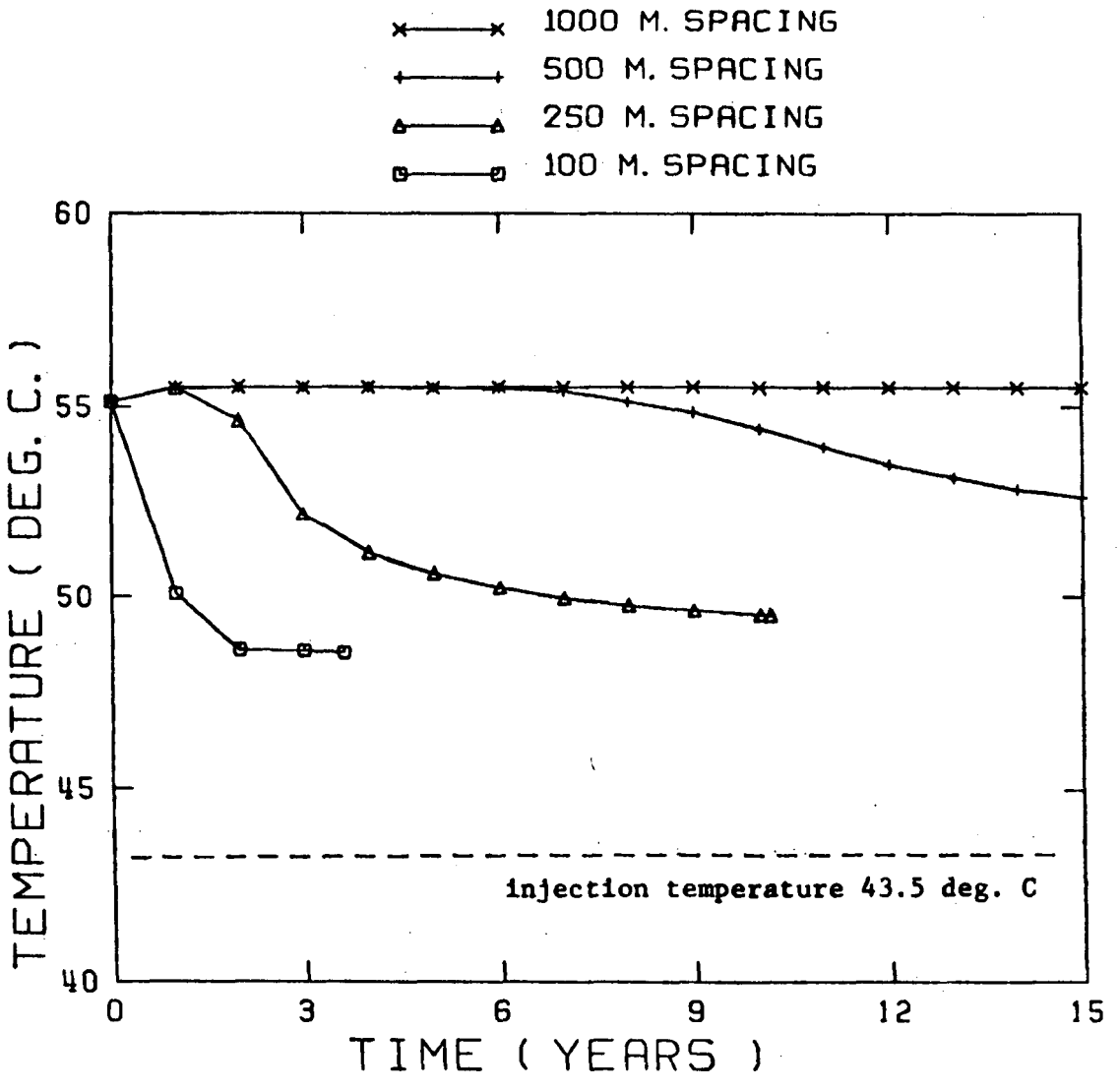

Figure 18: Production temperature versus time plot as in Figure 12 except system permeability and pumping-injection rate raised to 1000 md and 500 gpm, respectively.

Table 4 - Amount of energy extracted in Btu's per hour for the various well spacings in the simulated "typical" Atlantic Coastal Plain geothermal system.

k	100	250	500	1000 m spacings	q
1000 md	521640.	869097.	1087732.	1088640. Btu's/hr	100 gpm
100 md	522542.	903571.	1087732.	1088640.	100 gpm
1000 md	2204496	2644488.	3982608.	5438664.	500 gpm
100 md	2281608.	2726136.	4150440.	5443220.	500 gpm

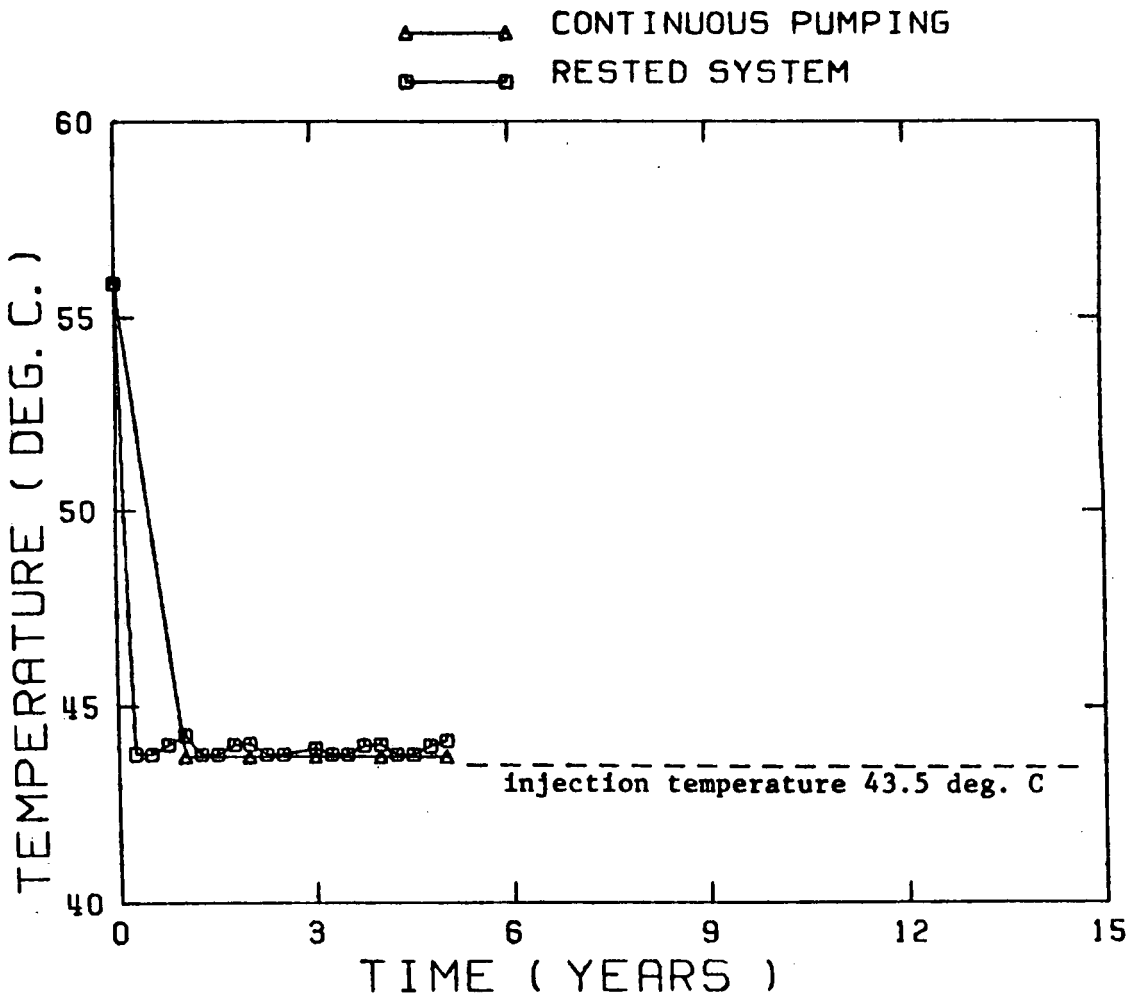

Figure 19: Plot comparing temperature at the injection well (average of the temperatures recorded at both injection elements) versus time in a continuously pumped and rested system with a well spacing of 100 meters.

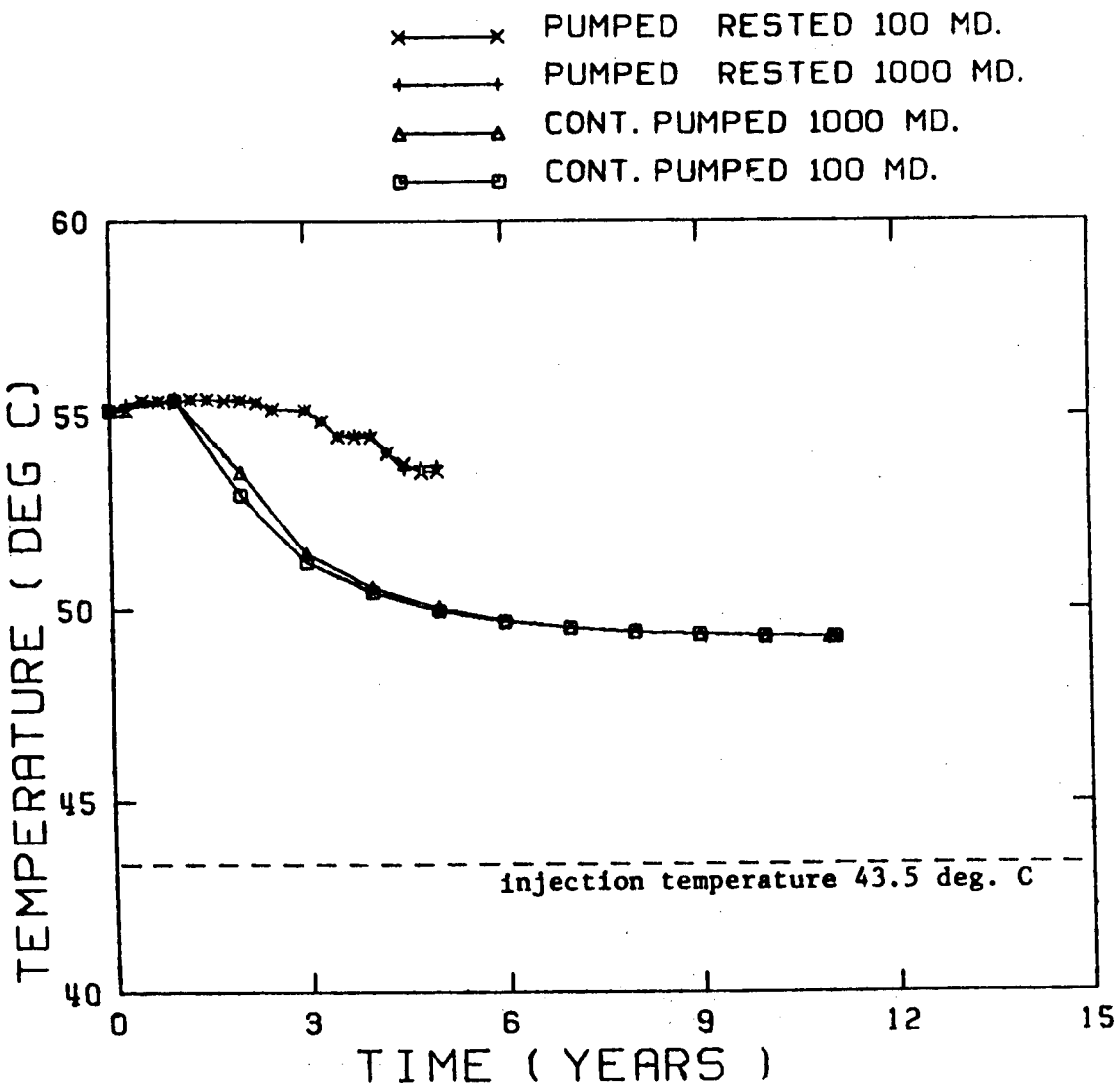

Figure 20: Plot of production temperature versus time in a continuously pumped and a rested system. Production temperature is the average of the temperatures recorded at both pumping elements. Curves compare permeabilities of 100 and 1000 md in a system with a 100 meter well spacing.

small gain of heat in the rested system. Varying the permeability, again has little effect on the system.

CONCLUSION

Information about piping, drilling, equipment and land acquisition costs are needed for a complete evaluation of the economics of the system, but the results of the modelling quantifies, without doubt, the existence of potential useful geothermal resources in the Atlantic Coastal Plain. Heat from a groundwater source (the aquifers of the Atlantic Coastal Plain) is adequate to run heat pumps at a high coefficient of performance (Neiss, 1979). A doublet system with direct injection back into the reservoir is shown by the simulations to be a feasible method of extracting heat in the low-temperature liquid-dominated geothermal systems of the Atlantic Coastal Plain. The 1000 meter spacing pumped at 500 gpm produces around 5.5 million Btu's per hour. Assuming a value of 70,000 Btu's per hour for energy expenditure to heat an average insulated home, the system would support over 75 households. If pumped for only six months a year, the thermal life-span of the system is shown to be at least 30 years.

The optimum geologic environment for the implementation of a groundwater geothermal system is one in which the highest temperatures are encountered at the shallowest depths. It is postulated that throughout the Atlantic Coastal Plain there exist areas where isotherms are warped upward over radiogenic heat-producing granites within the crystalline basement beneath the Coastal Plain sediments Costain et al., 1980). In the future shallow aquifers over these radiogenic heat sources may be located. In tapping these shallower geothermal reservoirs, drilling costs would be reduced and the use of lower energy output systems could be economically justified. Systems with close well spacings and/or low pumping-injection rates could then be implemented depending on the energy needs of the individual or community.

Modifications of the injection scheme intended to increase the thermal life-span of the system, for example, injection into an independent reservoir or injection into a zone separated by a low permeability lens should be carefully analyzed before being implemented. In the low permeability deeper reservoirs of the Atlantic Coastal Plain, the influence of the injection well is shown by this research to be necessary in order to maintain sufficient fluid pressures within the system. This influence of the injection well is required and must be taken into account in the design of a successful heat extraction system.

Reinjection of the thermally spent cooler water back into an independent or semi-independent reservoir may cause adverse chemical or physical reactions within that reservoir. In this case, extensive modelling of the total system should be performed. The program used in the modelling should not only allow for the solutions of the heat and mass flow equations but simultaneously solve for hydrodynamic dis-

persion and heat production due to the decomposition of reactants. The sensitivity of the reservoir water to the injected water and the resulting chemical reactions should be completely understood and incorporated into the program.

In-depth studies of each proposed Atlantic Coastal Plain geothermal system are strongly recommended before any actual application. These studies should include extensive hydrologic and geothermal (heat flow) data collection. The data should then be used in numerical models to analyze various system designs. Numerous computer programs are available in the literature (Bachmat et al., 1978 and Appel and Bredehoeft, 1976) to solve for the various physical phenomena taking place in a particular geothermal system. Program CCC is applicable and appropriate for the evaluation of the low-temperature geothermal systems of the Atlantic Coastal Plain. The collection of the data needed by the program and the actual running of the program require large amounts of time and money. This research can aid in future numerical simulations of Atlantic Coastal Plain geothermal systems. Where financial limitations inhibit adequate data collection or where computer funds are limited, the results of the present study will hopefully contribute to the development and design of reliable heat extraction systems in the Atlantic Coastal Plain.

NOMENCLATURE
(units given in parentheses)

A = area of the interface between nodel elements m and n (L^2)
c = fluid specific heat at a constant volume (L^2/t^2t)
d = horizontal distance between source and sink well (L)
D = distance between nodal elements m and n (L)
g = gravity (L/T^2)
h = total head or fluid potential (L)
H = aquifer thickness (L)
Hc = heat capacity of fluid (L^2/t^2T)
k = intrinsic permeability (L^2)
K = hydraulic conductivity (L/t)
Ke = thermal conductivity (ML/t^3T)
Mc = fluid mass capacity (M/L)
N = unit outer normal to a surface
q = fluid flow rate per unit volume (1/t)
q_e = energy injection rate per unit volume (M/Lt^3)
Q = element mass source or sink term (M/T)
Qp = pumping-injection rate (m^3/t)
Sp = specific storage or specific fluid capacity (1/L)
t = time (t)
T = temperature (T)
U = conductance of the interface between elements (L^2/T)
V = volume (L^3)
v_d = Darcy flow fluid flow velocity (L/t)
w_t = weight concentration of total dissolved solids, wt.%
β = thermal expansivity (1/T)
γ = second coefficient of thermal expansion ($1/T^2$)
λ = weight given to the backward-differencing operation in the implicit scheme
δT = difference between the mean temperature in the volume element and that on the surface interface (T)
μ = viscosity of the fluid (M/Lt)
ρ = density of the fluid (M/L^3)
$(\rho c)_M$ = volume of the solid-flux mixture (M/Lt^2T) interval

Subscripts

b = subscript used to denote boundary node
m = subscript used to denote nodal element in question
n = subscript used to denote adjacent nodal elements
m,n = subscript used to describe interface between elements m and n
o = subscript used to denote reference quantity
w = subscript to denote properties of pure water

Superscripts

0 = superscript to indicate previous value in the time interval

Abbreviations

CCC = computer program Conduction-Convection-Consolidation

gpm = gallon(s) per minute
IFDM = Integrated Finite Difference Method
m = meter(s)
md = millidarcy(s)
ppm = parts per million
Pa = pascal(s)

REFERENCES CITED

Appel, C. A. and J. D. Bredehoeft, 1976, Status of Groundwater Modeling in the U. S. Geological Survey, U. S. Geol. Surv. Circular 737.

Bachmat, Y., B. Andrews, D. Holtz, and S. Sebastian, 1978, Utilization of Numerical Groundwater Models for Water Resource Management, U. S. Environmental Protection Agency Report EPA-600/8-78-012.

Brown, D. L. and W. D. Silvey, 1972, Artificial Recharge to a Freshwater-Sensitive Brackish Water Sand Aquifer, Norfolk, Virginia, Geological Survey Professional Paper 939.

CalComp, 1973, GPCP, A general purpose contouring program, California Computer Products, Inc., 2411 W. LaPalma, Anaheim, CA 92801.

Cederstrom, D. J., 1945, Geology and Ground-water Resources of the Coastal Plain in Southeastern Virginia: Virginia Geol. Surv. Bull. 63, 384 p.

Claesson, J., B. Eftring, G. Hellstrom, and P. Olanders, 1978, Theoretical Analysis and Computer Simulation of Solid-Fluid Heat Storage Systems in the Ground. Extraction of Earth Heat, Department of Mathematical Physics and Building Science, Lund Institute of Technology, Lund, Sweden.

Cooley, R. L., 1971, A Finite Difference Method for Variably Saturated Porous Media: Application to a Single Pumping Well, Water Resources Research, Vol 7 No. 6.

Costain, J. K., L. Glover, III, and A. K. Sinha, 1980, Low Temperature Geothermal Reservoirs in the Eastern United States, EOS Transactions, American Geophysicl Union, Vol 61, No. 1.

Dashevsky, S and W. McClung, 1979, Summary of Temperature Logging at the Crisfield , Maryland Geothermal Test Hole , Evaluation and Targeting of Geothermal Energy Resources in the Southeastern United States, VPI&SU-78ET-27001-6. Available from National Technical Information Service, Springfield, VA.

Edwards, A. L., 1972, TRUMP: A Computer Program for Transient and Steady State Temperature Distributions in Multidimensional Systems, Lawrence Livermore Laboratory, Rpt. UCRL-14754, Rev. 3.

Gringerten, A. C. and J. P. Sauty, 1975, A Theoretical Study of Heat Extraction from Aquifers with Uniform Regional Flow, Jour. Geophys. Res., Vol 80 No. 35.

Hartsock, J. H., 1979, Analysis of Test Data from DOE Crisfield Airport Well No. 1, Geothermal Energy and the Eastern U.S., Minutes, APL/JHU, QM-79-261.

Ingenjorsbyran, A. AB, 1972, Heat Storage in Natural Ground Water Basins, Scandinavian Engineering Corporation.

Lippmann, M. J. and D. Mangold, 1977, Preparation of Input Data for Program CCC, Lawrence Berkeley Laboratory, Earth Science Division, Berkeley, CA.

Lippmann, M. J., C. F. Tsang, and P. A. Witherspoon, 1977, Analysis of Response of Geothermal Resources under Injection and Production Procedures, Paper Number 6537, Society of Petroleum Engr., Lawrence Berkeley Laboratory, Berkeley, CA.

MacNeal, R. H., 1953, An Asymmetric Finite Difference Network, Quart. Appl. Math., Vol 2.

Mercer, J. W., 1973, Finite Element Approach to the Modelling of Hydrothermal Systems, Ph. D. dissertation, University of Illinois.

Narasimhan, T. N., 1975, A unified Numerical Model for Saturated-Unsaturated Groundwater Flow, Ph. D. Thesis, Univ. of CA, Berkeley.

Narasimhan, T. N. and Witherspoon, P. A., 1976, An Integrated Finite-Difference Method for Analyzing Fluid Flow in a Porous Media, Water Resources Research, Vol. 12 No. 1.

Narasimhan, T. N. and Witherspoon, P. A., 1978, Numerical Model for Saturated - Unsaturated Flow in Deformable Porous Media. 2: The Algorithm, Water Resource Res., 14(2), 255-261.

Narasimhan, T. N., Witherspoon, P. A., and Edwards, A. L., 1978, Numerical Model for Saturated-Unsaturated Flow in A Deformable Porous Media 2. The Algorithm, Water Resources Research, Vol. 14, No. 2.

Neiss, R. C., 1979, Utilization of Geothermal Energy with an Emphasis on Heat Pumps, A Symposium of Geotherma Energy and it's Direct Uses in the Eastern United States, Geothermal Resources Council, Davis, CA.

O'Brien, G. G., M. A. Hyman, and S. Kaplin, 1951, A Study of the Numerical Solution of Partial Differential Equations, Jour. of Math. Phys., Vol 29.

Paddison, F. C., C. S. Leffel Jr., W. J. Toth, and R. S. P. Weissbrod, 1978, Direct Applications of Geothermal Energy in the Eastern United States and Estimates of Life Cycle Costs, Applied Physics Laboratory, Laurel, MD.

Richtmeyer, R. D. and K. W. Morton, 1967, Difference Methods for Initial Value Problems, Interscience, New York.

Sorey, M. L., 1975, Modeling of Liquid Geothermal Systems, Ph. D. Thesis, Univ. of CA, Berkeley.

Todd, D. K., 1959, Ground Water Hydrology, John Wiley, New York.

Tyson, H. N. and E. M. Weber, 1964, Groundwater Management for the Nations of the Future-Computer Simulation of Groundwater Basins, J. Hydraul. Div. ASCE, 90(HY4).

U. S. Geological Survey, 1967, The Status of Ground-Water Resources 1967 Nansemond County and Isle of Wight County Virginia, Geraghty & Miller, Consulting Ground-Water Geologists.

Wahl, F. E., 1977, Geothermal Energy Utilization, John Wiley, New York.

Westinghouse Electric Corporation, 1977, Templifier Heat Pump, Staunton, VA.

White, D. E. and D. L. Williams, 1975, Assessment of Geothermal Resources of the United States-1975, Introduction, Geological Survey Circular 726.

Heat Flow and Heat Generation in the Atlantic Coastal Plain

Lawrence D. Perry, Steven P. Higgins, and Margaret M. McKinney
Regional Geophysics Laboratory

Figure 1 shows the locations of holes drilled by VPI&SU in the Atlantic Coastal Plain for which new heat flow values have been calculated. Table 1 summarizes the heat flow data for all the holes and lists the heat generation values for those holes from which basement core was obtained.

The heat flow values of several of the holes (C24, C25, C26, C29, C55, and C59) have been reported previously in VPI&SU-5648-5. They are repeated here because a different procedure has been adopted for measuring the thermal conductivity. The core is currently being saturated in the laboratory, whereas previously it was measured in the same condition it came from the field.

The highest heat flow values (81 mW/m^2) found to date by the VPI&SU exploration program is in hole C25A at Portsmouth, VA; but the highest heat generation was found at hole ED1 in the Cuffytown Creek pluton of the Piedmont. The ED1 heat generation is approximately 25% higher than the heat generation at hole C25A. It is reasonable to expect the plutons beneath the Atlantic Coastal Plain to have the same distribution of U and Th as the plutons of the Piedmont; therefore, heat flow values even higher than C25A may be predicted.

Figure 2 is a plot of heat flow vs heat generation values from the basement of the Atlantic Coastal Plain. Hole C15 at Camp Lejuene, NC is the only hole that plots within a 90% confidence interval of the previously established Piedmont relationship.

It is tempting to try and establish the same type of linear relationship between heat flow and heat generation of the basement of the Atlantic Coastal Plain as has been shown to exist for plutons in the Piedmont. However, the data available to date do not define a significant relationship of their own. A least squares fit to the heat flow - heat generation data of Table 1 yields the line

$$q = 50 + 7.0A$$

with a regression coefficient of 0.64. While this is not as statistically significant as the Piedmont relationship it does indicate an interesting trend which should be explored with more holes penetrating the basement.

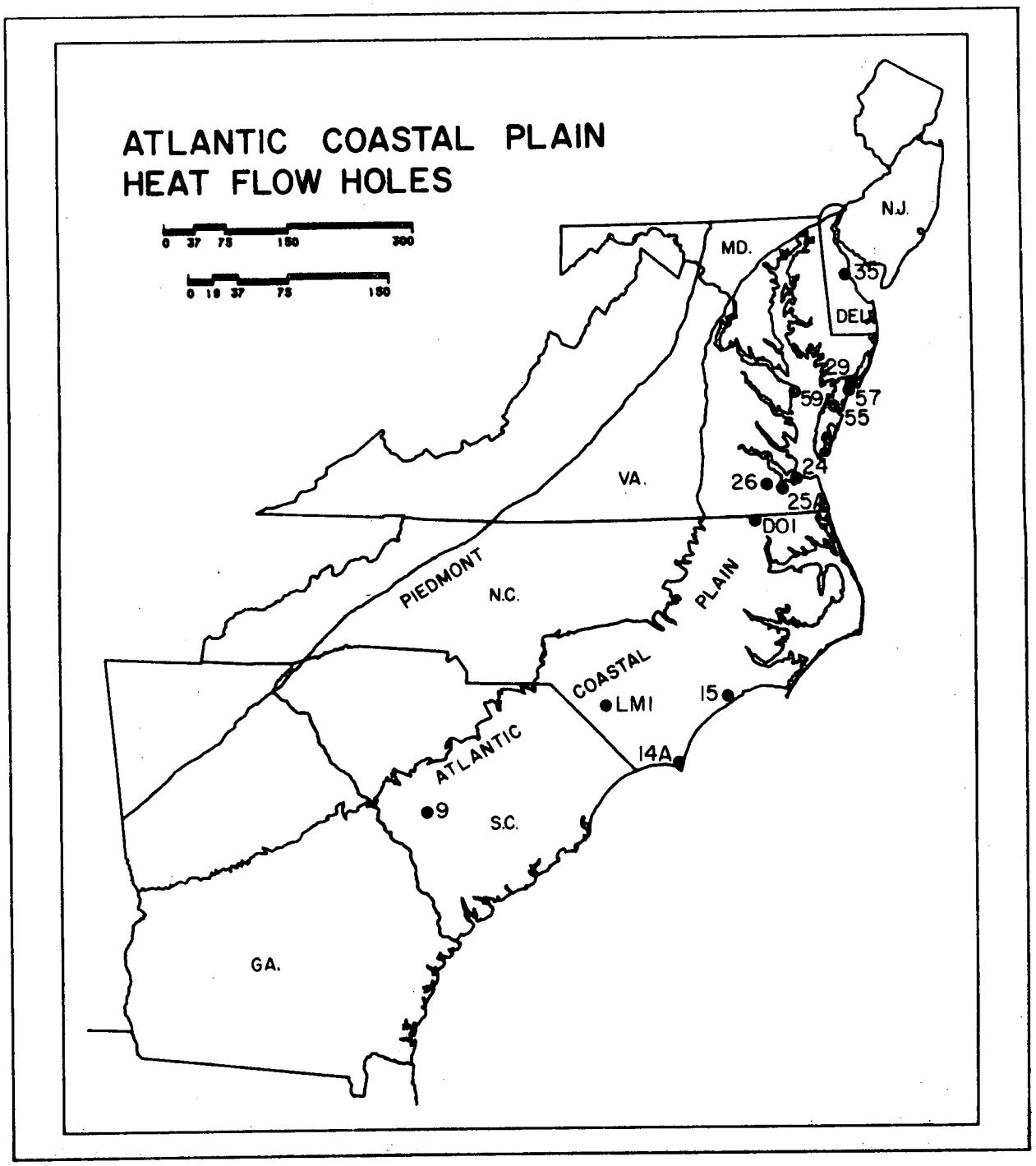

Figure 1: Heat flow holes on the Atlantic Coastal Plain

SUMMARY of HEAT FLOW and HEAT PRODUCTION DATA

LOCATION HOLE	LATITUDE (NORTH)	LONGITUDE (WEST)	DEPTH INTERVAL, (m)	GRADIENT, C/Km	THERMAL CONDUCTIVITY, W/m-°C	HEAT FLOW, q, mW/m^2	HEAT PRODUCTION, A, W/m^3
SALLEY, NC							
C9(SL1)	33°26'18"	81°16'54"	292.5-346.9	21.32+/-0.03(1.000 108)1	3.29+/- 0.17(34)2	70.1+/- 3.6B	2.7+/-0.3(5)2
SOUTHPORT, NC							
C14A	33°58'00"	77°58'12"	200.8-207.4	27.74+/-0.42(0.997 14)	1.91+/- 0.44(19)	53.0+/-12.3S	
C14A			358.5-373.3	27.27+/-0.29(0.997 30)	2.01+/- 0.42(59)	54.8+/-11.4S	
C14A			478.2-545.4	18.62+/-0.02(1.000 133)	2.89+/- 0.37(18)	53.7+/- 6.8B	
					BEST VALUE FOR C14A	53.8+/- 0.9	0.7+/-0.2(10)
JACKSONVILLE (CAMP LEJEUNE), NC							
C15	34°39'00"	77°19'00"	558.5-594.6	18.80+/-0.03(1.000 72)	2.73+/- 0.12(10)	51.4+/- 2.3	2.0+/-0.7(6)
NORFOLK, VA							
C24	36°57'24"	76°16'12"	161.3-173.0	46.56+/-1.47(0.979 24)	1.40+/- 0.23(72)	65.3+/-10.7	
CHESAPEAKE, VA							
C25A	36°54'06"	76°28'50"	294.8-307.6	34.30+/-0.22(0.999 26)	2.43+/- 0.30(48)	83.5+/-10.4S	
C25A			555.4-612.4	22.74+/-0.02(1.000 113)	3.48+/- 0.15(27)	79.1+/- 3.4B	
					BEST VALUE FOR C25A	81.3+/-3.1	4.2+/-0.2(6)
ISLE OF WIGHT, VA							
C26	36°54'31"	76°42'08"	287.1-332.4	21.77+/-0.20(0.999 10)	2.29+/- 0.18(11)	49.9+/- 4.0B	
WALLOPS ISLAND, VA							
C29	37°56'36"	75°27'16"	177.5-187.2	43.38+/-0.69(0.995 20)	1.82+/- 0.40(31)	78.8+/-17.2S	
DOVER AFB, DEL							
C35	39°06'42"	75°27'41"	235.6-242.7	48.31+/-0.72(0.997 15)	1.28+/- 0.17(60)	62.0+/- 8.5S	
TASLEY, VA							
C55	37°42'32"	75°42'51"	164.9-174.6	31.70+/-0.36(0.998 20)	2.05+/- 0.23(81)	65.0+/- 7.4S	
ATLANTIC, VA							
C57	37°53'14"	75°30'02"	174.0-186.2	42.47+/-0.37(0.998 25)	1.63+/- 0.34(110)	69.1+/-14.6S	
SMITH POINT, VA							
C59	37°53'12"	76°15'05"	143.6-154.3	52.42+/-0.80(0.995 22)	1.24+/- 0.09(77)	64.9+/- 5.0S	
DORT, NC							
DO1	36°31'43"	76°52'32"	326.8-346.1	23.53+/-0.04(1.000 39)	2.77+/- 0.14(16)	65.3+/- 3.3B	1.6+/-0.1(4)
LUMBERTON, NC							
LM1	34°34'12"	78°56'18"	250.8-272.7	21.13+/-0.03(1.000 44)	3.27+/- 0.18(5)	69.2+/- 3.8B	
LM1			292.5-300.7	22.61+/-0.10(1.000 17)	2.77+/- 0.13(3)	62.5+/- 3.0B	
LM1			306.8-328.7	19.92+/-0.03(1.000 44)	2.94+/- 0.33(4)	58.6+/- 6.6B	
					BEST VALUE FOR LM1	63.4+/- 5.4	1.1+/-0.1(3)
COLONEL'S ISLAND, GA							
CI1	31°08'12"	81°32'34"	479.4-492.6	18.46+/-0.12(0.999 27)	2.06+/- 0.44(2)	38.0+/- 8.1	
CI1			549.6-560.3	21.07+/-0.15(0.999 22)	1.85+/- 0.12(2)	38.9+/- 2.5	
					BEST VALUE FOR CI1	38.5+/- 0.6	

1... values in parentheses are the coefficient of linear regression and the number of data pairs in the interval
2... value in parentheses is the number of thermal conductivity values used to compute the mean
B... indicates a heatflow value from the basement of the Atlantic Coastal Plain
S... indicates a heatflow value from the sediments of the Atlantic Coastal Plain

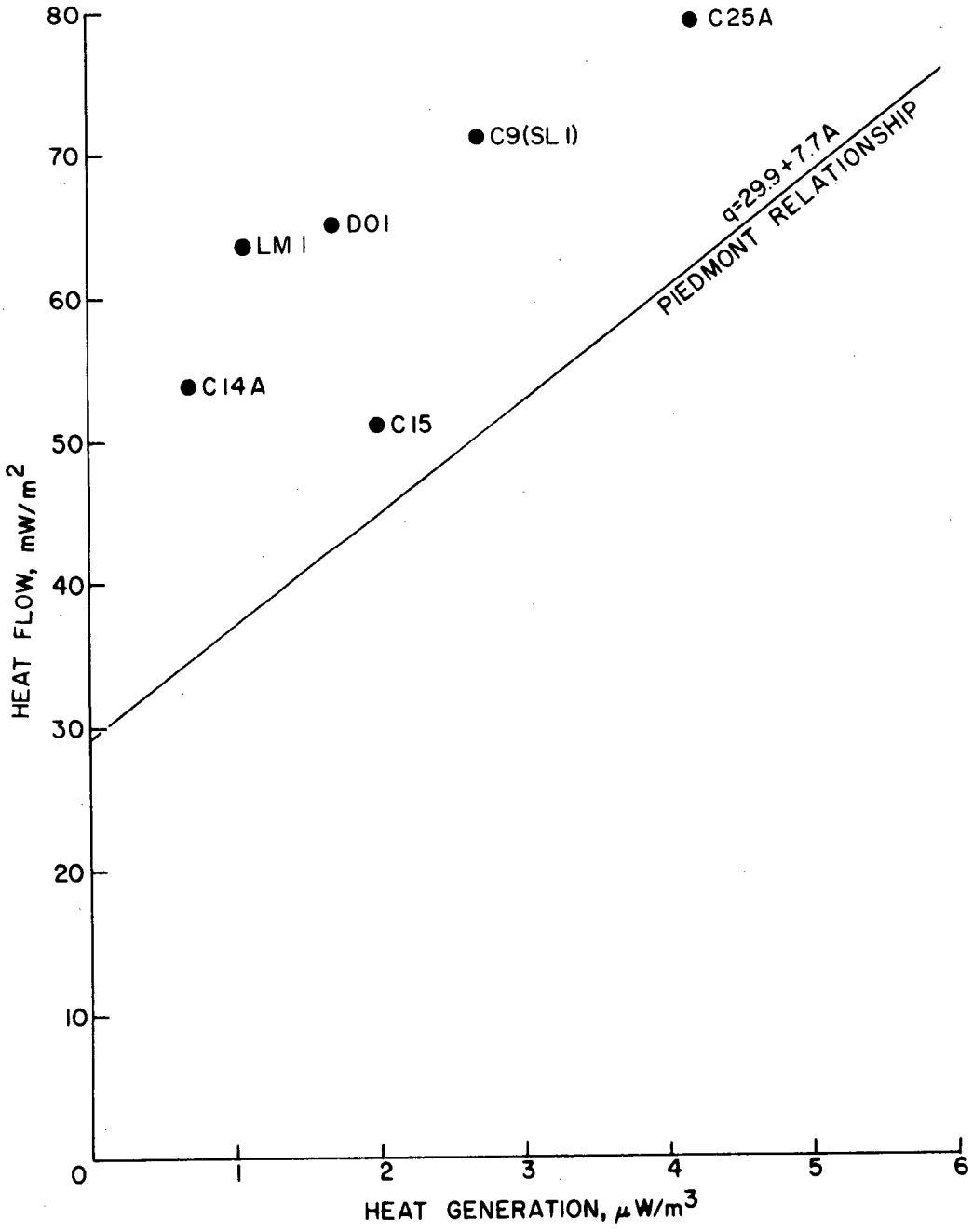

Figure 2: Heat flow versus heat generation in the Atlantic Coastal Plain.

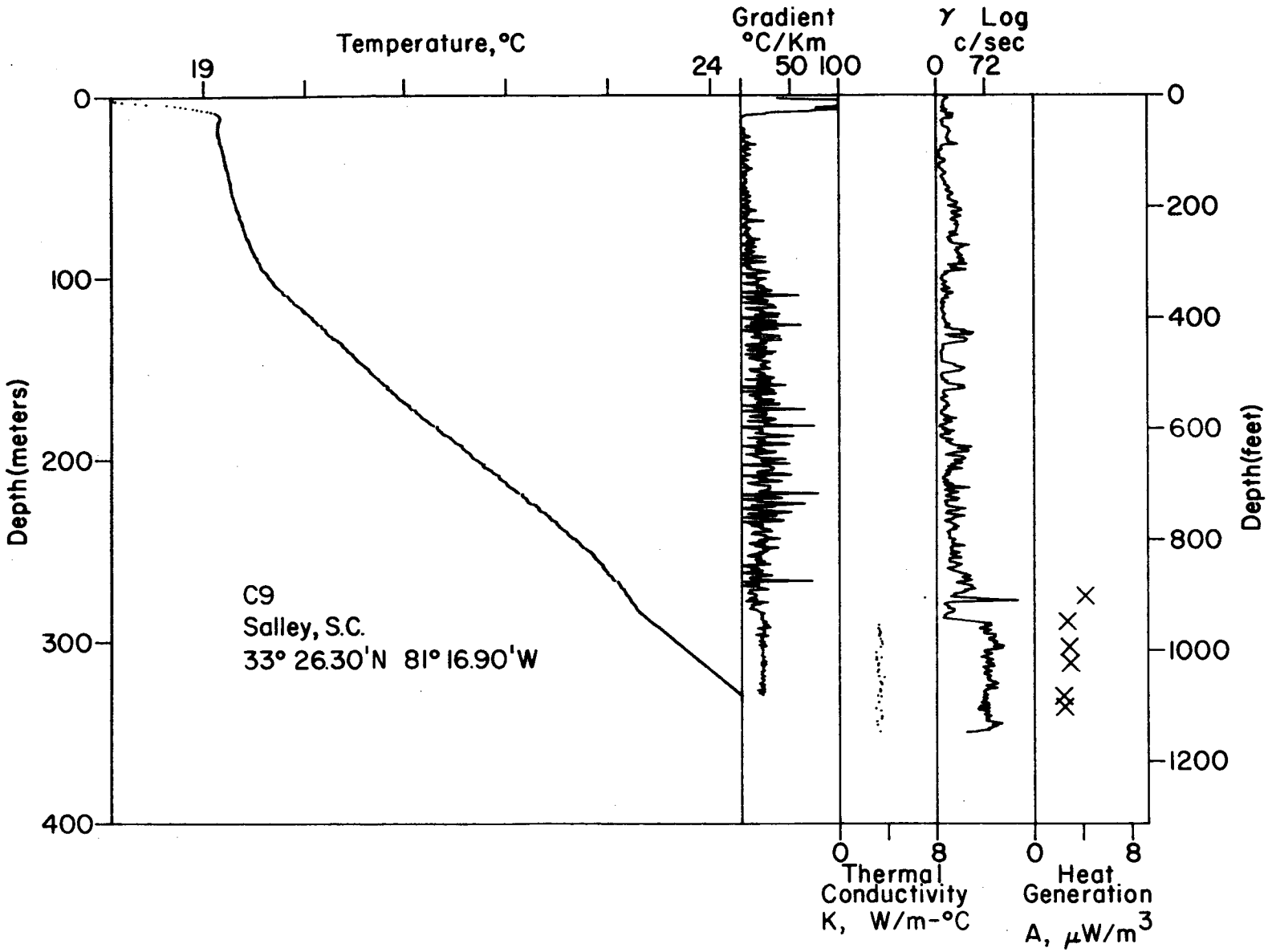
Temperature, °C
19
24
Gradient
°C/Km
50 100
γ Log
c/sec
0 72
0
100
200
300
400
Depth(meters)
0
200
400
600
800
1000
1200
Depth(feet)
C9
Salley, S.C.
33° 26.30'N 81° 16.90'W
0
8
Thermal
Conductivity
K, W/m-°C
0
8
Heat
Generation
A, μW/m3

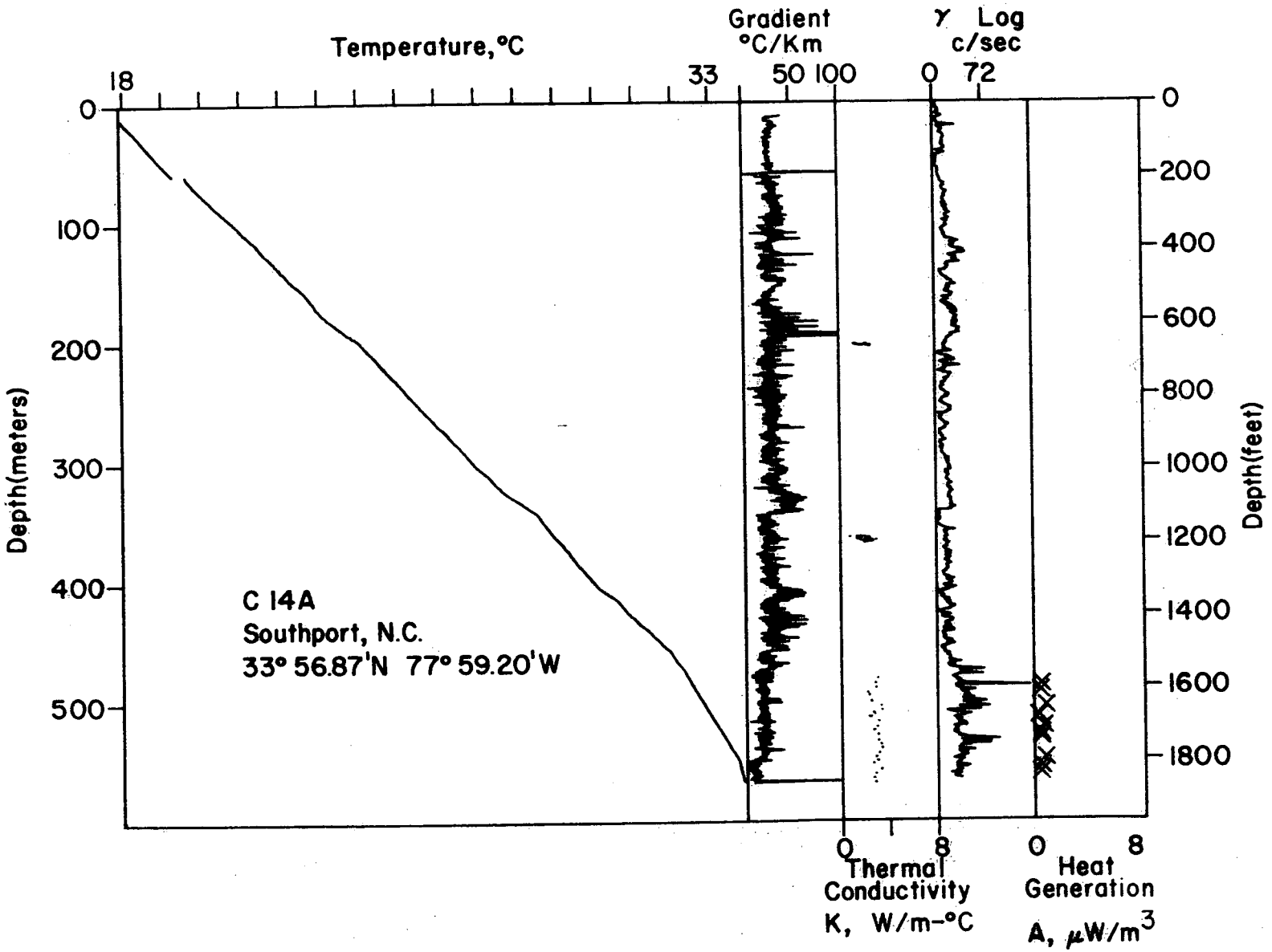
Temperature, °C
18
33
Gradient
°C/Km
50 100
γ Log
c/sec
0 72
0
100
200
300
400
500
Depth(meters)
0
200
400
600
800
1000
1200
1400
1600
1800
Depth(feet)
C 14A
Southport, N.C.
33° 56.87'N 77° 59.20'W
0 8
Thermal
Conductivity
K, W/m-°C
0 8
Heat
Generation
A, μW/m3

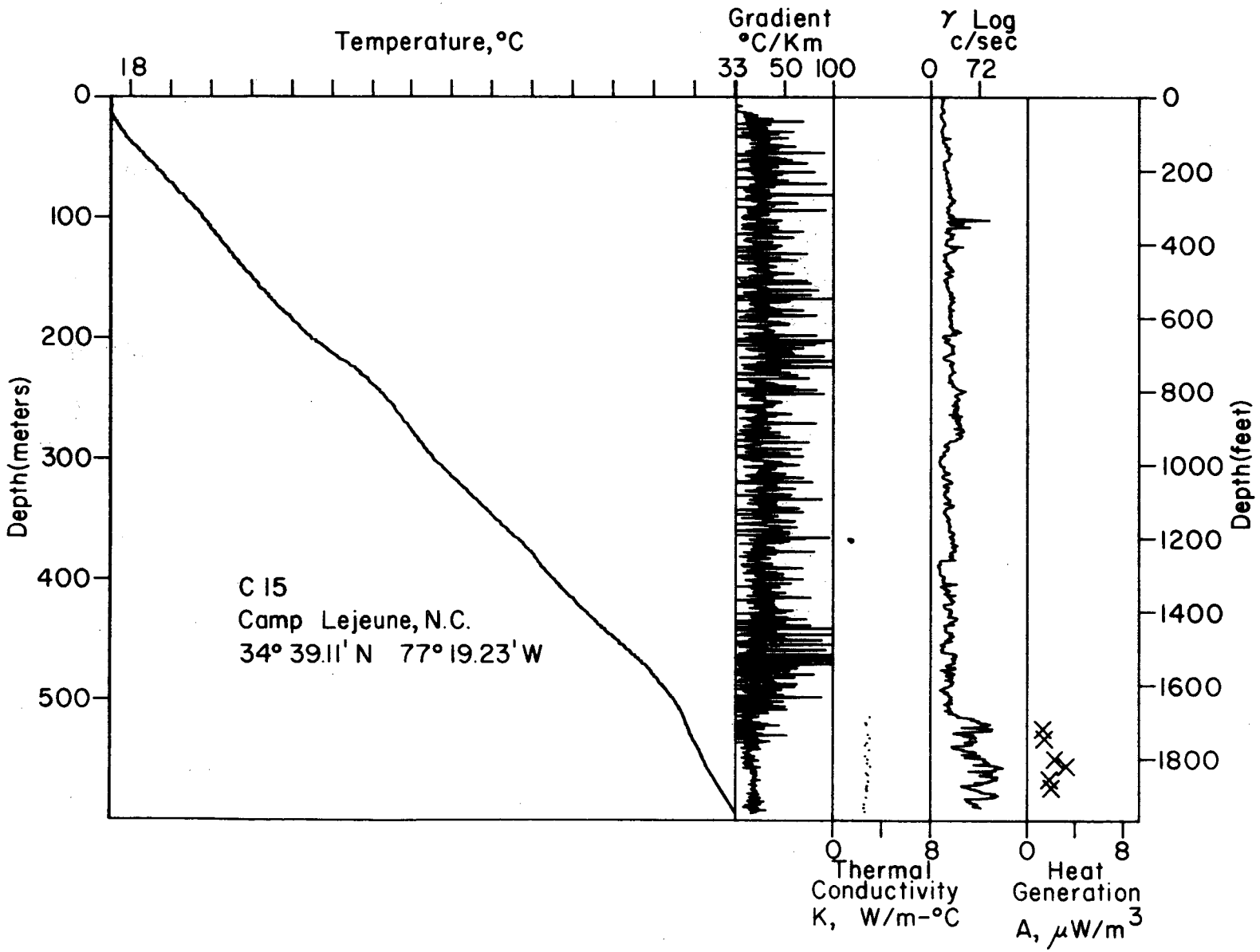
Temperature, °C
18
0
Gradient
°C/Km
33 50 100
γ Log
c/sec
0 72
100
200
300
400
500
Depth(meters)
C 15
Camp Lejeune, N.C.
34° 39.11' N 77° 19.23' W
0
200
400
600
800
1000
1200
1400
1600
1800
Depth(feet)
0 8
Thermal
Conductivity
K, W/m-°C
0 8
Heat
Generation
A, μW/m3

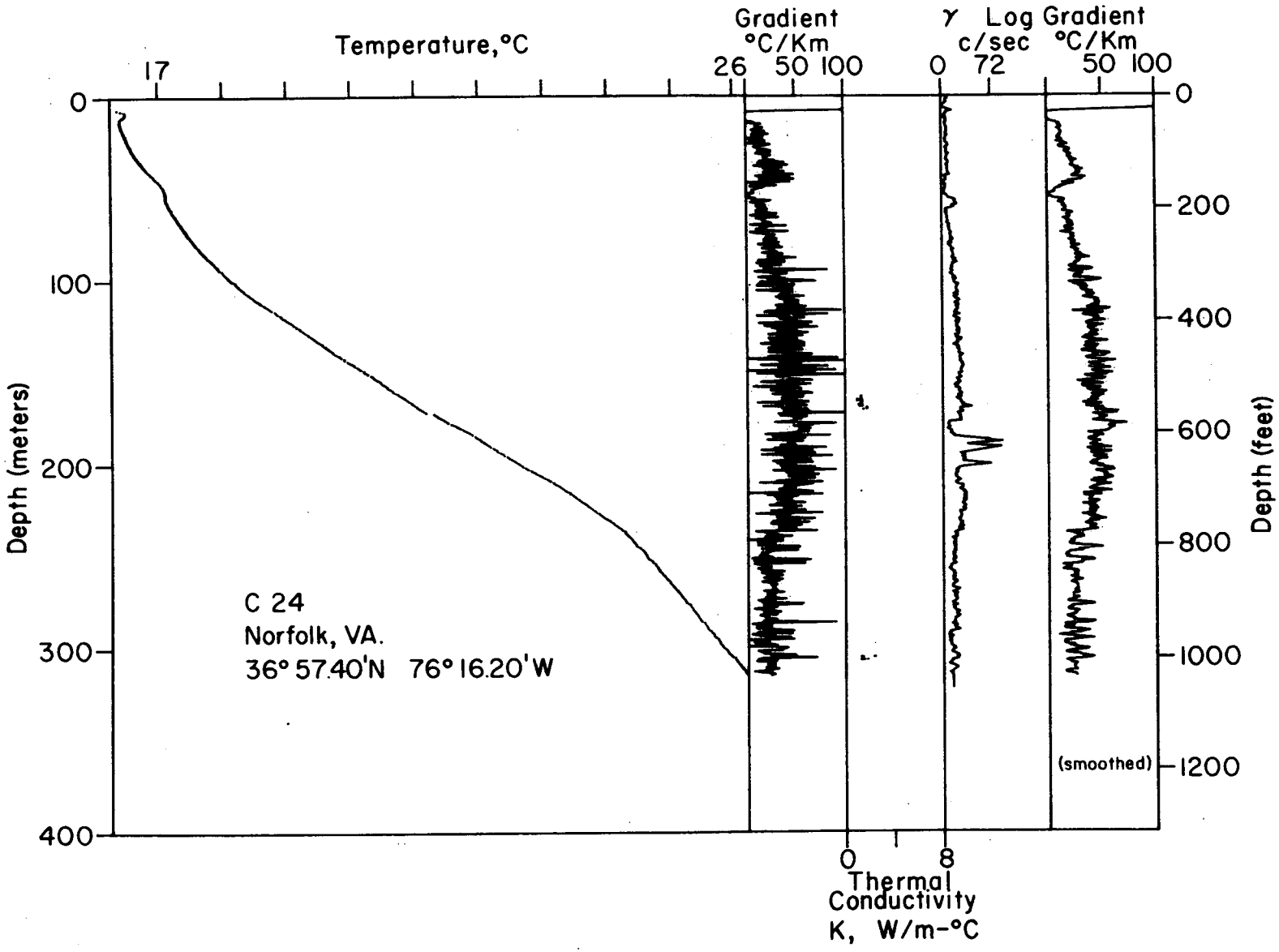
Temperature, °C
17
Gradient
°C/Km
26 50 100
γ Log
c/sec
0 72
Gradient
°C/Km
50 100
0
100
200
300
400
Depth (meters)
0
200
400
600
800
1000
1200
Depth (feet)
C 24
Norfolk, VA.
36° 57.40'N 76° 16.20'W
(smoothed)
0 8
Thermal
Conductivity
K, W/m-°C

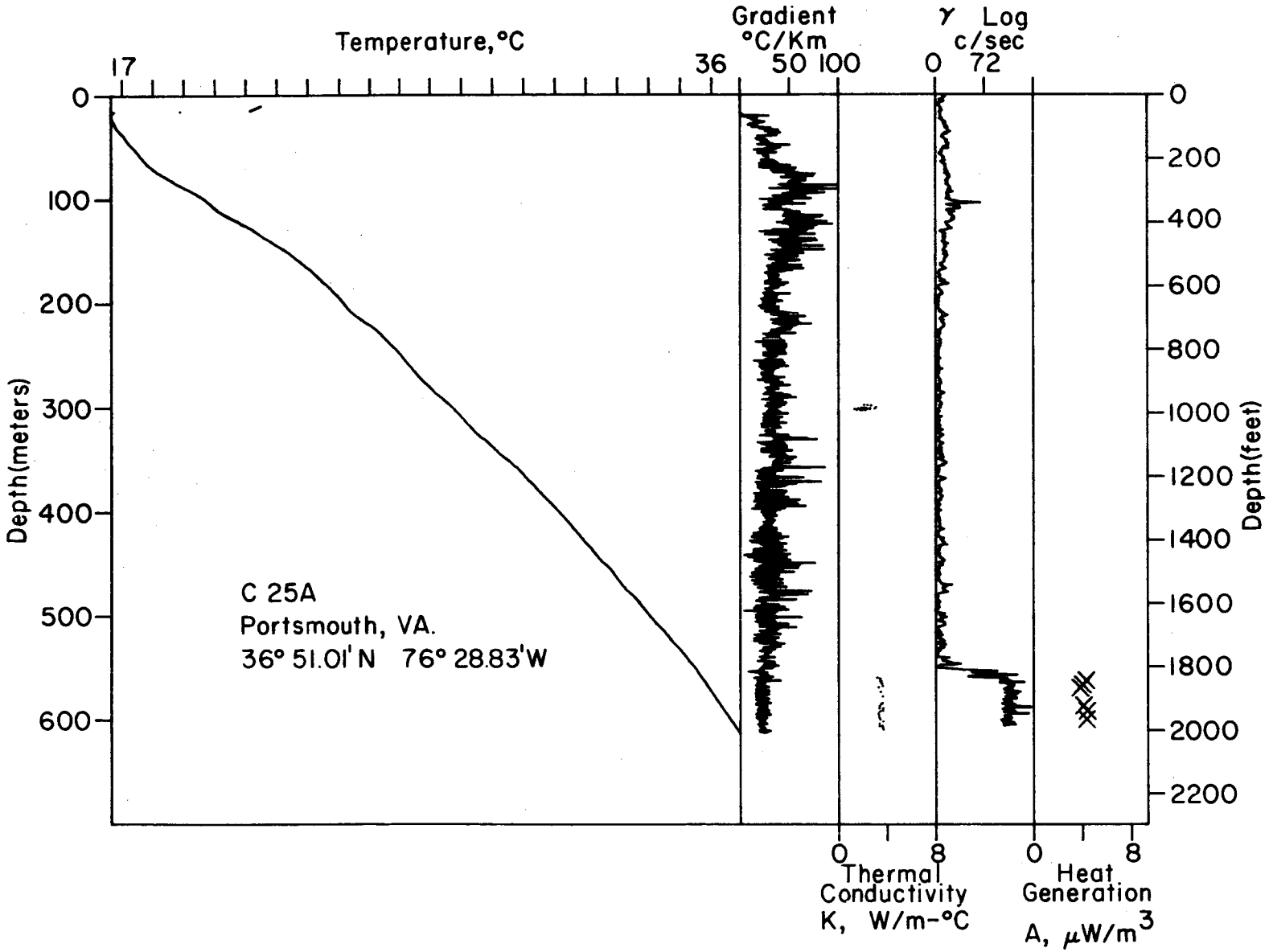
Temperature, °C
17
0
Gradient
°C/Km
36
50
100
γ Log
c/sec
0
72
Depth(meters)
0
100
200
300
400
500
600
Depth(feet)
0
200
400
600
800
1000
1200
1400
1600
1800
2000
2200
C 25A
Portsmouth, VA.
36° 51.01' N 76° 28.83' W
0
8
Thermal
Conductivity
K, W/m-°C
0
8
Heat
Generation
A, μW/m3

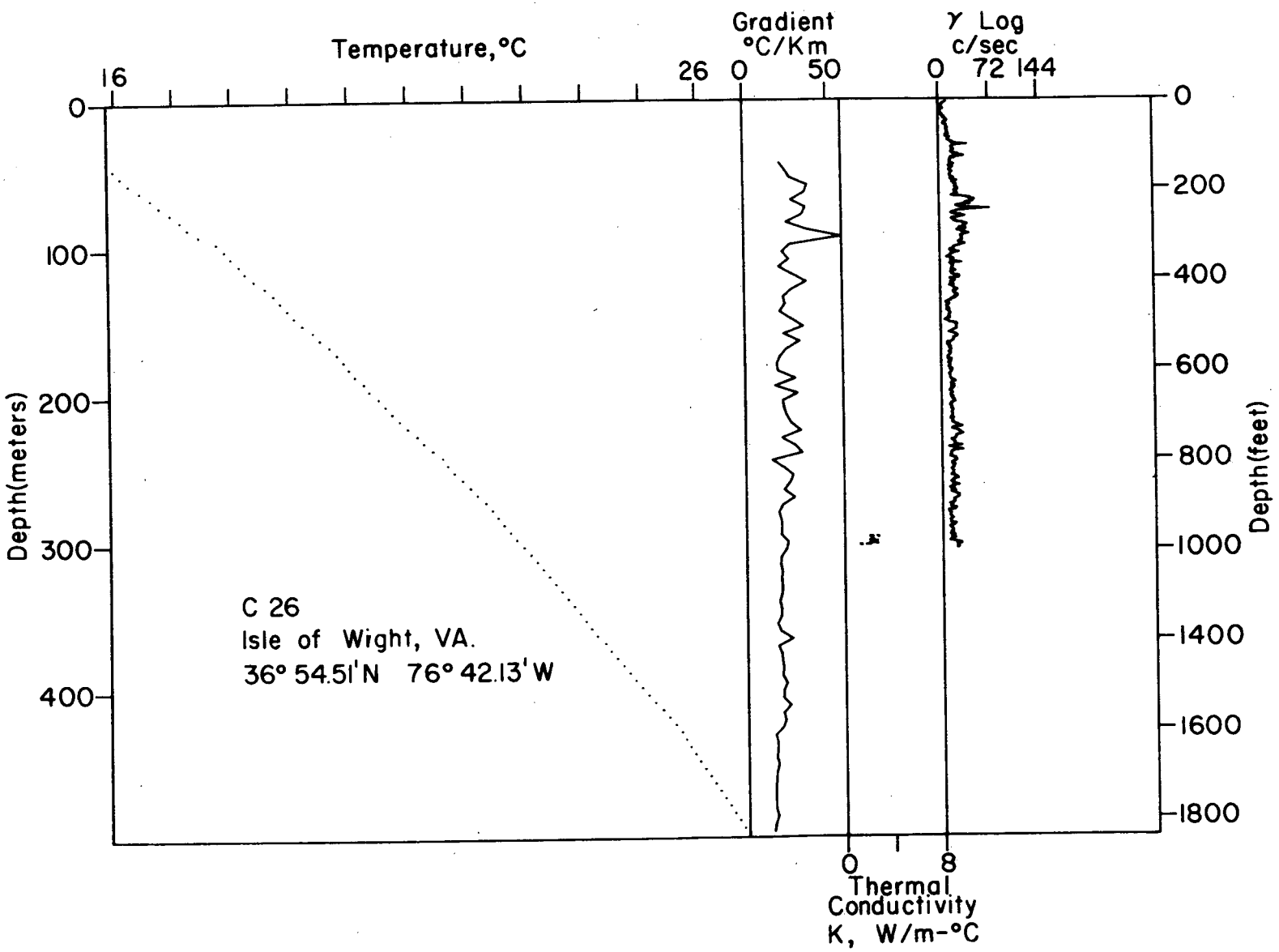
Temperature, °C
16
26
Gradient
°C/Km
0
50
γ Log
c/sec
0
72
144
0
100
200
300
400
Depth(meters)
0
200
400
600
800
1000
1400
1600
1800
Depth(feet)
C 26
Isle of Wight, VA.
36° 54.51'N 76° 42.13'W
0
8
Thermal
Conductivity
K, W/m-°C

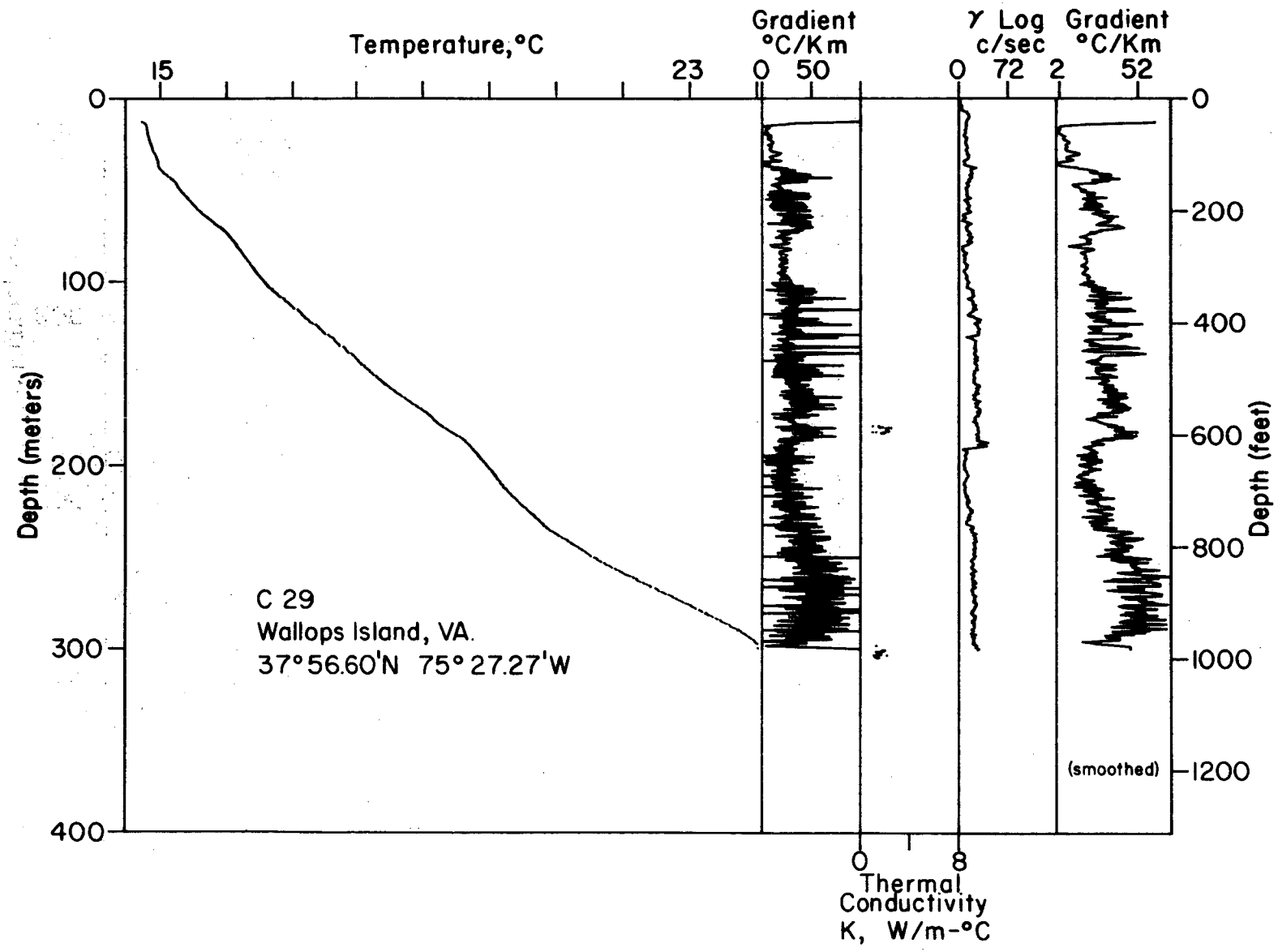
Temperature,°C
15
23
Gradient
°C/Km
0 50
γ Log
c/sec
0 72
Gradient
°C/Km
2 52
0
100
200
300
400
Depth (meters)
C 29
Wallops Island, VA.
37°56.60'N 75°27.27'W
0
200
400
600
800
1000
1200
Depth (feet)
(smoothed)
0 8
Thermal
Conductivity
K, W/m-°C

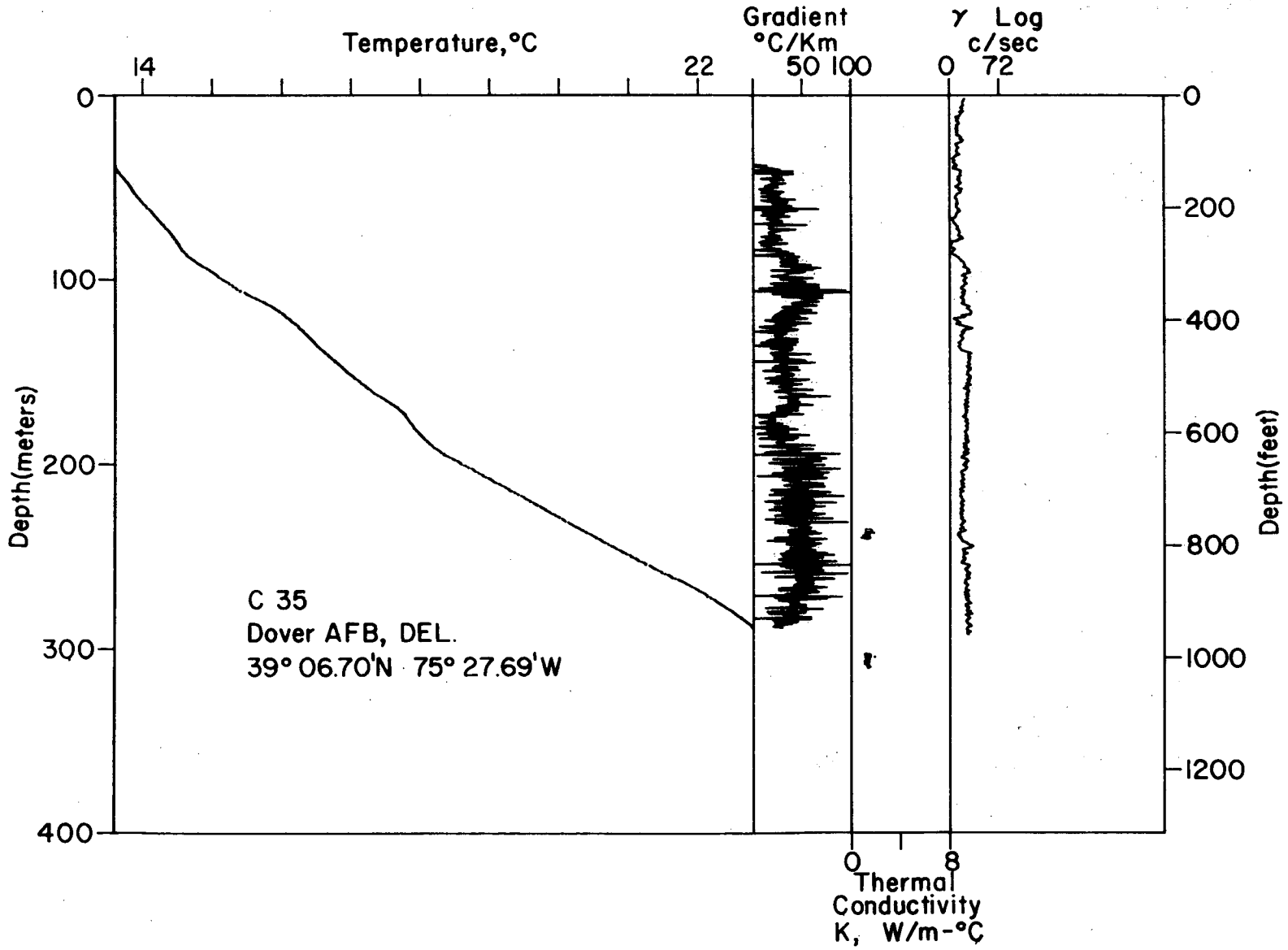
Temperature, °C
14
22
Gradient
°C/Km
50 100
γ Log
c/sec
0 72
0
100
200
300
400
Depth(meters)
0
200
400
600
800
1000
1200
Depth(feet)
C 35
Dover AFB, DEL.
39° 06.70'N 75° 27.69'W
0
8
Thermal
Conductivity
K, W/m-°C

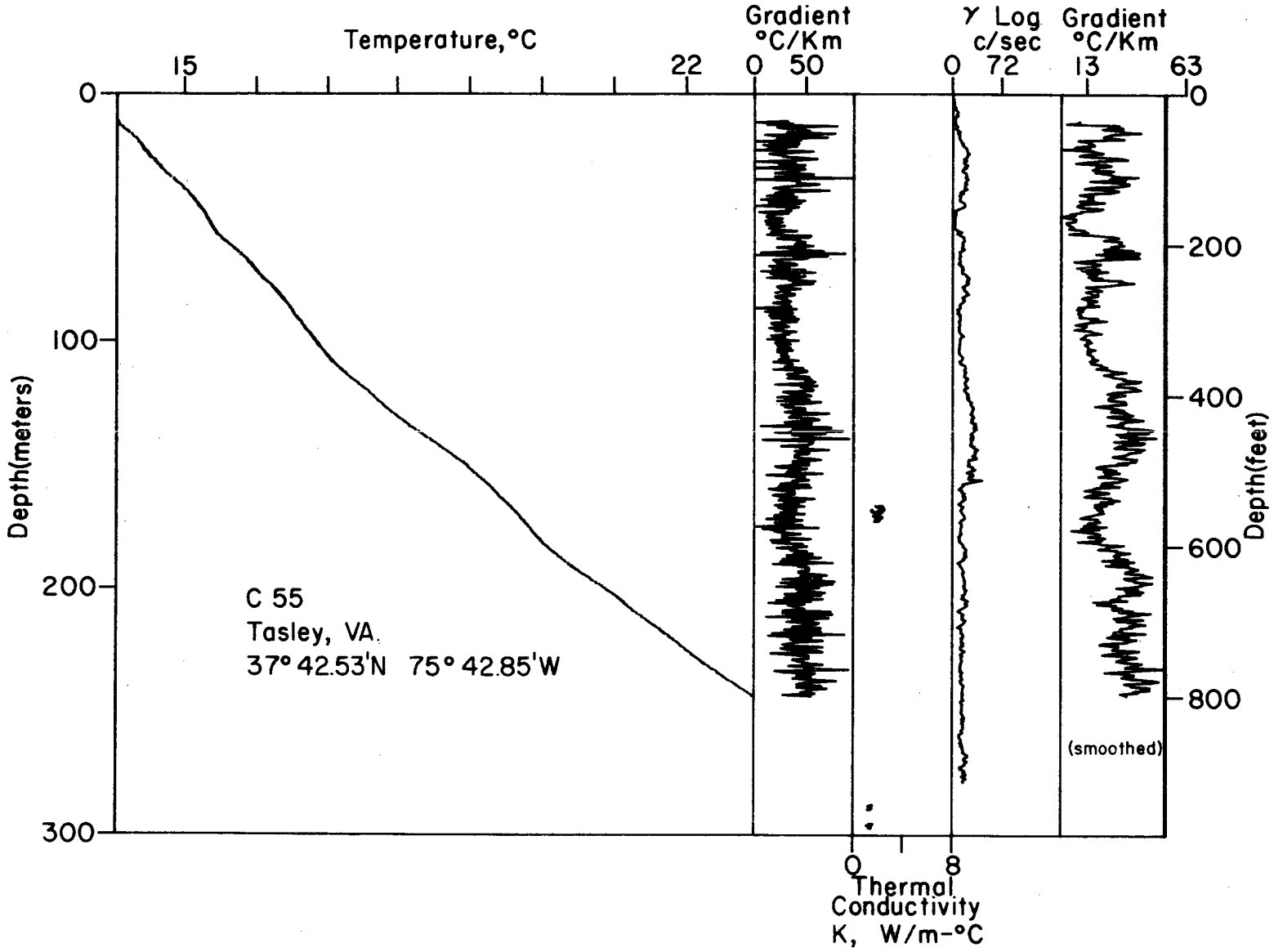
Temperature, °C
15
22
Gradient
°C/Km
0
50
γ Log
c/sec
0
72
Gradient
°C/Km
13
63
0
100
200
300
Depth(meters)
0
200
400
600
800
Depth(feet)
C 55
Tasley, VA.
37° 42.53'N 75° 42.85'W
(smoothed)
0
8
Thermal
Conductivity
K, W/m-°C

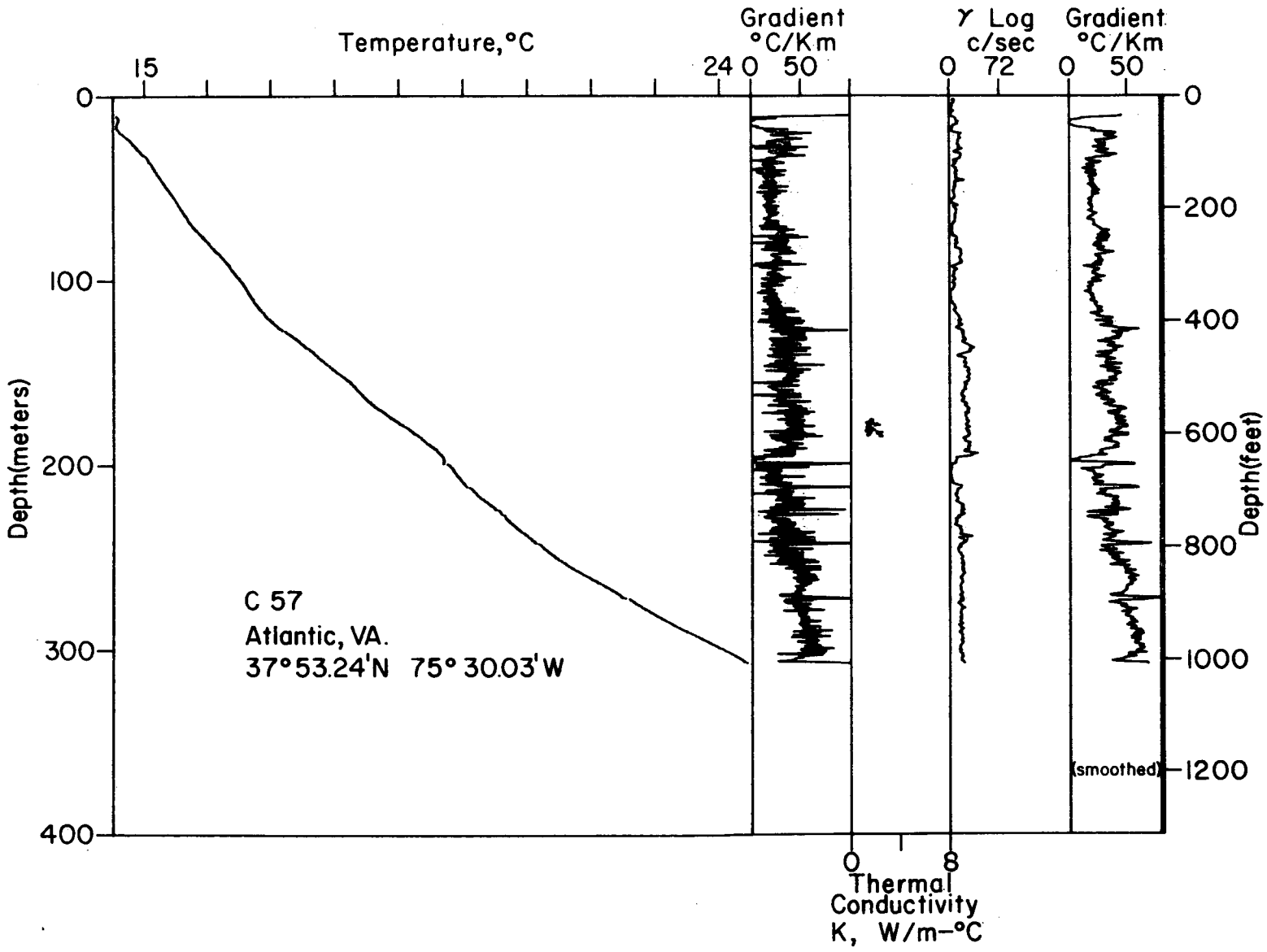
Temperature,°C
15
0
Gradient
°C/Km
24 0 50
γ Log
c/sec
0 72
Gradient
°C/Km
0 50
0
100
200
300
400
Depth(meters)
200
400
600
800
1000
1200
Depth(feet)
(smoothed)
C 57
Atlantic, VA.
37°53.24'N 75° 30.03'W
0 8
Thermal
Conductivity
K, W/m-°C

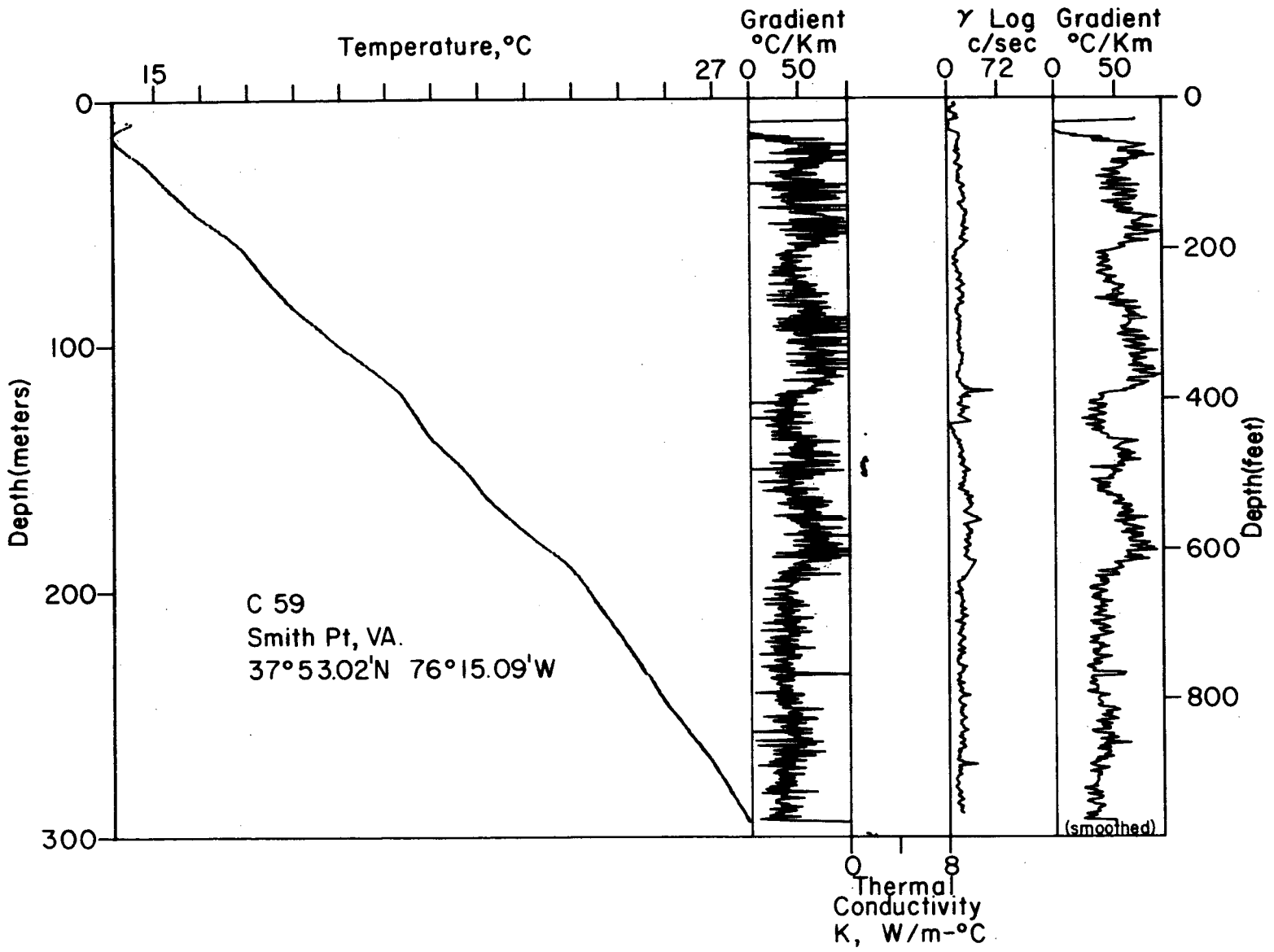
Temperature, °C
15
27
Gradient
°C/Km
0
50
γ Log
c/sec
0
72
Gradient
°C/Km
0
50
0
100
200
300
Depth(meters)
0
200
400
600
800
Depth(feet)
C 59
Smith Pt, VA.
37°53.02'N 76°15.09'W
(smoothed)
0
8
Thermal
Conductivity
K, W/m-°C

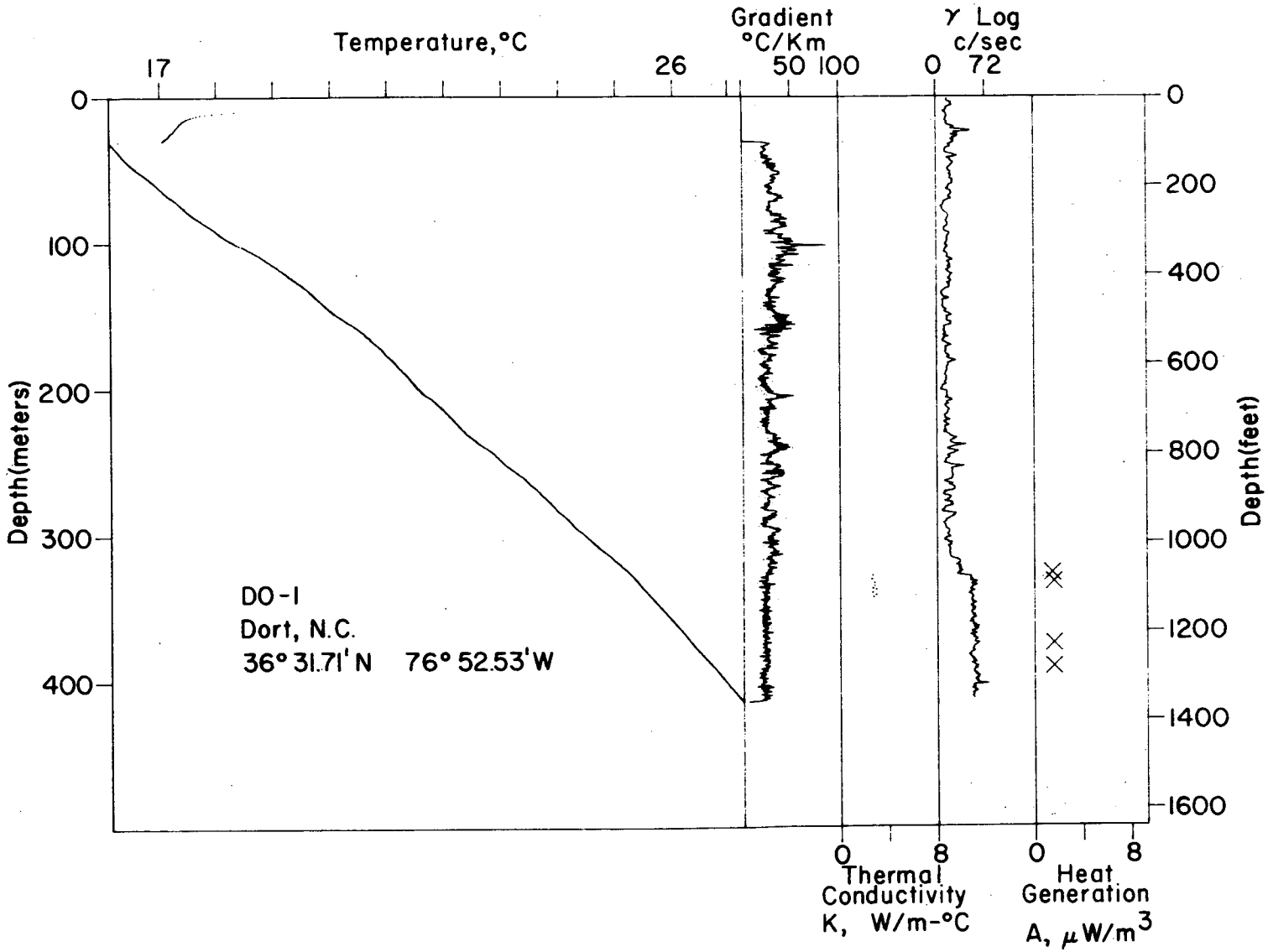
Temperature, °C
17
26
Gradient
°C/Km
50 100
γ Log
c/sec
0 72
Depth(meters)
0
100
200
300
400
Depth(feet)
0
200
400
600
800
1000
1200
1400
1600
DO-1
Dort, N.C.
36° 31.71' N 76° 52.53' W
0 8
Thermal
Conductivity
K, W/m-°C
0 8
Heat
Generation
A, μW/m3

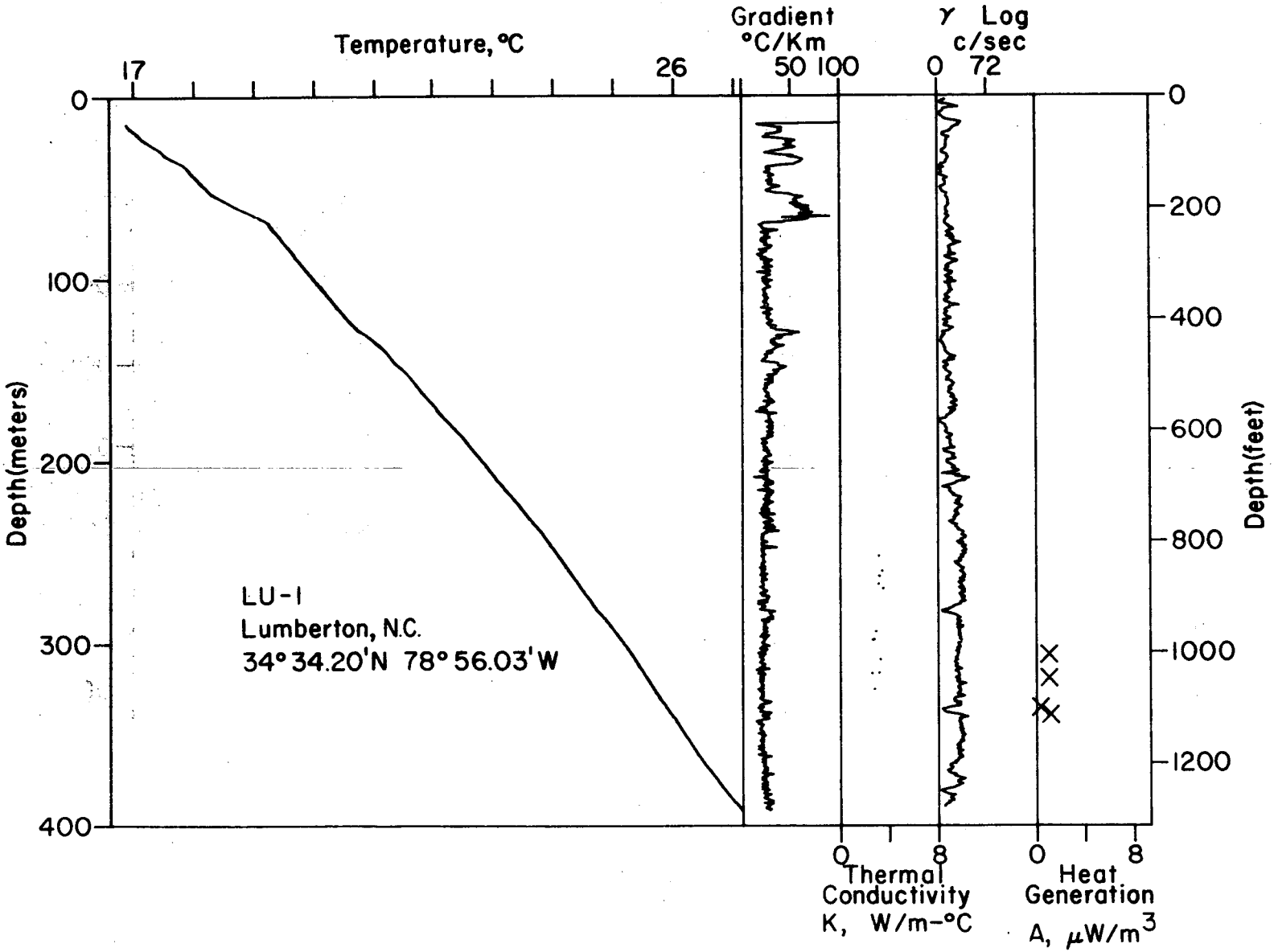
Temperature, °C
17
26
Gradient
°C/Km
50 100
γ Log
c/sec
0 72
0
100
200
300
400
Depth(meters)
0
200
400
600
800
1000
1200
Depth(feet)
LU-1
Lumberton, N.C.
34° 34.20'N 78° 56.03'W
0 8
Thermal
Conductivity
K, W/m-°C
0 8
Heat
Generation
A, μW/m3

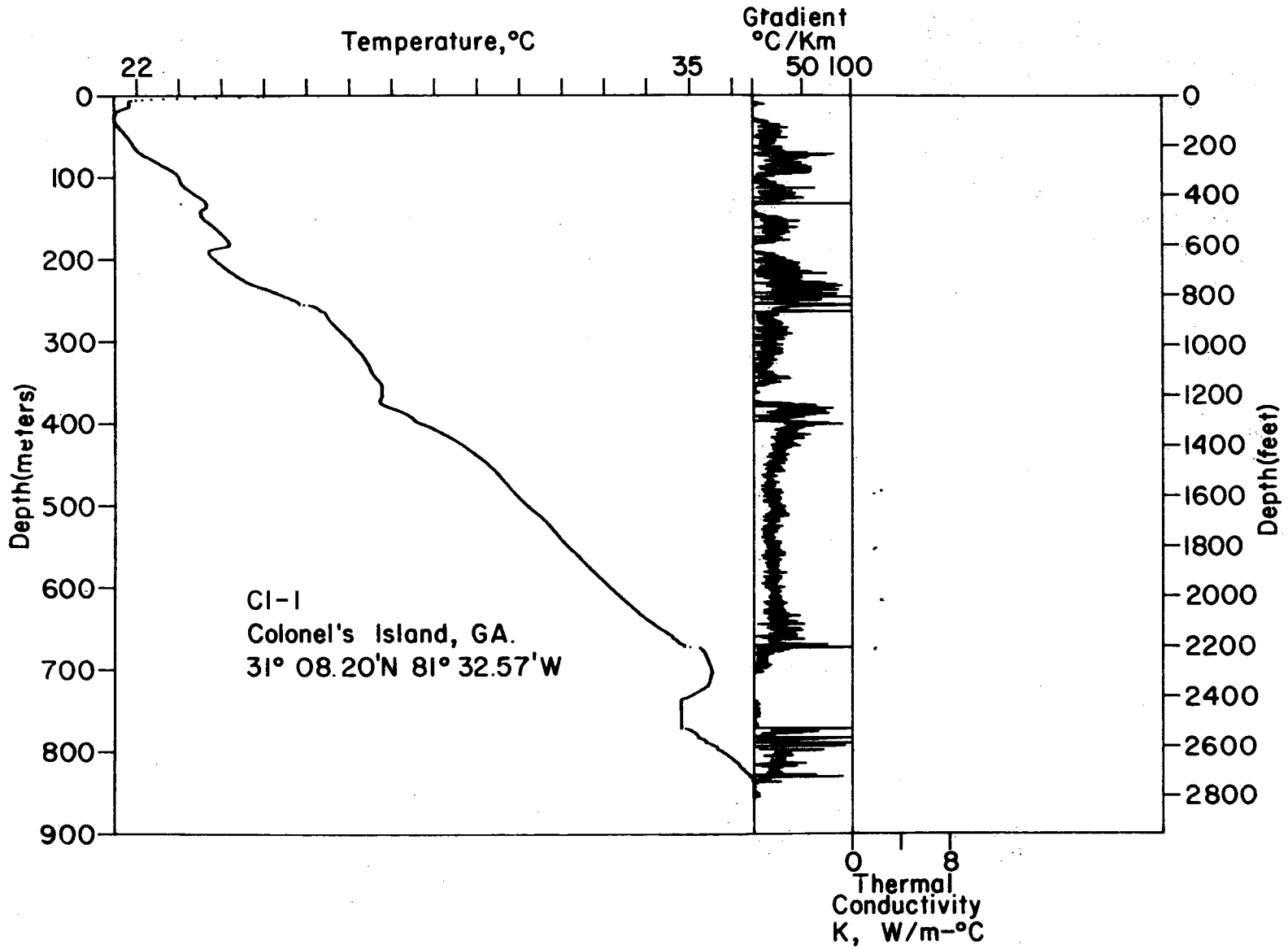
Temperature, °C
22
35
Gradient
°C/Km
50 100
0
100
200
300
400
500
600
700
800
900
Depth(meters)
0
200
400
600
800
1000
1200
1400
1600
1800
2000
2200
2400
2600
2800
Depth(feet)
CI-1
Colonel's Island, GA.
31° 08.20'N 81° 32.57'W
0
8
Thermal
Conductivity
K, W/m-°C

HEAT GENERATION DATA FROM CORE OF DRILL HOLE SL1

LOCATION	SAMPLE NO. DEPTH(m)	DENSITY, gm/cm^3	URANIUM (U),ppm	THORIUM (TH),ppm	POTASSIUM (K),%	RATIO, TH/U	HEAT GENERATION, A X 10^{-6} W/m^3
SALLEY	SC SL1-275	2.67	15.9	1.7	0.4	0.1	4.2
SALLEY	SC SL1-289	2.67	5.4	15.1	3.4	2.8	2.7
SALLEY	SC SL1-303	2.67	6.2	14.6	3.4	2.4	2.9
SALLEY	SC SL1-312	2.67	5.0	20.4	3.5	4.1	3.0
SALLEY	SC SL1-330	2.67	4.5	14.1	3.2	3.1	2.4
SALLEY	SC SL1-336	2.67	5.1	13.1	3.4	2.6	2.5

HEAT GENERATION DATA FROM CORE OF DRILL HOLE C14A

LOCATION	SAMPLE NO. DEPTH(m)	DENSITY, gm/cm^3	URANIUM (U),ppm	THORIUM (TH),ppm	POTASSIUM (K),%	RATIO, TH/U	HEAT GENERATION, A X 10^{-6} W/m^3
SOUTHPORT	NC 14A486	2.67	1.0	3.6	1.2	3.6	0.6
SOUTHPORT	NC 14A941	2.67	0.8	3.4	1.1	4.4	0.5
SOUTHPORT	NC 14A504	2.67	2.0	5.5	1.5	2.8	1.0
SOUTHPORT	NC 14A512	2.67	0.7	1.8	0.9	2.7	0.4
SOUTHPORT	NC 14A521	2.67	1.5	5.1	1.1	3.4	0.8
SOUTHPORT	NC 14A527	2.67	0.6	4.4	1.3	7.4	0.6
SOUTHPORT	NC 14A530	2.67	0.9	4.0	1.1	4.4	0.6
SOUTHPORT	NC 14A548	2.67	1.7	5.9	1.3	3.5	1.0
SOUTHPORT	NC 14A555	2.67	0.8	4.0	1.4	4.9	0.6
SOUTHPORT	NC 14A560	2.67	0.7	3.8	1.1	5.4	0.5

HEAT GENERATION DATA FROM CORE OF DRILL HOLE C15

LOCATION	SAMPLE NO. DEPTH(m)	DENSITY, gm/cm^3	URANIUM (U),ppm	THORIUM (TH),ppm	POTASSIUM (K),%	RATIO, TH/U	HEAT GENERATION, A X 10^{-6} W/m^3
CAMP LEJEUNE	NC C15524	2.67	1.7	9.9	2.1	6.0	1.3
CAMP LEJEUNE	NC C15532	2.67	2.4	6.4	3.9	2.6	1.4
CAMP LEJEUNE	NC C15549	2.67	4.0	15.0	2.5	3.7	2.3
CAMP LEJEUNE	NC C15555	2.67	6.8	18.4	2.8	2.7	3.3
CAMP LEJEUNE	NC C15566	2.67	3.2	13.3	1.6	4.2	1.8
CAMP LEJEUNE	NC C15573	2.67	3.5	13.0	2.5	3.7	2.0

HEAT GENERATION DATA FROM CORE OF DRILL HOLE C25A

LOCATION	SAMPLE NO. DEPTH(m)	DENSITY, gm/cm^3	URANIUM (U),ppm	THORIUM (TH),ppm	POTASSIUM (K),%	RATIO, TH/U	HEAT GENERATION, A X 10^{-6} W/m^3
PORTSMOUTH-25A-569M	VA 25A569	2.67	8.0	20.6	3.7	2.6	3.8
PORTSMOUTH	VA 25A562	2.67	9.0	24.1	4.0	2.7	4.3
PORTSMOUTH	VA 25A566	2.67	9.1	20.6	3.4	2.3	4.0
PORTSMOUTH	VA 25A586	2.67	9.8	19.1	3.5	2.0	4.1
PORTSMOUTH	VA 25A591	2.67	9.6	23.8	3.7	2.5	4.4
PORTSMOUTH	VA 25A599	2.67	9.2	24.8	3.4	2.7	4.4

HEAT GENERATION DATA FROM CORE OF DRILL HOLE DO1

LOCATION	SAMPLE NO. DEPTH(m)	DENSITY, gm/cm^3	URANIUM (U),ppm	THORIUM (TH),ppm	POTASSIUM (K),%	RATIO, TH/U	HEAT GENERATION, A X 10^{-6} W/m^3
DORT	NC DO1326	2.67	2.2	9.8	2.7	4.5	1.5
DORT	NC DO1332	2.67	2.0	12.1	2.8	5.9	1.6
DORT	NC DO1374	2.67	2.2	10.8	3.0	4.9	1.6
DORT	NC DO1390	2.67	2.8	9.0	3.0	3.3	1.6

HEAT GENERATION DATA FROM CORE OF DRILL HOLE LM1

LOCATION	SAMPLE NO. DEPTH(m)	DENSITY, gm/cm^3	URANIUM (U),ppm	THORIUM (TH),ppm	POTASSIUM (K),%	RATIO, TH/U	HEAT GENERATION, A X 10^{-6} W/m^3
LUMBERTON	NC LM1306	2.67	1.8	6.6	1.3	3.6	1.0
LUMBERTON	NC LM1319	2.69	1.9	5.9	1.8	3.1	1.0
LUMBERTON	NC LM1335	2.91	0.4	1.4	1.2	3.5	0.3
LUMBERTON	NC LM1339	2.65	1.8	6.9	2.4	3.8	1.2

THERMAL CONDUCTIVITY VALUES FROM CORE OF DRILL HOLE SL1
(SAMPLES ARE 2.680 CM IN DIAMETER BY 1.270 CM THICK)

SAMPLE NAME	DEPTH (METERS)	K, W/m-°C	SAMPLE NAME	DEPTH (METERS)	K, W/m-°C
SL1 - 905	275.8	7.02	SL1 - 1039	316.7	3.12
SL1 - 954	290.8	3.23	SL1 - 1047	319.1	3.25
SL1 - 960.4	292.7	3.19	SL1 - 1049	319.7	3.68
SL1 - 963.9	293.8	3.29	SL1 - 1057	322.2	3.36
SL1 - 968	295.0	3.37	SL1 - 1059	322.8	3.45
SL1 - 970.9	295.9	3.30	SL1 - 1061.2	323.5	3.47
SL1 - 973.8	296.8	3.24	SL1 - 1070.4	326.3	3.34
SL1 - 979.3	298.5	3.36	SL1 - 1074	327.4	3.35
SL1 - 984.2	300.0	3.47	SL1 - 1082	329.8	3.15
SL1 - 988.9	301.4	3.53	SL1 - 1083.8	330.3	3.45
SL1 - 994	303.0	3.37	SL1 - 1093.8	333.4	3.23
SL1 - 1003.8	306.0	3.00	SL1 - 1104.8	336.7	2.97
SL1 - 1013	308.8	3.04	SL1 - 1109	338.0	3.41
SL1 - 1013	308.8	3.45	SL1 - 1119	341.1	3.51
SL1 - 1017	310.0	3.03	SL1 - 1123.7	342.5	3.44
SL1 - 1023.8	312.1	3.21	SL1 - 1127.8	343.8	3.06
SL1 - 1027.6	313.2	3.17	SL1 - 1134.5	345.8	3.14
SL1 - 1035	315.5	3.22	SL1 - 1146.2	349.4	3.33
SL1 - 1036	315.8	3.20			

THERMAL CONDUCTIVITY VALUES FROM CORE OF DRILL HOLE C14A

SAMPLE NAME		DEPTH (METERS)	K, W/m-°C	SAMPLE NAME		DEPTH (METERS)	K, W/m-°C
C14A-663.5	s	202.2	1.3	C14A-1197.0	s	364.8	1.4
C14A-663.5	s	202.2	1.3	C14A-1197.0	s	364.8	1.6
C14A-663.5	s	202.2	1.4	C14A-1197.5	s	365.0	1.7
C14A-663.5	s	202.2	2.3	C14A-1197.5	s	365.0	1.8
C14A-664.5	s	202.5	2.2	C14A-1198.0	s	365.2	1.7
C14A-664.5	s	202.5	2.2	C14A-1198.0	s	365.2	1.8
C14A-664.5	s	202.5	2.3	C14A-1198.5	s	365.3	1.8
C14A-665.5	s	202.8	1.4	C14A-1198.5	s	365.3	1.8
C14A-665.5	s	202.8	1.5	C14A-1199.0	s	365.5	2.2
C14A-665.5	s	202.8	1.5	C14A-1199.0	s	365.5	2.4
C14A-665.5	s	202.8	1.7	C14A-1199.0	s	365.5	2.5
C14A-666.5	s	203.1	1.7	C14A-1199.5	s	365.6	2.1
C14A-666.5	s	203.1	1.8	C14A-1199.5	s	365.6	3.0
C14A-666.5	s	203.1	1.8	C14A-1200.5	s	365.9	1.7
C14A-666.5	s	203.1	2.0	C14A-1200.5	s	365.9	1.9
C14A-667.5	s	203.5	2.3	C14A-1200.5	s	365.9	2.1
C14A-667.5	s	203.5	2.4	C14A-1200.5	s	365.9	2.7
C14A-667.5	s	203.5	2.6	C14A-1201.5	s	366.2	2.3
C14A-667.5	s	203.5	2.6	C14A-1201.5	s	366.2	2.4
C14A-1191.0	s	363.0	0.8	C14A-1201.5	s	366.2	2.6
C14A-1191.0	s	363.0	1.4	C14A-1201.5	s	366.2	2.6
C14A-1191.0	s	363.0	1.5	C14A-1202.5	s	366.5	2.6
C14A-1191.0	s	363.0	1.7	C14A-1202.5	s	366.5	2.7
C14A-1192.0	s	363.3	2.0	C14A-1202.5	s	366.5	2.7
C14A-1192.0	s	363.3	2.1	C14A-1202.5	s	366.5	2.7
C14A-1192.0	s	363.3	2.1	C14A-1203.5	s	366.8	2.0
C14A-1192.0	s	363.3	2.3	C14A-1203.5	s	366.8	2.0
C14A-1193.0	s	363.6	1.6	C14A-1203.5	s	366.8	2.1
C14A-1193.0	s	363.6	1.7	C14A-1203.5	s	366.8	2.2
C14A-1193.0	s	363.6	2.1	C14A-1204.5	s	367.1	2.1
C14A-1193.0	s	363.6	2.4	C14A-1204.5	s	367.1	2.2
C14A-1194.0	s	363.9	1.7	C14A-1204.5	s	367.1	2.3
C14A-1194.0	s	363.9	1.7	C14A-1204.5	s	367.1	2.3
C14A-1194.0	s	363.9	1.8	C14A-1205.5	s	367.4	2.0
C14A-1194.0	s	363.9	1.9	C14A-1205.5	s	367.4	2.0
C14A-1195.5	s	364.4	1.4	C14A-1205.5	s	367.4	2.1
C14A-1195.5	s	364.4	1.5	C14A-1205.5	s	367.4	2.1
C14A-1196.0	s	364.5	1.6	C14A-1578.4	b	481.1	3.02
C14A-1196.0	s	364.5	1.7	C14A-1591.6	b	485.1	2.83
C14A-1196.5	s	364.7	1.5	C14A-1604.5	b	489.1	2.88
C14A-1196.5	s	364.7	1.8	C14A-1617	b	492.9	2.18

THERMAL CONDUCTIVITY VALUES FROM CORE OF DRILL HOLE C14A

SAMPLE NAME		DEPTH (METERS)	K, W/m-°C	SAMPLE NAME		DEPTH (METERS)	K, W/m-°C
C14A-1624.4	b	495.1	2.29	C14A-1759.6	b	536.3	3.26
C14A-1641	b	500.2	2.48	C14A-1769.5	b	539.3	3.34
C14A-1653.5	b	504.0	3.31	C14A-1783	b	543.5	3.11
C14A-1665.5	b	507.6	3.37	C14A-1793.8	b	546.8	2.85
C14A-1672	b	509.6	2.67	C14A-1804.6	b	550.0	2.97
C14A-1683.8	b	513.2	2.39	C14A-1812	b	552.3	2.61
C14A-1695.8	b	516.9	3.10	C14A-1828.6	b	557.4	3.30
C14A-1710.8	b	521.5	2.95	C14A-1841	b	561.1	2.80
C14A-1720	b	524.3	2.68	C14A-1851.9	b	564.5	2.65
C14A-1732.7	b	528.1	3.02	C14A-1863	b	568.1	2.78
C14A-1748.3	b	532.9	3.05				

THERMAL CONDUCTIVITY VALUES FROM CORE OF DRILL HOLE C15

SAMPLE NAME		DEPTH (METERS)	K, W/m-°C	SAMPLE NAME		DEPTH (METERS)	K, W/m-°C
C15-1202.5	s	366.5	1.3	C15-1208.5	s	368.4	1.6
C15-1202.5	s	366.5	1.3	C15-1209.5	s	368.7	1.5
C15-1202.5	s	366.5	1.4	C15-1210.5	s	369.0	1.5
C15-1202.5	s	366.5	1.4	C15-1686.5	b	514.0	3.04
C15-1202.5	s	366.5	1.5	C15-1702.3	b	518.9	2.69
C15-1203.5	s	366.8	1.4	C15-1706.7	b	520.2	2.76
C15-1203.5	s	366.8	1.5	C15-1734.5	b	528.7	2.89
C15-1203.5	s	366.8	1.5	C15-1744.2	b	531.6	3.04
C15-1203.5	s	366.8	1.5	C15-1757	b	535.5	2.79
C15-1203.5	s	366.8	1.6	C15-1763.8	b	537.6	2.66
C15-1204.5	s	367.1	1.5	C15-1776.3	b	541.4	2.98
C15-1204.5	s	367.1	1.5	C15-1793	b	546.5	2.63
C15-1204.5	s	367.1	1.5	C15-1802.3	b	549.3	2.84
C15-1204.5	s	367.1	1.6	C15-1813.4	b	552.7	2.84
C15-1204.5	s	367.1	1.6	C15-1822	b	555.3	3.09
C15-1205.5	s	367.4	1.3	C15-1839.2	b	560.6	2.72
C15-1205.5	s	367.4	1.5	C15-1844.2	b	562.1	2.87
C15-1205.5	s	367.4	1.5	C15-1862	b	567.5	2.91
C15-1205.5	s	367.4	1.5	C15-1875.2	b	571.6	2.80
C15-1205.5	s	367.4	1.5	C15-1882.7	b	573.8	2.76
C15-1206.5	s	367.7	1.4	C15-1887.9	b	575.4	2.79
C15-1206.5	s	367.7	1.4	C15-1906.1	b	581.0	2.74
C15-1206.5	s	367.7	1.5	C15-1924.5	b	586.6	2.57
C15-1206.5	s	367.7	1.5	C15-1935.2	b	589.8	2.54
C15-1207.5	s	368.0	1.5	C15-1945	b	592.8	2.64

THERMAL CONDUCTIVITY VALUES FROM CORE OF DRILL HOLE C24

SAMPLE NAME		DEPTH (METERS)	K, W/m-°C	SAMPLE NAME		DEPTH (METERS)	K, W/m-°C
C24-535.5	s	163.2	1.3	C24-543.5	s	165.7	1.2
C24-535.5	s	163.2	1.3	C24-543.5	s	165.7	1.3
C24-535.5	s	163.2	1.3	C24-543.5	s	165.7	1.3
C24-535.5	s	163.2	1.4	C24-543.5	s	165.7	1.3
C24-535.5	s	163.2	1.4	C24-544.5	s	166.0	1.2
C24-536.5	s	163.5	1.3	C24-544.5	s	166.0	1.3
C24-536.5	s	163.5	1.3	C24-544.5	s	166.0	1.3
C24-536.5	s	163.5	1.3	C24-544.5	s	166.0	1.3
C24-536.5	s	163.5	1.3	C24-544.5	s	166.0	1.3
C24-536.5	s	163.5	1.3	C24-545.5	s	166.3	1.3
C24-537.5	s	163.8	1.3	C24-545.5	s	166.3	1.5
C24-537.5	s	163.8	1.4	C24-546.5	s	166.6	1.3
C24-537.5	s	163.8	1.4	C24-546.5	s	166.6	1.3
C24-537.5	s	163.8	1.4	C24-547.5	s	166.9	1.4
C24-537.5	s	163.8	1.5	C24-547.5	s	166.9	1.5
C24-538.5	s	164.1	1.3	C24-548.5	s	167.2	1.4
C24-538.5	s	164.1	1.3	C24-548.5	s	167.2	1.5
C24-538.5	s	164.1	1.3	C24-549.5	s	167.5	1.5
C24-538.5	s	164.1	1.4	C24-551.0	s	167.9	1.6
C24-538.5	s	164.1	1.4	C24-552.0	s	168.2	1.5
C24-539.5	s	164.4	1.3	C24-553.0	s	168.6	1.6
C24-539.5	s	164.4	1.3	C24-554	s	168.9	1.6
C24-539.5	s	164.4	1.3	C24-555.5	s	169.3	1.5
C24-539.5	s	164.4	1.3	C24-555.5	s	169.3	1.7
C24-539.5	s	164.4	1.3	C24-556.5	s	169.6	2.3
C24-540.5	s	164.7	1.0	C24-557.5	s	169.9	1.9
C24-540.5	s	164.7	1.0	C24-557.5	s	169.9	1.9
C24-540.5	s	164.7	1.3	C24-558.5	s	170.2	1.9
C24-540.5	s	164.7	1.3	C24-558.5	s	170.2	2.1
C24-540.5	s	164.7	1.3	C24-559.5	s	170.5	1.7
C24-541.5	s	165.0	1.1	C24-559.5	s	170.5	1.9
C24-541.5	s	165.0	1.2	C24-1005A	s	306.3	1.8
C24-541.5	s	165.0	1.3	C24-1005A	s	306.3	2.0
C24-541.5	s	165.0	1.3	C24-1005A	s	306.3	2.0
C24-541.5	s	165.0	1.5	C24-1005A	s	306.3	2.5
C24-542.5	s	165.4	1.2	C24-1005B	s	306.3	1.8
C24-542.5	s	165.4	1.3	C24-1005B	s	306.3	1.8
C24-542.5	s	165.4	1.3	C24-1005B	s	306.3	1.8
C24-542.5	s	165.4	1.4	C24-1005B	s	306.3	1.8
C24-542.5	s	165.4	1.5	C24-1005C	s	306.3	1.8
C24-543.5	s	165.7	1.2	C24-1005C	s	306.3	1.8

THERMAL CONDUCTIVITY VALUES FROM CORE OF DRILL HOLE C24

SAMPLE NAME		DEPTH (METERS)	K, W/m-°C	SAMPLE NAME		DEPTH (METERS)	K, W/m-°C
C24-1005C	s	306.3	1.9	C24-1005I1	s	306.3	1.4
C24-1005C	s	306.3	1.9	C24-1005J	s	306.3	1.3
C24-1005D	s	306.3	1.5	C24-1005J	s	306.3	1.3
C24-1005D	s	306.3	1.6	C24-1005J2	s	306.3	2.5
C24-1005D	s	306.3	1.7	C24-1005J2	s	306.3	2.5
C24-1005E	s	306.3	1.5	C24-1005J2	s	306.3	2.6
C24-1005E	s	306.3	1.6	C24-1005K	s	306.3	1.9
C24-1005E	s	306.3	1.7	C24-1005K	s	306.3	2.3
C24-1005E	s	306.3	1.8	C24-1005K2	s	306.3	2.1
C24-1005F	s	306.3	1.5	C24-1005K2	s	306.3	2.3
C24-1005F	s	306.3	1.6	C24-1005L	s	306.3	2.6
C24-1005F	s	306.3	1.6	C24-1005L	s	306.3	2.7
C24-1005F	s	306.3	1.6	C24-1005L	s	306.3	2.7
C24-1005F1	s	306.3	1.2	C24-1005L1	s	306.3	2.6
C24-1005F1	s	306.3	1.3	C24-1005L1	s	306.3	2.7
C24-1005F2	s	306.3	1.1	C24-1005L1	s	306.3	2.7
C24-1005F2	s	306.3	1.2	C24-1005L1	s	306.3	2.7
C24-1005G	s	306.3	1.3	C24-1005L2	s	306.3	1.7
C24-1005G	s	306.3	1.5	C24-1005L2	s	306.3	2.0
C24-1005G1	s	306.3	1.5	C24-1005L2	s	306.3	2.4
C24-1005G1	s	306.3	1.5	C24-1005M	s	306.3	2.2
C24-1005H	s	306.3	1.4	C24-1005M	s	306.3	2.2
C24-1005H	s	306.3	1.5	C24-1005M	s	306.3	2.3
C24-1005H1	s	306.3	1.5	C24-1005M1	s	306.3	1.5
C24-1005H1	s	306.3	1.5	C24-1005M1	s	306.3	1.5
C24-1005I	s	306.3	1.5	C24-1005M1	s	306.3	1.5
C24-1005I	s	306.3	1.5				

Core interval between 1005° - 1035° was not fully recovered; therefore, the depths were recorded as removed from coring barrel. (Using A thru M)

THERMAL CONDUCTIVITY VALUES FROM CORE OF DRILL HOLE C25A

SAMPLE NAME		DEPTH (METERS)	K, W/m-°C	SAMPLE NAME		DEPTH (METERS)	K, W/m-°C
C25-976.5	s	297.6	2.1	C25-990.5	s	301.9	2.6
C25-976.5	s	297.6	2.3	C25-990.5	s	301.9	2.5
C25-976.5	s	297.6	2.1	C25-991.5	s	302.2	2.3
C25-977.5	s	297.9	2.6	C25-991.5	s	302.2	2.2
C25-977.5	s	297.9	2.4	C25-991.5	s	302.2	2.3
C25-977.5	s	297.9	2.4	C25-991.5	s	302.2	2.3
C25-977.5	s	297.9	2.4	C25-991.8	s	302.3	2.0
C25-978.5	s	298.2	2.2	C25-992.0	s	302.4	2.1
C25-978.5	s	298.2	2.1	C25-992.0	s	302.4	2.1
C25-978.5	s	298.2	2.1	C25-992.0	s	302.4	2.1
C25-978.5	s	298.2	2.0	C25A-1835	b	559.3	3.17
C25-979.5	s	298.6	2.1	C25A-1839	b	560.5	3.42
C25-979.5	s	298.6	1.9	C25A-1845.5	b	562.5	3.48
C25-979.5	s	298.6	3.1	C25A-1848	b	563.3	3.43
C25-979.5	s	298.6	2.1	C25A-1854	b	565.1	3.56
C25-985.0	s	300.2	2.8	C25A-1862	b	567.5	3.64
C25-985.0	s	300.2	2.8	C25A-1865	b	568.5	3.28
C25-985.0	s	300.2	2.6	C25A-1880	b	573.0	3.46
C25-985.0	s	300.2	2.9	C25A-1894.3	b	577.4	3.62
C25-986.0	s	300.5	3.0	C25A-1914.2	b	583.4	3.62
C25-986.0	s	300.5	2.8	C25A-1918.1	b	584.6	3.49
C25-986.0	s	300.5	2.8	C25A-1924.5	b	586.6	3.37
C25-986.0	s	300.5	2.5	C25A-1931.1	b	588.6	3.33
C25-987.0	s	300.8	3.1	C25A-1931.1	b	588.6	3.67
C25-987.0	s	300.8	2.8	C25A-1937.8	b	590.6	3.63
C25-987.0	s	300.8	2.8	C25A-1940.7	b	591.5	3.41
C25-987.0	s	300.8	2.7	C25A-1947.2	b	593.5	3.27
C25-988.0	s	301.1	2.3	C25A-1953.6	b	595.5	3.34
C25-988.0	s	301.1	2.4	C25A-1960.1	b	597.4	3.33
C25-988.0	s	301.1	2.5	C25A-1966.2	b	599.3	3.41
C25-988.0	s	301.1	2.3	C25A-1972.7	b	601.3	3.67
C25-988.8	s	301.4	2.5	C25A-1979.7	b	603.4	3.37
C25-989.5	s	301.6	2.5	C25A-1986.2	b	605.4	3.60
C25-989.5	s	301.6	2.4	C25A-1987.6	b	605.8	3.35
C25-989.5	s	301.6	2.6	C25A-1990.5	b	606.7	3.62
C25-989.5	s	301.6	2.5	C25A-1994.2	b	607.8	3.65
C25-990.5	s	301.9	2.4	C25A-1999.1	b	609.3	3.71
C25-990.5	s	301.9	2.4				

THERMAL CONDUCTIVITY VALUES FROM CORE OF DRILL HOLE C26

SAMPLE NAME		DEPTH (METERS)	K, W/m-°C	SAMPLE NAME		DEPTH (METERS)	K, W/m-°C
C26-261.5	s	79.7	2.0	C26-267.5	s	81.5	1.3
C26-261.5	s	79.7	2.1	C26-267.5	s	81.5	1.3
C26-261.5	s	79.7	2.1	C26-267.5	s	81.5	1.4
C26-261.5	s	79.7	2.2	C26-267.5	s	81.5	1.4
C26-262.5	s	80.0	2.2	C26-268.5	s	81.8	1.5
C26-262.5	s	80.0	2.2	C26-268.5	s	81.8	1.5
C26-262.5	s	80.0	2.4	C26-268.5	s	81.8	1.5
C26-262.5	s	80.0	2.4	C26-268.5	s	81.8	1.6
C26-263.5	s	80.3	2.0	C26-269.5	s	82.1	1.3
C26-263.5	s	80.3	2.1	C26-269.5	s	82.1	1.4
C26-263.5	s	80.3	2.1	C26-269.5	s	82.1	1.4
C26-263.5	s	80.3	2.1	C26-269.5	s	82.1	1.5
C26-264.5	s	80.6	1.4	C26-987.5	s	301.0	2.2
C26-264.5	s	80.6	1.4	C26-988.0	s	301.1	2.1
C26-264.5	s	80.6	1.4	C26-988.0	s	301.1	2.2
C26-264.5	s	80.6	1.5	C26-988.0	s	301.1	2.3
C26-265.5	s	80.9	1.4	C26-987.7	s	301.1	2.7
C26-265.5	s	80.9	1.5	C26-989.0	s	301.4	2.2
C26-265.5	s	80.9	1.5	C26-989.0	s	301.4	2.3
C26-265.5	s	80.9	1.5	C26-989.0	s	301.4	2.4
C26-266.5	s	81.2	1.5	C26-990.0	s	301.8	2.1
C26-266.5	s	81.2	1.5	C26-990.0	s	301.8	2.2
C26-266.5	s	81.2	1.6	C26-990.0	s	301.8	2.5
C26-266.5	s	81.2	1.6				

THERMAL CONDUCTIVITY VALUES FROM CORE OF DRILL HOLE C29

SAMPLE NAME		DEPTH (METERS)	K, W/m-°C	SAMPLE NAME		DEPTH (METERS)	K, W/m-°C
C29-584.5	s	178.2	1.0	C29-984.0	s	299.9	2.0
C29-584.5	s	178.2	1.5	C29-984.0	s	299.9	2.1
C29-585.5	s	178.5	1.5	C29-984.5	s	300.1	1.8
C29-585.5	s	178.5	1.5	C29-984.5	s	300.1	1.8
C29-586.5	s	178.8	1.6	C29-984.5	s	300.1	1.8
C29-586.5	s	178.8	1.8	C29-985.5	s	300.4	1.8
C29-587.5	s	179.1	2.3	C29-985.5	s	300.4	2.0
C29-587.5	s	179.1	2.5	C29-986.5	s	300.7	1.8
C29-588.5	s	179.4	2.1	C29-986.5	s	300.7	1.8
C29-588.5	s	179.4	2.2	C29-987.5	s	301.0	1.7
C29-589.5	s	179.7	2.2	C29-987.5	s	301.0	1.8
C29-589.5	s	179.7	2.2	C29-988.5	s	301.3	1.3
C29-590.5	s	180.0	2.2	C29-988.5	s	301.3	1.4
C29-590.5	s	180.0	2.2	C29-989.5	s	301.6	1.5
C29-591.5	s	180.3	2.1	C29-989.5	s	301.6	1.5
C29-591.5	s	180.3	2.2	C29-990.5	s	301.9	1.5
C29-592.5	s	180.6	2.1	C29-990.5	s	301.9	1.6
C29-592.5	s	180.6	2.1	C29-991.5	s	302.2	1.6
C29-594.5	s	181.2	2.3	C29-991.5	s	302.2	1.7
C29-595.5	s	181.5	1.0	C29-992.5	s	302.5	1.5
C29-595.5	s	181.5	1.3	C29-992.5	s	302.5	1.5
C29-596.5	s	181.8	1.8	C29-993.5	s	302.8	1.6
C29-596.5	s	181.8	2.0	C29-993.5	s	302.8	1.7
C29-597.5	s	182.1	1.7	C29-994.5	s	303.1	1.1
C29-597.5	s	182.1	1.8	C29-994.5	s	303.1	1.3
C29-599.0	s	182.6	1.5	C29-994.5	s	303.1	2.2
C29-599.0	s	182.6	1.5	C29-995.5	s	303.4	1.2
C29-599.0	s	182.6	1.6	C29-995.5	s	303.4	1.2
C29-599.5	s	182.7	1.5	C29-996.5	s	303.7	1.3
C29-599.5	s	182.7	1.5	C29-996.5	s	303.7	1.3
C29-599.5	s	182.7	1.5	C29-997.5	s	304.0	1.2
C29-977.5	s	297.9	1.3	C29-998.5	s	304.3	1.3
C29-983.0	s	299.6	1.7	C29-998.5	s	304.3	1.5
C29-983.0	s	299.6	2.1	C29-999.5	s	304.6	1.4
C29-983.0	s	299.6	2.2	C29-999.5	s	304.6	1.5

THERMAL CONDUCTIVITY VALUES FROM CORE OF DRILL HOLE C35

SAMPLE NAME		DEPTH (METERS)	K, W/m-°C	SAMPLE NAME		DEPTH (METERS)	K, W/m-°C
C35-772.5	s	235.5	1.2	C35-783.5	s	238.8	1.2
C35-772.5	s	235.5	1.2	C35-783.5	s	238.8	1.3
C35-772.5	s	235.5	1.5	C35-783.5	s	238.8	1.4
C35-772.5	s	235.5	1.5	C35-784.5	s	239.1	1.0
C35-773.5	s	235.8	1.3	C35-784.5	s	239.1	1.2
C35-773.5	s	235.8	1.3	C35-785.5	s	239.4	1.0
C35-773.5	s	235.8	1.4	C35-785.5	s	239.4	1.0
C35-773.5	s	235.8	1.6	C35-785.5	s	239.4	1.2
C35-774.5	s	236.1	1.3	C35-785.5	s	239.4	1.3
C35-774.5	s	236.1	1.3	C35-785.5	s	239.4	1.3
C35-774.5	s	236.1	1.4	C35-786.5	s	239.7	0.8
C35-774.5	s	236.1	1.5	C35-786.5	s	239.7	1.0
C35-775.5	s	236.4	1.5	C35-786.5	s	239.7	1.3
C35-775.5	s	236.4	1.6	C35-786.5	s	239.7	1.3
C35-776.0	s	236.5	1.3	C35-786.5	s	239.7	1.5
C35-777.0	s	236.8	1.2	C35-878.5	s	240.0	0.8
C35-777.0	s	236.8	1.2	C35-787.5	s	240.0	1.1
C35-777.0	s	236.8	1.2	C35-787.5	s	240.0	1.2
C35-777.0	s	236.8	1.5	C35-787.5	s	240.0	1.3
C35-778.0	s	237.1	1.3	C35-787.5	s	240.0	1.4
C35-778.0	s	237.1	1.3	C35-994.5	s	303.1	1.1
C35-778.0	s	237.1	1.5	C35-994.5	s	303.1	1.1
C35-779.0	s	237.4	1.2	C35-994.5	s	303.1	1.2
C35-779.0	s	237.4	1.2	C35-994.5	s	303.1	1.2
C35-779.0	s	237.4	1.3	C35-995.5	s	303.4	1.2
C35-779.0	s	237.4	1.4	C35-995.5	s	303.4	1.3
C35-780.0	s	237.7	1.3	C35-995.5	s	303.4	1.3
C35-780.0	s	237.7	1.4	C35-995.5	s	303.4	1.5
C35-780.0	s	237.7	1.4	C35-996.5	s	303.7	1.2
C35-780.0	s	237.7	1.4	C35-996.5	s	303.7	1.2
C35-781.0	s	238.0	1.2	C35-996.5	s	303.7	1.3
C35-781.0	s	238.0	1.2	C35-996.5	s	303.7	1.3
C35-781.0	s	238.0	1.3	C35-997.5	s	304.0	1.2
C35-781.0	s	238.0	1.3	C35-997.5	s	304.0	1.3
C35-782.5	s	238.5	1.0	C35-997.5	s	304.0	1.3
C35-782.5	s	238.5	1.0	C35-997.5	s	304.0	1.5
C35-782.5	s	238.5	1.2	C35-998.5	s	304.3	1.3
C35-782.5	s	238.5	1.2	C35-998.5	s	304.3	1.4
C35-782.5	s	238.5	1.2	C35-998.5	s	304.3	1.4
C35-783.5	s	238.8	0.7	C35-998.5	s	304.3	1.5
C35-783.5	s	238.8	1.1	C35-999.5	s	304.6	1.1

THERMAL CONDUCTIVITY VALUES FROM CORE OF DRILL HOLE C35

SAMPLE NAME		DEPTH (METERS)	K, W/m-°C	SAMPLE NAME		DEPTH (METERS)	K, W/m-°C
C35-999.5	s	304.6	1.5	C35-1007.0	s	306.9	1.2
C35-999.5	s	304.6	1.9	C35-1008.0	s	307.2	1.3
C35-1001.0	s	305.1	1.2	C35-1008.0	s	307.2	1.3
C35-1001.0	s	305.1	1.3	C35-1008.0	s	307.2	1.4
C35-1001.0	s	305.1	1.4	C35-1008.0	s	307.2	1.4
C35-1001.0	s	305.1	1.4	C35-1009.0	s	307.5	1.3
C35-1002.0	s	305.4	1.3	C35-1009.0	s	307.5	1.3
C35-1002.0	s	305.4	1.3	C35-1009.0	s	307.5	1.4
C35-1002.0	s	305.4	1.3	C35-1009.0	s	307.5	1.4
C35-1002.0	s	305.4	1.4	C35-1010.0	s	307.8	1.2
C35-1003.0	s	305.7	1.3	C35-1010.0	s	307.8	1.3
C35-1003.0	s	305.7	1.3	C35-1010.0	s	307.8	1.3
C35-1003.0	s	305.7	1.3	C35-1010.0	s	307.8	1.3
C35-1003.0	s	305.7	1.4	C35-1011.0	s	308.2	1.1
C35-1004.0	s	306.0	1.3	C35-1011.0	s	308.2	1.1
C35-1004.0	s	306.0	1.3	C35-1011.0	s	308.2	1.2
C35-1004.0	s	306.0	1.3	C35-1011.0	s	308.2	1.2
C35-1004.0	s	306.0	1.3	C35-1013.0	s	308.8	1.3
C35-1004.0	s	306.0	1.4	C35-1013.0	s	308.8	1.3
C35-1005.0	s	306.3	1.3	C35-1014.0	s	309.1	1.3
C35-1005.0	s	306.3	1.3	C35-1014.0	s	309.1	1.3
C35-1005.0	s	306.3	1.3	C35-1015.0	s	309.4	1.3
C35-1005.0	s	306.3	1.3	C35-1015.0	s	309.4	1.4
C35-1006.0	s	306.6	1.2	C35-1016.0	s	309.7	1.4
C35-1006.0	s	306.6	1.2	C35-1016.0	s	309.7	1.4
C35-1006.0	s	306.6	1.3	C35-1017.0	s	310.0	1.4
C35-1006.0	s	306.6	1.3	C35-1017.0	s	310.0	1.5
C35-1007.0	s	306.9	1.1	C35-1018.0	s	310.3	1.3
C35-1007.0	s	306.9	1.1	C35-1018.0	s	310.3	1.4
C35-1007.0	s	306.9	1.1				

THERMAL CONDUCTIVITY VALUES FROM CORE OF DRILL HOLE C55

SAMPLE NAME		DEPTH (METERS)	K, W/m-°C	SAMPLE NAME		DEPTH (METERS)	K, W/m-°C
C55-546.0	s	166.4	1.8	C55-555.5	s	169.3	2.0
C55-546.0	s	166.4	2.1	C55-555.5	s	169.3	2.0
C55-546.0	s	166.4	2.2	C55-556.5	s	169.6	1.9
C55-546.0	s	166.4	2.3	C55-556.5	s	169.6	2.0
C55-547.0	s	166.7	1.9	C55-556.5	s	169.6	2.0
C55-547.0	s	166.7	2.1	C55-556.5	s	169.6	2.1
C55-547.0	s	166.7	2.1	C55-557.5	s	169.9	1.8
C55-547.0	s	166.7	2.3	C55-557.5	s	169.9	1.8
C55-548.0	s	167.0	2.2	C55-557.5	s	169.9	1.8
C55-548.0	s	167.0	2.3	C55-557.5	s	169.9	1.8
C55-548.0	s	167.0	2.4	C55-558.5	s	170.2	2.0
C55-549.0	s	167.3	2.2	C55-558.5	s	170.2	2.1
C55-549.0	s	167.3	2.2	C55-558.5	s	170.2	2.1
C55-549.0	s	167.3	2.3	C55-558.5	s	170.2	2.1
C55-549.0	s	167.3	2.4	C55-559.5	s	170.5	1.6
C55-550.5	s	167.8	2.1	C55-559.5	s	170.5	1.8
C55-550.5	s	167.8	2.2	C55-559.5	s	170.5	1.8
C55-550.5	s	167.8	2.3	C55-559.5	s	170.5	1.8
C55-550.5	s	167.8	2.5	C55-561.0	s	171.0	2.1
C55-551.0	s	167.9	1.5	C55-561.0	s	171.0	2.1
C55-551.5	s	168.1	2.1	C55-561.0	s	171.0	2.1
C55-551.5	s	168.1	2.3	C55-561.0	s	171.0	2.3
C55-551.5	s	168.1	2.3	C55-562.0	s	171.3	2.3
C55-551.5	s	168.1	2.4	C55-562.0	s	171.3	2.3
C55-552.0	s	168.2	1.5	C55-562.0	s	171.3	2.3
C55-552.5	s	168.4	2.1	C55-562.0	s	171.3	2.3
C55-552.5	s	168.4	2.2	C55-563.0	s	171.6	1.8
C55-552.5	s	168.4	2.3	C55-563.0	s	171.6	1.9
C55-552.5	s	168.4	2.4	C55-563.0	s	171.6	2.1
C55-553.0	s	168.6	1.5	C55-563.0	s	171.6	2.1
C55-553.5	s	168.7	1.9	C55-564.0	s	171.9	1.8
C55-553.5	s	168.7	2.1	C55-564.0	s	171.9	1.8
C55-553.5	s	168.7	2.2	C55-564.0	s	171.9	1.8
C55-553.5	s	168.7	2.3	C55-564.0	s	171.9	1.9
C55-554.0	s	168.9	1.6	C55-565.5	s	172.4	2.0
C55-554.5	s	169.0	2.1	C55-565.5	s	172.4	2.0
C55-554.5	s	169.0	2.1	C55-565.5	s	172.4	2.1
C55-554.5	s	169.0	2.2	C55-566.5	s	172.7	1.7
C55-554.5	s	169.0	2.3	C55-566.5	s	172.7	1.8
C55-555.5	s	169.3	1.8	C55-566.5	s	172.7	2.0
C55-555.5	s	169.3	1.9	C55-944.5	s	287.9	1.5

THERMAL CONDUCTIVITY VALUES FROM CORE OF DRILL HOLE C55

SAMPLE NAME		DEPTH (METERS)	K, W/m-°C	SAMPLE NAME		DEPTH (METERS)	K, W/m-°C
C55-944.5	s	287.9	1.5	C55-969.5	s	295.5	1.5
C55-944.5	s	287.9	1.5	C55-969.5	s	295.5	1.5
C55-944.5	s	287.9	1.5	C55-969.5	s	295.5	1.6
C55-945.5	s	288.2	1.2	C55-970.5	s	295.8	1.3
C55-945.5	s	288.2	1.3	C55-970.5	s	295.8	1.4
C55-945.5	s	288.2	1.3	C55-970.5	s	295.8	1.4
C55-945.5	s	288.2	1.3	C55-970.5	s	295.8	1.5
C55-946.5	s	288.5	1.5	C55-971.5	s	296.1	1.1
C55-946.5	s	288.5	1.5	C55-971.5	s	296.1	1.2
C55-946.5	s	288.5	1.5	C55-971.5	s	296.1	1.3
C55-946.5	s	288.5	1.5	C55-971.5	s	296.1	1.3
C55-948.5	s	289.1	1.3	C55-972.5	s	296.4	1.3
C55-948.5	s	289.1	1.4	C55-972.5	s	296.4	1.3
C55-948.5	s	289.1	1.5	C55-972.5	s	296.4	1.3
C55-948.5	s	289.1	1.5	C55-972.5	s	296.4	1.3
C55-949.5	s	289.4	1.3	C55-973.5	s	296.7	1.3
C55-949.5	s	289.4	1.3	C55-973.5	s	296.7	1.4
C55-949.5	s	289.4	1.4	C55-973.5	s	296.7	1.4
C55-949.5	s	289.4	1.4	C55-973.5	s	296.7	1.4
C55-950.5	s	289.7	1.2	C55-974.5	s	297.0	1.3
C55-950.5	s	289.7	1.3	C55-974.5	s	297.0	1.3
C55-950.5	s	289.7	1.3	C55-974.5	s	297.0	1.3
C55-950.5	s	289.7	1.3	C55-974.5	s	297.0	1.4
C55-969.5	s	295.5	1.3				

THERMAL CONDUCTIVITY VALUES FROM CORE OF DRILL HOLE C57
(SAMPLES ARE 2.680 CM IN DIAMETER BY 1.270 CM THICK)

SAMPLE NAME	DEPTH (METERS)	K, W/m-°C	SAMPLE NAME	DEPTH (METERS)	K, W/m-°C
C57-575.5	175.4	1.6	C57-587.5	179.1	1.4
C57-575.5	175.4	1.6	C57-587.5	179.1	1.5
C57-575.5	175.4	1.6	C57-587.5	179.1	1.5
C57-575.5	175.4	1.7	C57-587.5	179.1	1.5
C57-576.5	175.7	1.6	C57-588.5	179.4	1.3
C57-576.5	175.7	1.6	C57-588.5	179.4	1.3
C57-576.5	175.7	1.7	C57-588.5	179.4	1.3
C57-576.5	175.7	1.7	C57-588.5	179.4	1.4
C57-577.5	176.0	1.6	C57-589.5	179.7	1.3
C57-577.5	176.0	1.7	C57-589.5	179.7	1.4
C57-577.5	176.0	1.7	C57-589.5	179.7	1.5
C57-577.5	176.0	1.7	C57-590.5	180.0	1.5
C57-578.5	176.3	1.6	C57-590.5	180.0	1.5
C57-578.5	176.3	1.6	C57-590.5	180.0	1.5
C57-578.5	176.3	1.6	C57-590.5	180.0	1.7
C57-578.5	176.3	1.6	C57-591.5	180.3	1.4
C57-579.5	176.6	1.4	C57-591.5	180.3	1.4
C57-579.5	176.6	1.5	C57-591.5	180.3	1.4
C57-579.5	176.6	1.5	C57-591.5	180.3	1.6
C57-579.5	176.6	1.6	C57-592.5	180.6	1.3
C57-580.5	176.9	1.3	C57-592.5	180.6	1.4
C57-580.5	176.9	1.3	C57-592.5	180.6	1.4
C57-582.5	177.5	1.8	C57-592.5	180.6	1.5
C57-582.5	177.5	2.1	C57-593.5	180.9	1.5
C57-582.5	177.5	2.1	C57-593.5	180.9	1.8
C57-583.5	177.9	1.5	C57-593.5	180.9	1.8
C57-583.5	177.9	1.5	C57-593.5	180.9	1.9
C57-583.5	177.9	1.6	C57-594.5	181.2	1.2
C57-583.5	177.9	2.0	C57-594.5	181.2	1.3
C57-580.5	178.2	1.2	C57-594.5	181.2	1.4
C57-584.5	178.2	1.9	C57-594.5	181.2	1.4
C57-584.5	178.2	2.2	C57-595.5	181.5	1.3
C57-584.5	178.2	2.3	C57-595.5	181.5	1.4
C57-585.5	178.5	1.4	C57-595.5	181.5	1.4
C57-585.5	178.5	1.4	C57-595.5	181.5	1.5
C57-585.5	178.5	1.5	C57-595.5	181.5	1.6
C57-584.5	178.5	2.0	C57-596.5	181.8	1.2
C57-586.5	178.8	1.3	C57-596.5	181.8	1.3
C57-586.5	178.8	1.4	C57-596.5	181.8	1.3
C57-586.5	178.8	1.4	C57-596.5	181.8	1.3
C57-586.5	178.8	1.5	C57-597.5	182.1	2.1

THERMAL CONDUCTIVITY VALUES FROM CORE OF DRILL HOLE C57
(SAMPLES ARE 2.680 CM IN DIAMETER BY 1.270 CM THICK)

SAMPLE NAME	DEPTH (METERS)	K, W/m-°C	SAMPLE NAME	DEPTH (METERS)	K, W/m-°C
C57-597.5	182.1	2.1	C57-602.5	183.6	1.3
C57-597.5	182.1	2.2	C57-602.5	183.6	1.4
C57-597.5	182.1	2.5	C57-602.5	183.6	1.4
C57-598.5	182.4	1.5	C57-602.5	183.6	1.5
C57-598.5	182.4	1.6	C57-603.5	183.9	1.3
C57-598.5	182.4	2.3	C57-603.5	183.9	1.4
C57-600.5	183.0	2.1	C57-603.5	183.9	1.4
C57-600.5	183.0	2.3	C57-603.5	183.9	1.4
C57-600.5	183.0	2.3	C57-604.5	184.3	2.3
C57-600.5	183.0	2.4	C57-604.5	184.3	2.4
C57-601.5	183.3	1.4	C57-604.5	184.3	2.5
C57-601.5	183.3	1.4	C57-604.5	184.3	2.5
C57-601.5	183.3	1.4	C57-605.0	184.4	2.3
C57-601.5	183.3	1.4	C57-605.0	184.4	2.4

THERMAL CONDUCTIVITY VALUES FROM CORE OF DRILL HOLE C59

SAMPLE NAME		DEPTH (METERS)	K, W/m-°C	SAMPLE NAME		DEPTH (METERS)	K, W/m-°C
C59-477.5	s	145.5	1.2	C59-491.5	s	149.8	1.1
C59-477.5	s	145.5	1.2	C59-491.5	s	149.8	1.2
C59-477.5	s	145.5	1.4	C59-491.5	s	149.8	1.2
C59-478.5	s	145.8	1.2	C59-492.5	s	150.1	1.0
C59-478.5	s	145.8	1.3	C59-492.5	s	150.1	1.0
C59-478.5	s	145.8	1.3	C59-492.5	s	150.1	1.1
C59-479.5	s	146.2	1.2	C59-493.5	s	150.4	1.0
C59-479.5	s	146.2	1.3	C59-493.5	s	150.4	1.2
C59-479.5	s	146.2	1.3	C59-493.5	s	150.4	1.2
C59-480.5	s	146.5	1.1	C59-494.5	s	150.7	1.1
C59-480.5	s	146.5	1.2	C59-494.5	s	150.7	1.2
C59-480.5	s	146.5	1.3	C59-494.5	s	150.7	1.2
C59-481.5	s	146.7	1.4	C59-495.5	s	151.0	1.0
C59-481.5	s	146.8	1.1	C59-495.5	s	151.0	1.1
C59-481.5	s	146.8	1.2	C59-495.5	s	151.0	1.2
C59-482.5	s	147.1	1.3	C59-496.5	s	151.3	1.2
C59-482.5	s	147.1	1.3	C59-496.5	s	151.3	1.3
C59-482.5	s	147.1	1.4	C59-497.5	s	151.6	1.3
C59-483.5	s	147.4	1.3	C59-497.5	s	151.6	1.3
C59-483.5	s	147.4	1.3	C59-497.5	s	151.6	1.3
C59-483.5	s	147.4	1.3	C59-498.9	s	152.1	1.3
C59-484.5	s	147.7	1.2	C59-498.9	s	152.1	1.3
C59-484.5	s	147.7	1.3	C59-498.9	s	152.1	1.3
C59-484.5	s	147.7	1.3	C59-499.9	s	152.4	1.1
C59-485.5	s	148.0	1.2	C59-499.9	s	152.4	1.3
C59-485.5	s	148.0	1.3	C59-499.9	s	152.4	1.4
C59-486.5	s	148.3	1.3	C59-500.9	s	152.7	1.2
C59-486.5	s	148.3	1.3	C59-500.9	s	152.7	1.2
C59-486.5	s	148.3	1.3	C59-500.9	s	152.7	1.2
C59-487.5	s	148.6	1.2	C59-501.9	s	152.9	1.3
C59-487.5	s	148.6	1.2	C59-501.9	s	152.9	1.3
C59-487.5	s	148.6	1.2	C59-501.9	s	153.0	1.3
C59-488.5	s	148.9	1.3	C59-501.9	s	153.0	1.3
C59-488.5	s	148.9	1.3	C59-502.9	s	153.3	1.1
C59-489.5	s	149.2	1.2	C59-502.9	s	153.3	1.2
C59-489.5	s	149.2	1.3	C59-502.9	s	153.3	1.3
C59-489.5	s	149.2	1.3	C59-979.5	s	298.5	1.9
C59-485.5	s	149.5	1.3	C59-979.5	s	298.6	1.4
C59-490.5	s	149.5	1.3	C59-979.5	s	298.6	1.7
C59-490.5	s	149.5	1.3	C59-980.5	s	298.9	1.8
C59-490.5	s	149.5	1.3	C59-980.5	s	298.9	1.8

THERMAL CONDUCTIVITY VALUES FROM CORE OF DRILL HOLE C59

SAMPLE NAME		DEPTH (METERS)	K, W/m-°C	SAMPLE NAME		DEPTH (METERS)	K, W/m-°C
C59-980.5	s	298.9	1.9	C59-982.5	s	299.5	1.8
C59-981.5	s	299.2	2.0	C59-982.5	s	299.5	1.9
C59-981.5	s	299.2	2.1	C59-983.5	s	299.8	1.5
C59-981.5	s	299.2	2.1	C59-983.5	s	299.8	1.5

THERMAL CONDUCTIVITY VALUES FROM CORE OF DRILL HOLE DO1
(SAMPLES ARE 2.680 CM IN DIAMETER BY 1.270 CM THICK)

SAMPLE NAME	DEPTH (METERS)	K, W/m-°C	SAMPLE NAME	DEPTH (METERS)	K, W/m-°C
DO1 - 1075	327.7	2.67	DO1 - 1107	337.4	2.97
DO1 - 1084	330.4	2.59	DO1 - 1107	337.4	2.97
DO1 - 1084	330.4	2.59	DO1 - 1114	339.5	2.64
DO1 - 1092	332.8	2.83	DO1 - 1114	339.5	2.67
DO1 - 1092	332.8	2.83	DO1 - 1119	341.1	2.97
DO1 - 1099	335.0	2.83	DO1 - 1119	341.1	2.99
DO1 - 1105	336.8	2.68	DO1 - 1124	342.6	2.73
DO1 - 1105	336.8	2.68	DO1 - 1124	342.6	2.74

THERMAL CONDUCTIVITY VALUES FROM CORE OF DRILL HOLE LM1
(SAMPLES ARE 2.680 CM IN DIAMETER BY 1.270 CM THICK)

SAMPLE NAME	DEPTH (METERS)	K, W/m-°C	SAMPLE NAME	DEPTH (METERS)	K, W/m-°C
LM1 - 827	252.1	3.14	LM1 - 977	297.8	2.76
LM1 - 854.5	260.5	3.42	LM1 - 978	298.1	2.64
LM1 - 864	263.3	3.18	LM1 - 1013	308.8	3.27
LM1 - 878	267.6	3.12	LM1 - 1037.5	316.2	3.16
LM1 - 886	270.1	3.51	LM1 - 1038	316.4	2.57
LM1 - 963	293.5	2.90	LM1 - 1067	325.2	2.76

THERMAL CONDUCTIVITY VALUES FROM CORE OF DRILL HOLE CI1
(SAMPLES ARE 2.680 CM IN DIAMETER BY 1.270 CM THICK)

SAMPLE NAME	DEPTH (METERS)	K, W/m-°C	SAMPLE NAME	DEPTH (METERS)	K, W/m-°C
CI1 - 1580	481.6	2.37	CI1 - 1815	553.2	1.76
CI1 - 1593	485.5	1.75	CI1 - 2017.5	614.9	2.38
CI1 - 1810	551.7	1.93	CI1 - 2212	674.2	1.83

Heat Flow and Heat Generation in the Piedmont

Lawrence D. Perry, Steven P. Higgins, and Margaret M. McKinney

Figure 1 shows the location of holes drilled in the Piedmont by VPI&SU from which both heat flow and heat generation values have been obtained. Table 1 summarizes geothermal gradients, thermal conductivity values, heat flow calculations, and heat generation values.

Six new heat flow - heat generation values have been determined from holes PT2 and PT3 in the Petersburg granite, RM1 near Rocky Mount, NC, RL5 in the Rolesville Pluton, PG1 in the Pageland granite and BG1 in the Baltimore gabbro. The heat flow - heat generation values from holes PT2, PT3, RM1, and RL5 all plot quite close to the previous line determined for the Piedmont and are included in the calculation of a new (but not significantly different) relationship.

The heat flow - heat generation values from the Pageland hole, PG1, do not conform to the previously determined linear relationship between heat flow and heat generation. Apparently the heat flow value is too low as a result of water circulation disturbing the normal geothermal gradient in this hole. Close inspection of a Pageland temperature log shows a zone of disturbance between 195 m and 220 m depth; just below the interval for which the heat flow was calculated. The Pageland heat flow - heat generation values are not included in the calculation of the linear relationship between heat flow and heat generation.

The heat flow - heat generation data from hole BG1 in the Baltimore gabbro is not included in the linear relationship between heat flow and heat generation because the gabbro is underlain by crustal material which must contain higher U and Th concentrations than the gabbro. The heat flow observed (50 mW/m^2) is a result of the radiogenic heat produced below the gabbro. It is interesting to note that if the BG1 heat flow is plotted versus the overall mean heat generation (2.9) of all the data in Table 1, the point plots precisely on the line described by

$$q = 29.9 + 7.7A \quad (r^2 = 0.95)$$

which is the least squares fit to all the heat flow - heat generation data of Table 1 except holes CS1, BG1, PM1, and PG1. All the remaining holes fall within a 90% confidence interval about the regression line. The data and regression line are plotted in Figure 2.

Two additional heat flow values are reported for holes MN1 near Mineral, VA and CL1 near Pearisburg, VA. Hole MN1 was deviated from vertical by approximately 55° at the bottom of the hole. A deviation survey supplied by Callahan Mining Corporation was used to correct the temperature profile to vertical. The heat flow values reported are based on gradients calculated from the corrected temperature log.

Hole CL1 near Pearisburg, VA in the Valley and Ridge Province was drilled when warm water was encountered in a nearby hole drilled by the Alanses Corp(?). CL1 is drilled on the hanging wall of the Narrows fault. The unusually high heat flow value (123 mW/m^2) is probably caused by warm water entering the Narrows fault zone at depth and rising along the fault zone to be discharged at the surface in topographic lows. The nearest topographic low is the bottom of the New River.

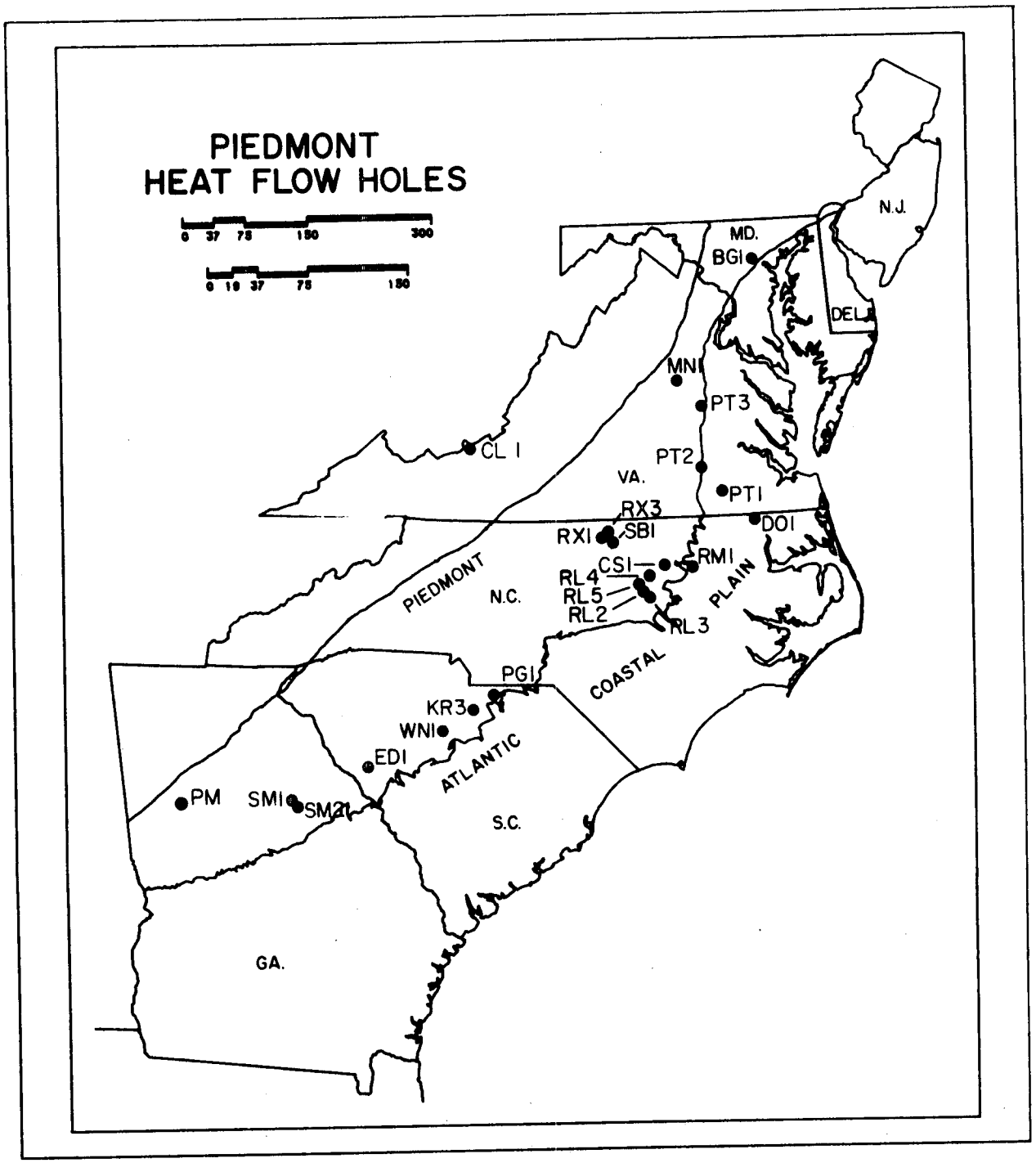
PIEDMONT
HEAT FLOW HOLES
0 37 75 150 300
0 19 37 75 150
N.J.
MD.
BGI
DEL.
MNI
PT3
PT2
PT1
CL 1
VA.
RX3
RX1
SB1
DO1
RM1
CS1
RL4
RL5
RL2
RL3
PIEDMONT
N.C.
PLAIN
COASTAL
PG1
KR3
WN1
ED1
ATLANTIC
S.C.
PM
SM1
SM2
GA.

SUMMARY of HEAT FLOW and HEAT PRODUCTION DATA

LOCATION HOLE	LATITUDE (NORTH)	LONGITUDE (WEST)	DEPTH INTERVAL, (m)	GRADIENT, C/Km	THERMAL CONDUCTIVITY, W/m-°C	HEAT FLOW, q, mW/m^2	HEAT PRODUCTION, A, μW/m^3
CUFFYTOWN PLUTON, SC							
ED1	33°55'11"	82°07'10"	182.5-285.0	17.65+/-0.03(1.000 42)1	3.84+/- 0.10(29)2	67.7+/- 1.7	5.2+/-0.4(17)[2]
LIBERTY HILL-KERSHAW PLUTON, NC							
KR3	34°32'20"	80°44'51"	351.8-384.3	14.90+/-0.01(1.000 14)	3.08+/- 0.30(12)	45.9+/- 4.5	2.3+/-0.6(23)
PETERSBURG GRANITE, VA							
PT1	36°49'45"	77°19'15"	190.0-251.0	18.92+/-0.08(0.998 123)	2.75+/- 0.31(23)	52.0+/- 5.9	2.6+/-0.2(10)
PT2	37°05'44"	77°35'37"	70.1-210.1	17.30+/-0.01(1.000 276)	3.28+/- 0.18(61)	56.8+/- 3.2	3.1+/-0.7(15)
PT3	37°45'11"	77°33'02"	107.3-201.0	18.37+/-0.02(1.000 185)	3.19+/- 0.10(42)	58.6+/- 1.8	3.7+/-0.7(15)
ROLESVILLE BATHOLITH AND CASTALIA PLUTON, NC							
CS1	36°04'15"	78°07'15"	142.2-209.7	19.26+/-0.03(1.000 28)	3.15+/- 0.16(26)	60.7+/- 3.1	2.3+/-0.1(2)
RL2	35°47'28"	78°25'04"	192.2-204.7	18.77+/-0.04(1.000 6)	2.97+/- 0.14(5)	55.7+/- 2.7	
RL2			104.7-114.7	16.84+/-0.08(1.000 5)	3.08+/- 0.18(5)	51.9+/- 3.1	
					BEST VALUE FOR RL2	53.8+/- 2.7	2.5+/-0.3(1)
RL3	35°57'05"	78°20'00"	42.4- 94.9	13.57+/-0.15(22)	3.44+/- 0.29(12)	46.9+/- 4.6	
RL3			97.4-129.9	13.79+/-0.10(14)	3.29+/- 0.45(15)	45.6+/- 6.7	
					BEST VALUE FOR RL3	46.3+/- 0.9	
RL4	35°57'05"	78°19'45"	155.2-192.2	16.91+/-0.05(1.000 16)	2.96+/- 0.27(16)	50.0+/- 4.5	2.8+/-0.5(19)
RL5	35°51'17"	78°28'54"	174.8-209.8	16.97+/-0.04(1.000 15)	2.90+/- 0.17(12)	49.2+/- 2.9	2.3+/-0.5(10)
ROXBORO METAGRANITE, NC							
RX1	36°23'12"	78°58'00"	149.3-169.3	10.81+/-0.04(1.000 9)	3.80+/- 0.06(10)	41.1+/- 0.6	
RX1			229.3-246.8	10.71+/-0.07(1.000 8)	3.82+/- 0.07(10)	40.9+/- 0.8	
					BEST VALUE FOR RX1	41.0+/- 0.7	1.8+/-0.1(7)
RX2	36°25'31"	79°01'53"	131.8-209.3	11.14+/-0.03(1.000 32)	3.67+/- 0.17(28)	40.9+/- 1.9	1.6+/-0.2(8)
RX3	36°25'39"	78°53'42"	139.9-194.9	10.31+/-0.15(0.998 10)	3.48+/- 0.24(14)	35.9+/- 2.6	1.1+/-0.2(7)
SLATE BELT, NC							
SB1	36°19'40"	78°50'00"	124.2-209.2	11.99+/-0.06(0.999 26)	3.36+/- 0.28(28)	40.3+/- 3.3	1.4+/-0.1(5)
SILOAM PLUTON, GA							
SM1	32°27'17"	83°08'53"	172.6-199.1	19.07+/-0.05(1.000 54)	3.38+/- 0.23(11)	64.4+/- 4.4	4.7+/-0.6(16)
SM2	33°28'41"	83°11'45"	104.5-205.5	19.30+/-0.03(1.000 203)	3.33+/- 0.29(28)	64.2+/- 5.6	4.5+/-0.5(14)
RION PLUTON, SC							
WN1	34°18'48"	81°08'42"	166.7-316.7	18.34+/-0.03(1.000 61)	3.38+/- 0.10(5)	62.0+/- 1.9	4.3+/-0.6(15)
N BALTIMORE GABBRO, MD							
BG1	39°19'15"	76°46'16"	254.6-282.6	15.56+/-0.04(1.000 56)	3.20+/- 0.32(14)	49.8+/- 5.0	0
ROCKY MOUNT, NC							
RM1	36°02'10"	77°45'14"	91.5-126.7	19.16+/-0.02(1.000 71)	3.11+/- 0.08(18)	59.6+/- 1.6	3.4+/-0.3(5)
PAGELAND, VA							
PG1	34°34'25"	80°50'05"	170.0-187.5	12.91+/-0.07(1.000 44)	3.10+/- 0.15(9)	40.1+/- 1.9	3.0+/-0.5(1)

MINERAL, VA						
MN1		284.0-319.3	16.26+/-0.04(0.999	111)	2.38+/- 0.19(11)	38.7+/- 3.2
MN1		326.5-350.1	17.34+/-0.06(0.999	79)	2.13+/- 0.31(7)	37.0+/- 5.4
					BEST VALUE FOR MN1	37.8+/- 0.6
PEARISBURG, VA (VR)						
CL1	37°20'31" 80°46'11"	113.4-171.4	18.90+/-0.04(0.999	115)	6.07+/- 0.24(28)	114.7+/- 4.5
CL1		188.2-195.4	21.11+/-0.16(0.999	15)	6.23+/- 0.06(3)	131.6+/- 1.7
					BEST VALUE FOR CL1(VR)	123.2+/-11.9
PALMETTO						
PM1	33°29'55" 84°41'58"	89.5-148.5	14.74+/-0.04(	118)	2.55+/- 0.42(20)	37.5+/- 3.3
PM1		149.5-160.0	11.92+/-0.14(	21)	3.13+/- 0.46(4)	37.3+/- 5.7
PM1		161.4-205.0	17.08+/-0.30(	90)	2.45+/- 0.20(20)	41.9+/- 3.6
					BEST VALUE FOR PM1	38.9+/- 2.5 3.0+/-2.5

VR - - - VALLEY AND RIDGE PROVINCE

1... values in parentheses are the coefficient of linear regression and the number of data pairs in the interval
2... value in parentheses is the number of thermal conductivity values used to compute the mean
B... indicates a heatflow value from the basement of the Atlantic Coastal Plain
S... indicates a heatflow value from the sediments of the Atlantic Coastal Plain

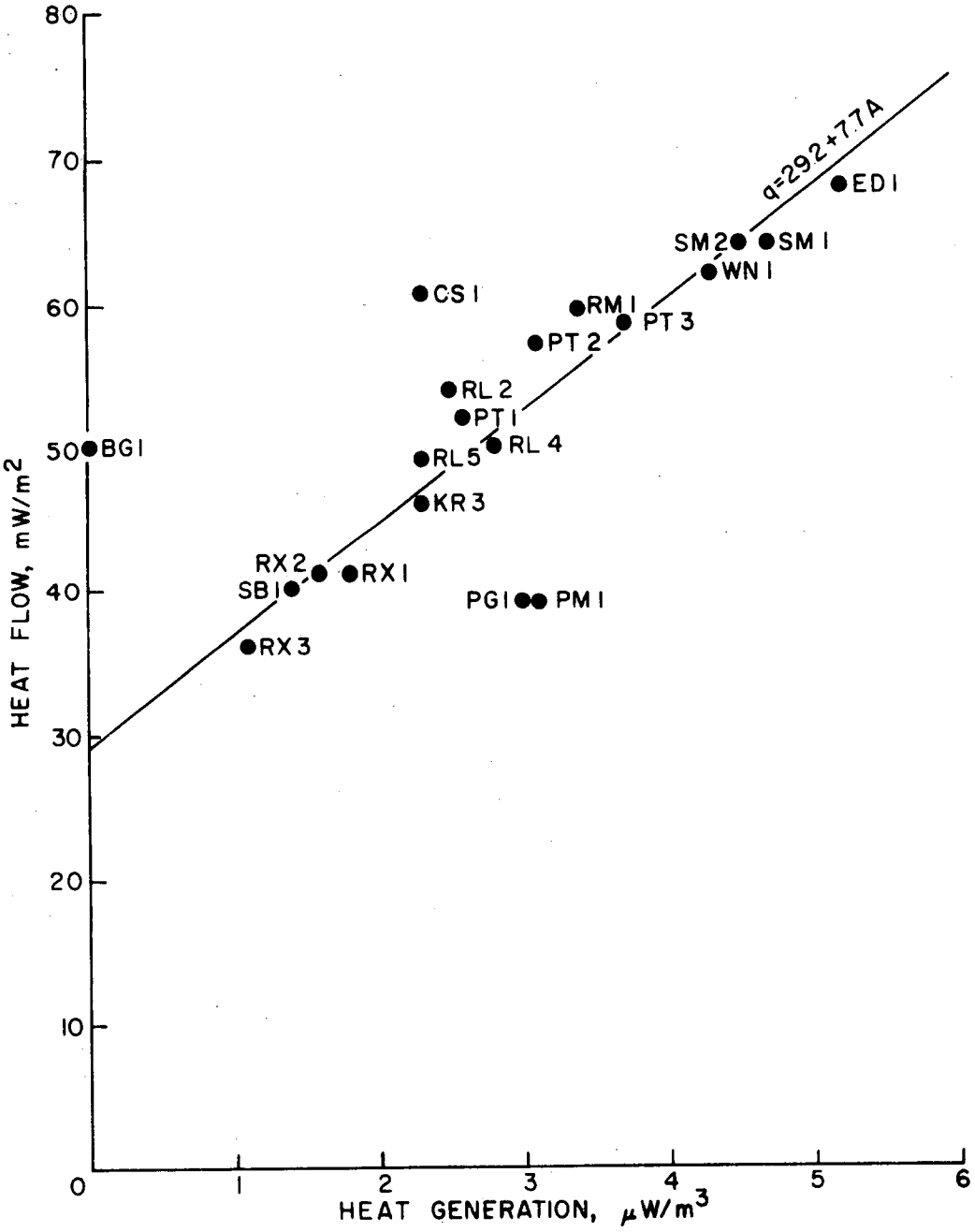
80
70
60
50
40
30
20
10
0
1
2
3
4
5
6
HEAT FLOW, mW/m2
HEAT GENERATION, μW/m3
q=29.2+7.7A
ED1
SM2
SM1
WN1
CS1
RM1
PT3
PT2
RL2
PT1
RL4
RL5
BG1
KR3
RX2
RX1
SB1
PG1
PM1
RX3

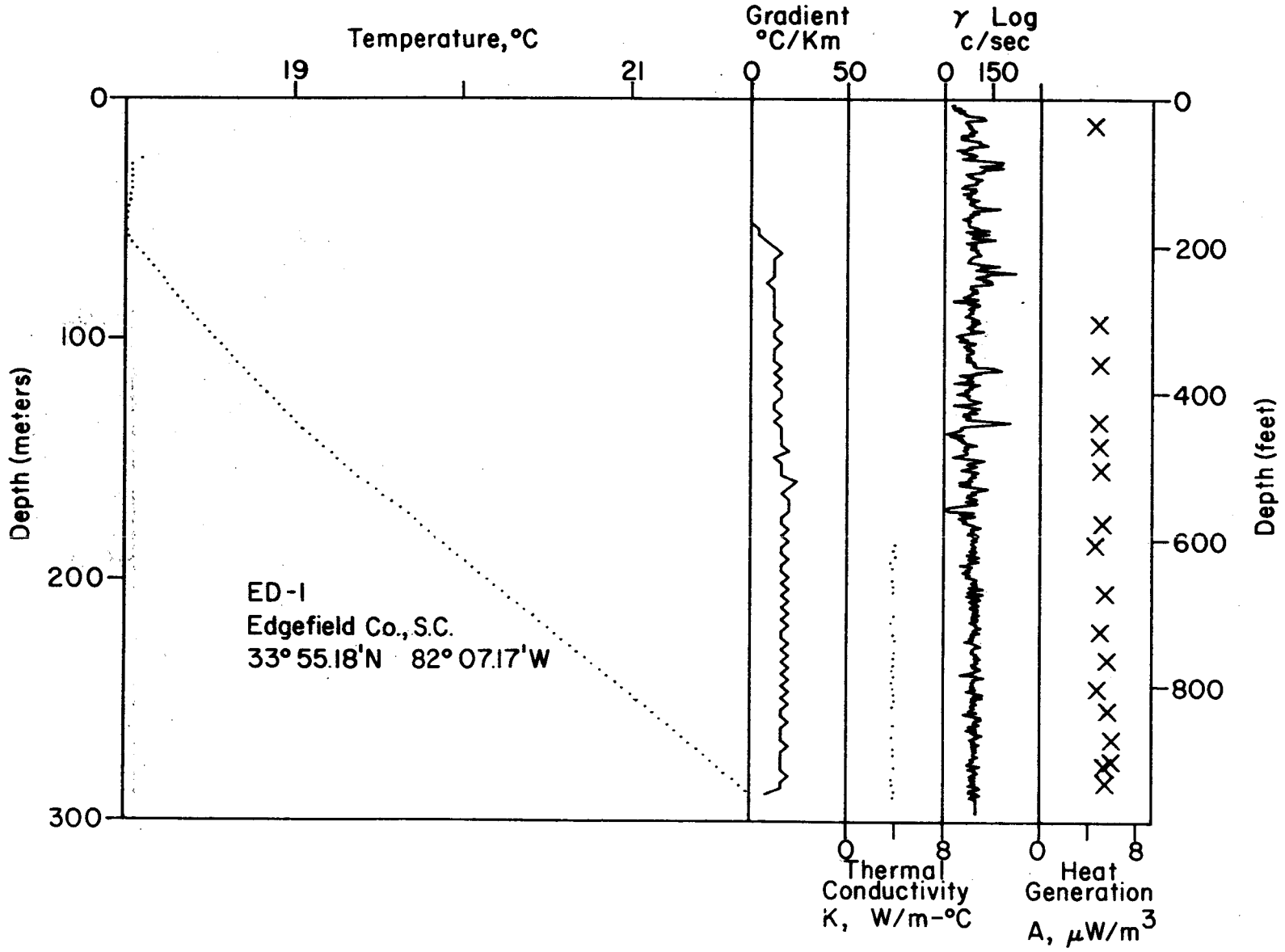
Temperature, °C
19
21
Gradient
°C/Km
0
50
γ Log
c/sec
0
150
0
100
200
300
Depth (meters)
ED-1
Edgefield Co., S.C.
33° 55.18'N 82° 07.17'W
0
200
400
600
800
Depth (feet)
0
8
Thermal
Conductivity
K, W/m-°C
0
8
Heat
Generation
A, μW/m3

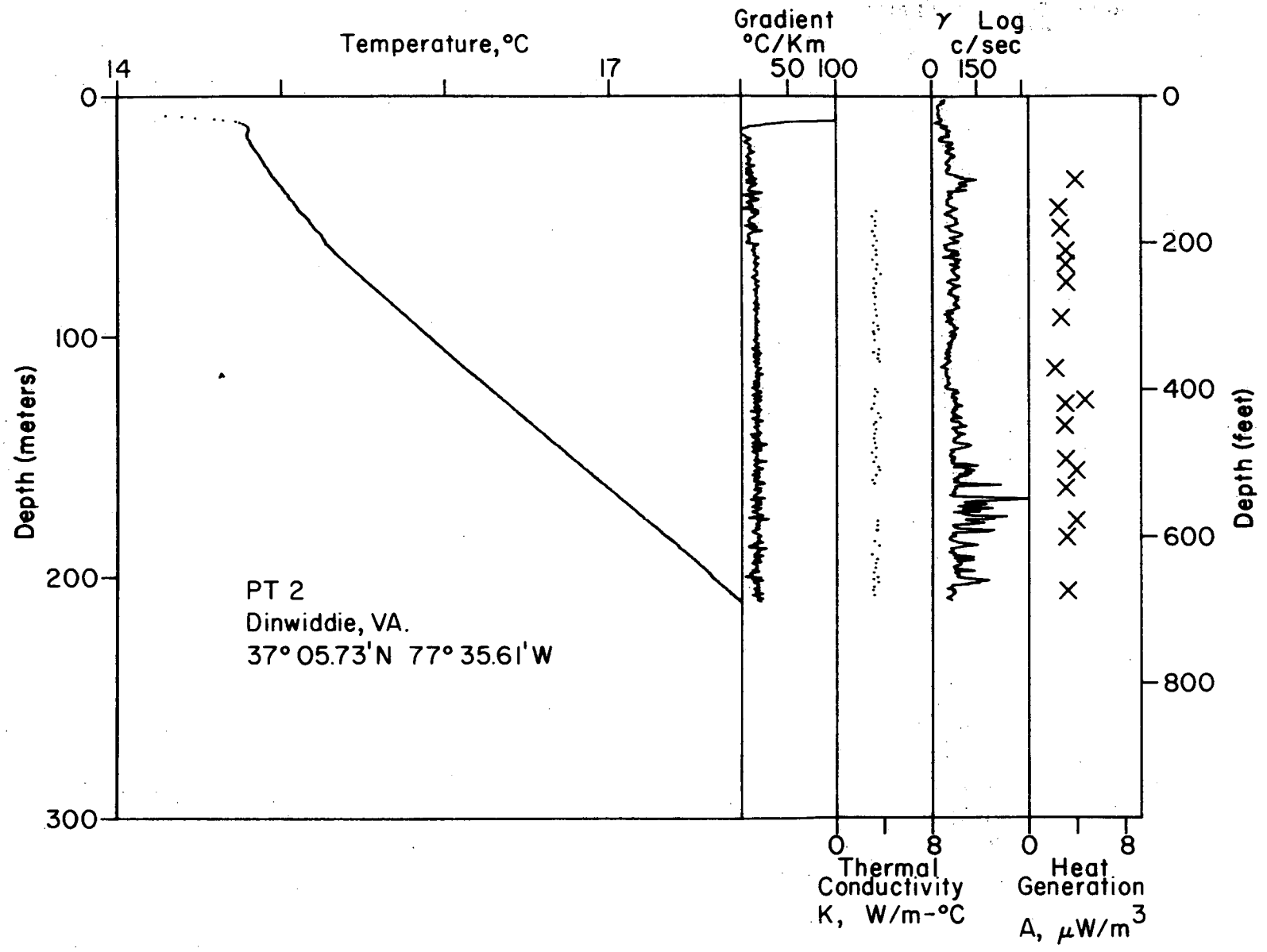
Temperature, °C
14
17
Gradient
°C/Km
50 100
γ Log
c/sec
0 150
0
100
200
300
Depth (meters)
0
200
400
600
800
Depth (feet)
PT 2
Dinwiddie, VA.
37° 05.73'N 77° 35.61'W
0
8
Thermal
Conductivity
K, W/m-°C
0
8
Heat
Generation
A, μW/m3

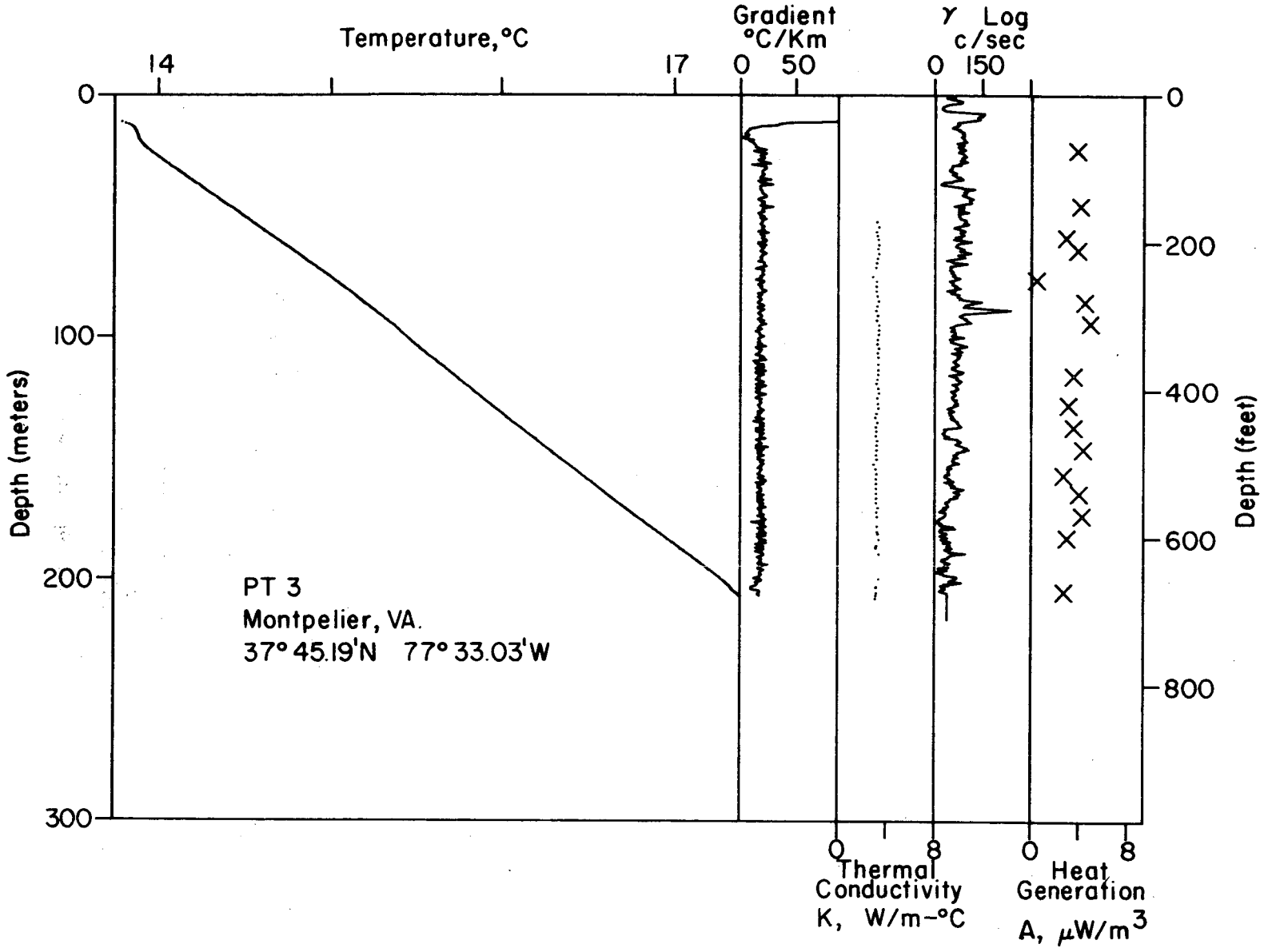
Temperature, °C
14
17
Gradient
°C/Km
0
50
γ Log
c/sec
0
150
0
100
200
300
Depth (meters)
0
200
400
600
800
Depth (feet)
PT 3
Montpelier, VA.
37° 45.19'N 77° 33.03'W
0
8
Thermal
Conductivity
K, W/m-°C
0
8
Heat
Generation
A, μW/m3

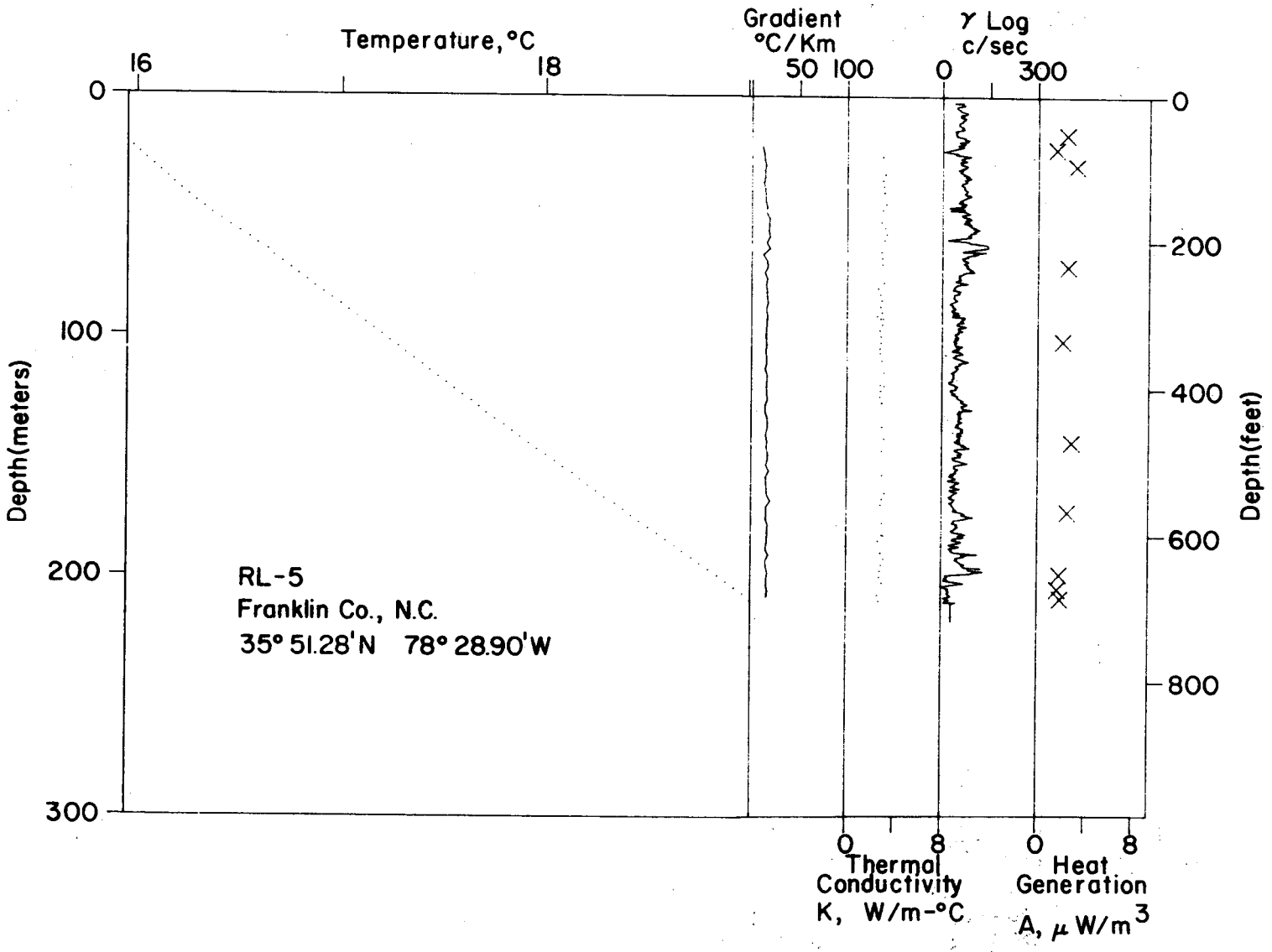
Temperature, °C
16
18
Gradient
°C/Km
50 100
γ Log
c/sec
0
300
0
100
200
300
Depth(meters)
0
200
400
600
800
Depth(feet)
RL-5
Franklin Co., N.C.
35° 51.28'N 78° 28.90'W
0
8
Thermal
Conductivity
K, W/m-°C
0
8
Heat
Generation
A, μ W/m3

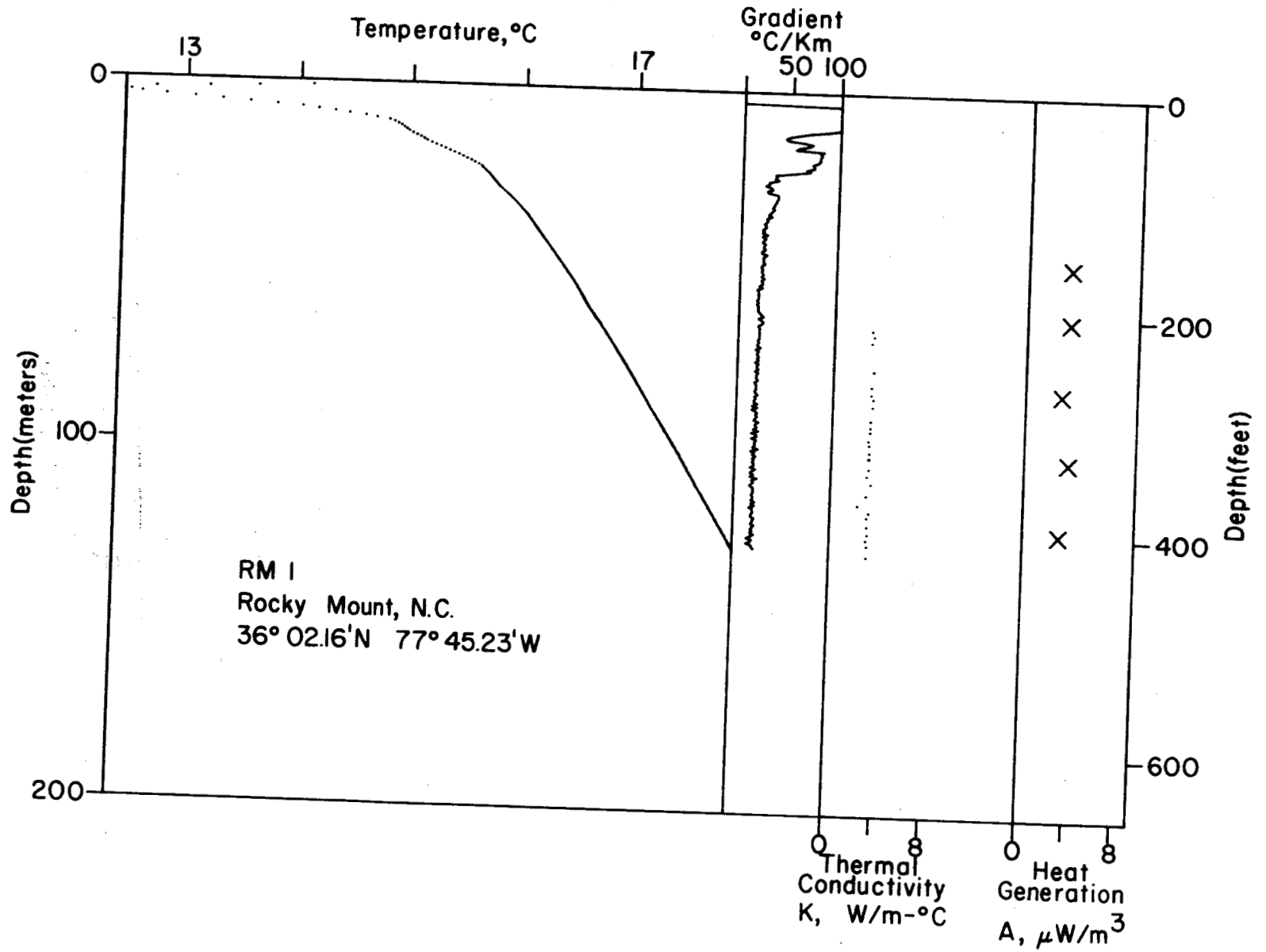
Temperature, °C
13
17
Gradient
°C/Km
50 100
0
Depth(meters)
100
200
RM 1
Rocky Mount, N.C.
36° 02.16'N 77° 45.23'W
0
200
400
600
Depth(feet)
0
8
Thermal
Conductivity
K, W/m-°C
0
8
Heat
Generation
A, μW/m3

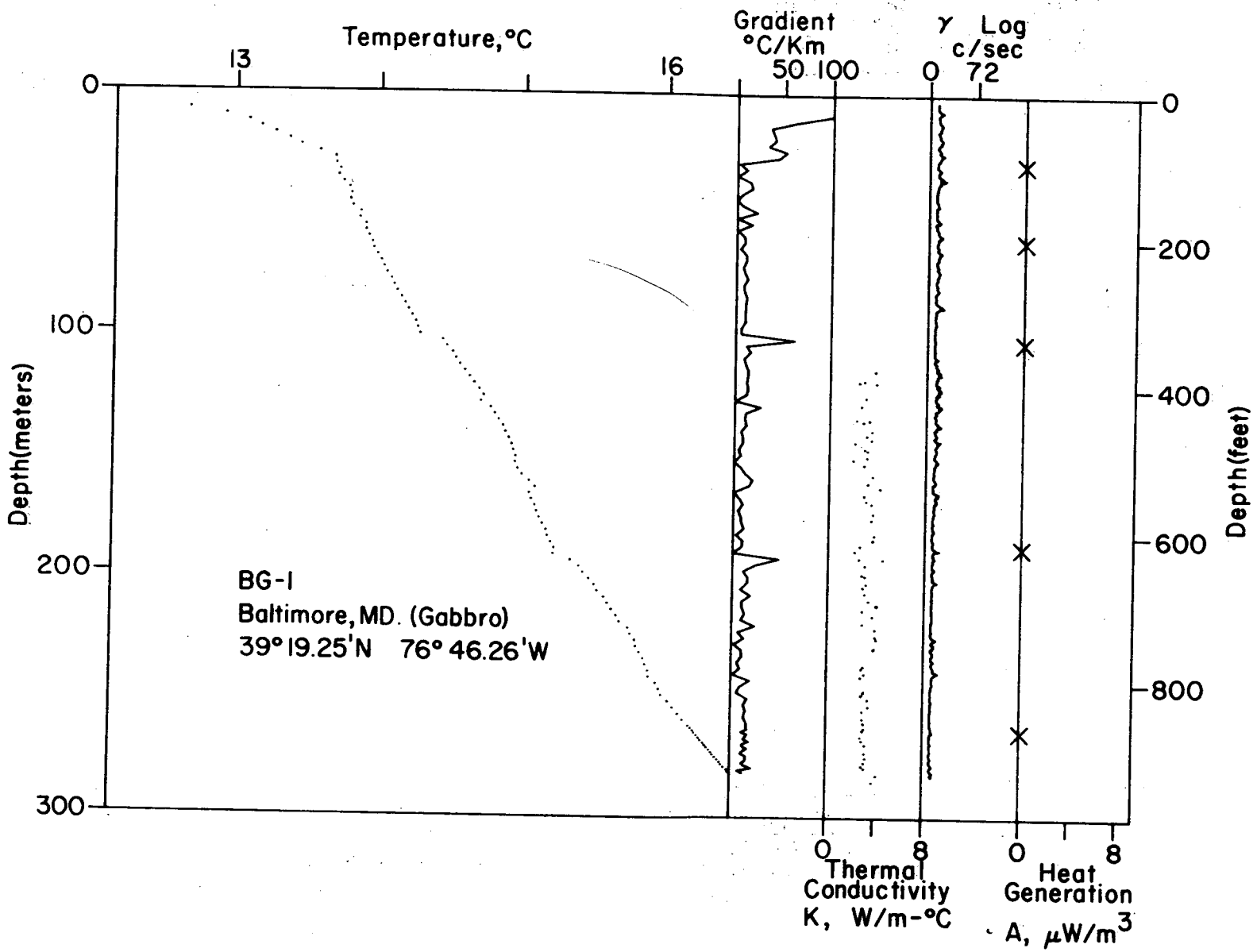
Temperature, °C
13
16
Gradient
°C/Km
50 100
γ Log
c/sec
0 72
0
100
200
300
Depth(meters)
0
200
400
600
800
Depth(feet)
BG-1
Baltimore, MD. (Gabbro)
39° 19.25'N 76° 46.26'W
0 8
Thermal
Conductivity
K, W/m-°C
0 8
Heat
Generation
A, μW/m3

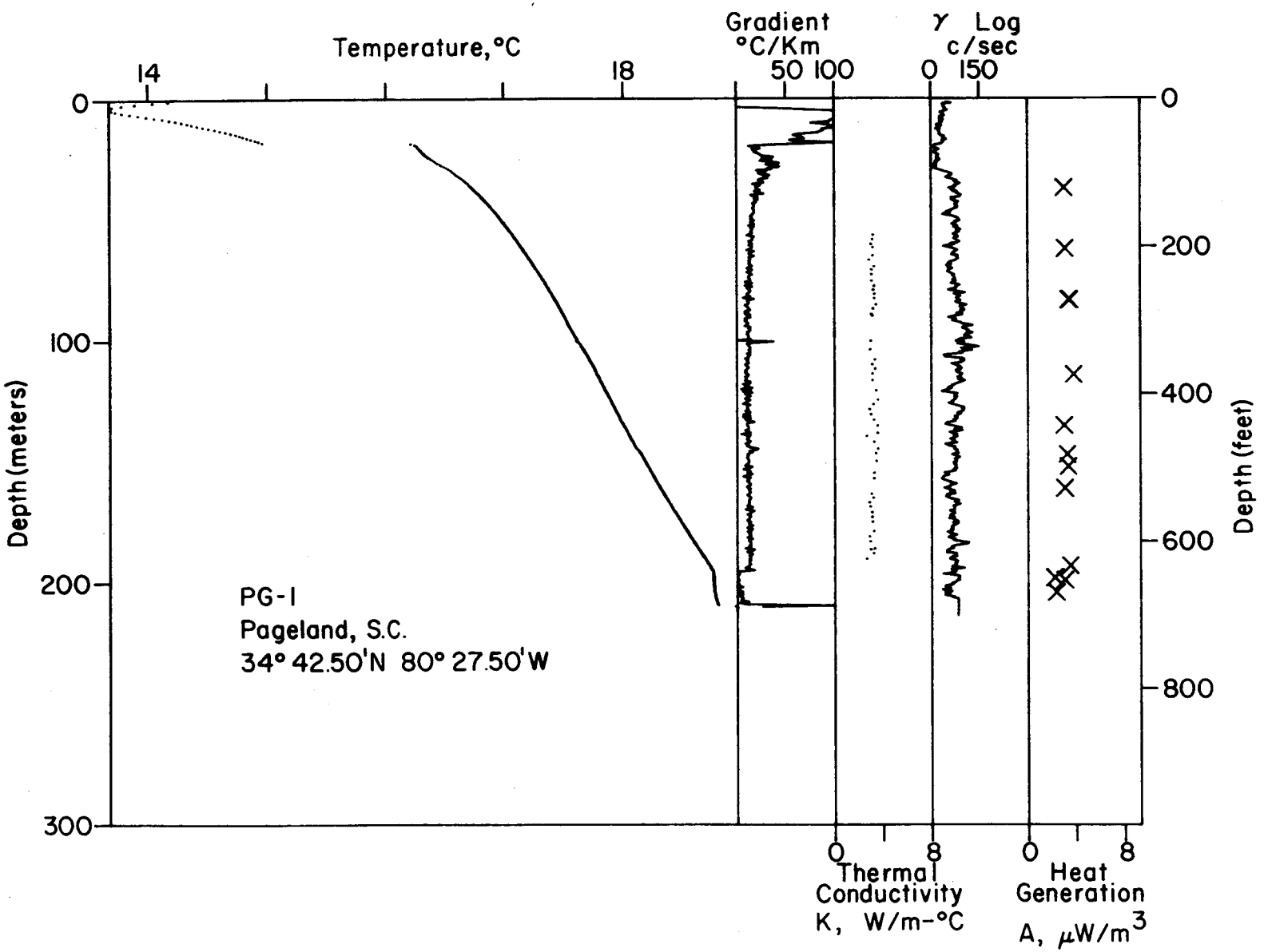
Temperature, °C
14
18
Gradient
°C/Km
50 100
γ Log
c/sec
0 150
0
100
200
300
Depth (meters)
0
200
400
600
800
Depth (feet)
PG-1
Pageland, S.C.
34° 42.50'N 80° 27.50'W
0
8
Thermal
Conductivity
K, W/m-°C
0
8
Heat
Generation
A, μW/m3

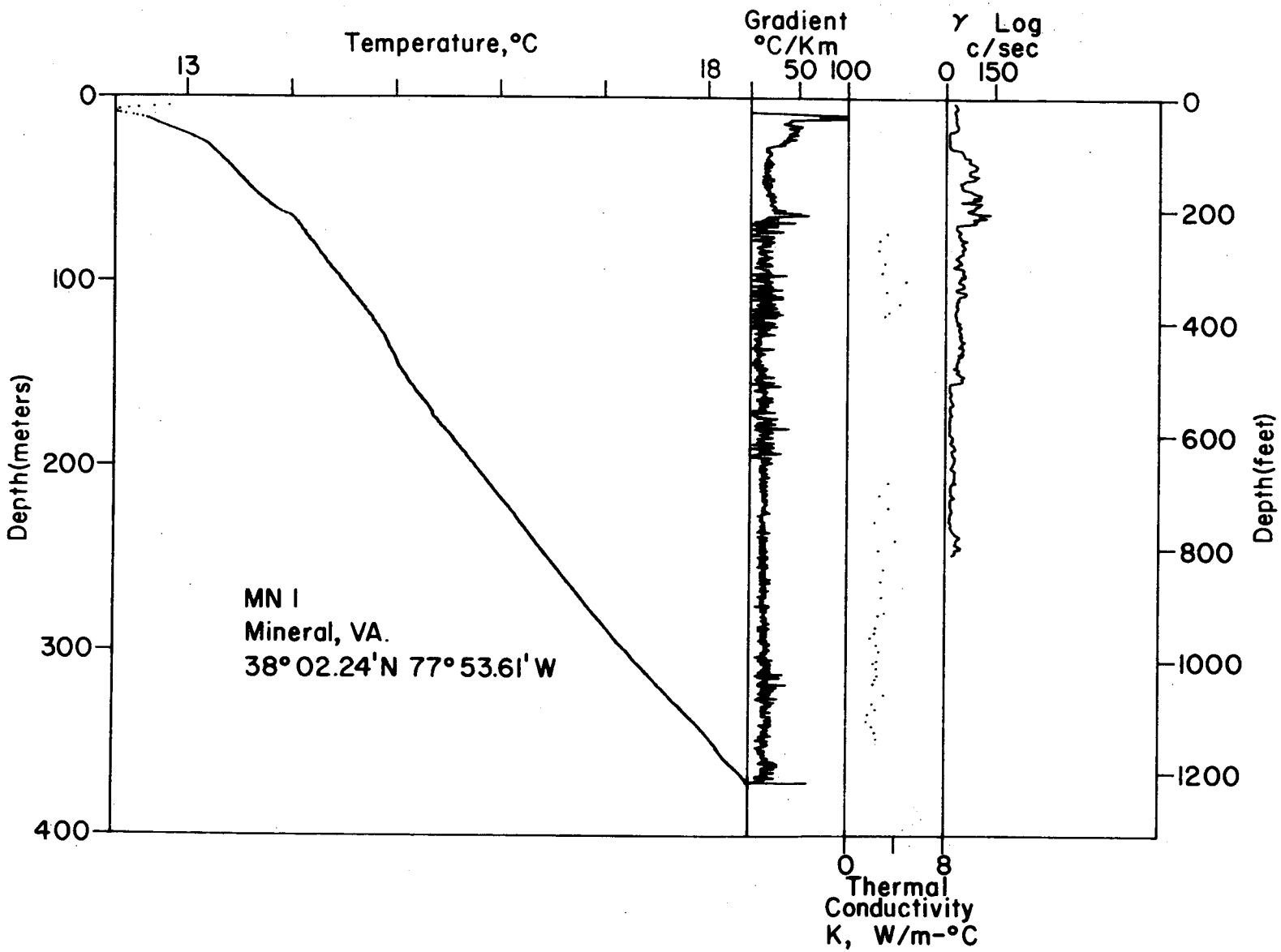
Temperature, °C
13
18
Gradient
°C/Km
50 100
γ Log
c/sec
0 150
0
100
200
300
400
Depth(meters)
0
200
400
600
800
1000
1200
Depth(feet)
MN 1
Mineral, VA.
38° 02.24'N 77° 53.61'W
0
8
Thermal
Conductivity
K, W/m-°C

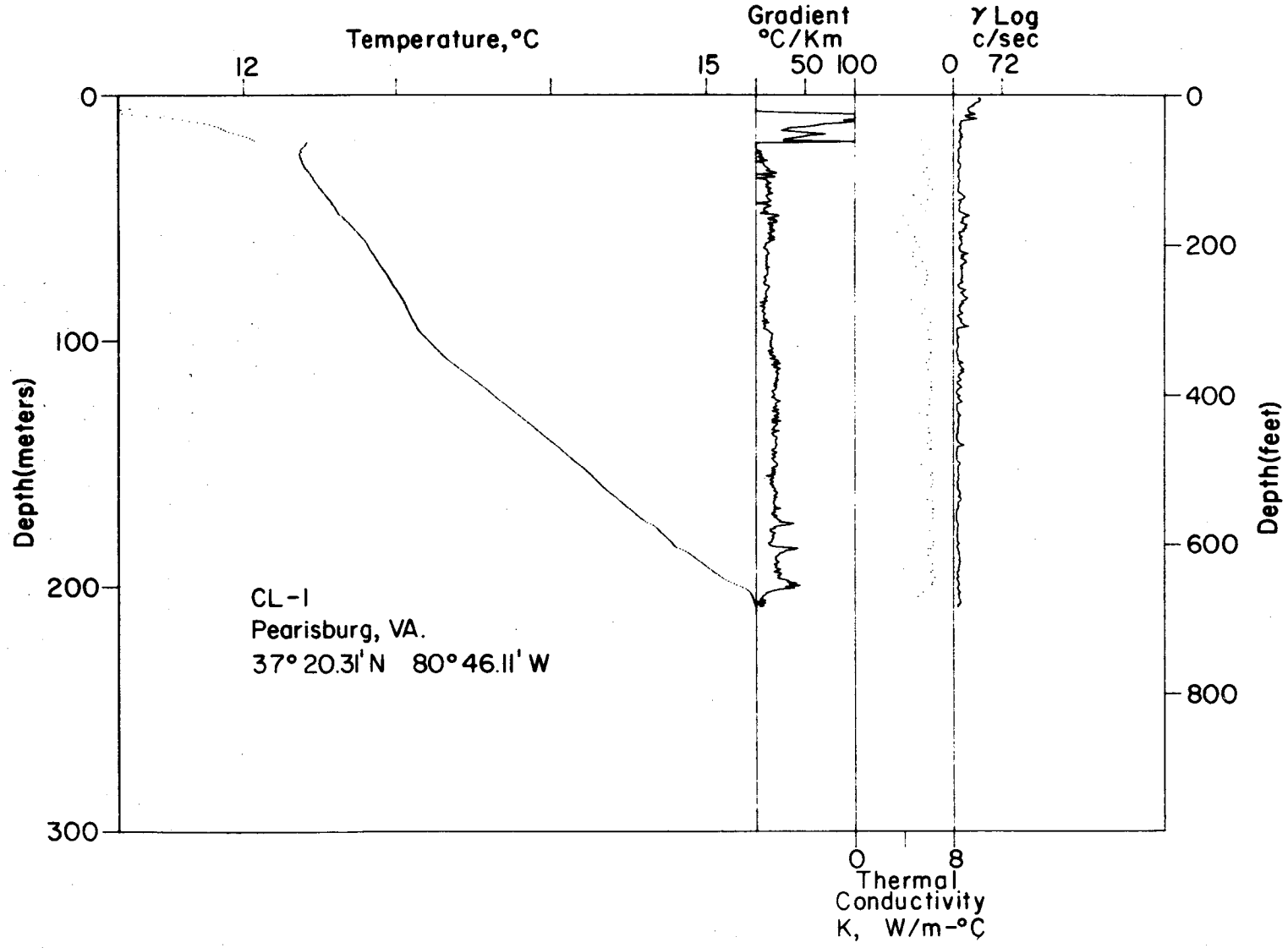
Temperature, °C
12
15
Gradient
°C/Km
50 100
γ Log
c/sec
0 72
0
100
200
300
Depth(meters)
0
200
400
600
800
Depth(feet)
CL-1
Pearisburg, VA.
37° 20.31' N 80° 46.11' W
0 8
Thermal
Conductivity
K, W/m-°C

HEAT GENERATION DATA FROM CORE OF DRILL HOLE PT2

LOCATION	SAMPLE NO. DEPTH(m)	DENSITY, gm/cm^3	URANIUM (U),ppm	THORIUM (TH),ppm	POTASSIUM (K),%	RATIO, TH/U	HEAT GENERATION, A X 10^{-6} W/m^3
PETERSBURG-2	VA PT2114	2.67	9.3	17.2	3.5	1.8	3.8
PETERSBURG-2	VA PT2152	2.67	4.1	16.2	3.5	4.0	2.5
PETERSBURG-2	VA PT2180	2.67	5.2	15.2	3.1	2.9	2.6
PETERSBURG-2	VA PT2211	2.67	5.9	18.7	3.3	3.2	3.0
PETERSBURG-2	VA PT2229	2.67	6.4	16.8	3.4	2.6	3.0
PETERSBURG-2	VA PT2254	2.67	5.9	18.8	3.2	3.2	3.1
PETERSBURG-2	VA PT2302	2.67	5.0	16.1	3.5	3.2	2.7
PETERSBURG-2	VA PT2371	2.67	3.6	14.1	3.3	3.9	2.2
PETERSBURG-2	VA PT2414	2.67	11.5	20.2	3.5	1.8	4.6
PETERSBURG-2	VA PT2419	2.67	6.6	15.2	3.4	2.3	3.0
PETERSBURG-2	VA PT2449	2.67	6.0	16.6	3.5	2.8	3.0
PETERSBURG-2	VA PT2495	2.67	6.1	17.4	3.3	2.9	3.0
PETERSBURG-2	VA PT2510	2.67	10.1	15.6	3.2	1.5	4.0
PETERSBURG-2	VA PT2534	2.67	6.5	16.3	3.4	2.5	3.0
PETERSBURG-2	VA PT2578	2.67	9.2	18.3	3.4	2.0	4.0
PETERSBURG-2	VA PT2601	2.67	6.4	17.7	3.2	2.8	3.1
PETERSBURG-2	VA PT2674	2.67	6.3	18.9	3.3	3.0	3.2

HEAT GENERATION DATA FROM CORE OF DRILL HOLE PT3

LOCATION	SAMPLE NO. DEPTH(m)	DENSITY, gm/cm^3	URANIUM (U),ppm	THORIUM (TH),ppm	POTASSIUM (K),%	RATIO, TH/U	HEAT GENERATION, A X 10^{-6} W/m^3
PETERSBURG-3	VA PT3075	2.67	8.7	18.8	3.8	2.2	3.8
PETERSBURG-3	VA PT3150	2.67	7.0	28.4	4.0	4.1	4.1
PETERSBURG-3	VA PT3193	2.63	5.5	17.7	4.1	3.2	3.0
PETERSBURG-3	VA PT3210	2.67	4.7	34.2	3.9	7.2	3.9
PETERSBURG-3	VA PT3250	2.67	0.6	3.1	1.1	5.5	0.5
PETERSBURG-3	VA PT3280	2.67	6.6	35.6	3.8	5.4	4.5
PETERSBURG-3	VA PT3309	2.67	8.5	35.5	4.0	4.2	5.0
PETERSBURG-3	VA PT3380	2.67	5.6	26.4	3.8	4.7	3.5
PETERSBURG-3	VA PT3420	2.67	4.2	24.9	4.0	5.9	3.1
PETERSBURG-3	VA PT3450	2.67	5.8	25.1	4.0	4.3	3.5
PETERSBURG-3	VA PT3480	2.67	6.3	35.1	3.7	5.6	4.3
PETERSBURG-3	VA PT3515	2.67	4.4	18.4	3.8	4.2	2.7
PETERSBURG-3	VA PT3540	2.67	6.8	28.3	4.0	4.2	4.0
PETERSBURG-3	VA PT3570	2.67	5.3	36.9	4.3	7.0	4.3
PETERSBURG-3	VA PT3600	2.67	4.9	20.8	4.0	4.3	3.0
PETERSBURG-3	VA PT3673	2.67	4.8	16.7	4.2	3.5	2.8

HEAT GENERATION DATA FROM CORE OF DRILL HOLE RL5

LOCATION	SAMPLE NO. DEPTH(m)	DENSITY, gm/cm^3	URANIUM (U),ppm	THORIUM (TH),ppm	POTASSIUM (K),%	RATIO, TH/U	HEAT GENERATION, A X 10^{-6} W/m^3
ROLESVILLE-5	NC RL5016	2.62	3.1	19.8	3.6	6.3	2.4
ROLESVILLE-5	NC RL5022	2.67	2.1	8.0	4.9	3.9	1.5
ROLESVILLE-5	NC RL5029	2.64	6.0	20.3	3.5	3.4	3.2
ROLESVILLE-5	NC RL5071	2.64	2.8	22.6	3.6	8.1	2.5
ROLESVILLE-5	NC RL5102	2.64	2.5	17.8	3.3	7.2	2.1
ROLESVILLE-5	NC RL5144	2.65	6.5	13.8	3.1	2.1	2.9
ROLESVILLE-5	NC RL5173	2.65	4.2	17.6	3.4	4.2	2.5
ROLESVILLE-5	NC RL5199	2.64	2.2	15.5	3.2	7.1	1.9
ROLESVILLE-5	NC RL5205	2.64	2.1	13.5	3.2	6.5	1.7
ROLESVILLE-5	NC RL5209	2.63	2.3	15.6	3.7	6.7	5.6

HEAT GENERATION DATA FROM CORE OF DRILL HOLE BG1

LOCATION	SAMPLE NO. DEPTH(m)	DENSITY, gm/cm^3	URANIUM (U),ppm	THORIUM (TH),ppm	POTASSIUM (K),%	RATIO, TH/U	HEAT GENERATION, A X 10^{-6} W/m^3
BALTIMORE GABBRO	MD BG1-029	2.67	0.0	0.2	0.1	99.2	0.0
BALTIMORE GABBRO	MD BG1-061	2.67	0.1	0.2	0.1	1.9	0.0
BALTIMORE GABBRO	MD BG1-103	2.67	0.1	0.2	0.0	3.1	0.0
BALTIMORE GABBRO	MD BG1-188	2.67	0.0	0.2	0.1	4.6	0.0
BALTIMORE GABBRO	MD BG1-264	2.67	0.2	0.3	0.0	1.4	0.1

HEAT GENERATION DATA FROM CORE OF DRILL HOLE RM1

LOCATION	SAMPLE NO. DEPTH(m)	DENSITY, gm/cm^3	URANIUM (U),ppm	THORIUM (TH),ppm	POTASSIUM (K),%	RATIO, TH/U	HEAT GENERATION, A X 10^{-6} W/m^3
ROCKY MOUNT	NC RM1-047	2.66	7.6	20.6	3.5	2.7	3.6
ROCKY MOUNT	NC RM1-062	2.69	6.6	24.1	2.9	3.6	3.6
ROCKY MOUNT	NC RM1-082	2.69	6.8	14.9	3.0	2.2	3.0
ROCKY MOUNT	NC RM1-101	2.69	7.9	21.1	2.9	2.7	3.7
ROCKY MOUNT	NC RM1-121	2.69	6.7	15.9	2.8	2.4	3.0

HEAT GENERATION DATA FROM CORE OF DRILL HOLE PG1

LOCATION	SAMPLE NO. DEPTH(m)	DENSITY, gm/cm^3	URANIUM (U),ppm	THORIUM (TH),ppm	POTASSIUM (K),%	RATIO, TH/U	HEAT GENERATION, A X 10^{-6} W/m^3
PAGELAND	SC PG1037	2.65	5.4	19.7	3.4	3.7	3.0
PAGELAND	SC PG1062	2.65	5.1	21.8	3.3	4.3	3.1
PAGELAND	SC PG1083	2.40	8.8	18.5	3.2	2.1	3.4
PAGELAND	SC PG1083	2.40	8.5	20.6	3.5	2.4	3.5
PAGELAND	SC PG1114	2.63	7.8	22.8	3.4	2.9	3.8
PAGELAND	SC PG1135	2.65	6.1	16.9	3.6	2.8	3.0
PAGELAND	SC PG1147	2.67	5.4	22.6	3.9	4.2	3.3
PAGELAND	SC PG1152	2.67	5.3	24.3	3.7	4.6	3.3
PAGELAND	SC PG1161	2.67	6.5	15.6	3.6	2.4	3.0
PAGELAND	SC PG1193	2.67	5.9	24.4	3.8	4.1	3.5
PAGELAND	SC PG1198	2.67	3.9	13.1	3.4	3.4	2.2
PAGELAND	SC PG1199	2.67	5.7	19.1	3.5	3.4	3.0
PAGELAND(Z)	SC PG1198	2.67	3.9	13.1	3.4	3.4	2.2
PAGELAND630-671,678-680	SC PG1204	2.67	4.1	13.9	3.6	3.4	2.3

THERMAL CONDUCTIVITY VALUES FROM CORE OF DRILL HOLE PT2
(SAMPLES ARE 2.680 CM IN DIAMETER BY 1.270 CM THICK)

SAMPLE NAME	DEPTH (METERS)	K, W/m-°C	SAMPLE NAME	DEPTH (METERS)	K, W/m-°C
PT2 - 157.6	48.0	3.34	PT2 - 419.6	127.9	3.13
PT2 - 164.6	50.2	2.99	PT2 - 426.2	129.9	2.93
PT2 - 171	52.1	3.26	PT2 - 432.3	131.8	3.48
PT2 - 177.6	54.1	3.28	PT2 - 438.2	133.6	3.66
PT2 - 184.9	56.4	3.03	PT2 - 444.7	135.5	3.28
PT2 - 191.4	58.3	3.22	PT2 - 447.9	136.5	3.10
PT2 - 197.8	60.3	3.39	PT2 - 454.3	138.5	3.29
PT2 - 204.4	62.3	3.10	PT2 - 460.3	140.3	3.15
PT2 - 210.3	64.1	3.33	PT2 - 466.6	142.2	3.13
PT2 - 216.9	66.1	3.35	PT2 - 473.1	144.2	3.20
PT2 - 223.4	68.1	3.03	PT2 - 479.6	146.2	3.31
PT2 - 229.6	70.0	3.42	PT2 - 486.2	148.2	2.95
PT2 - 236.2	72.0	3.34	PT2 - 492.6	150.1	3.30
PT2 - 242.7	74.0	3.70	PT2 - 499.1	152.1	3.11
PT2 - 249.3	75.9	3.15	PT2 - 505.5	154.1	3.49
PT2 - 255.2	77.8	3.32	PT2 - 510.1	155.5	3.60
PT2 - 261.8	79.8	3.13	PT2 - 516.6	157.5	3.29
PT2 - 268.3	81.8	3.14	PT2 - 523.3	159.5	3.00
PT2 - 273.6	83.4	3.27	PT2 - 528.3	161.0	3.16
PT2 - 283.8	86.5	3.21	PT2 - 578.7	176.4	3.44
PT2 - 291.1	88.7	3.29	PT2 - 585.1	178.3	3.40
PT2 - 299.6	91.3	3.37	PT2 - 591.6	180.3	3.37
PT2 - 309.1	94.2	3.10	PT2 - 591.6	180.3	3.39
PT2 - 313.2	95.5	3.46	PT2 - 606.6	184.9	3.17
PT2 - 318.2	97.0	3.53	PT2 - 612.7	186.8	3.55
PT2 - 321.2	97.9	3.09	PT2 - 624.6	190.4	2.96
PT2 - 324.7	99.0	3.17	PT2 - 631.2	192.4	3.40
PT2 - 333.1	101.5	3.20	PT2 - 637.3	194.2	3.27
PT2 - 345.2	105.2	3.55	PT2 - 643.1	196.0	3.25
PT2 - 349.4	106.5	3.09	PT2 - 649.6	198.0	3.11
PT2 - 352.3	107.4	3.51	PT2 - 655.7	199.9	3.44
PT2 - 358.3	109.2	3.44	PT2 - 658.8	200.8	3.10
PT2 - 362.3	110.4	3.60	PT2 - 662.7	202.0	3.49
PT2 - 399.7	121.8	3.23	PT2 - 669.1	203.9	3.14
PT2 - 403.7	123.0	3.41	PT2 - 673.7	205.3	3.05
PT2 - 409	124.7	3.19	PT2 - 680.1	207.3	3.15

THERMAL CONDUCTIVITY VALUES FROM CORE OF DRILL HOLE PT3
(SAMPLES ARE 2.680 CM IN DIAMETER BY 1.270 CM THICK)

SAMPLE NAME	DEPTH (METERS)	K, W/m-°C	SAMPLE NAME	DEPTH (METERS)	K, W/m-°C
PT3 - 171.2	52.2	3.17	PT3 - 423.5	129.1	3.32
PT3 - 178.1	54.3	3.35	PT3 - 430.9	131.3	3.15
PT3 - 185	56.4	3.13	PT3 - 436.4	133.0	3.04
PT3 - 190.1	57.9	3.23	PT3 - 442.9	135.0	3.23
PT3 - 195.1	59.5	3.31	PT3 - 449.2	136.9	3.11
PT3 - 202.3	61.7	3.34	PT3 - 454.9	138.7	3.14
PT3 - 207.8	63.3	3.26	PT3 - 461.2	140.6	3.10
PT3 - 214.2	65.3	3.33	PT3 - 467.8	142.6	3.20
PT3 - 220.6	67.2	3.22	PT3 - 474.2	144.5	3.15
PT3 - 226.7	69.1	3.16	PT3 - 480.7	146.5	3.16
PT3 - 232.8	71.0	3.10	PT3 - 487.2	148.5	3.11
PT3 - 245.1	74.7	2.83	PT3 - 493.2	150.3	3.17
PT3 - 251.6	76.7	3.16	PT3 - 499.8	152.3	2.90
PT3 - 258.1	78.7	3.13	PT3 - 506.1	154.3	3.09
PT3 - 264.6	80.7	3.15	PT3 - 512.7	156.3	3.17
PT3 - 271.4	82.7	3.21	PT3 - 519.6	158.4	3.09
PT3 - 278.1	84.8	3.33	PT3 - 526	160.3	3.12
PT3 - 284.7	86.8	3.19	PT3 - 532.8	162.4	3.11
PT3 - 291.1	88.7	3.13	PT3 - 539.3	164.4	3.12
PT3 - 297.6	90.7	3.26	PT3 - 545.8	166.4	3.14
PT3 - 304.1	92.7	3.16	PT3 - 552.2	168.3	3.14
PT3 - 310.6	94.7	3.36	PT3 - 558.6	170.3	3.27
PT3 - 317.1	96.7	3.36	PT3 - 564.7	172.1	3.16
PT3 - 323.5	98.6	3.34	PT3 - 571.2	174.1	3.20
PT3 - 330.5	100.7	3.24	PT3 - 584.4	178.1	3.21
PT3 - 336.4	102.5	3.22	PT3 - 591.4	180.3	3.21
PT3 - 342.2	104.3	3.36	PT3 - 594.5	181.2	3.29
PT3 - 348.3	106.2	3.25	PT3 - 602	183.5	3.37
PT3 - 354.7	108.1	3.31	PT3 - 610.2	186.0	3.15
PT3 - 364.2	111.0	3.30	PT3 - 613.2	186.9	3.11
PT3 - 371.6	113.3	3.28	PT3 - 622.1	189.6	3.38
PT3 - 378.1	115.2	3.28	PT3 - 655.7	199.9	3.33
PT3 - 384.4	117.2	3.22	PT3 - 666.2	203.1	3.17
PT3 - 390.3	119.0	3.14	PT3 - 667	203.3	3.11
PT3 - 396.8	120.9	3.29	PT3 - 674.4	205.6	3.18
PT3 - 403.2	122.9	3.37	PT3 - 678.3	206.7	3.11
PT3 - 409.7	124.9	3.19	PT3 - 682.5	208.0	3.07
PT3 - 417.2	127.2	3.29			

THERMAL CONDUCTIVITY VALUES FROM CORE OF DRILL HOLE RL5
(SAMPLES ARE 2.680 CM IN DIAMETER BY 1.270 CM THICK)

SAMPLE NAME	DEPTH (METERS)	K, W/m-°C	SAMPLE NAME	DEPTH (METERS)	K, W/m-°C
RL5 - 82	25.0	2.97	RL5 - 344.5	105.0	2.76
RL5 - 106.5	32.5	3.18	RL5 - 351	107.0	2.80
RL5 - 114.8	35.0	2.97	RL5 - 360.9	110.0	2.93
RL5 - 123	37.5	3.05	RL5 - 377.3	115.0	3.10
RL5 - 131.5	40.1	3.10	RL5 - 393.7	120.0	2.80
RL5 - 131.5	40.1	3.10	RL5 - 395.5	120.5	3.10
RL5 - 147.5	45.0	3.26	RL5 - 401.9	122.5	2.80
RL5 - 155.8	47.5	2.97	RL5 - 410.1	125.0	2.76
RL5 - 172.2	52.5	2.85	RL5 - 418.3	127.5	2.93
RL5 - 180.4	55.0	3.18	RL5 - 451.1	137.5	2.93
RL5 - 188.6	57.5	3.31	RL5 - 467.5	142.5	3.14
RL5 - 196.8	60.0	3.10	RL5 - 483.9	147.5	2.93
RL5 - 213.2	65.0	2.85	RL5 - 516.7	157.5	2.97
RL5 - 221.5	67.5	2.93	RL5 - 541.3	165.0	3.18
RL5 - 229.6	70.0	2.97	RL5 - 549.5	167.5	2.97
RL5 - 254.5	77.6	3.10	RL5 - 557.7	170.0	2.85
RL5 - 262.5	80.0	2.59	RL5 - 582.3	177.5	3.01
RL5 - 270.7	82.5	2.80	RL5 - 598.7	182.5	2.97
RL5 - 278.9	85.0	2.93	RL5 - 599.4	182.7	3.14
RL5 - 287	87.5	2.80	RL5 - 606.9	185.0	2.64
RL5 - 295	89.9	2.93	RL5 - 623.4	190.0	2.89
RL5 - 300.3	91.5	2.51	RL5 - 631.6	192.5	3.14
RL5 - 303.5	92.5	2.85	RL5 - 639.8	195.0	2.93
RL5 - 303.5	92.5	3.05	RL5 - 648	197.5	2.85
RL5 - 311.7	95.0	2.97	RL5 - 656.2	200.0	2.80
RL5 - 319.7	97.4	2.76	RL5 - 664.4	202.5	3.01
RL5 - 328.1	100.0	2.85	RL5 - 680.8	207.5	2.64
RL5 - 336.3	102.5	2.85	RL5 - 689	210.0	2.76

THERMAL CONDUCTIVITY VALUES FROM CORE OF DRILL HOLE BG1
(SAMPLES ARE 2.680 CM IN DIAMETER BY 1.270 CM THICK)

SAMPLE NAME	DEPTH (METERS)	K, W/m-°C	SAMPLE NAME	DEPTH (METERS)	K, W/m-°C
BG1 - 376	114.6	3.78	BG1 - 678.5	206.8	3.10
BG1 - 389	118.6	2.88	BG1 - 688	209.7	3.40
BG1 - 391	119.2	2.45	BG1 - 694	211.5	4.11
BG1 - 392	119.5	3.87	BG1 - 694.5	211.7	4.08
BG1 - 412	125.6	3.01	BG1 - 701.5	213.8	2.91
BG1 - 423	128.9	2.64	BG1 - 709	216.1	3.77
BG1 - 442	134.7	2.26	BG1 - 719.5	219.3	2.94
BG1 - 442.5	134.9	3.32	BG1 - 726.5	221.4	3.99
BG1 - 445	135.6	2.83	BG1 - 736.5	224.5	3.98
BG1 - 457	139.3	3.57	BG1 - 740	225.6	4.10
BG1 - 463.5	141.3	3.11	BG1 - 752	229.2	3.93
BG1 - 468.9	142.9	3.52	BG1 - 753.7	229.7	3.86
BG1 - 473	144.2	2.14	BG1 - 777.0	236.8	3.04
BG1 - 482	146.9	2.95	BG1 - 780	237.7	2.90
BG1 - 484	147.5	3.19	BG1 - 787.5	240.0	3.16
BG1 - 493	150.3	3.16	BG1 - 791.5	241.2	2.84
BG1 - 496.5	151.3	2.02	BG1 - 810.9	247.2	3.12
BG1 - 503.5	153.5	2.93	BG1 - 812	247.5	3.10
BG1 - 518.5	158.0	3.65	BG1 - 815.8	248.7	2.91
BG1 - 528.5	161.1	3.25	BG1 - 816.1	248.7	2.93
BG1 - 535	163.1	4.25	BG1 - 821.9	250.5	3.48
BG1 - 545	166.1	2.95	BG1 - 831.4	253.4	3.51
BG1 - 552.5	168.4	3.12	BG1 - 838	255.4	3.01
BG1 - 556	169.5	3.56	BG1 - 848.1	258.5	3.04
BG1 - 570	173.7	3.70	BG1 - 854	260.3	3.14
BG1 - 578	176.2	3.58	BG1 - 861.1	262.5	3.18
BG1 - 599	182.6	3.82	BG1 - 864	263.3	3.05
BG1 - 605.5	184.6	3.69	BG1 - 873.5	266.2	2.90
BG1 - 614	187.1	2.66	BG1 - 878	267.6	3.01
BG1 - 621	189.3	2.23	BG1 - 884	269.4	3.27
BG1 - 631	192.3	2.61	BG1 - 895.1	272.8	3.26
BG1 - 632	192.6	4.56	BG1 - 902	274.9	3.31
BG1 - 640	195.1	3.07	BG1 - 908	276.8	3.19
BG1 - 653	199.0	2.84	BG1 - 913	278.3	3.00
BG1 - 655	199.6	3.11	BG1 - 916	279.2	3.23
BG1 - 665	202.7	3.21	BG1 - 926	282.2	4.22
BG1 - 670	204.2	2.93	BG1 - 935.2	285.0	3.88

THERMAL CONDUCTIVITY VALUES FROM CORE OF DRILL HOLE RM1
(SAMPLES ARE 2.680 CM IN DIAMETER BY 1.270 CM THICK)

SAMPLE NAME	DEPTH (METERS)	K, W/m-°C	SAMPLE NAME	DEPTH (METERS)	K, W/m-°C
RM1 - 214	65.2	3.14	RM1 - 330	100.6	3.12
RM1 - 219	66.8	3.30	RM1 - 330.5	100.7	3.12
RM1 - 225	68.6	3.12	RM1 - 339.8	103.6	3.13
RM1 - 251	76.5	3.32	RM1 - 346	105.5	3.00
RM1 - 265	80.8	3.18	RM1 - 353.3	107.7	3.34
RM1 - 272	82.9	3.17	RM1 - 364	110.9	2.97
RM1 - 276	84.1	3.34	RM1 - 373	113.7	2.27
RM1 - 283	86.3	3.30	RM1 - 379.6	115.7	3.21
RM1 - 296	90.2	3.17	RM1 - 384	117.0	3.04
RM1 - 302	92.0	3.16	RM1 - 392	119.5	3.09
RM1 - 306	93.3	3.16	RM1 - 399.2	121.7	3.15
RM1 - 314	95.7	3.04	RM1 - 405	123.4	3.02
RM1 - 318	96.9	3.11	RM1 - 410	125.0	3.12
RM1 - 325	99.1	3.13	RM1 - 420.3	128.1	3.11

THERMAL CONDUCTIVITY VALUES FROM CORE OF DRILL HOLE PG1
(SAMPLES ARE 2.680 CM IN DIAMETER BY 1.270 CM THICK)

SAMPLE NAME	DEPTH (METERS)	K, W/m-°C	SAMPLE NAME	DEPTH (METERS)	K, W/m-°C
PG1 - 184.5	56.2	3.21	PG1 - 414.4	126.3	3.20
PG1 - 190.8	58.2	3.15	PG1 - 421	128.3	2.89
PG1 - 197.3	60.1	3.03	PG1 - 427.9	130.4	3.02
PG1 - 201.6	61.4	3.18	PG1 - 435.3	132.7	3.26
PG1 - 212.5	64.8	3.18	PG1 - 443.1	135.1	3.56
PG1 - 218.5	66.6	2.85	PG1 - 453.1	138.1	3.53
PG1 - 227.3	69.3	3.29	PG1 - 457.5	139.4	2.64
PG1 - 231.7	70.6	3.06	PG1 - 465.1	141.8	3.26
PG1 - 238	72.5	3.09	PG1 - 474.7	144.7	3.59
PG1 - 246.7	75.2	3.10	PG1 - 481.1	146.6	3.39
PG1 - 253.6	77.3	3.31	PG1 - 491.4	149.8	3.46
PG1 - 259	78.9	3.21	PG1 - 507.7	154.7	3.25
PG1 - 264.5	80.6	3.31	PG1 - 515.1	157.0	3.23
PG1 - 270.3	82.4	3.30	PG1 - 535.6	163.3	3.03
PG1 - 278.9	85.0	3.45	PG1 - 541.1	164.9	3.20
PG1 - 284.6	86.7	3.19	PG1 - 547.3	166.8	2.86
PG1 - 291.8	88.9	3.05	PG1 - 553.2	168.6	2.95
PG1 - 294.1	89.6	3.15	PG1 - 560.8	170.9	3.09
PG1 - 328.1	100.0	3.00	PG1 - 567.1	172.9	3.11
PG1 - 340	103.6	2.94	PG1 - 573.6	174.8	3.13
PG1 - 353.7	107.8	3.33	PG1 - 586.4	178.7	3.25
PG1 - 360.1	109.8	3.11	PG1 - 593.5	180.9	2.88
PG1 - 366.5	111.7	3.36	PG1 - 600.1	182.9	2.96
PG1 - 372.8	113.6	3.12	PG1 - 609.5	185.8	3.33
PG1 - 381.9	116.4	3.15	PG1 - 610.8	186.2	2.96
PG1 - 395.8	120.6	3.45	PG1 - 616.6	187.9	3.22
PG1 - 408.1	124.4	3.60	PG1 - 623.6	190.1	2.63

THERMAL CONDUCTIVITY VALUES FROM CORE OF DRILL HOLE MN1
(SAMPLES ARE 2.680 CM IN DIAMETER BY 1.270 CM THICK)

SAMPLE NAME	DEPTH (METERS)	K, W/m-°C	SAMPLE NAME	DEPTH (METERS)	K, W/m-°C
MN1 - 240.5	73.3	3.23	MN1 - 918.6	280.0	2.58
MN1 - 252.9	77.1	2.62	MN1 - 940	286.5	2.38
MN1 - 270.5	82.4	2.54	MN1 - 949.5	289.4	2.31
MN1 - 293.3	89.4	3.03	MN1 - 958	292.0	1.97
MN1 - 310.4	94.6	2.82	MN1 - 971.1	296.0	2.47
MN1 - 325.5	99.2	4.79	MN1 - 982.6	299.5	2.68
MN1 - 343.8	104.8	3.18	MN1 - 999.7	304.7	2.51
MN1 - 365.8	111.5	4.30	MN1 - 1003.6	305.9	2.22
MN1 - 380.6	116.0	3.39	MN1 - 1013	308.8	2.49
MN1 - 387.1	118.0	3.05	MN1 - 1025.9	312.7	2.54
MN1 - 683.7	208.4	3.37	MN1 - 1032.1	314.6	2.37
MN1 - 705.6	215.1	2.66	MN1 - 1040.7	317.2	2.21
MN1 - 728	221.9	3.39	MN1 - 1060	323.1	3.07
MN1 - 752.6	229.4	2.26	MN1 - 1075.5	327.8	2.14
MN1 - 785.7	239.5	3.97	MN1 - 1086	331.0	2.40
MN1 - 803.1	244.8	2.57	MN1 - 1094.8	333.7	1.78
MN1 - 837.3	255.2	2.99	MN1 - 1107.3	337.5	1.66
MN1 - 858.6	261.7	2.77	MN1 - 1116.5	340.3	2.11
MN1 - 886.1	270.1	2.85	MN1 - 1126.9	343.5	2.37
MN1 - 914.1	278.6	3.09	MN1 - 1138.5	347.0	2.47

THERMAL CONDUCTIVITY VALUES FROM CORE OF DRILL HOLE CL1
(SAMPLES ARE 2.680 CM IN DIAMETER BY 1.270 CM THICK)

SAMPLE NAME	DEPTH (METERS)	K, W/m-°C	SAMPLE NAME	DEPTH (METERS)	K, W/m-°C
CL1 - 60.3	18.4	5.37	CL1 - 342.8	104.5	6.17
CL1 - 72.4	22.1	6.03	CL1 - 344.3	104.9	6.16
CL1 - 80.3	24.5	5.54	CL1 - 352.3	107.4	5.99
CL1 - 97.3	29.7	5.83	CL1 - 356.8	108.8	5.80
CL1 - 102.7	31.3	5.57	CL1 - 366.2	111.6	5.93
CL1 - 112.4	34.3	6.03	CL1 - 382.5	116.6	6.19
CL1 - 120.5	36.7	5.91	CL1 - 389.8	118.8	6.13
CL1 - 125.7	38.3	6.29	CL1 - 389.8	118.8	6.23
CL1 - 133.4	40.7	4.72	CL1 - 394.1	120.1	6.23
CL1 - 133.4	40.7	4.80	CL1 - 401.3	122.3	5.55
CL1 - 139.5	42.5	5.87	CL1 - 405.5	123.6	6.06
CL1 - 145.7	44.4	5.37	CL1 - 413.5	126.0	6.02
CL1 - 154.1	47.0	5.74	CL1 - 426.9	130.1	5.86
CL1 - 160.5	48.9	3.90	CL1 - 426.9	130.1	5.90
CL1 - 167.2	51.0	5.19	CL1 - 444.2	135.4	5.96
CL1 - 173.1	52.8	4.33	CL1 - 450.7	137.4	6.02
CL1 - 182.4	55.6	3.45	CL1 - 450.7	137.4	6.06
CL1 - 189.1	57.6	4.83	CL1 - 460.8	140.5	6.19
CL1 - 189.1	57.6	4.86	CL1 - 464.8	141.7	5.84
CL1 - 195.7	59.6	4.95	CL1 - 472.3	144.0	6.05
CL1 - 202.9	61.8	5.23	CL1 - 472.3	144.0	6.18
CL1 - 209.5	63.9	4.72	CL1 - 493.1	150.3	5.36
CL1 - 215.3	65.6	4.71	CL1 - 504.3	153.7	6.28
CL1 - 221.9	67.6	5.47	CL1 - 507.1	154.6	6.12
CL1 - 228.8	69.7	4.91	CL1 - 513.3	156.5	6.33
CL1 - 233.7	71.2	5.81	CL1 - 519.3	158.3	6.27
CL1 - 239.9	73.1	5.88	CL1 - 523.1	159.4	6.17
CL1 - 246.5	75.1	5.82	CL1 - 539.7	164.5	5.85
CL1 - 252.6	77.0	5.65	CL1 - 539.7	164.5	5.87
CL1 - 272.5	83.1	4.54	CL1 - 541.8	165.1	6.27
CL1 - 284.3	86.7	5.67	CL1 - 552.5	168.4	6.30
CL1 - 291.1	88.7	5.44	CL1 - 552.5	168.4	6.35
CL1 - 302.7	92.3	6.13	CL1 - 557.8	170.0	6.31
CL1 - 312.9	95.4	5.92	CL1 - 565.3	172.3	6.30
CL1 - 325.7	99.3	6.01	CL1 - 581.6	177.3	6.04
CL1 - 325.7	99.3	6.21			

THERMAL CONDUCTIVITY VALUES FROM CORE OF DRILL HOLE CL1
(SAMPLES ARE 2.680 CM IN DIAMETER BY 1.270 CM THICK)

SAMPLE NAME	DEPTH (METERS)	K, W/m-°C	SAMPLE NAME	DEPTH (METERS)	K, W/m-°C
CL1 - 596.3	181.8	6.36	CL1 - 637.3	194.2	6.16
CL1 - 601.5	183.3	6.31	CL1 - 644.5	196.4	6.48
CL1 - 605.5	184.6	5.91	CL1 - 650.9	198.4	6.27
CL1 - 605.5	184.6	6.12	CL1 - 653.5	199.2	6.23
CL1 - 614.8	187.4	5.91	CL1 - 664.1	202.4	5.52
CL1 - 626.8	191.0	6.27	CL1 - 670.4	204.3	5.08
CL1 - 634.8	193.5	6.27			

Seismic Data Processing Facility

Cahit Coruh
Regional Geophysics Laboratory

We have developed software for demultiplexing, true amplitude recovery, spherical divergence corrections, VIBROSEIS crosscorrelation, deconvolution, velocity analysis (spectra), cdp stacking, filtering, section plotting, etc., etc., for use on the University's 370/158 computer system. (The Computing Center at VPI&SU is built around three large computer system: an IBM 3032 system operating under MVS, an IBM 370/158 dual processor system operating under VM/CMS and a Honeywell 68/60 MULTICS system). Though the facilities we have in the University's Computing Center, memory requirements of seismic processing jobs and desirability of rapid turn-around time required a dedicated computer to process our VIBROSEIS data. After a detailed study we purchased a new minicomputer system free-standing for VIBROSEIS data.

The minicomputer system called DISCO and specially designed for seismic data processing which consist of:

1. VAX 11/780 CPU with 1 megabyte expandable memory

2. two CDC Model 9766 300-megabyte disk subsystems

3. three triple-density 125 ips tape drives

4. electrostatic plotter, Varian 9222, 200 dot/inch, 22 inch wide

5. array processor, FPS AP120B with 64K words internal fast memory

6. six terminals for remote and interactive processing

System includes DIGICON's basic and advanced seismic data processing software packages. The new software packages also include autostatics, crooked-line and wave equation migration processing options.

The new seismic data processing system is capable of processing the data coming from our VIBROSEIS field system in a timely manner.